Title

New Donor-Acceptor Charge-Transfer Complexes of Transition Metals Incorporating Redox-Active Ligands

Permalink

Author

Seraya, Elaine

Publication Date

2016

UNIVERSITY OF CALIFORNIA,
IRVINE

New Donor-Acceptor Charge-Transfer Complexes of Transition Metals
Incorporating Redox-Active Ligands

DISSERTATION

submitted in partial satisfaction of the requirements
for the degree of

DOCTOR OF PHILOSOPHY

in Chemistry

by

Elaine Victoria Seraya

Dissertation Committee:
Professor Alan F. Heyduk, Chair
Professor Andrew S. Borovik
Professor Elizabeth R. Jarvo

2016

DEDICATION

To

my Mom

TABLE OF CONTENTS

LIST OF FIGURES

LIST OF TABLES

LIST OF SCHEMES

ACKNOWLEDGMENTS

CURRICULUM VITAE

Elaine Victoria Seraya

Education
University of California, Irvine   2011–2016
PhD. Candidate, Organic Chemistry
PhD. Dissertation: New Donor-Acceptor Charge-Transfer Complexes of Transition Metals Incorporating Redox-Active Ligands

California State University, Fullerton   2007–2010
BSc. Biochemistry, Magna cum Laude
Thesis Title: Stereoselective Gold(I)-Catalyzed Rearrangement of Highly Strained Cyclopropenyl Acetates

Research Experience
Graduate Researcher, University of California, Irvine   2012–2016
Graduate Advisor: Alan F. Heyduk
- Designed, synthesized, and characterized several families of charge-transfer coordination complexes including those of palladium, ruthenium, and rhodium.
- Systematically studied and optimized the charge-transfer parameters of new coordination complexes by synthetic and analytical solution techniques.
- Devised and performed multistep syntheses of new redox-active ligands with chemical linkers (anchor groups) for binding on solid supports.
- Developed suitable deprotection strategies for chemical anchoring groups of the redox-active ligands and their complexes.

Research Intern, Corning West Technology Center, CA   Summer 2016
Research Supervisor: Jeffrey King
- Developed new optical sensors for detection of hazardous gases on the surface of glass materials.
- Designed methods to verify sensing capabilities of glass products.

Visiting Researcher, University of California, Irvine   Spring–Summer 2011
Advisor: Suzanne Blum
- Explored new methods for synthesizing stereodefined gold(I) complexes using dual palladium and gold catalysis.

Visiting Researcher, University of Illinois at Chicago   Summer 2010
Advisor: Vladimir Gevorgyan
- Explored methods for the activation of aromatic C−H bond with palladium catalysis.

Undergraduate Researcher, California State University, Fullerton   2008–2010

Undergraduate Advisor: Christopher T. Hyland

- Discovered and established new gold-catalyzed methodology targeting ring-strain relief in three-membered organic compounds.
- Synthesized and characterized energetically strained cyclopropenes and methylenecyclopropanes.

Publications

- King, J.; **Seraya**, **E**.; Mazumber, P. Invention disclosure, patent pending (filed September, **2016**)
- **Seraya**, **E**.; Ziller, J. W.; Heyduk, A.F "Synthesis and Characterization of Rhodium(I) and Rhodium(III) Complexes Supported by the "Redox-Uncertain" β-Ketoamine Ligand." *Manuscript in preparation*
- **Seraya**, **E**.; Luan, Z.; Law, M.; Heyduk, A.F. "Synthesis of Catecholate Ligands with Phosphonate Anchoring Groups," *Inorg. Chem.* **2015**, *54*, 7571–7578
- **Seraya**, **E**.; Slack, E.; Ariafard, A.; Yates, B. F.; Hyland, C.T. "Experimental and Theoretical Investigation into the Gold-Catalyzed Reactivity of Cyclopropenylmethyl Acetates," *Org. Lett.* **2010**, 12 (21), 4768–4771

Contributed Presentations

- **Seraya**, **E**.; Heyduk, A.F. "Photoredox-Active Ligands: Optical Trends of the β-Ketoamine Ligand on Rhodium Centers." 251st ACS National Meeting, San Diego, CA, March 13, 2016 (Oral presentation)
- **Seraya**, **E**.; Heyduk, A.F. "Modular Donor-Acceptor Complexes of Palladium(II) for Hole-Injecting Dye-Sensitized Solar Cell Applications." 248th ACS National Meeting, San Francisco, CA, August 12, 2014 (Oral presentation)
- **Seraya**, **E**.; Heyduk, A.F. "Synthesis of Tunable (Donor)Pd[II](Acceptor) Charge-Transfer Complexes for Application in Dye-Sensitized Solar Cells." Center for Solar Energy Colloquium, University of California, Irvine, December 3, 2012 (Oral presentation).
- **Seraya**, **E**.; Heyduk, A.F. "Synthesis of Functionalized Donor Ligands and Their Charge-Transfer Complexes for Sensitizing Oxide Surfaces." Southern California Inorganic Photochemistry Conference, Catalina, CA, September 9, 2012. (Oral presentation)
- **Seraya**, **E**.; Hyland, C.T. "Facile Stereoselective Synthesis of Acyloxy Dienes from Cyclopropenyl Acetates." 239th ACS National Meeting, San Francisco, CA, March 23, 2010 (Poster)
- **Seraya**, **E**.; Hyland, C.T. "Facile Stereoselective Synthesis of Acyloxy Dienes from Cyclopropenyl Acetates." 22nd Annual California State University Biotechnology Symposium, Santa Clara, CA, January 9, 2010 (Poster).

Teaching Experience

Teaching Assistant, Department of Chemistry, UC Irvine   2011–2016
- Taught lower and upper division laboratory courses: organic, inorganic, general chemistry

Instructional Assistant, Viet My Learning Center, CA   2010–2011
- Taught biology and chemistry subjects at an afterschool learning program

Professional Experience

Graduate Professional Success-BIOMED Trainee, UC Irvine   2015
- Attended training and workshop sessions on leadership and career skills

Steering Committee, Department of Chemistry, UC Irvine   2013–2014
- Coordinated inorganic chemistry student-seminar series to facilitate scientific discussions among graduate students and post-docs

Project Coordinator, Volunteer and Service Center, Cal State Univ. Fullerton   2007
- Planned and supervised bimonthly visits to the Orangewood Children's Home

Professional Affiliations
- American Chemical Society   2009–2016
- University of California, Irvine Center for Solar Energy   2012
- California State University Program for Education and Research in Biotechnology   2009-2010
- Student Health Professions Association   2007

Honors and Awards
- Taihi Hong Memorial Graduate Student Education Award   2013
- American Institute of Chemists Foundation Award   2010
- National Science and Mathematics Access to Retain Talent Grant   2010
- Howard Hughes Medical Institute Research Scholarship   2008–2010
- National Science Foundation REU Award   2008

ABSTRACT OF THE DISSERTATION

New Donor-Acceptor Charge-Transfer Complexes of Transition Metals
Incorporating Redox-Active Ligands

By

Elaine Victoria Seraya

Doctor of Philosophy in Chemistry

University of California, Irvine, 2016

Professor Alan F. Heyduk, Chair

The work described in this dissertation is subdivided into two main parts. Part 1 addresses how new donor-acceptor charge-transfer complexes, of mixed redox-active ligands, can be realized with coordinatively saturated transition-metal centers. Part 2 details synthetic strategies for installing phosphonic acid anchoring groups on frequently used redox-active ligands.

Chapter 1 provides a general background on redox-active ligands and their donor-acceptor charge-transfer complexes. The molecular structure of classical donor-acceptor complexes is introduced along with their benefits and inherent deficiencies. The need for improved molecular designs is highlighted through several non-classical donor-acceptor complexes of coordinatively saturated metal ions.

Chapter 2 discusses the coordination and reactivity patterns of the new β-ketoaminato ligand, $(acNac^{Ph})^-$, on square-planar Rh^I and octahedral Rh^{III} centers. Oxidation of the Rh^I structure, $(acNac^{Ph})Rh(dmbpy)$ (dmbpy = 4,4-dimethyl-2,2-bipyridine), by two electrons produces two different forms of the Rh^{III} complex: the electron donor $(acNac^{Ph})^-$

and the electron-acceptor dmbpy are found either in a coplanar arrangement or non-coplanar arrangement. The propensity of (acNac^{Ph})$^-$ to participate in ligand-to-ligand charge-transfer (LL'CT) on Rh^{III} centers is scrutinized by optical spectroscopic methods, revealing that the ligand is primarily redox innocent.

Chapter 3 reports on the synthesis and characterization of octahedral Ru^{II} centers coordinated by the redox-active catecholate donor and bipyridine acceptor ligands. Solid-state analysis of two independent products indicates that both contain Ru^{II} in a six-coordinate environment with non-coplanar donor-acceptor pairs.   However, characterization of the putative products by solution spectroscopic techniques provides evidence that alternative ruthenium configurations must also be prevalent.

Chapter 4 introduces the concept of chemical anchoring groups for covalent modification of metallic oxide surfaces.   The intrinsic advantages, suitable syntheses, and the real-life applications of phosphonic acid anchors are discussed. The current and future role of the phosphonate group is highlighted in the context of redox-active ligands.

Chapter 5 compares the redox properties of two new catecholate ligands containing protected phosphonate diester groups in the 4-position of the catecholate ring. The electronic properties of the phosphonate anchors are assessed in solution through a series of (catecholate)Pd(diimine) charge-transfer complexes.   Direct attachment of the phosphonate group to the catecholate ligand significantly perturbs the electron donor ability of the ligand whereas the incorporation of a single methylene linker between the phosphonate group and the catecholate ring effectively preserves the donating properties of the ligand. The charge-transfer complexes of the catecholate ligands with deprotected phosphonic acids are shown to bind strongly on the surface of titanium dioxide.

Chapter 6 outlines a modular synthetic approach for the redox-active β-diketiiminyl ligand, (NacNac^{Phos})$^-$, functionalized with a phosphonate diester substituent at the central carbon of the ligand backbone. The new ligand is coordinated on Rh^I and Rh^{III} centers, (NacNac^{Phos})Rh(phdi) and (NacNac^{Phos})RhCl$_2$(phdi) (phdi = phenanthrene-9,10-diimine), respectively. For the Rh^{III} structure, significant involvement of the (NacNac^{Phos})$^-$ donor ligand in ligand-to-ligand charge-transfer is verified through systematic comparisons with reported (NacNac^R)RhCl$_2$(phdi) complexes (R = CH$_3$ or CF$_3$ at the 1,3-positions of the ligand backbone). The LL'CT band energy is directly influenced by the donor-ligand substitution according to the trend: (NacNac^{CF3})$^-$ > (NacNac^{Phos})$^-$ > (NacNac^{CH3})$^-$.

Chapter 7 details a general route for the preparation of redox-active amido-bis(phenolate) ligands, [ONO], with doubly substituted phosphonate diester substituents. Based on this route, two independent ONO-ligand derivatives are accessed with different solubility characteristics, which is attributed to the presence of bulky *tert*-butyl substituents at the 3-position of the aromatic rings or lack thereof.

Part 1: Chapter 1

Introduction to Donor-Acceptor Complexes of the Redox-Active Ligands

1.1 Redox-Active Ligands

Transition metal complexes with a "classical" redox behavior are defined by their ability to undergo oxidation or reduction at the metal center while maintaining the ligand oxidation states unaffected. In alternative cases, when the ligand may play a non-spectator role in the redox process, the pertinent coordination complexes are classified as ones having "redox-active" or "redox non-innocent" ligands.[1] While both classifications are frequently interchangeable, the former term, "redox-active", most commonly refers to a species that can exist in multiple oxidation states upon coordination to a metal (Figure 1.1). Furthermore, the prospective oxidation states of the redox-active species are rendered stable (isolable), reversible, and assignable. Conversely, the use of the term "redox non-innocence" is deemed appropriate whenever unambiguous assignments of the metal and ligand oxidation states cannot be made. The commonly witnessed occurence within the redox non-innocent situation is the close separation in energy between the metal and ligand valence electronic levels.[2] The close energy levels of the metal- and ligand-centered orbitals may in turn result in equilibria between different electronic and charge-based distributions of the same species (redox isomers), via an intramolecular electron transfer process described as valence tautomerism.
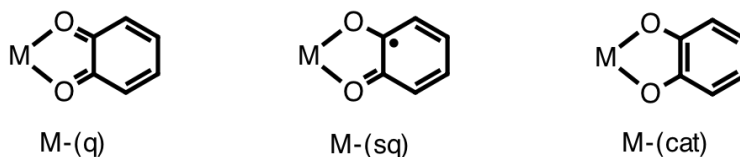
Figure 1.1. Redox-active metal-quinonoid chelates shown in three different charge-localized electronic forms: quinone (q), semiquinone (sq), and catecholate (cat) (where M is a transition metal ion).

Coordination complexes supported by the redox-active or non-innocent ligands are exemplified extensively in the literature with transition metals incorporating ligands of the dioxolene family. As summarized in Figure 1.1, three distinct oxidation states are accessible to the dioxolenyl ligand motif including the oxidized *ortho*-quinone (q), the singly-reduced semiquinone (sq), and the doubly-reduced catecholate (cat). Over the past decades, research strides involving metal-quinonoid systems have contributed to a deeper understanding of their unique valence, spin, and electron-transfer properties.[1,3] In particular, ruthenium-quinonoid systems have garnered continuous interest owing to their fundamental capacity to produce molecular frameworks with extensively delocalized metal- and ligand-based orbitals. Earlier studies were pioneered by Lever and coworkers and helped establish the delocalized bonding phenomena at the ruthenium-quinonoid interface.[4] Figure 1.2a depicts the prototypic bis-quinonoid complex of the formula bis(dioxolene)(bipyridine)ruthenium that presents inherent vulnerability in defining a precise electronic structure. Access to multiple oxidation states, with respect to ruthenium (+2, +3, +4) and the quinonoid ligands (q, sq, cat), and the strong orbital mixing together can create ambiguities in the oxidation-state assignments. In this regard, multiple electronic structures can be invoked, with two dominant resonance contributors shown as $(sq)_2(bpy)Ru^{II}$ and $(cat)(sq)(bpy)Ru^{III}$ (bpy = bipyridine), to describe the highly delocalized system of ruthenium.[4] The two postulated electronic descriptions share the same ground-state energy minimum and, thus, are related with resonance arrows. Conversely, the isostructural bis(dioxolene)(bipyridine) complex of cobalt exemplifies the archetypal situation of valence tautomeric behavior shown in Figure 1.2b.[5] The pertinent $(sq)_2(bpy)Co^{II}$ and $(cat)(sq)(bpy)Co^{III}$ structures make up a chemical equilibrium, rather

3

than two limiting descriptions of a delocalized system, wherein the two redox isomers possess distinct energy minima related by shifts in charge distribution through intramolecular charge-transfer (CT) processes.
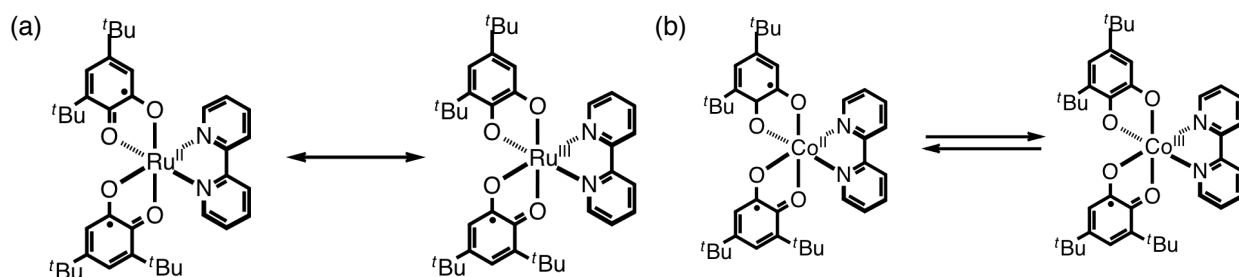
Figure 1.2. (a) Possible representation of electronic arrangements in a highly delocalized bis(dioxolene)(bipyridine) system of ruthenium, described as a sum of two limiting resonance structures. (b) Representation of a chemical equilibrium in the bis(dioxolene)(bipyridine) system of cobalt showing two redox isomers with different electronic properties.

Earlier studies of ruthenium- and cobalt-quinonoid complexes illuminated the inherent complexities in establishing precise valence state configurations within the metal-ligand framework. Building upon this insight, Lever's work proved instrumental in resolving some of the fundamental implications associated with incorporating more than one redox-active ligand into the same coordination complex. Much in the same way that the metal- and ligand-based orbital mixing leads to a combination of interactions based on ligand-to-metal donation (σ and π) and metal-to-ligand π-back-donation, the electronic interactions between a pair of redox-active ligands may be potentially coupled into a ligand(L)-to-ligand(L') donation (where L and L' represent an identical ligand set or two electronically distinct redox-active ligands). The extent of orbital mixing between the individual ligands is greatly dependent on the electronic nature of the species involved. For the quinonoid ligands of ruthenium(II) centers (where quinone = *ortho*-quinone, *ortho*-iminoquinone, and *ortho*-diiminoquinone), the degree of interligand orbital mixing was

demonstrated to be greatly perturbed by systematic substitutions of the ligand oxygen donor atoms with less electronegative nitrogen donor atoms.[6] On the basis of this study, it is now well-recognized that metal complexes with two electronically identical quinonates, but in two different oxidations states (cat and q), favor symmetric electronic configurations resulting in homoleptic diradical, bis(semiquinonate)-metal motifs (Figure 1.3a).[7] In contrast, for two electronically distinct ligands, where the oxygen atoms of one ligand are substituted for nitrogen groups, asymmetric electronic configurations[8] are rendered at the expense of significantly different electrochemical potentials: the difference in the ligand redox potentials encourages one ligand to adopt the reduced oxidation form (catecholate) while the other the oxidized form (*ortho*-diiminoquinone) (Figure 1.3b).

Fundamentally, the heteroleptic bis(quinonato)-metal frameworks with asymmetric electronic configurations can support ligand-to-ligand charge-transfer (LL'CT) photochemistry. The preponderance of LL'CT complexes with mixed redox-active ligands is well documented in the literature.[9] These complexes are uniquely poised to take part in photoinduced charge-transfer processes by leveraging the complementary redox properties of the two ligands: one ligand acts as an electron donor and the other as an electron acceptor. As shown in Figure 1.3c, the heteroleptic LL'CT complexes possess inherently photoactive frontier molecular orbitals localized mainly on the redox-active ligands themselves with the metal valence electronic levels displaced out of the FMO set. An attractive feature of the donor-acceptor configuration is the ease with which the HOMO and LUMO of the molecule can be independently tuned.
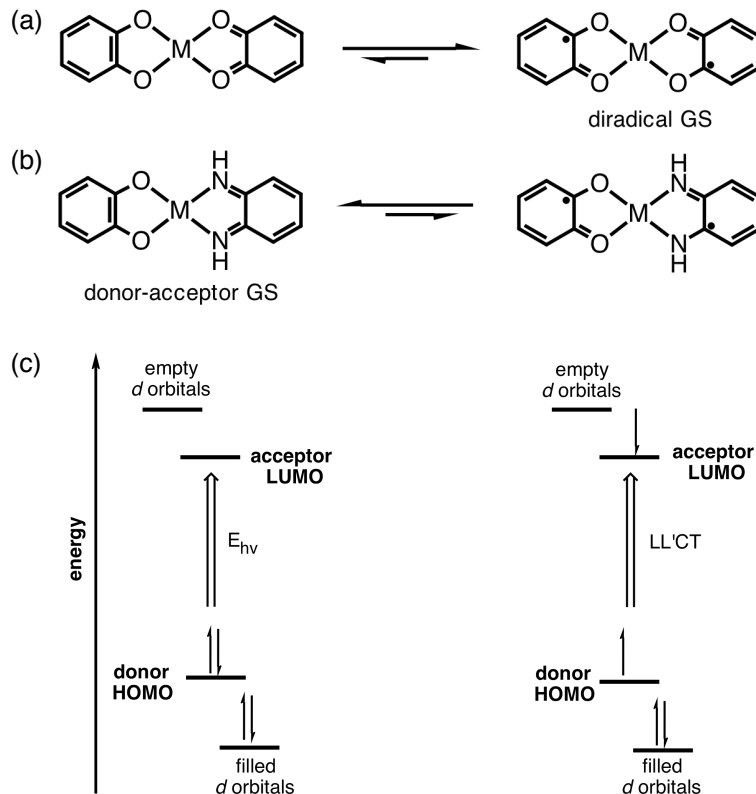
Figure 1.3. Representation of square-planar metal-quinonoid complexes containing (a) a symmetric ground-state (GS) electronic structure derived from the same redox-active ligands and (b) an asymmetric, GS structure derived from two electronically different redox-active ligands. (c) MO diagram for donor-acceptor complexes with the asymmetric electronic configuration (where M = Pt, Pd, or Ni). E_{hv} corresponds to the energy of the absorbed photon, which is equivalent to ligand-to-ligand charge-transfer (LL'CT).

1.2 Classical Ligand-to-Ligand Charge-Transfer Complexes

Classical LL'CT systems are exemplified by square-planar complexes of platinum with the formula (dithiolene)Pt(diimine). Over the past three decades, Eisenberg and coworkers systematically studied electrochemical and emissive behavior of the (dithiolene)Pt(diimine) complexes by varying the chemical substituents of the dithiolene and diimine ligands (Table 1.1). This study led to the observation that the excited-state energy can be tuned by up to 1 eV.[10] Apart from their large excited-state redox potentials, Eisenberg's complexes afford other interesting characteristics including long-lived solution

6

luminescence, solvatochromism, large molecular hyperpolarizabilities, and intense and

tunable absorption energies. With the exception of photoluminescence, most of the

aforementioned properties are also common to the (dithiolene)(diimine) complexes of

palladium and nickel[10] as well as their (catecholate)(diimine) counterparts[9] (in the donor-

acceptor systems other than platinum, the often non-emissive excited states are depleted

by non-radiative relaxation).

Table 1.1. Classical Donor-Acceptor LL'CT Complexes of the Formula (dithiolene)Pt(diimine).[a]
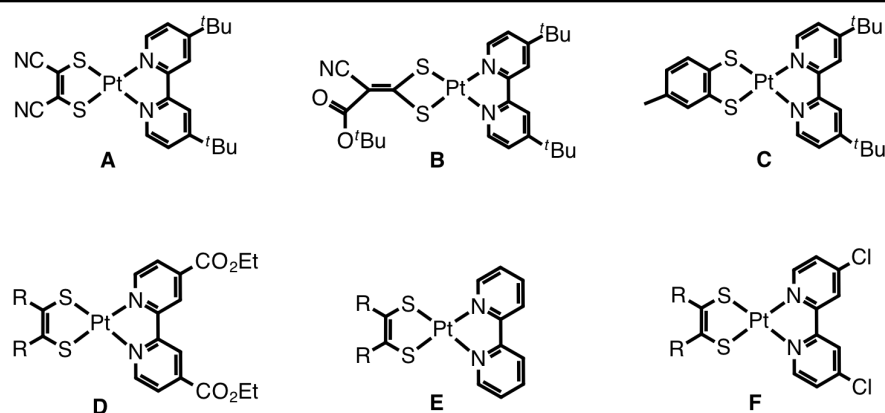
[a]R denotes commonly modified carbon substituents of the dithiolenyl ligand.

In general, the absorptive features of square-planar donor-acceptor complexes

exhibit a diagnostic LL'CT band in the visible or vis-NIR spectral range, which is conferred

by the transfer of an electron from the donor ligand to the acceptor ligand. The low-energy

LL'CT transition is both conveniently controlled by systematic variation of the individual

ligand components and highly directional in nature as a result of asymmetric electronic

configuration of the ground-state molecule. Collectively, the key features of the donor-

acceptor LL'CT complexes make them attractive candidates for elaboration into schemes

that target bimolecular photoinduced electron-transfer and energy-transfer processes.

Indeed, the donor-acceptor frameworks of group 10 metals have drawn increasing research

interest for use in solar energy conversion,[11] supramolecular assemblies,[12] photocatalysis,[13] nonlinear optics[14], and photonic molecular devices.[10a]

Despite their prominent role in various applications, classical LL'CT complexes possess inherent deficiencies with respect to their molecular structure, which can greatly impact the overall charge-transfer performance. Especially in those cases where molecular photosensitizers (dyes) are sought, the square-planar donor-acceptor complexes generally underform with respect to long-term dye stability and photocurrent quantum yields. While technically saturated, the four-coordinate environment of a d^8 metal complex introduces the proclivity toward ligand-exchange reactions. Even for chelating ligands such as the redox-active quinonoid derivatives, the exchange of ligands may be activated by exogenous coordinating species. As such, the redox-active chelates can be associatively displaced from the 16-electron complex, which will compromise charge transfer and the long-term stability of the molecule. Furthermore, the planar nature of the d^8-metal configuration may promote self-quenching reactions between the ground- and excited-state species,[15] via intermolecular $\pi-\pi$ stacking interactions of the metal-diimine motifs or via aggregation of flat-lying (collapsed) complexes on the electrode surface interface.[16] Both phenomena will potentially quench the directional charge transfer, through scrambling and thermal relaxation of charge carriers, and suppress bimolecular CT processes between the excited-state dye and the semiconducting electrode: this energy-conversion step is essential to realize photocurrent. The existing limitations associated with the square-planar framework may be potentially resolved by directing new research into alternative donor-acceptor LL'CT platforms.

1.3 Alternative Ligand-to-Ligand Charge-Transfer Complexes

   Though most developed with d^8 metal complexes of mixed redox-active ligands, the donor-acceptor LL'CT framework is not restricted to square-planar geometry of group 10 metals. Coordination complexes of octahedral d^6 metals that support LL'CT transitions are also known, albeit significantly less explored. For example, optical manifestations of interligand charge-transfer bands in the visible region were originally reported for Lever's bis(bipyridine)(catecholate) complexes of ruthenium (Figure 1.4a).[4c] Such transitions were characterized by ill-resolved and weakly intense absorptions, ascribed to a combination of poorly overlapped ligand-based orbitals and the significant reorganization energy that follows in response to the LL'CT photoexcitation of the ground-state complex. As shown in Figure 1.4a, the octahedral donor-acceptor system of ruthenium differs from the classical square-planar configuration in that the catecholate donor and bipyridine acceptor chelates adopt a non-coplanar arrangement to accommodate the six-coordinate environment of a d^6 metal center. The resulting arrangement imposes significant constraints on the directional probability of intramolecular electron transfer between the two weakly coupled redox-active ligands, both from a physical and electronic standpoint. Hence, the spectra of such complexes are typically dominated by alternative CT transitions and, in particular, the transition with metal-to-ligand charge-transfer (MLCT) is prominent due to the energetically favored coupling of the metal d orbitals and the low-lying π^* orbitals of bpy.[4] In this regard, the relative arrangement of the donor and acceptor ligands appears to influence the degree to which the LL'CT transition is accessible. Furthermore, access to the non-coplanar ligand arrangement hints at the synthetic implications associated with including two mixed redox-active ligands at coordinatively saturated metal centers.

Research interests into the donor-acceptor LL'CT platforms of coordinatively saturated rhodium centers have been on the rise in recent years. A novel bimetallic system of rhodium was reported recently by Turro and coworkers[17] wherein the role of the donor and acceptor components was fulfilled by formamidinate and dipyridoquinoxaline ligands, respectively (Figure 1.4b). The dirhodium species revealed a singlet excited state of LL'CT character that produced a low-energy electronic absorption band in the 500-600 nm range. Detailed investigation of the electronic structure and the photophysical properties of the bimetallic confirmed the ligand-centered nature of the charge-transfer transition with significant formamidinate- and diimine-ligand contributions to the HOMO and LUMO, respectively. However, the visible charge-transfer transition was rather weak (ε = 800-3000 $M^{-1}cm^{-1}$) with shoulder-like characteristics. Though not addressed directly by Turro, the weak intensity of the LL'CT transition is likely justifiable by the paddle-wheel-shaped framework of dimeric rhodium with bridging formamidinate donor ligands. As a result, the electronic communication required for directional charge transer may be weakened between the juxtaposed donor and acceptor ligands.
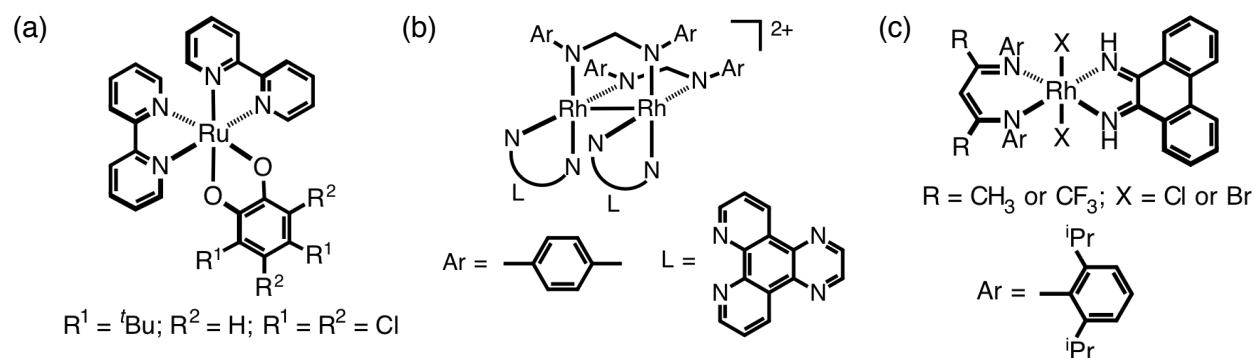
Figure 1.4. Octahedral LL'CT frameworks of the formulae (a) (bpy)$_2$Ru(cat) (where bpy = bypiridine; cat = 3,5-di-*tert*-butylcatecholate or tetrachlorocatecholate), (b) *cis*-[Rh$_2$(μ-DTolF)$_2$(L)$_2$]$^{2+}$ (where DTolF = *p*-ditolylformamidinate; L = dipyridoquinoxaline), and (c) (NacNac)RhX$_2$(phdi) (where NacNac = *β*-diimine; phdi =phenanthrene-9,10-diimine; X = Cl or Br).

10

Access to complementary donor-acceptor platforms of mononuclear rhodium was recently demonstrated in our own laboratory.[18] We reported the synthesis and characterization of (NacNac^R)RhX$_2$(phdi) complexes {NacNac^R = *N*,*N*-bis(2,6-diisopropylphenyl)pentane-2,4-diimine, *N*,*N*-bis(2,6-diisopropylphenyl)hexafluoropentane-2,4-diimine; phdi = phenanthrene-9,10-diimine; X = Cl or Br} where the pertinent ligand-to-ligand charge-transfer behavior was derivable through the coplanar juxtaposition of an oxidizable *β*-diimine donor ligand (NacNac) and a reducible *α*-diimine acceptor ligand (phdi) at the bridging Rh^{III} center (Figure 1.4c). The LL'CT transition of octahedral rhodium revealed increased sensitivity to the NacNac^R donor-ligand identity. Namely, systematic substitution of the NacNac ligand-backbone methyl groups with trifluoromethyl groups caused the respective LL'CT absorption bands to differ in energy by more than 3000 cm^{-1}. Furthermore, the same electronic transition yielded well-resolved absorption profiles with molar extinction coefficients of up to 4000 M^{-1} cm^{-1}, making it one of the first of its class to confer relatively strong and well-defined LL'CT characteristics on an octahedral metal center.

1.4 Contributions of This Dissertation

The premise of the initial three chapters of this work was tailored toward making strides in the area of new donor-acceptor LL'CT complexes of d^6 metals. The current chapter has provided background and motivation for pursuing coordinatively saturated donor-acceptor frameworks of mixed redox-active ligands. Chapter 2 details the synthesis and characterization of a series of octahedral rhodium complexes, inspired by the original (NacNac^R)RhX$_2$(phdi) platform, incorporating a "redox-uncertain" *β*-ketoaminato donor ligand and a bipyridine acceptor ligand. The chapter specifically addresses how

perturbations of the electronic structure associated with the new ligand scaffold may shut down interligand charge-transfer pathways on rhodium metal even when the critical coplanar arrangement of the donor-acceptor motif is preserved. Chapter 3 describes the synthesis and preliminary characterization of octahedral ruthenium centers supported by the redox-active catecholate donor and bipyridine acceptor ligands.

1.5 References

[1] (a) Kaim, W.; Schwederski, B. *Coord. Chem. Rev.* **2010**, *254*, 1580–1588. (b) Kaim, W. *Coord. Chem. Rev*. **1987**, *76*, 187–235.

[2] (a) Hendrickson, D. N.; Pierpont, C. G. *Top Curr Chem*. **2004**, *234*, 63–95. (b) Pierpont, C. G. *Coord. Chem. Rev*. **2001**, *216–217*, 99–125.

[3] Boyer, J. L.; Rochform, J.; Tsai, M-K.; Muckerman, J. T.; Fujita, E. *Coord. Chem. Rev*. **2010**, *254*, 309–330.

[4] (a) Gorelsky, S. I.; Lever. A. B. P.; Ebadi, M. *Coord. Chem. Rev*. **2002**, *97,* 97–105. (b) Lever, A. B. P.; Masui, H.; Metcalfe, R. A.; Stufkens, D. J.; Dodsworth, E. S.; Auburn, P. R. *Coord. Chem. Rev*. **1993**, *125*, 317–331 (c) Haga, M.-A.; Dodsworth, E. S.; Lever, A. B. P. *Inorg. Chem*. **1986**, *25*, 447–353.

[5] Buchanan, R. M.; Pierpont, C. G. *J. Am. Chem.* Soc. **1980**, *102*, 4951–4957.

[6] Masui, H.; Lever, A. B. P.; Auburn, P. R. *Inorg. Chem*. **1991**, *30*, 2402–2410.

[7] (a) Chaudhuri, P.; Verani, C. N.; Bill, E.; Bothe, E.; Weyhermüller, T.; Wieghardt, K. *J. Am. Chem. Soc*. **2001**, *123,* 2213–2223. (b) Herebian, D.; Bothe, E.; Bill, E.; Weyhermüller, T.; Wieghardt, K. *J. Am. Chem. Soc*. **2001**, *123*, 10012–10023. (c) Bachler, V.; Olbrich, G.; Neese, F.; Wieghardt, K. *Inorg. Chem*. **2002**, *41*, 4179–4193. (d) Herebian, D.; Bothe, E.; Neese, F.; Weyhermüller, T.; Wieghardt, K. *J. Am. Chem. Soc*. **2003**, *125*, 9116–9128. (e) Kokatam, S.; Weyhermüller, T.; Bothe, E.; Chaudhuri, P.; Wieghardt, K. *Inorg. Chem*. **2005**, *44*, 3709–3717 (f) Ray, K.; Weyhermuller, T.; Neese, F.; Wieghardt, K. *Inorg. Chem*. **2005**, *44*, 5345–5360.

[8] (a) Kramer, W. W.; Cameron, L. A.; Zarkesh, R. A.; Ziller, J. W.; Heyduk, A. F. *Inorg. Chem*. **2014**, *53*, 8825–8837. (b) Seraya, E.; Luan, Z.; Law, M.; Heyduk, A.F. *Inorg. Chem.* **2015**, *54*, 7571–7578 (c) Pevny, F.; Zabel, M.; Winter, R. F.; Rausch, A. F.; Yersin, H.; Tuczek, F.; Záliš, S. *Chem. Commun*. **2011**, *47*, 6302–6304. (d) J. A. Weinstein, J. A.; Tierney, M. T.; Davies, E. S.; Base, K.; Robeiro, A. A.; Grinstaff, M. W. *Inorg. Chem*. **2006**, *45*, 4544–4555. (e) Best, J.; Sazanovich, I. V.; Adams, H.; Bennett, R. D.; Davies, E. S.; Meijer, A. J. H. M.; Towrie, M.; Tikhomirov, S. A.; Bouganov, O. V.; Ward, M. D.; Weinstein, J. A. *Inorg. Chem*. **2010**, *49*, 10041–10056. (f) Anbalagan, V.; Srivastava, T. *Polyhedron* **2004**, *23*, 3173–3183.

9 (a) Hissler, M.; McGarrah, J. E.; Connick, W. B.; Geiger, D. K.; Cummings, S. D.; Eisenberg, R. *Coord. Chem. Rev.*, **2000**, 208, 115–137. (b) Zuleta, J. A.; Bevilacqua, J. M.; Rehm, J. M.; Eisenberg, R. *Inorg. Chem*. **1992**, *31*, 1332–1337. (c) Cummings, S. D.; Eisenberg, R. *J. Am. Chem. Soc.* **1996**, *118*, 1949–1960. (d) Paw, W.; Cummings, S. D.; Mansour, M. A.; Connick, W. B.; Geiger, D. K.; Eisenberg, R. *Coord. Chem. Rev.* **1998**, *171*, 125–150. (e) Connick, W. B.; Geiger, D.; Eisenberg, R. *Inorg. Chem.* **1999**, *38*, 3264–3265.

10 (a) Cocker, T. M.; Bachman, R. E. *Inorg. Chem*. **2001**, *40*, 1550–1556. (b) Chen, C.-T.; Liao, S.-Y.; Lin, K.-J.; Chen, C.-H.; Lin, T.-Y. J. *Inorg. Chem*. **1999**, *38*, 2734–2741. (c) Vogler, A.; Kunkely, H.; Hlavatsch, J.; Merz, A. *Inorg. Chem*. **1984**, *23*, 506–509. (d) Wootoon, J. L.; Zink, J. I. *J. Phys. Chem*. **1995**, *99*, 7251–7257.

11 (a) Linfoot, C. L.; Richardson, P.; McCall, K. L.; Durrant, J. R.; Morandeira, A.; Robertson, N. *Solar Energy* **2011**, *85*, 1195–1203. (b) Geary, E. A. M.; Yellowlees, L. J.; Jack, L. A.; Oswald, I. D. H.; Parsons, S.; Hirata, N.; Durrant, J. R.; Robertson, N. *Inorg. Chem*. **2005**, *44*, 242–250 (c) Islam, A.; Sugihara, H.; Hara, K.; Singh, L. P.; Katoh, R.; Yanagida, M.; Takahashi, Y.; Murata, S.; Arakawa, H.; Fujihashi, G. *Inorg. Chem*. **2001**, *40*, 5371–5380. (d) Diwan, K.; Chauhan, R.; Singh, S. K.; Singh, B.; Drew, M. G. B.; Bahadur, L.; Singh, N. *New J. Chem*. **2014**, *38*, 97–108. (e) Verma, S.; Kar, P.; Das, A.; Ghosh, H. N. *Chem. Eur. J.* **2011**, *17*, 1561–1568. (f) Archer, S.; Weinstein, J. A. *Coord. Chem. Rev*. **2012**, *256*, 2530–2561.

12 (a) Smucker, B. W.; Hudson, J. M.; Omary, M. A.; Dunbar, K. R. *Inorg. Chem*. **2003**, *42*, 4714–4723. (b) Honda, H.; Matsumoto, T.; Sakamoto, M.; Kobayashi, A.; Chang, H.-C.; Kato, M. *Inorg. Chem*. **2013**, *52*, 4324–4334.

13 (a) Zheng, B.; Sabatini, R. P.; Fu, W.-F.; Eum, M.-S.; Brennessel, W. W.; Wang, L.; McCamant, D. W.; Eisenberg, R. *Proc. Natl. Acad. Sci*. **2015**, *112*, E3987–E3996. (b) Zhang, D.; Bin, Y.; Tallorin, L.; Tse, F.; Hernandez, B.; Mathias, E. V.; Stewart, T.; Bau, R.; Selke, M. *Inorg. Chem*. **2013**, *52*, 1676–1678. (c) Zarkadoulas, A.; Koutsouri, E.; Mitsopoulou, C. A. *Coord. Chem. Rev*. **2012**, *256*, 2424–2434. (d) Zhang, J.; Du, P.; Schneider, J.; Jarosz, P.; Eisenberg, R. *J. Am. Chem. Soc.* **2007**, *129*, 7726–7727.

14 (a) Base, K.; Tierney, M. T.; Fort, A.; Muller, J.; Grinstaff, M. W. *Inorg. Chem*. **1999**, *38*, 287–289. (b) Pilia, L.; Pizzotti, M.; Tessore, F.; Robertson, N. *Inorg. Chem*. **2014**, *53*, 4517–4526.

15 Fleeman, W. L.; Connick, W. B. *Comments Inorg. Chem*. **2010**, *23*, 205–230.

16 (a) Connick, W. B.; Henling; L. M.; Marsh, R. E.; Gray, H. B. *Inorg. Chem.* **1996**, *35*, 6261–6265. (b) Houlding, V. H.; Miskowski, V. M. *Coord. Chem. Rev*. **1991**, *111*, 145–152.

17 Li, Z.; Leed, N. A.; Dickson-Karn, N. M.; Dunbar, K. R.; Turro, C. *Chem. Sci*. **2014**, *5*, 727–737.

18 Shaffer, D. W.; Ryken, S. A.; Zarkesh, R. A.; Heyduk, A. F. *Inorg. Chem*. **2012**, *51*, 12122–12131.

Chapter 2

Synthesis and Characterization of Rhodium(I) and Rhodium(III)

Complexes Supported by the "Redox-Uncertain" β-Ketoamine Ligand

2.1 Introduction

Photoredox-active ligands have garnered increasing attention recently in the field of electron-transfer photochemistry[1] and solar-energy conversion.[2] Chelating ligands of this class are prone to photoinduced oxidation-state changes, when coordinated on a metal ion, which allows the organic ligand to function either as an electron-donor equivalent or an electron-acceptor equivalent during charge transfer (Figure 2.1). Heteroleptic complexes of the photoredox-active ligands, containing electron-donor as well as electron-acceptor ligands, are well established in the literature for their unique charge-transfer (CT) properties.[3,4] Such complexes are characterized by inherently photoactive frontier molecular orbitals localized mainly on the redox-active ligands themselves; the degree of orbital mixing between the ligand-centered orbitals and the valence set of the metal d orbitals is generally negligible, though in some cases appreciable contributions from the metal d orbitals are also observed.[4h,4i] The resulting electronic configuration of the donor-acceptor complex leads to a lowest-energy electronic transition that is classified as either LL'CT (ligand-to-ligand charge-transfer) or MMLL'CT (mixed-metal-ligand-to-ligand charge-transfer). Furthermore, this transition is tunable across the visible to NIR region of the electromagnetic spectrum. The origin of the observed tunability is ascribed to the independent manipulations of the HOMO and LUMO, with the former orbital composed mainly of the donor ligand and the latter of the acceptor ligand. In addition to their tunable absorptions, the donor-acceptor charge-transfer complexes yield other interesting characteristics including tunable redox potentials, large excited-state energies, solvatochromism, and in certain cases long-lived solution luminescence.[3,4]
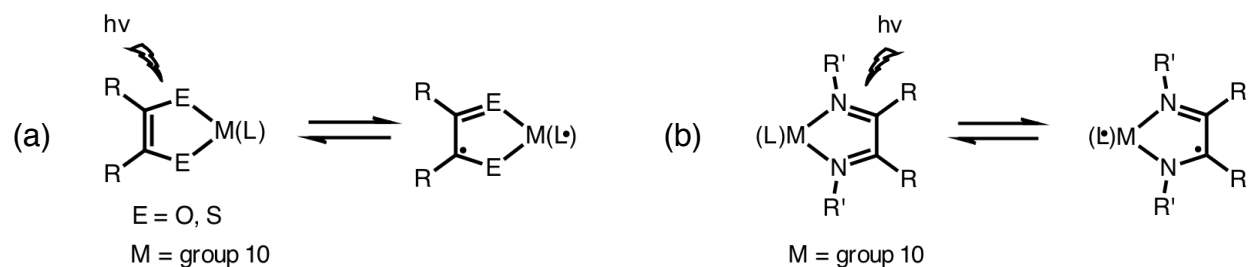
Figure 2.1. Photoredox-active ligand behavior of (a) quinonate or dithiolate donor ligands and (b) bipyridine acceptor ligands in the donor-acceptor charge-transfer complexes of group 10 metals. L represents a complementary photoredox-active ligand set for storing electrons and holes, respectively.

Neutral bipyridine ligands (bpy) are well documented for their role as reducible, electron-acceptor equivalents in the donor-acceptor charge-transfer complexes of group 10 metals[3,4] (Figure 2.1b) as well in the Ru-bpy metal-to-ligand charge-transfer (MLCT) congeners.[5] Dianionic quinonate and dithiolate ligands have in turn proven valuable as oxidizable, electron-donor equivalents in the same donor-acceptor complexes of group 10 metal ions (Figure 2.1a).[3,4] On the other hand, until recently monoanionic ligands of the β-ketonate family, such as 2,4-pentanedione (acetyacetonato, (acac)$^-$) and its Schiff-base derivatives (Figure 2.3), have been regarded as passive, redox innocent spectators to the electron-transfer processes of transition-metal coordination complexes. The redox innocent (acac)$^-$ ligand[6] and its Schiff-base counterparts, the β-ketoaminate ((acNac)$^-$) and the β-diketiminate ((NacNac)$^-$) ligands, enjoy vast applications as supporting ligands[7] in transition-metal and rare-earth coordination chemistry,[8,9] main-group chemistry,[10] polymerization,[11] and small-molecule activation chemistry.[12]

Recently, the involvement of β-diketiminate ligands in redox events has become increasingly documented with several metal and p-block coordination complexes supported by these ligands, providing new insights into their electronic and magnetic properties. Weighardt[13] and Itoh[14] independently demonstrated the ability of a closed-shell

16

(NacNac)⁻ ligand to undergo a one-electron oxidation when coordinated to Ni[II] ions, forming the neutral p radical form of the ligand, (NacNac)• (Figure 2.2). The same ligand electronic configuration was also described by Nocera and coworkers[15] for the bis(β-diketiminato) system of Co[II]. Likewise, our group previously reported on the photo-oxidative behavior of the β-diketiminate ligands in the context of donor-acceptor charge-transfer complexes of octahedral Rh[III] centers.[16] Complementary redox properties of the (NacNac)⁻ ligand were also discovered recently with coordination complexes of aluminum[17] and ytterbium[18] whose electronic structures were described on the basis of one- and/or two-electron reduced forms of the ligand.
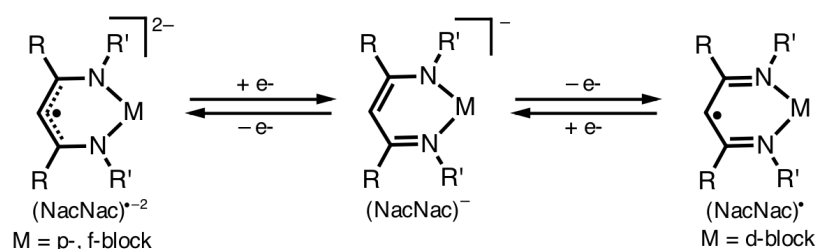
Figure 2.2. Possible oxidation states of a generic monoanionic (NacNac)⁻ ligand with commonly modified carbon positions labeled as R and R′.

While compelling evidence is beginning to emerge that β-diketimines are not completely redox-innocent ligands, the analogous redox chemistry of the β-ketoaminato ligand scaffold remains unexplored. The β-ketoamine ligand, (acNac)⁻, is an isoelectronic monoanion of the NacNac-ligand platform that contains two different donor atoms: the oxygen atom is a hard donor able to stabilize metals in higher oxidation states whereas the nitrogen atom, although still classified as a hard donor, is more suited to stabilize the high and low oxidation-state metal centers (Figure 2.3). Though the non-innocent electronic behavior of the (acNac)⁻ ligand is unprecedented, theoretically both of its donor atoms could help support a high-valent metal center with redox-stable nonbonding orbitals, such

as the t_{2g} orbital set of a d^6 metal ion, to facilitate oxidation of the ligand selectively over the metal. Fundamentally, the ligand-centered oxidation event demands that the removal of an electron from the valence shell of the acNac-based orbital is an energetically permitted process.
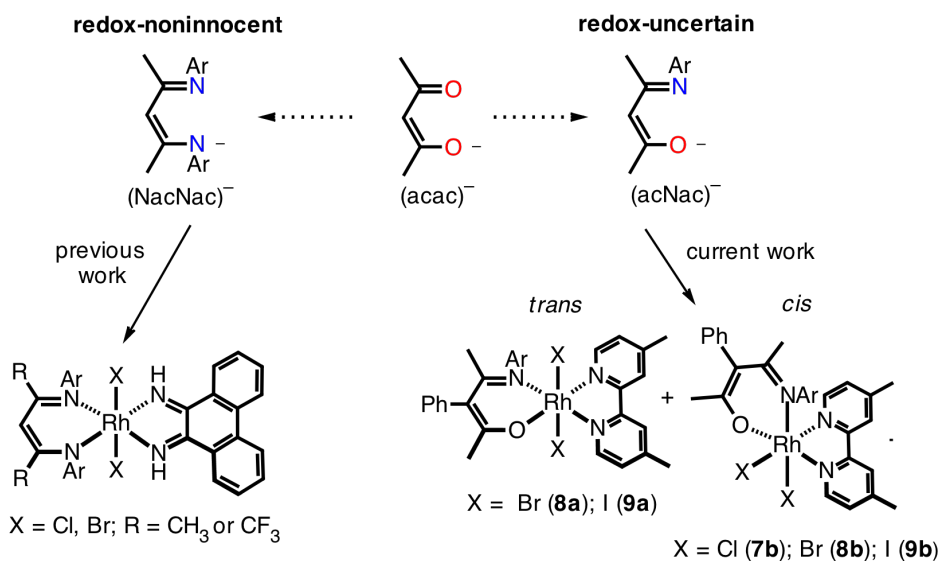
Figure 2.3. General chemical structures of monoanionic ligands of the β-ketonate family (top); Ar represents commonly modified aromatic rings. Rhodium charge-transfer complexes coordinated by established (NacNac^R)$^-$ ligands (bottom left) and the new (acNac^{Ph})$^-$ ligand (bottom right).

Access to the ligand-centered oxidation of the β-diketimine ligands, containing two nitrogen donor atoms, was previously demonstrated in our laboratory[16] with complexes of octahedral Rh^{III} centers (Figure 2.3). The pertinent complexes showed ligand-to-ligand charge-transfer (LL'CT) behavior owing to the juxtaposition of an oxidizable, β-diiminyl donor ligand (*N,N*-bis(aryl)pentane-2,4-diimine, (NacNac)$^-$) and a reducible, α-diiminyl acceptor ligand (phenanthrene-9,10-diimine, (phdi)) at the bridging rhodium ion. Namely, the LL'CT transitions of the donor-acceptor Rh^{III} complexes revealed a profound dependence on the electronic identity of the (NacNac^R)$^-$ donor whereby substitution of the ligand-backbone methyl groups with trifluoromethyl groups caused the absorption

18

energies of the respective complexes to differ by more than 200 nm. Motivated by our earlier work, we set out to probe the analogous interligand charge-transfer events with the "redox-uncertain" (acNac)$^-$ ligand coordinated on octahedral Rh^{III} centers of the general formulation [(acNac^{Ph})Rh(dmbpy)]X$_2$ (acNac^{Ph} = 4-(3,5-dimethylphenylamino)-3-phenyl-pent-3-en-2-one; dmbpy = 4,4-dimethyl-2,2-bipyridine; X$_2$ = *cis*-Cl$_2$, **7b**; *trans*-Br$_2$, **8a**; *cis*-Br$_2$, **8b**; *trans*-I$_2$, **9a**; *cis*-I$_2$, **9b**). The new (acNac^{Ph})$^-$ ligand was synthesized and coordinated on rhodium to establish its redox proclivity toward oxidation and assess the electronic influence of the ligand donor atoms (the N to O substitution) on the energy of the prospective LL'CT absorption. Here we demonstrate that the (acNac^{Ph})$^-$ monoanion behaves predominantly as a classical auxiliary ligand on Rh^{III} centers, albeit with a very subtle proclivity toward redox non-innocence.

2.2 Results and Discussion

2.2.1 Synthesis and Characterization of the *β*-Ketoamine Ligand

To examine the prospective viability of the *β*-ketoaminato motif as a redox-active donor ligand, the new proligand (acNac^{Ph})H (**3**) was accessed by a two-step strategy (Scheme 2.1). Ullman condensation of iodobenzene with 2,4-pentanedione under catalysis of CuI/L-proline afforded *α*-phenylacetylacetone, (acac^{Ph})H (**2**). In the next step, an aryl-protected nitrogen group was introduced on (acac^{Ph})H by an acid-catalyzed Schiff-base condensation with 3,5-dimethylaniline. Employment of excess amine was deemed necessary to drive the reaction to completion for the mono-Schiff base ligand (**3**). Interestingly, the addition of excess amine did not proceed to give the di-Schiff base product (NacNac^{Ph})H. In stark contrast, the analogous di-Schiff base (NacNac^{CH3})H is readily obtainable by the condensation of the parent 2,4-pentanedione with excess 3,5-

dimethylaniline.[19] Hence, the lack of the doubly condensed product suggests that the remaining keto group of (acNac^{Ph})H may be sterically and/or electronically deactivated from the introduction of an aromatic ring within the ligand backbone.

Scheme 2.1. Synthesis of (acNac^{Ph})H proligand (**3**).
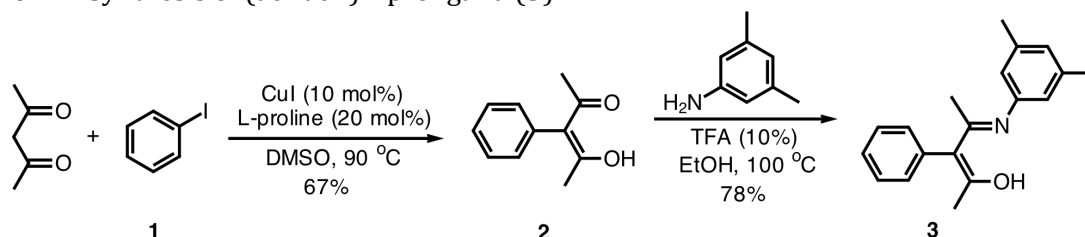
2.2.2 Synthesis, Characterization, and Reactivity of (acNac^{Ph})Rh(CO)$_2$

The installation of (acNac^{Ph})$^-$ onto rhodium was achieved by reaction of (acNac^{Ph})K with rhodium carbonyl chloride ([RhCl(CO)$_2$]$_2$) (Scheme 2.2). Treatment of (acNac^{Ph})H (**3**) with 1 equivalent of KH, at −78 °C in diethyl ether, formed a homogeneous solution of the ligand potassium salt. The addition of 0.5 equivalents of solid-red [RhCl(CO)$_2$]$_2$ dimer to the yellow suspension of (acNac^{Ph})K resulted in the precipitation of KCl. After stirring overnight at room temperature, (acNac^{Ph})Rh(CO)$_2$ (**4a**) was isolated as a yellow solid.

The ^{1}H NMR spectrum of **4a** in CDCl$_3$ displayed two chemically distinguishable methyl group resonances at 1.84 and 1.49 ppm, assignable to the keto- and amine-CH$_3$ groups, respectively. In the ^{13}C NMR spectrum of the complex, the same CH$_3$ resonances were evident at 27.4 ppm (keto) and 23.0 ppm (amine). In further support of C$_s$-symmetric structure, the ^{13}C NMR spectrum showed two distinguishable carbonyl signals at 185.8 ppm (d, J = 65.9 Hz) and 184.3 ppm (d, J = 72.6 Hz), with each carbon resonance split into a doublet due to coupling to monoisotopic nucleus of ^{103}Rh. The IR spectrum of the yellow solid of (acNac^{Ph})Rh(CO)$_2$ revealed two strong C≡O stretching vibrations at 2060 and 1986

cm^{-1}. The UV-vis spectrum of **4a** in THF showed a near-UV absorption band at 380 nm (ε = 12,000 M^{-1}cm^{-1}) (Figure 2.5).

Scheme 2.2. Preparation of (acNac^{Ph})Rh(CO)$_2$ (**4a**), (acNac^{Ph})Rh(CO)NMe$_3$ (**4b**), and (acNac^{Ph})Rh(CO)py (**4c**) from rhodium carbonyl chloride.
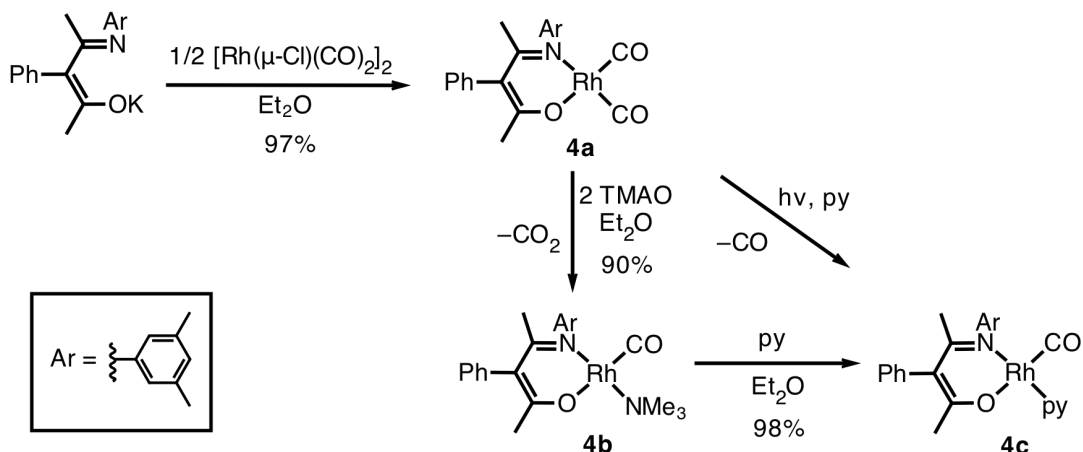
The new rhodium dicarbonyl complex, (acNac^{Ph})Rh(CO)$_2$ (**4a**), was subjected to oxidative decarbonylation with trimethylamine *N*-oxide (TMAO) in order to effect installation of the diimine acceptor ligand onto rhodium. The attempted strategy sought to replace the CO ligands from (acNac^{Ph})Rh(CO)$_2$ in the presence of 1 equivalent of 4,4-dimethyl-2,2-bipyridine (dmbpy) to yield (acNac^{Ph})Rh(dmbpy) (**6**), which could be used as synthon for new octahedral Rh complexes of the (acNac^{Ph})$^-$ ligand. However, all attempts to exchange the CO ligands of **4a** for dmbpy, using TMAO, gave rise to a new rhodium species of the formula (acNac^{Ph})Rh(CO)NMe$_3$ (**4b**). To aid in characterization of the new product, the CO-labilization reaction was performed in the absence of dmbpy, by addition of 2 equivalents of TMAO to a yellow diethyl ether solution of (acNac^{Ph})Rh(CO)$_2$, as shown in Scheme 2.2. After stirring overnight at room temperature, unreacted TMAO was separated by filtration and the new product, (acNac^{Ph})Rh(CO)NMe$_3$, was isolated as an orange solid.

The identity of (acNac^Ph)Rh(CO)NMe₃ (**4b**) was verifiable by spectroscopic means. In contrast to its parent precursor, (acNac^Ph)Rh(CO)₂, the ^{1}H NMR spectrum of (acNac^Ph)Rh(CO)NMe₃ in CDCl₃ showed a new signal at 2.68 ppm, displaying a singlet resonance which in-total integrates for nine protons of the NMe₃ group. The ^{13}C NMR spectrum of the complex revealed the presence of a new signal at 55.3 ppm, once again ascribable to the CH₃ groups of the tertiary amine. In the same spectrum, a single carbonyl-centered doublet was also evidenced at 191.3 ppm with a *J* coupling constant of 83.0 Hz. The IR spectrum of (acNac^Ph)Rh(CO)NMe₃ displayed a single strong absorption in the C≡O stretching region at 1942 cm^{-1}. On the basis of this analysis, the use of an exogenous oxidant (TMAO) was shown to effect the displacement of one but not both of the CO ligands from (acNac^Ph)Rh(CO)₂, which proceeds with a concomitant association of trimethylamine ligand, the byproduct of CO oxidation.
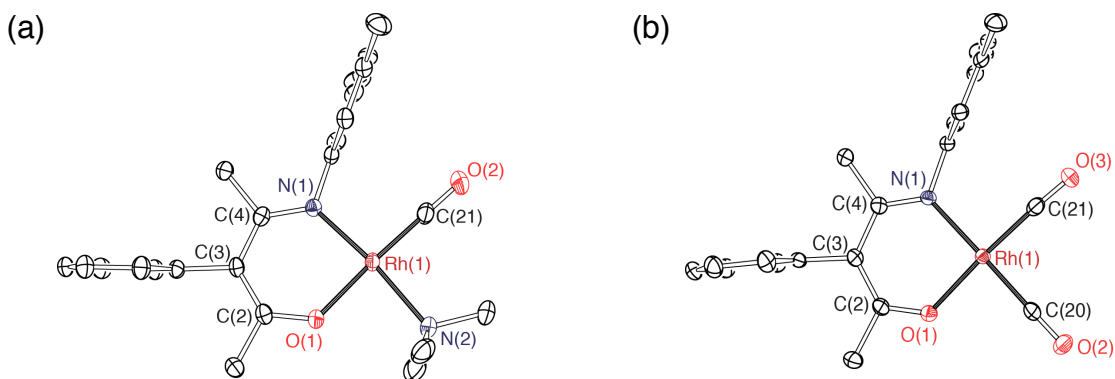
Figure 2.4. ORTEP diagrams of (a) (acNac^Ph)Rh(CO)NMe₃ (**4b**) and (b) (acNac^Ph)Rh(CO)₂ (**4a**). Ellipsoids are shown at 50% probability. Hydrogen atoms and solvent molecules have been omitted for clarity.

To further elucidate the electronic influence of coordinated (acNac^Ph)⁻ on the ligand-exchange reactivity at rhodium, single crystals of (acNac^Ph)Rh(CO)₂ (**4a**) and (acNac^Ph)Rh(CO)NMe₃ (**4b**) suitable for X-ray structural analysis were obtained by liquid-liquid diffusion methods. The ORTEP diagrams of **4a** and **4b** are shown in Figure 2.4 with

selected bond distances summarized in Table 2.1. The metal center of (acNac^{Ph})Rh(CO)NMe$_3$ exhibits a square-planar geometry pertaining to the N,O donor set of (acNac^{Ph})$^-$, the N-donor atom of the NMe$_3$ group, and the C atom of the CO ligand. In the same complex the most significant structural feature is the *trans* relationship between the nitrogen donor atom of (acNac^{Ph})$^-$ and the nitrogen donor atom of trimethylamine, with the pertinent N(2)-Rh(1)-N(1) angle equivalent to 173.43°(6). The Rh–N bond lengths are 2.0238(15) and 2.1433(16) Å for Rh(1)-N(1) and Rh(1)-N(2), respectively. The remaining bond lengths within the rhodium square plane are 2.0089(13) Å for Rh(1)-O(1) and 1.807(2) Å for Rh(1)-C(21).

The metric parameters of (acNac^{Ph})Rh(CO)NMe$_3$ (**4b**) compared well to those of (acNac^{Ph})Rh(CO)$_2$ (**4a**). As shown in Figure 2.4, the rhodium atom of **4a** is located in the center of a square-planar arrangement with the carbonyl ligand *trans*-disposed to the (acNac^{Ph})$^-$ fragment. The Rh(1)-N(1) distance of 2.0515(17) Å and the Rh(1)-O(1) distance of 2.0097(15) Å correspond to the (acNac^{Ph})$^-$ donor-atom distances and closely match those described for (acNac^{Ph})Rh(CO)NMe$_3$ (**4b**). For the same (acNac^{Ph})Rh(CO)$_2$ complex, the Rh(1)-C(20) bond length of 1.870(2) Å is slightly longer than the Rh(1)-C(21) bond length of 1.844(2) Å. Close examination of the C–O bond lengths of **4a** revealed a slight elongation of the C(21)-O(3) distance (1.142(3) Å) as compared to the C(20)-O(2) distance (1.135(3) Å), where the former occupies a *trans* position to the oxygen atom and the latter a *trans* position to the nitrogen atom of (acNac^{Ph})$^-$. Hence, the C–O distance *trans* to the nitrogen donor is closer to the value for free CO (1.128 Å),[20] which suggests weakened bonding with rhodium relative to the second CO ligand (*trans*-disposed to the oxygen donor of (acNac^{Ph})$^-$). Following loss of the CO ligand in the *trans* to N position, the remaining CO

ligand becomes even harder to displace from the more electron-rich rhodium center of (acNac^{Ph})Rh(CO)NMe$_3$ (**4b**). Relative to (acNac^{Ph})Rh(CO)$_2$ (**4a**), the metal-carbonyl interaction for **4b** shows a significant decrease in the Rh(1)-C(21) bond distance (1.807(2) Å) and increase in the C(21)-O(2) bond distance (1.156(2)Å) due to strong π back-donation.

Table 2.1. Selected Metrical Parameters for the Solid-State Structures of (acNac^{Ph})Rh(CO)$_2$ (**4a**) and (acNac^{Ph})Rh(CO)NMe$_3$ (**4b**).

Bond (Å) / Angle (deg)	**4a**	**4b**
Rh(1)-N(1)	2.0515(17)	2.0238(15)
Rh(1)-O(1)	2.0097(15)	2.0089(13)
O(1)-C(2)	1.285(3)	1.296(2)
C(1)-C(2)	1.514(3)	1.513(3)
C(2)-C(3)	1.393(3)	1.381(3)
C(3)-C(4)	1.432(3)	1.435(2)
C(4)-C(5)	1.509(3)	1.517(3)
N(1)-C(4)	1.325(3)	1.321(2)
Rh(1)-C(21)	1.844(2)	1.807(2)
Rh(1)-C(20)	1.870(2)	––
Rh(1)-N(2)	––	2.1433(16)
O(2)-C(20)	1.135(3)	––
O(3)-C(21)	1.142(3)	––
O(2)-C(21)	––	1.156(2)
O(1)-Rh(1)-N(1)	88.92(7)	89.32(6)
C(21)-Rh(1)-C(20)	86.94(9)	––
N(2)-Rh(1)-C(21)	––	92.45(8)
N(2)-Rh(1)-N(1)	––	173.43(6)

In sum, the electronic asymmetry of coordinated (acNac^{Ph})$^-$ ligand for complex **4a** produced *trans* directing influence associated with the ligand imido group as compared to the enolate oxygen group. Of the two available heteroatoms, the imido nitrogen is the stronger σ-donor and stronger π-acceptor ligand on rhodium. The former property manifests in the ground-state structure through the weakened metal-carbonyl bond in the *trans* to *N* position whereas the latter manifests physically by promoting the rate of CO ligand substitution derived from the same position (*trans* effect) on oxidation of **4a** with

TMAO. The product Rh–C and C–O bond distances for $(acNac^{Ph})Rh(CO)NMe_3$ (**4b**) were in support of enhanced orbital mixing between the Rh^I metal ion and the remaining carbonyl ligand (the n_{CO} to d_{Rh} and d_{Rh} to π^*_{CO} donations). As such, the resulting stability of the metal-carbonyl interaction must contribute to the seen lack of CO_2 liberation from complex **4b**.
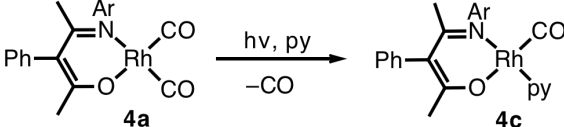
2.2.3 Photochemical Reactivity of $(acNac^{Ph})Rh(CO)_2$

The electronic structure of the $(acNac^{Ph})^-$ ligand had an impeding synthetic consequence with respect to the installation of the dmbpy ligand onto $(acNac^{Ph})Rh(CO)_2$ **4a**. To address the partial CO displacement, ultraviolet photolysis of **4a** was pursued using a Rayonet photochemical reactor and independently a Hanovia, 450-watt mercury vapor lamp (Scheme 2.2). Photochemical experiments were carried out in stoppered quartz cuvettes at a wavelength range controlled with long-pass filters (> 295 nm and > 395 nm). To aid in identification of photo-intermediates, all experiments were performed in the presence of excess pyridine, used as a ligand to stabilize the metal center upon loss of CO_2. The expected, singly photolyzed species $(acNac^{Ph})Rh(CO)py$ (**4c**) was independently prepared by chemical exchange of the NMe_3 with pyridine, according to Scheme 2.2. Compound **4c** was tested in a manner identical to that of $(acNac^{Ph})Rh(CO)_2$. In a typical experiment, a 2.2-2.3 mM solution of either complex, in benzene:pyridine (9:1), was subjected to a 6-hour irradiation with UV light. The progress of photolysis was examined by ^{1}H-NMR spectroscopy of crude samples in C_6D_6.

The results of photochemical CO displacement are summarized in Table 2.2. In general, incomplete photolytic conversion of $(acNac^{Ph})Rh(CO)_2$ (**4a**) to $(acNac^{Ph})Rh(CO)py$ (**4c**) was observed on irradiation of **4a** with UV light in all attempted cases, albeit with a slightly higher conversion ratio when photolyzed with the 295-nm filter, as compared to the

395-nm filter. Under the same conditions, the UV-light irradiation of $(acNac^{Ph})Rh(CO)py$

(4c) indicated no signs of photolytic CO cleavage to give $(acNac^{Ph})Rh(py)_2$, as confirmed by

^{1}H NMR spectroscopy. These results revealed that liberation of the second CO ligand does

not proceed, from either $(acNac^{Ph})Rh(CO)_2$ **(4a)** or $(acNac^{Ph})Rh(CO)py$ **(4c)**, which is once

again ascribable to the hindering *trans*-effect of the $(acNac^{Ph})$-ligand asymmetry.

Table 2.2. Photochemical Cleavage of CO Ligands from $(acNac^{Ph})Rh(CO)_2$ **(4a)**.[a]

entry	λ_{photo} (nm)	conversion (4c:4a)[d]
1	> 395[b]	1:8.5
2	> 295[b]	1:3.2
3	254[b]	1:4.7
4	> 395[c]	1:5.0
5	> 295[c]	1:4.5

[a]General conditions: 13 μmol of **4a**, 5 mL of benzene, 6.5 mmol of pyridine, irradiated at given wavelengths at room temperature for 6 hours. [b]Photolysis carried out with a Rayonet photochemical reactor. [c]Photolysis carried with a Hanovia mercury vapor lamp. [d]The product ratio estimated by integration of the ^{1}H NMR signals assignable to the keto-methyl groups of **4c** and **4a**.

2.2.4 Synthesis and Characterization of $(acNac^{Ph})Rh(dmbpy)$

The new $(acNac^{Ph})Rh(CO)_2$ species, supported by the asymmetric β-ketoaminato

ligand, proved largely recalcitrant toward formation of square-planar $(acNac^{Ph})Rh(dmbpy)$

complex. As such, a CO-free rhodium complex of the $(acNac^{Ph})^-$ ligand was independently

prepared for use as synthon. As shown in Scheme 2.3, the installation of $(acNac^{Ph})^-$ onto

rhodium was achieved by addition of 0.5 equivalents of orange $[RhCl(coe)_2]_2$ dimer (coe =

cyclooctene) to a diethyl ether suspension K($acNac^{Ph}$). After stirring overnight at room

temperature, KCl was separated by filtration and the solvent was removed to yield

$(acNac^{Ph})Rh(coe)_2$ **(5)** as a brown solid. The exchange of alkene ligands from square-planar

Rh^I centers is known to require high reaction temperatures.[21] Therefore, installation of 4,4-dimethyl-2,2-bipyridine on $(acNac^{Ph})Rh(coe)_2$ was realized by heating an equimolar diethyl ether solution of the two species at 120 °C, under airtight conditions. The new dark-green product, $(acNac^{Ph})Rh(dmbpy)$ (**6**), was isolated by cooling the saturated, diethyl ether reaction mixture of **6** to −35 °C.

Scheme 2.3. Synthesis of $(acNac^{Ph})Rh(dmbpy)$ (**6**).
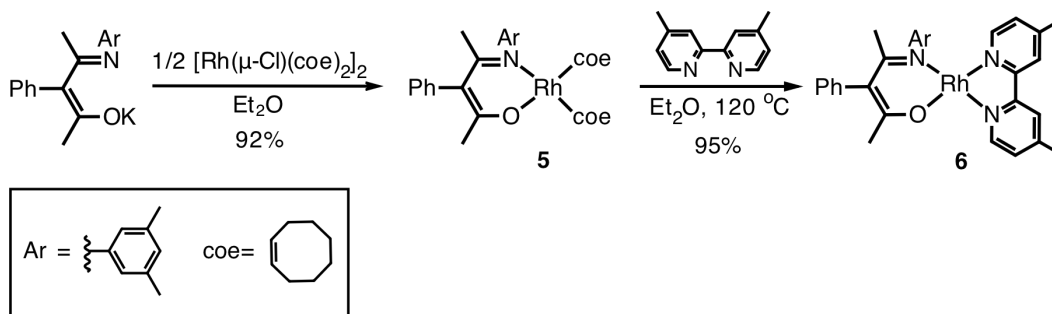
The structural identity of $(acNac^{Ph})Rh(dmbpy)$ was verifiable on the basis of NMR spectroscopy and is in agreement with square-planar geometry of a d^8 rhodium center of the complex. The ^1H NMR spectrum of **6** in C_6D_6 is dominated by five sets of methyl-group resonances in different chemical environments. The signals assignable to the CH_3 groups of the acNac-ligand backbone displayed two singlet resonances centered at 2.16 ppm (keto) and 1.71 ppm (amine). For the same ligand, the CH_3 substituents of the *N*-3,5-dimethylphenyl ring were found in the same environment, defined by a singlet resonance at 2.11 ppm (integration of 6H). The remaining two CH_3 signals assignable to the dmbpy-ligand backbone displayed individual resonances centered at 1.50 and 1.40 ppm. Further evidence of C_s-symmetric conformation was inferred from the split ^{13}C NMR signals associated with the $(acNac^{Ph})^-$ ligand and the bipyridine ligand core.

The optical characteristics of dark-green (acNac^{Ph})Rh(dmbpy) (**6**) were elucidated in solution. Figure 2.5 shows the UV-vis-NIR absorption spectrum of **6** recorded in THF at 298K. The UV-vis region of the electromagnetic spectrum is dominated by a strong absorption at 417 nm (ε = 7298 M^{-1}cm^{-1}), which is accompanied by a less intense absorption band in the lower-energy visible region (647 nm, ε = 4250 M^{-1}cm^{-1}). A distinct shoulder is also observed near the edge of the second absorption band, between 700 and 900 nm. The visible-energy transition at 647 nm and its closely associated shoulder at 750 nm are most likely derived from the molecular orbitals based predominantly on rhodium and the dmbpy ligand. The absence of analogous transitions in the electronic spectrum of (acNac^{Ph})Rh(CO)$_2$ further supports this contention (Figure 2.5).
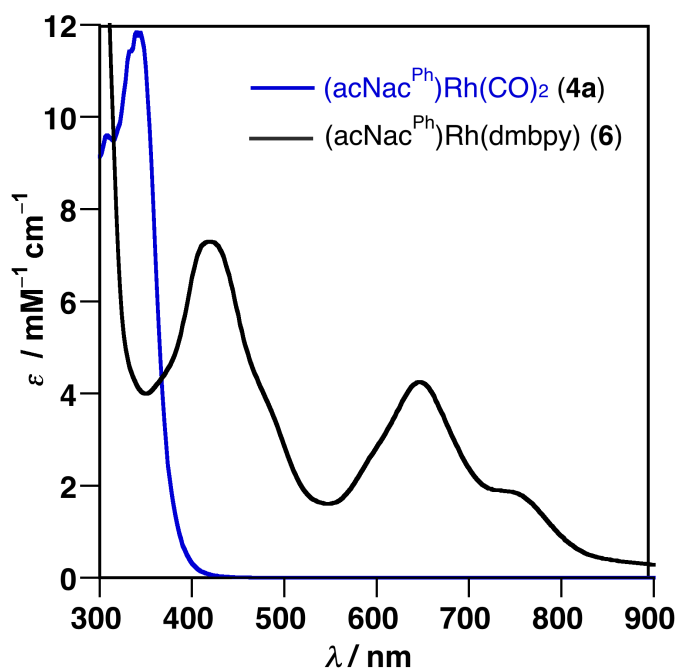
Figure 2.5. UV-vis-NIR absorption spectra of (acNac^{Ph})Rh(dmbpy) (**6**) and (acNac^{Ph})Rh(CO)$_2$ (**4a**).

Electrochemical analysis of (acNac^{Ph})Rh(dmbpy) (**6**) in solution revealed several redox processes within the solvent potential window. Figure 2.6 displays the cyclic voltammogram of **6** collected in THF using a glassy carbon disk electrode and 0.1 M

[^{n}Bu$_4$N][PF$_6$] as the supporting electrolyte. Complex **6** shows two well-behaved, one-electron reductions at –2.36 and –1.99 V (in reference to the Cp$_2$Fe$^{+/0}$ couple) and an irreversible oxidation at –0.27 V. The cathodic events are most likely dmbpy-centered in nature, which is consistent with formation of the singly-reduced (dmbpy$^{\bullet-}$) and the doubly-reduced (dmbpy^{2-}) redox states of the ligand. Furthermore, the respective values of –1.99 V and –2.36 V fall within the range reported for known bipyridine complexes of group 9 metals characterized by diimine-centered reductions.[22] The irreversible anodic event around –0.27 V may be due to oxidation of rhodium or the (acNac^{Ph})$^-$ ligand.
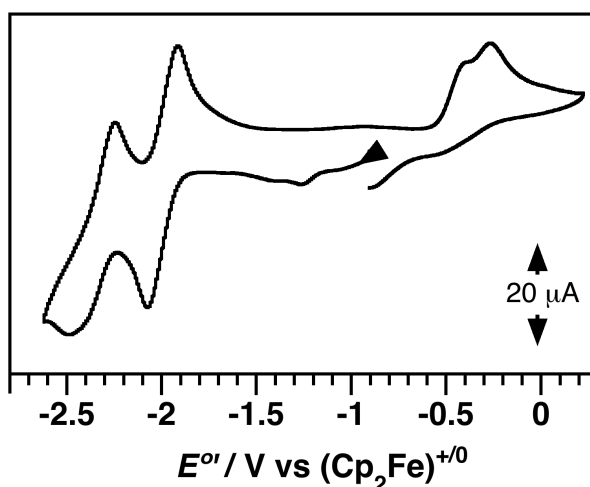
Figure 2.6. Cyclic voltammogram of (acNac^{Ph})Rh(dmbpy) (**6**). Measurements were made at a scan rate of 200 mV/s in THF with 1.0 mM analyte and 0.10 M [^{n}Bu$_4$N][PF$_6$]. Potentials referenced to Cp$_2$Fe$^{+/0}$ couple.

2.2.5 Oxidative Behavior of (acNac^{Ph})Rh(dmbpy)

The new (acNac^{Ph})Rh(dmbpy) complex (**6**) was probed as synthon for deriving octahedral donor-acceptor counterparts of the formula [(acNac^{Ph})Rh(dmbpy)]X$_2$ (where X = Cl, Br, or I). To this end, oxidative addition of halogens to the square-planar rhodium center of **6** was examined with a variety of oxidants including iodobenzene dichloride (PhICl$_2$), as an easy-to-handle Cl$_2$ surrogate, as well as with elemental bromine (Br$_2$) and iodine (I$_2$).

The details of oxidation are summarized in Table 2.3 In general, oxidative addition of halogens was found to give access to both *trans* and *cis* dihalo adducts of rhodium with the formulae $(acNac^{Ph})RhX_2(dmbpy)$ and $X_2\text{-}(acNac^{Ph})Rh(dmbpy)$, respectively. While both types of products were observed from the addition of $PhICl_2$ to **6**, the *cis* isomer was favored at elevated temperature, in benzene, while the *trans* isomer was slightly favored at room temperature in ethereal solvents. (Table 2.3, entries 1-5). Likewise, a mixture of both stereoisomers was identifiable from the room-temperature addition of Br_2 to **6** in diethyl ether, albeit with an opposite stereochemical outcome: the *trans*:*cis* ratio of the rhodium dibromide adducts was 4:1/**8a**:**8b** whereas the respective ratio of the rhodium dichloride adducts was 1:1.5/**7a**:**7b** (Table 2.3, entries 4, 6). Furthermore, the room-temperature oxidative addition with I_2 favored the *trans* stereoisomer (**9a**) as the sole product (Table 2.3, entry 7). We had also performed thermal equilibration experiments with isolated *trans* species of rhodium **8a** and **9a**, scaled for NMR spectroscopic analysis in $CDCl_3$, which revealed a very sluggish isomerization to the respective *cis* product counterparts after several days of heating at 180 °C (not shown). The two-electron oxidation of $(acNac^{Ph})Rh(dmbpy)$ was additionally examined with silver(I) salts of type AgX, where X is Cl^-, Br^-, or I^- (Table 2.3, entries 8-10). In contrast to the halogen oxidation, the same stereoselective outcome prevailed with silver, in all cases yielding the *cis* dihalo adducts from **6**.

Based on the observed reactivity of dihalogens with $(acNac^{Ph})Rh(dmbpy)$ (**6**), the formation of the *cis* product may be explained by a *trans-cis* isomerization of the *trans*-isomer counterpart, access to which is in turn favored by heterolytic bond cleavage. It is generally accepted that X–X bonds are activated heterolytically, in an S_N2-type process, at

30

square-planar, late d^8 transition metals. The heterolytic bond cleavage yields the *trans* isomer and shows sensitivity to solvents.[23] We examined the effect of solvent polarity on the product ratio from the PhICl$_2$ addition and found that the relevant amounts of the *trans* isomer could be increased on going from benzene (*trans*:*cis*/1:6) to THF (*trans*:*cis*/1:1), as presented in Table 2.3. While not detected in this work, the *trans* oxidative addition to rhodium most likely proceeds *via* an η^1-X$_2$ adduct[24,23a-b] that subsequently undergoes heterolysis of the X–X bond[25] to produce a charge-separated 5-coordinate intermediate. The isolation of the η^1-I$_2$ adduct was previously reported by us for a related square-planar rhodium(I) center defined as (NacNac^{CH3})Rh(phdi)(I$_2$).[16] Following the heterolytic cleavage of X$_2$, the 5-coordinate metal cation can give a complex where the two halogen ligands are located in the axial positions of an octahedron (**8a** and **9a**), with the parent square-planar configuration preserved through the equatorial ligands. However, the 5-coordinate intermediate may lack in stereochemical rigidity, leading to equilibration between the *trans* and *cis* isomers if thermodynamically favored.[26] The described process may involve pseudorotation of the 5-coordinate species preceded by dissociation of X$^-$ from the metal center. The lack of stereochemical rigidity was most likely responsible for giving significant amounts of the *cis* dichloro adduct of rhodium (**7b**) when the oxidation of **6** was carried out with PhICl$_2$ in benzene. Conversely, the relative amounts of the *trans* dichloro adduct of (**7a**) were found to increase when the same reaction was performed in coordinating solvents. The 5-coordinate intermediate can be better stabilized by such solvents, which would slow the *trans* to *cis* rearrangement (Table 2.3, entries 4, 5). On the other hand, the origin of observed *cis* selectivity with silver oxidants is likely to have emerged from alternative reactivity with Rh^I via homolytic bond cleavage[23i] (Table 2.3, entries 8-10).

Table 2.3. Two-Electron Oxidation of (acNac^{Ph})Rh(dmbpy) (**6**).

X = Cl (**7a**); Br (**8a**); I (**9b**)   X = Cl (**7b**); Br (**8b**); I (**9b**)
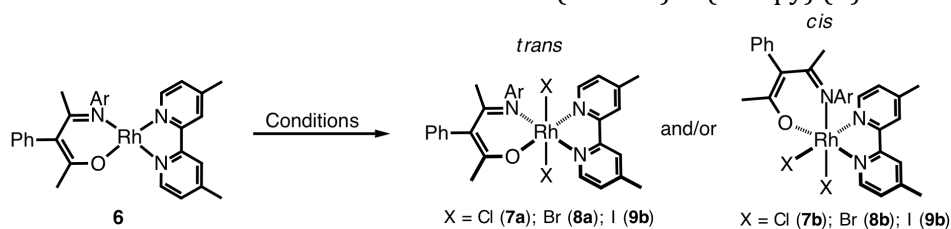
entry	oxidant	solvent	temp	stereoproduct[a]	yield(%)
1	PhICl$_2$ (1eq)	benzene	–5 °C	*trans*:*cis* / 1.3:1 (**7a**:**7b**)	--
2	PhICl$_2$ (1eq)	benzene	60 °C	*trans*:*cis* / 1:10 (**7a**:**7b**)	--
3	PhICl$_2$ (1eq)	benzene	rt	*trans*:*cis* / 1:6 (**7a**:**7b**)	--
4	PhICl$_2$ (1eq)	Et$_2$O	rt	*trans*:*cis* / 1:1.5 (**7a**:**7b**)	--
5	PhICl$_2$ (1eq)	THF	rt	*trans*:*cis* / 1:1 (**7a**:**7b**)	--
6	Br$_2$ (1eq)	Et$_2$O	rt	*trans*:*cis* /4:1 (**8a**:**8b**)	72
7	I$_2$ (1 eq)	Et$_2$O	rt	*trans* (**9a**)	67
8	AgCl (2 eq)	Et$_2$O	rt	*cis* (**7b**)	80
9	AgBr (2 eq)	Et$_2$O	rt	*cis* (**8b**)	83
10	AgI (2 eq)	Et$_2$O	rt	*cis* (**9b**)	63

[a]The *trans*/*cis* isomeric ratio was estimated from the ^{1}H NMR spectra of crude reaction mixtures by integration of respective keto-methyl groups.

2.2.6 Structural Assessment of [(acNac^{Ph})Rh(dmbpy)]X$_2$ Complexes

The structural features of the new octahedral complexes [(acNac^{Ph})Rh(dmbpy)]X$_2$ (where X$_2$ ligands are either *cis* or *trans*) were elucidated by solution NMR spectroscopy. Complete characterization was achieved for five of the six independently isolated rhodium complexes (**7b-9b**) whereas the solution structure of (acNac^{Ph})RhCl$_2$(dmbpy) (**7a**) was inferred from an inseparable *cis-trans* mixture of rhodium dichloride complexes (Table 2.3, entry 5). The reaction conditions used to synthesize **7b-9b** are included in Table 2.3 (entries 6-10). By and large, the most significant difference between the *trans* and *cis* isomers of the complexes in solution relates to the conformational mobility of the *N*-3,5-dimethylphenyl ring (*N*-xylyl). At room temperature, the *cis*-adduct series **7b**, **8b**, and **9b** revealed characteristic signs of a restricted N–C bond rotation, where N is the nitrogen donor group of (acNac^{Ph})$^-$ and C is a carbon atom of the 3,5-dimethylphenyl group.

Conversely, the spectral features of the *trans*-addition products **8a** and **9a** are in agreement with the N–C bond being mobile in solution.
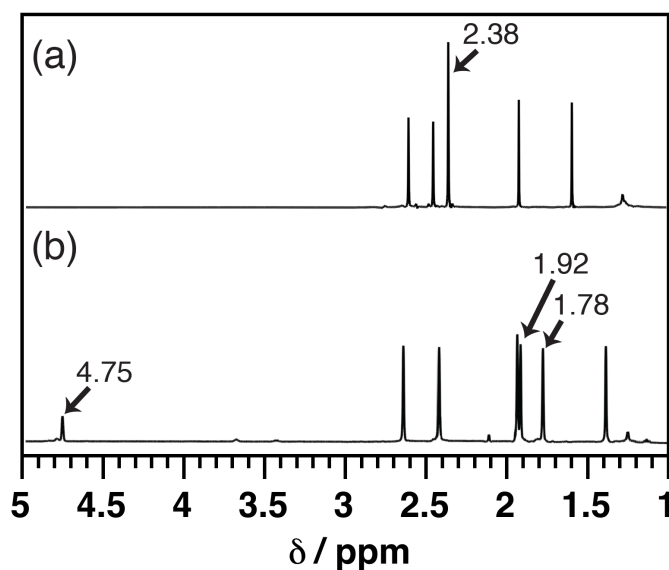
Figure 2.7. ^{1}H NMR spectra of the 1-5 ppm range of (a) (acNac[Ph])RhI$_2$(dmbpy) (**9a**) and (b) I$_2$-(acNac[Ph])Rh(dmbpy) (**9b**) in CD$_2$Cl$_2$ at 298K.

Figure 2.7 compares the ^{1}H NMR spectra of (acNac[Ph])RhI$_2$(dmbpy) (**9a**) and I$_2$-(acNac[Ph])Rh(dmbpy) (**9b**) in CD$_2$Cl$_2$, which are representative of all remaining *trans* and *cis* products, respectively. Complex **9b** shows signal splitting with respect to the CH$_3$ substituents of the *N*-xylyl group, displayed as individual singlets at 1.92 and 1.78 ppm. In contrast, the analogous CH$_3$ resonances for **9a** are found in the same chemical environment defined by a singlet resonance at 2.38 ppm. The proton spectrum of I$_2$-(acNac[Ph])Rh(dmbpy) (**9b**) additionally includes a diagnostic signal at 4.75 ppm as a singlet resonance assignable to one of the two *ortho* protons of the aromatic *N*-xylyl group. As established from 2D heteronuclear experiments, the shielded chemical shift of the aromatic *ortho* proton is unusually low and possibly results from a weak, intramolecular C–H···I interaction with a proximal iodide ligand, which is in agreement with the solid-state structure (*vide infra*). Conversely, the *ortho* protons of the 3,5-dimethylphenyl ring are chemically equivalent for

33

(acNac^{Ph})RhI$_2$(dmbpy) (**9a**) and appear within the usual ppm range of aromatic signals, as evidenced by a singlet resonance at 7.54 ppm with a total integration of 2 protons (not shown). The remaining proton-based characteristics revealed minimum individual differences between the solution structures **9a** and **9b**.
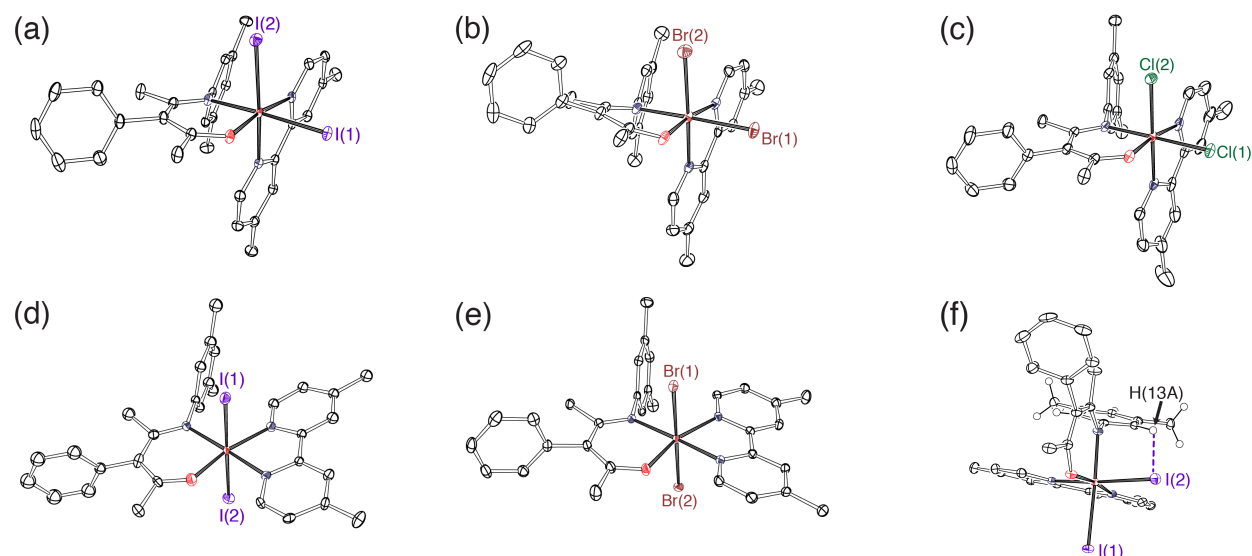
Figure 2.8. ORTEP diagrams of (a) I$_2$-(acNac^{Ph})Rh(dmbpy) (**9b**), (b) Br$_2$-(acNac^{Ph})Rh(dmbpy) (**8b**), (c) Cl$_2$-(acNac^{Ph})Rh(dmbpy) (**7b**), (d) (acNac^{Ph})RhI$_2$(dmbpy) (**9a**), and (e) (acNac^{Ph})RhBr$_2$(dmbpy) (**8a**). Ellipsoids are shown at 50% probability. Hydrogen atoms and solvent molecules have been omitted for clarity. (f) Rotated view of complex **9b** showing an intramolecular C–H···I contact interaction.

The absolute configuration of independent Rh^{III} centers was determined by obtaining X-ray quality crystals of [(acNac^{Ph})Rh(dmbpy)]X$_2$ complexes (**7b-9b**). The five individual structures are shown in Figure 2.8 in the form of ORTEP thermal ellipsoid plots, drawn at 50% probability. A collection of the most important bond lengths and angles for each complex is included in Table 2.4. Predictably, the geometry around rhodium is close to octahedral, in all cases with signs of small angular distortions. The C–O, C–N, and C–C bond lengths of the β-ketoaminato ligand for **7b-9b** fall within the range seen previously with (acNac^{Ph})Rh(CO)$_2$ (**4a**) and (acNac^{Ph})Rh(CO)NMe$_3$ (**4b**) (Table 2.1). The C–C and C–N bond

distances of the planar dmbpy ligand are in agreement with the bond metrics of reported Rh[III]-bipyridine complexes.[27]

Table 2.4. Selected Bond Lengths and Bond Angles of [(acNac[Ph])Rh(dmbpy)]X$_2$ Structures (**7b-9b**).

trans = X = Br (**8a**); I (**9a**)   cis = X = Cl (**7b**); Br (**8b**); I (**9b**)
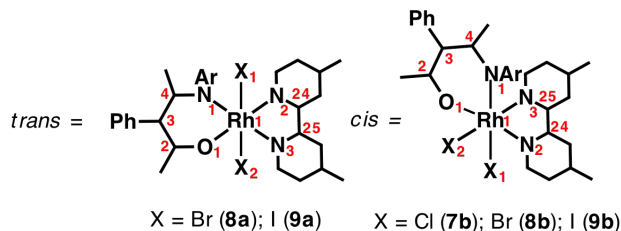
Bond (Å) / Angle (deg)	cis-Cl$_2$ (**7b**)	trans-Br$_2$ (**8a**)	cis-Br$_2$ (**8b**)	trans-I$_2$ (**9a**)	cis-I$_2$ (**9b**)
Rh(1)-N(1)	2.0267(18)	2.0425(16)	2.037(2)	2.076(7)	2.0628(16)
Rh(1)-O(1)	2.0028(16)	1.9851(14)	2.0010(17)	1.996(6)	1.9987(13)
O(1)-C(2)	1.295(3)	1.294(2)	1.305(3)	1.271(9)	1.291(2)
C(2)-C(3)	1.389(3)	1.377(3)	1.376(4)	1.407(11)	1.390(3)
C(3)-C(4)	1.440(3)	1.439(3)	1.436(4)	1.424(12)	1.436(3)
N(1)-C(4)	1.312(3)	1.314(3)	1.319(3)	1.316(10)	1.323(2)
Rh(1)-X(1)	2.3795(6)	2.4811(3)	2.5123(4)	2.6732(9)	2.6872(2)
Rh(1)-X(2)	2.3507(6)	2.4790(3)	2.4874(4)	2.6561(9)	2.6709(2)
Rh(1)-N(2)	2.0332(19)	2.1109(16)	2.035(2)	2.076(7)	2.0502(15)
Rh(1)-N(3)	2.0174(19)	2.0425(16)	2.022(2)	2.044(7)	2.0386(16)
N(2)-C(24)	1.361(3)	1.364(2)	1.359(3)	1.364(10)	1.362(2)
N(3)-C(25)	1.358(3)	1.346(2)	1.359(3)	1.349(10)	1.356(2)
X(2)-Rh(1)-X(1)	92.98(2)	179.021(10)	93.261(14)	179.51(3)	92.806(8)
O(1)-Rh(1)-N(2)	172.02(7)	164.12(6)	172.32(8)	165.2(2)	171.43(6)
N(3)-Rh(1)-N(1)	--	175.87(7)	--	176.5(3)	--
X(1)-Rh(1)-N(1)	179.19(6)	--	178.39(7)	--	177.22(5)
N(3)-Rh(1)-X(2)	177.53(6)	--	175.99(6)	--	174.95(4)
O(1)-Rh(1)-N(1)	91.89(7)	90.06(6)	90.22(8)	89.8(2)	90.90(6)
N(3)-Rh(1)-N(2)	--	78.55(6)	--	78.2(3)	--
X(1)-Rh(1)-N(2)	86.03(6)	--	85.06(6)	--	87.75(4)
C(13)-H(13A)···X(2)	2.972	--	3.437	--	3.548

Several key structural and conformational differences are discernible between the complementary isomers of *cis* and *trans* addition. For example, the equatorial plane of (acNac[Ph])RhI$_2$(dmbpy) (**9a**) is defined by two nitrogen atoms of the dmbpy ligand and the

nitrogen and oxygen atoms of the (acNac^{Ph})$^-$ ligand (Figure 2.8d); where the pertinent O(1)-Rh(1)-N(1) and N(3)-Rh(1)-N(2) bond angles are 89.8(2)° and 78.2(3)°, respectively. In constrast, the basal coordination plane of I$_2$-(acNac^{Ph})Rh(dmbpy) (**9b**) is comprised of the (acNac^{Ph})$^-$ donor atoms, one of the nitrogen atoms of the dmbpy ligand, and one of the two iodide ligands, defined by the O(1)-Rh(1)-N(1) bond angle of 90.90(6)° and the I(1)-Rh(1)-N(2) bond angle of 87.75(4)° (Figure 2.8a). Both of the iodides of (acNac^{Ph})RhI$_2$(dmbpy) (**9a**) occupy *trans* positions of the basal coordination plane, with the I(2)-Rh(1)-I(1) bond angle of 179.51(3)°. Conversely, the iodide ligands of I$_2$-(acNac^{Ph})Rh(dmbpy) (**9b**) occupy one axial and one equatorial vertex with the relevant I(2)-Rh(1)-I(1) bond angle of 92.806(8)°. Close examination of the Rh–I bond lengths revealed a slight elongation of the Rh(1)-I(1) and Rh(1)-I(2) distances in the *cis* complex **9b** as compared to those of the *trans* isomer **9a**; where the former bond distances are 2.6872(2) Å and 2.6709(2) Å and the latter are 2.6732(9) Å and 2.6561(9), respectively. As determined from the room-temperature solution structure of **9b**, the complex exhibits signs of a locked conformation with respect to the N–C bond of its *N*-3,5-dimethylphenyl group (*vide supra*). Consistent with the restricted N–C bond rotation is the presence of an intramolecular contact interaction between the axial iodide ligand and the *ortho* proton of the *N*-xylyl ring closest to the top axial face of the octahedron. In the solid-state structure of I$_2$-(acNac^{Ph})Rh(dmbpy) (**9b**) the pertinent C–H···I distance measures 3.548 Å (Figure 2.8f), which is within the reported range (3.517-3.633 Å) for Rh^{III} complexes containing intramolecular C–H···I contacts, classified as either weak electrostatic interactions or weak hydrogen bonds.[28] The analogous intramolecular C–H···X contacts measure 3.437 Å for the *cis*-Br$_2$ variant (**8b**) and 2.972 Å for the *cis*-Cl$_2$ variant (**7b**) (Table 2.4). Once again the

respective distances lie within the reported C–H⋯Br and C–H⋯Cl ranges (3.442-3.678 Å and 2.751-3.164 Å, respectively).[29,30]

2.2.7 Charge-Transfer Characteristics of [(acNac^{Ph})Rh(dmbpy)]X$_2$ Complexes

The charge-transfer (CT) features of [(acNac^{Ph})Rh(dmbpy)]X$_2$ complexes (where X$_2$ ligands are either *cis* or *trans*) were assessed by electronic absorption spectroscopy, measured in CH$_2$Cl$_2$ at 298K. As shown in Figure 2.9a, the absorptive characteristics of **7b-9b** are generally restricted to the UV-vis portions of the electromagnetic spectrum, with strong absorptions namely found in the 300-400 nm range. While the near-UV transition of (acNac^{Ph})RhI$_2$(dmbpy) (**9a**) is characterized by a well resolved absorption band maximum at 368 nm (ε = 8410 M^{-1}cm^{-1}), the analogous transitions have blue-shifted to higher energy in the remaining rhodium counterparts. On closer inspection of the visible spectral region notable differences are evident among the complexes. For example, the low-energy absorption spectra of (acNac^{Ph})RhI$_2$(dmbpy) (**9a**) and I$_2$-(acNac^{Ph})Rh(dmbpy) (**9b**) are compared in Figure 2.9b. The *trans* conformer **9a** displays a weak shoulder spanning the 500-750 nm range with a sensibly broad peak centered at λ_{max} = 555 nm (ε = 634 M^{-1}cm^{-1}). In contrast, the analogous spectrum of the *cis* isomer **9b** lacks in a comparable transition, as evidenced by the baseline character of its vis-NIR region. Less discernable yet optically parallel differences are manifested for the absorptive properties of the rhodium dibromide isomers, (acNac^{Ph})RhBr$_2$(dmbpy) (**8a**) and Br$_2$-(acNac^{Ph})Rh(dmbpy) (**8b**). As shown in Figure 2.9c, the 500-750 nm region of **8a** revealed a weak shoulder at λ_{max} ≈ 555 nm525 nm (ε = 443 M^{-1}cm^{-1}), albeit partially obscured by the near-UV electronic transition. Once again, the analogous shoulder-like feature is absent from the visible region of the *cis*

product counterpart (**8b**). Likewise, no appreciable optical density was derivable from the low-energy region of Cl_2-(acNac^{Ph})Rh(dmbpy) (**7b**).
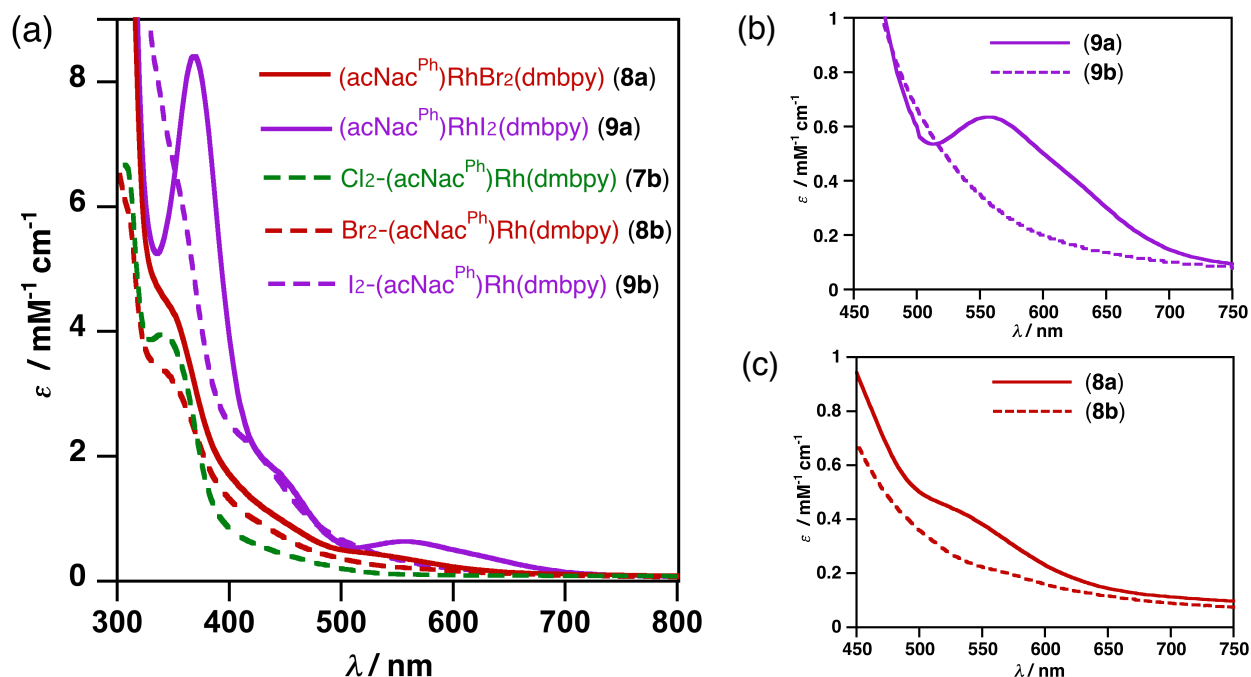
Figure 2.9. Solution UV-vis absorption spectra of (a) [(acNac^{Ph})Rh(dmbpy)]X$_2$ complexes **7b-9b** recorded in CH_2Cl_2 at 298K. Overlaid spectra of (b) [(acNac^{Ph})Rh(dmbpy)]I$_2$ and (c) [(acNac^{Ph})Rh(dmbpy)]Br$_2$ complexes showing interligand CT bands or lack thereof.

The development of a weak, visible-energy transition demonstrated a marked sensitivity toward conformational changes about the octahedral rhodium center. As established from the electronic absorption spectra of **7b-9b**, the prevalence of low-intensity shoulders was noted for the *trans* isomers of rhodium while the absence of analogous shoulders was common to the *cis* isomers of rhodium. As such, the emergence of the 500-750 nm absorption appears to be largely influenced by the coplanar juxtaposition of the (acNac^{Ph})$^-$ donor and the dmbpy acceptor ligands, with the remaining halogens occupying axial positions of an octahedron (**8a** and **9a**). The growth of the CT transition may be further promoted by the axial-halogen p orbitals through the local electronic coupling with the donor- and acceptor-based orbitals. For example, the development of a

well-resolved and slightly red-shifted absorption for $(acNac^{Ph})RhI_2(dmbpy)$ (**9a**), as compared to $(acNac^{Ph})RhBr_2(dmbpy)$ (**8a**), points to the likely influence of the halide identity on the electronic transition. However, the postulated assignment does not reflect the absorptive features of $(acNac^{Ph})RhCl_2(dmbpy)$ (**7a**), the independent characterization of which was deemed unsuccessful. In contrast, the capacity to derive the same LL'CT-like features appears to be shut down for the geometric isomers of the formula X_2-$(acNac^{Ph})Rh(dmbpy)$ (**7b**, **8b**, and **9b**). As determined through X-ray crystallography, the metal coordination environment for the *cis* stereoisomers is comprised of orthogonally juxtaposed ligand planes, between $(acNac^{Ph})^-$ and the dmbpy ligand, which would be expected to preclude the electronic coupling of respective orbitals for interligand charge transfer. Hence, the lack of coplanarity between the prospective donor and acceptor ligands leads to a net elimination of the weak charge-transfer transition.

2.3 Summary

Synthesis of the β-ketoaminato ligand, $(acNac^{Ph})^-$, allowed the development and investigation of new rhodium complexes with the formulae $(acNac^{Ph})Rh(CO)_2$ (**4a**), $(acNac^{Ph})Rh(CO)NMe_3$ (**4b**), $(acNac^{Ph})Rh(dmbpy)$ (**6**), and $[(acNac^{Ph})Rh(dmbpy)]X_2$ (dmbpy = 4,4-dimethyl-2,2-bipyridine; X_2 = *cis*-Cl_2, **7b**; *trans*-Br_2, **8a**; *cis*-Br_2, **8b**; *trans*-I_2, **9a**; *cis*-I_2, **9b**). As established through a combination of spectroscopic, structural, and photochemical studies of $(acNac^{Ph})Rh(CO)_2$ (**4a**), the electronic asymmetry of the $(acNac^{Ph})$-ligand donor atoms precluded the parent dicarbonyl complex from being used as synthon. Instead, access to $(acNac^{Ph})Rh(dmbpy)$ (**6**) was sought from $(acNac^{Ph})Rh(coe)_2$ (coe = cyclooctene) by means of thermal displacement of the alkene ligands. Five octahedral complexes of Rh^{III} centers were independently derived from $(acNac^{Ph})Rh(dmbpy)$ by oxidative addition of

elemental halogens or two-electron oxidation with silver(I) halides. In general, the addition of halogens to (acNac^{Ph})Rh(dmbpy) gave mixtures of *trans* and *cis* dihalo adducts, with access to the *trans* isomers of rhodium favored in polar solvents and access to the *cis* isomers of rhodium promoted by thermal *cis*-to-*trans* rearrangements. Conversely, the two-electron oxidation with silver was found to proceed in a stereoselective fashion, in all cases yielding the *cis* dihalo rhodium isomers. The relative and absolute configurations of the individual complexes were confirmed using a combination of X-ray crystallographic analysis and NMR spectroscopy. The *trans*-isomer assignment corresponds to the structures where the added halogens are mutually *trans* disposed, as seen with (acNac^{Ph})RhBr$_2$(dmbpy) (**8a**) and (acNac^{Ph})RhI$_2$(dmbpy) (**9a**). The *cis*-isomer assignment corresponds to the structures where the two halogens are *cis*-diposed, occupying one axial and one equatorial positions of an octahedron, as seen with Cl$_2$-(acNac^{Ph})Rh(dmbpy) (**7b**), Br$_2$-(acNac^{Ph})Rh(dmbpy) (**8b**), and I$_2$-(acNac^{Ph})Rh(dmbpy) (**9b**).

The individual charge-transfer properties of (acNac^{Ph})RhX$_2$(dmbpy) and X$_2$-(acNac^{Ph})Rh(dmbpy) complexes were elucidated by electronic absorption spectroscopy. All five complexes revealed intense near-UV absorptions, in most cases with poorly resolved characteristics. While the *trans* adducts of rhodium also displayed a weak charge-transfer transition in the visible region of the absorption spectrum, the analogous transition was absent from the spectra of the *cis* adducts of rhodium. The consequential activation and deactivation of the CT band appears to correlate with conformational changes around the central metal ion. Hence, the described trend bears evidence of weak, interligand charge transfer, which may proceed by photoexcitation of an electron from a filled (acNac^{Ph})-based

orbital into the π^* orbital of the dmbpy fragment, fundamentally demanding coplanarity or near-coplanarity of juxtaposed ligand orbitals.
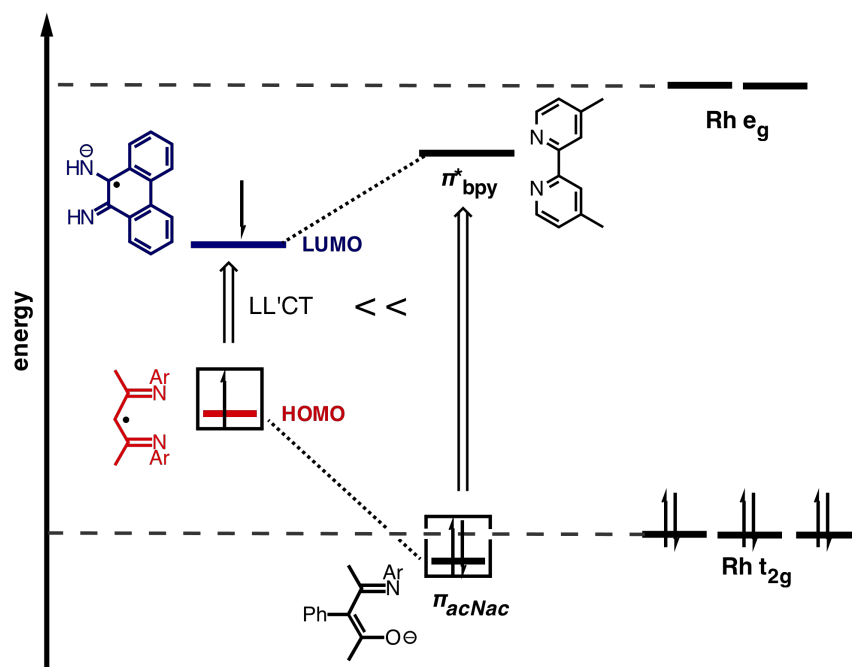
Figure 2.10. Qualitative description of molecular-orbital energy differences in the ligand-centered orbitals of (acNac^{Ph})RhX$_2$(dmbpy) and those of (NacNac^{R})RhX$_2$(phdi).

While fundamentally the conformationally sensitive electronic transition may be LL'CT in character, the weak transition intensity signals that it is accessed with a very low probability. In this regard, the described behavior contrasts the strong vis-NIR LL'CT features that we reported previously for related (NacNac^{R})RhX$_2$(phdi) complexes.[16] These differences suggest that the N,N to N,O donor-atom substitution has significantly perturbed the electronic manifold of the β-ketoaminato-centered orbital. As suggested in Figure 2.10, retention of the hard oxygen atom for (acNac^{Ph})$^-$ must have lowered the energy of the donor-based orbital, in reference to (NacNac^{R})$^-$, which was also coupled with a high-lying π^* orbital of the dmbpy acceptor ligand, in reference to phdi. The combined electronic effect of the more contracted donor and acceptor orbitals has substantially raised the

photoexcitation energy required for LL'CT, thus promoting the near-UV transition of the complexes into the dominant electronic transition. On the basis of this assessment, the examined β-ketoaminato motif is found to serve primarily as a traditional chelating ligand on octahedral rhodium centers, though their conformationally switchable CT features hint at the marginal proclivity of the ligand toward redox non-innocence.

2.4 Experimental

General Considerations. The complexes described are air- and moisture-sensitive, necessitating their synthesis to be carried out under an inert atmosphere of nitrogen using standard Schlenk, vacuum-line, and glovebox techniques. All reactions were carried out in dry and degassed solvents. Hydrocarbon solvents were sparged with argon and then deoxygenated and dried by passage through Q5 and activated alumina columns, respectively. Ethereal and halogenated solvents were sparged with argon and dried by passage through two activated alumina columns. All manipulations involving the ligand synthesis were performed under air, unless otherwise noted, employing reagents and solvents purchased from commercial suppliers and used as received. Column chromatography was performed with 230-400 mesh silica gel using flash column techniques. The ligand precursor 3-phenylpentane-2,4-dione ((acac^{Ph})H (**2**) was prepared by a previously described method.[31]

Physical Methods. NMR spectra were collected on Bruker Avance 400 and 500 MHz spectrometers. Chemical shifts were reported using the standard δ notation in parts per million and referenced using residual ^{1}H and ^{13}C isotopic impurities of the solvent. Infrared spectra were recorded as KBr pellets, neat solids, or neat liquids using the Perkin-Elmer Spectrum One FTIR and Jasco FT/IR-4700-ATR-PRO ONE spectrophotometers. Electronic

absorption spectra were recorded in dry, degassed THF or benzene solvents in one-centimeter cuvettes using a Shimadzu UV-1700 Spectrometer.

Electrochemical Methods. Cyclic voltammetry (CV) experiments were performed on a Gamry Series G 300 Potentiostat/Galvanostat/ZRA (Gamry Instruments, Warminster, PA, U.S.A.) using a 3.0 mm glassy carbon working electrode, a platinum wire auxiliary electrode, and a silver wire reference electrode. Measurements were recorded in a nitrogen-filled glovebox at ambient temperature and a scan rate of 200 mV/s. Sample concentrations were based on 1.0 mM THF solutions containing 100 mM [$^nBu_4N$][PF_6] as the supporting electrolyte. All potentials were referenced to the [$Cp_2Fe^{+/0}$] couple using ferrocene as an internal standard.[32] Tetrabutylammonium hexafluorophosphate was recrystallized from ethanol three times and dried under vacuum.

Photolytic Cleavage of CO ligands. Photolytic studies were performed in sealed quartz cuvettes placed in a Rayonet photochemical reactor (model RPR-100) at an operating temperature of 35 °C and intensity of 1.65×10^{16} photon·s^{-1} cm^{-3}. Samples were placed 1.5 inches from the lamp and irradiated with UV light at 254 nm or at a wavelength range controlled with long-pass filters (> 295 nm or > 395 nm). Additional photolytic studies were conducted with a Hanovia medium pressure, 450-watt, mercury vapor lamp (PC451050/610741), inside of a fume hood equipped with aluminum foil covered windows. The temperature in the hood was maintained between 25 and 27 °C by storing the 5.5 inch long UV lamp inside a 13 inch x 1.5 inch diameter S3 cavity of a double-walled quartz water cooling jacket. Samples were placed adjacent to the outer wall of the cooling jacket (1.5 inches away) and irradiated at the wavelength range controlled with long-pass filters (> 295 nm or > 395 nm). For studies monitored by absorption spectroscopy, samples

were prepared by a 25-fold dilution of 2.5 μM stock benzene solution containing (acNac^{Ph})Rh(CO)$_2$ (**4a**) or (acNac^{Ph})Rh(CO)py (**4c**) to afford final volumes of 5 mL of benzene, which were combined with 15 μL of pyridine. NMR-scale experiments were performed in quartz cuvettes, using samples prepared by dissolving 6.0 mg of **4a** (13 μmol) or 5.0 mg of **4c** (13 μmol) in 5mL solutions of benzene:pyridine / 4.5 mL:0.5mL.

4-(3,5-dimethylphenylamino)-3-phenylpent-3-en-2-one ((acNac^{Ph})H, 3):   A solution of (acac^{Ph})H (**2**) (809 mg, 4.59 mmol) and 3,5-dimethylaniline (2.29 mL, 18.3 mmol) in ethanol (30 mL) was heated at reflux for 12 h, in the presence of 3 drops of trifluoroacetic acid. The reaction mixture was cooled to room temperature and the solvent was removed under reduced pressure. The crude material was purified by column chromatography on silica-gel (ethyl acetate:hexanes/48:52) to give (acNac^{Ph})H (**3**) as an off-white solid (1.0 g, 78%). ^{1}H NMR (500 MHz, CDCl$_3$) δ 13.52 (s, 1H), 7.37 (appar t, J = 7.4 Hz, 2H), 7.29 (appar t, J = 7.3 Hz, 1H), 7.22 (d, J = 7.0 Hz, 2H), 6.84 (s, 1H), 6.78 (s, 2H), 2.31 (s, 6H), 1.89 (s, 3H), 1.74 (s, 3H); ^{13}C NMR (126 MHz, CDCl$_3$) δ 195.9 (C=O), 160.0 (C−N), 141.0 (xylyl-C−N), 139.10 (aryl-qC), 139.06 (xylyl-qC), 132.3 (aryl-C), 128.9 (aryl-C), 127.7 (aryl-C), 127.0 (xylyl-C), 123.4 (xylyl-C), 111.5 (α-qC), 27.0 (acyl-C), 21.6 (xylyl-CH$_3$), 18.8 (CH$_3$); FTIR (KBr) v/cm^{-1} 3412 st (N−H), 1569 br (C=O, C=C); HRMS (ESI) m / z calcd for C$_{19}$H$_{21}$NO (M + Na)$^+$ 302.1521, found 302.1516.

(acNac^{Ph})Rh(CO)$_2$ (4a):   To a cooled solution of (acNac^{Ph})H (**3**) (279 mg, 1.00 mmol) in diethyl ether (5 mL, −78 °C) was added potassium hydride (42 mg, 1.0 mmol). After stirring at room temperature for 12 h, to the resulting suspension was added [Rh(μ-Cl)(CO)$_2$]$_2$ (194 mg, 0.500 mmol) and the reaction mixture was stirred at the same temperature for another 12 h. The dark solution was filtered and the solvent was removed

to afford (acNac^{Ph})Rh(CO)$_2$ (**4a**) as a bright yellow solid (350 mg, 97%). ^{1}H NMR (500 MHz, CDCl$_3$) δ 7.34 (appar t, J = 7.6 Hz, 2H), 7.27 (appar t, J = 7.1 Hz, 1H), 7.15 (d, J = 7.8 Hz, 2H), 6.79 (s, 1H), 6.71 (s, 2H), 2.30 (s, 6H), 1.84 (s, 3H), 1.49 (s, 3H); ^{13}C NMR (126 MHz, CDCl$_3$) δ 185.5 (d, J = 65.9 Hz, C≡O), 184.3 (d, J = 72.6 Hz, C≡O), 176.6 (C=O), 165.9 (C–N), 158.4 (aryl-qC), 142.7 (xylyl-C–N), 138.9 (xylyl-qC), 132.1 (aryl-C), 129.1 (aryl-C), 127.2 (aryl-C), 127.0 (xylyl-C), 121.9 (xylyl-C), 112.2 (α-qC), 27.4 (keto-CH$_3$), 23.0 (amine-CH$_3$), 21.6 (xylyl-CH$_3$); FTIR (KBr) v/cm^{-1} 2060 st (C≡O), 1986 st (C≡O); HRMS (ESI) m / z calcd for C$_{21}$H$_{20}$NO$_3$Rh (M + K)$^+$ 476.0135, found 476.0144.

(acNac^{Ph})Rh(CO)NMe$_3$ (4b): A solution of (acNac^{Ph})Rh(CO)$_2$ (**4a**) (100 mg, 0.23 mmol) and trimethylamine N-oxide (TMAO) (35 mg, 0.47 mmol) was stirred in diethyl ether (10 mL) for 12h at room temperature. The orange reaction mixture was filtered to remove unreacted TMAO and the solvent removed *in vacuo* to afford (acNac^{Ph})Rh(CO)NMe$_3$ (**4b**) as an orange solid (97 mg, 90%), which required no further purification. ^{1}H NMR (500 MHz, CDCl$_3$) δ 7.30 (appar t, J = 7.4 Hz, 2H), 7.23–7.18 (m, 3H), 6.66 (s, 1H), 6.62 (s, 2H), 2.68 (s, 9H), 2.26 (s, 6H), 1.72 (s, 3H), 1.36 (s, 3H); ^{13}C NMR (126 MHz, CDCl$_3$) δ 191.5 (d, J = 83 Hz, C≡O), 173.0 (C=O), 164.3 (C–N), 159.3 (aryl-qC), 143.7 (xylyl-C–N), 138.1 (xylyl-qC), 132.5 (aryl-C), 128.8 (aryl-C), 126.4 (aryl-C), 126.0 (xylyl-C), 121.8 (xylyl-C), 112.8 (α-qC), 55.5 (N(CH$_3$)$_3$, 27.1 (keto-CH$_3$), 23.5 (amine-CH$_3$), 21.7 (xylyl-CH$_3$); FTIR (KBr) v/cm^{-1} 1942 st (C≡O).

(acNac^{Ph})Rh(CO)py (4c): A diethyl ether (3mL) solution of (acNac^{Ph})Rh(CO)NMe$_3$ (**4b**) (50 mg, 0.11 mmol) was treated with excess pyridine (300 μL). After stirring for 12 hours at room temperature, the solvent was removed *in vacuo* to afford (acNac^{Ph})Rh(CO)py (**4c**) as an orange solid (51 mg, 98%), which required no further purification. ^{1}H NMR (500

MHz, CDCl$_3$) δ 8.86 (d, J = 4.6 Hz, 2H), 7.71 (t, J = 7.2 Hz, 1H), 7.34–7.29 (m, 3H), 7.24–7.18 (m, 4H), 6.71 (s, 3H), 2.28 (s, 6H), 1.74 (s, 3H), 1.43 (s, 3H); ^{13}C NMR (126 MHz, CDCl$_3$) δ 190.7 (d, J = 81.1 Hz, C≡O), 173.8 (C=O), 164.0 (C–N), 159.8 (aryl-qC), 154.2 (py-C), 143.9 (xylyl-C–N), 138.2 (xylyl-qC), 136.9 (py-C), 132.6 (aryl-C), 128.8 (aryl-C), 126.5 (aryl-C), 126.1 (xylyl-C), 124.9 (py-C), 121.9 (xylyl-C), 112.6 (α-qC), 27.3 (keto-CH$_3$), 23.5 (amine-CH$_3$), 21.6 (xylyl-CH$_3$); FTIR (KBr) ν/cm^{-1} 1940 st (C≡O);

(acNac^{Ph})Rh(dmbpy) (6): To a cooled solution of (acNac^{Ph})H (**3**) (220 mg, 0.79 mmol) in diethyl ether (10 mL, −78 °C) was added potassium hydride (33 mg, 0.82 mmol). After stirring at room temperature for 12 h, to the resulting suspension was added solid [Rh(μ-Cl)(coe)$_2$]$_2$ (282 mg, 0.393 mmol) and the reaction mixture was stirred at the same temperature for another 12 h. The reaction mixture was stripped to dryness, redissolved in toluene, and filtered to remove KCl. Upon removal of solvent under reduced pressure, intermediate (acNac^{Ph})Rh(coe)$_2$ (**5**) was obtained as a green-brown solid (436 mg, 92% yield), which was used directly in the next step to prepare (acNac^{Ph})Rh(dmbpy) (**6**) by the following procedure: An air-tight, 50 mL Straus tube was charged with a light brown diethyl ether (6mL) solution of **5** (432 mg, 0.719 mmol) and solid 4,4′-dimethyl-2,2′-bipyridine (dmbpy) (132 mg, 0.719 mmol). The headspace was evacuated and the reaction tube was sealed followed by heating behind a glass shield at 120 °C for 12 h. The resulting reaction mixture was stripped down to a minimum amount of diethyl ether (2mL) and filtered under a glovebox atmosphere. Multiple washings of the crude solid with cold diethyl ether (10 mL, −35 °C) followed by cold pentane (10 mL, −35 °C) yielded (acNac^{Ph})Rh(dmbpy) (**6**) as a dark green solid (387 mg, 95% yield).^{1}H NMR (500 MHz, C$_6$D$_6$) δ 10.52 (d, J = 6.5 Hz, 1H), 7.46 (d, J = 6.5 Hz, 1H), 7.28 (m, 3H), 7.21 (appar t, J = 7.5

Hz, 3H), 7.08 (appar t, J = 7.3 Hz, 2H), 6.76 (s, 1H), 6.70 (m, 2H), 6.35 (d, J = 6.5 Hz, 1H), 2.16 (s, 3H), 2.11 (s, 6H), 1.71 (s, 3H), 1.50 (s, 3H), 1.40 (s, 3H); ^{13}C NMR (126 MHz, py-d_5) δ 172.3 (C=O), 160.0 (C–N), 157.2 (dmbpy-C=N), 156.4 (dmbpy-C=N), 150.8 (aryl-C), 147.7 (aryl-C), 145.5 (xylyl-C–N), 142.7 (dmbpy-qC), 141.5 (dmbpy-qC), 139.2 (xylyl-qC), 133.5 (aryl-C), 129.2 (aryl-C), 126.5 (aryl-C), 125.2 (xylyl-C), 124.3 (aryl-C), 123.4 (aryl-C), 122.7 (xylyl-C), 122.6 (α-qC), 28.0 (keto-CH$_3$), 25.8 (amine-CH$_3$), 21.63 (dmbpy-CH$_3$), 21.62 (xylyl-CH$_3$), 21.3 (dmbpy-CH$_3$); FTIR (KBr) ν/cm^{-1} 2914, 2852, 1734, 1689, 1532, 1411 st, 1367 st, 1246, 1019, 830, 705.

Cl$_2$-(acNac^{Ph})Rh(dmbpy) (7b): To a solution of (acNac^{Ph})Rh(dmbpy) (**6**) (22 mg, 0.039 mmol) in diethyl ether (3 mL) was added solid AgCl (11 mg, 0.078 mmol). The reaction mixture was stirred at room temperature for 12 h in the absence of light. The resulting reaction mixture was stripped to dryness, redissolved in CH$_2$Cl$_2$, and filtered through a plug of celite. The removal of solvent yielded Cl$_2$-(acNac^{Ph})Rh(dmbpy) (**7b**) as a light orange solid (20 mg, 80 % yield). X-ray quality crystals of **7b** were grown from cold CH$_2$Cl$_2$ solution (–35 °C). ^{1}H NMR (500 MHz, CDCl$_3$) δ 9.29 (d, J = 5.7 Hz, 1H), 8.70 (d, J = 5.7 Hz, 1H), 7.80 (s, 1H), 7.48(m, 2H), 7.35 (m, 4H), 7.16 (s, 1H), 7.04 (m, 1H), 6.66 (s, 1H), 6.33 (s, 1H), 4.82 (s, 1H), 2.61 (s, 3H), 2.38 (s, 3H), 2.08 (s, 3H), 1.97 (s, 3H), 1.74 (s, 3H), 1.37 (s, 3H); ^{13}C NMR (126 Hz, CDCl$_3$) δ 177.7 (C=O), 164.2 (qC–N), 157.3 (dmbpy-C=N), 155.9 (dmbpy-C=N), 153.1 (aryl-C), 151.5 (dmbpy-qC), 149.9 (dmbpy-qC), 149.8 (aryl-C), 148.7 (aryl-C–N), 143.0 (aryl-qC), 138.7 (xylyl-qC), 137.4 (xylyl-qC), 128.5 (aryl-C), 127.5 (aryl-C), 126.8 (aryl-C), 126.6 (aryl-C), 126.4 (xylyl-C), 125.6 (aryl-C), 124.6 (aryl-C), 123.3 (xylyl-C), 122.4 (aryl-C), 121.1 (xylyl-o-C), 110.6 (α-qC), 27.6 (dmbpy-CH$_3$), 24.9 (dmbpy-CH$_3$), 21.9 (keto-CH$_3$), 21.4 (xylyl-CH$_3$), 21.2 (xylyl-CH$_3$), 21.1 (amine-CH$_3$); FTIR (ATR) ν/cm^{-1} 2970,

2890, 1615, 1427 st, 1890 st, 1055 st, 683; HRMS (ESI) m / z calcd for $C_{31}H_{32}Cl_2N_3ORh$ (M +

K)$^+$ 674.0615, found 674.0590.

Br$_2$-(acNac^{Ph})Rh(dmbpy) (8b): This complex was prepared in a manner similar to

that described for Cl$_2$-(acNac^{Ph})Rh(dmbpy) (**7b**) by addition of 3 mL of a diethyl ether

solution of **6** (24 mg, 0.043 mmol) to solid AgBr (16 mg, 0.086 mmol). Compound Br$_2$-

(acNac^{Ph})Rh(dmbpy) (**8b**) was afforded as a light brown solid (28 mg, 83% yield). X-ray

quality crystals of **8b** were grown from cold CH_2Cl_2 solution (-35 °C). ^{1}H NMR (500 MHz,

CD_2Cl_2) δ 9.47 (dd, J = 5.9 Hz, 1H), 8.65 (d, J = 5.8 Hz, 1H), 7.78 (s, 1H), 7.54 (dd, J = 5.8, 0.9

Hz, 1H), 7.46 (s, 1H), 7.40–7.33 (m, 3H), 7.29–7.24 (m, 2H), 7.12 (dd, J = 5.9, 1.0 Hz, 1H),

6.59 (s, 1H), 6.38 (s, 1H), 4.78 (s, 1H), 2.64 (s, 3H), 2.42 (s, 3H), 2.00 (s, 3H), 1.97 (s, 3H),

1.77 (s, 3H), 1.38 (s, 3H); ^{13}C NMR (126 MHz, CD_2Cl_2) δ 177.2 (C=O), 164.4 (qC–N), 157.3

(dmbpy-C=N), 156.1 (dmbpy C=N), 154.7 (aryl-C), 151.9 (dmbpy-qC), 150.2 (dmbpy-qC),

149.3 (aryl-C), 148.0 (xylyl-C–N), 143.0 (aryl-qC), 138.8 (xylyl-qC), 137.8 (xylyl-qC), 127.6

(aryl-C), 126.81 (aryl-C), 126.76 (aryl-C), 124.4 (aryl-C), 123.5 (aryl-C), 122.6 (aryl-C),

121.2 (xylyl-o-C), 111.1 (α-qC), 26.9 (dmbpy-CH$_3$), 25.0 (dmbpy-CH$_3$), 21.7 (keto-CH$_3$), 21.2

(xylyl-CH$_3$), 21.0 (xylyl-CH$_3$), 20.8 (amine-CH$_3$); FTIR (ATR) v/cm^{-1} 2956, 2913, 1624, 1564

st, 1417 st, 1281, 1162, 1127, 1022; HRMS (ESI) m / z calcd for $C_{31}H_{32}Br_2N_3ORh$ (M + Na)$^+$

745.9865, found 745.9869.

I$_2$-(acNac^{Ph})Rh(dmbpy) (9b): This complex was prepared in a manner similar to

that described for Cl$_2$-(acNac^{Ph})Rh(dmbpy) (**7b**) by addition of 3 mL of a diethyl ether

solution of **6** (47 mg, 0.083 mmol) to solid AgI (39 mg, 0.17 mmol). Compound I$_2$-

(acNac^{Ph})Rh(dmbpy) (**9b**) was afforded as a brown solid (43 mg, 63% yield). X-ray quality

crystals of **9b** were grown from a cold CH_3CN solution (-35 °C). ^{1}H NMR (500 MHz, CD_2Cl_2)

δ 9.72 (d, *J* = 5.9 Hz, 1H), 8.65 (d, *J* = 5.8 Hz, 1H), 7.74 (s, 1H), 7.56 (d, *J* = 5.8 Hz, 1H), 7.42 (s, 1H), 7.37–7.34 (m, 3H), 7.28–7.25 (m, 2H), 7.07 (d, *J* = 5.9 Hz, 1H), 6.62 (s, 1H), 6.38 (s, 1H), 4.75 (s, 1H), 2.65 (s, 3H), 2.43 (s, 3H), 1.94 (s, 3H), 1.92 (s, 3H), 1.78 (s, 3H), 1.39 (s, 3H); ^{13}C NMR (126 MHz, CD$_2$Cl$_2$) δ 177.5 (C=O), 164.3 (qC–N), 158.00 (aryl-C), 157.96 (dmbpy-C=N), 155.9 (dmbpy-C=N), 151.64 (dmbpy-qC), 149.7 (dmbpy-qC), 148.7 (aryl-C), 147.4 (xylyl-C–N), 143.2 (aryl-qC), 138.8 (xylyl-qC), 137.7 (xylyl-qC), 127.4 (aryl-C), 127.1 (aryl-C), 126.8 (aryl-C), 126.6 (aryl-C), 124.2 (aryl-C), 123.4 (aryl-C), 122.7 (aryl-C), 121.4 (xylyl-o-C), 112.1 (α-qC), 26.7 (dmbpy-CH$_3$), 25.1 (dmbpy-CH$_3$), 21.7 (xylyl-CH$_3$), 21.1 (keto-CH$_3$), 21.0 (xylyl-CH$_3$), 20.9 (amine-CH$_3$); FTIR (ATR) *v*/cm^{-1} 2970, 2859, 1622, 1566 st, 1406 st, 1278, 1028, 996 st, 846; HRMS (ESI) *m / z* calcd for C$_{31}$H$_{32}$I$_2$N$_3$ORh (M + Na)$^+$ 841.9587, found 841.9605.

(acNac^{Ph})RhBr$_2$(dmbpy) (8a): To a solution of (acNac^{Ph})Rh(dmbpy) (**6**) (54 mg, 0.095 mmol) in diethyl ether (3 mL) was added Br$_2$ (97 µL, 0.095 mmol, 0.98 M in benzene). The reaction mixture was stirred at room temperature for 12 h after which point it was filtered and the crude solid washed with cold diethyl ether (10 mL, –35 °C). Drying of the product under reduced pressure afforded an inseparable mixture of regioisomers (acNac^{Ph})RhBr$_2$(dmbpy) (**8a**) and Br$_2$-(acNac^{Ph})Rh(dmbpy) (**8b**) in a 4-to-1 ratio as a brown solid, in a combined yield of 72% (50 mg). X-ray quality crystals of **8a** were grown from cold CDCl$_3$ solution (–35 °C) using the mixture of isomers. Characterization data for **8b** is reported above; characterization data for **8a** is as follows: ^{1}H NMR (500 MHz, CD$_2$Cl$_2$) δ 9.62 (d, *J* = 5.9 Hz, 1H), 7.92 (s, 1H), 7.82 (s, 1H), 7.52 (dd, *J* = 5.9, 1.0 Hz, 1H),), 7.37–7.35 (m, 3H), 7.30–7.24 (m, 3H), 7.06 (s, 1H), 6.78 (dd, *J* = 6.1, 1.2 Hz, 1H), 6.13 (d, *J* = 6.1 Hz, 1H), 2.60 (s, 3H), 2.44 (s, 3H), 2.35 (s, 6H), 1.99 (s, 3H), 1.63 (s, 3H); ^{13}C NMR (126 MHz, CD$_2$Cl$_2$)

δ 174.2 (C=O), 166.50 (qC–N), 157.4 (dmbpy-C=N), 156.5 (dmbpy-C=N), 153.1(aryl-C), 152.7 (dmbpy-qC), 151.4 (dmbpy-qC), 151.0 (xylyl-C–N), 148.8 (aryl-C), 143.3 (aryl-qC), 140.0 (xylyl-qC), 133.0 (aryl-C), 129.0 (aryl-C), 128.0 (aryl-C), 126.9 (aryl-C), 126.7 (aryl-C), 126.0 (aryl-C), 125.3 (aryl-C), 123.3 (aryl-C), 110.3 (α-qC), 26.7 (dmbpy-CH$_3$), 26.4 (dmbpy-CH$_3$), 21.6 (keto-CH$_3$), 21.5 (xylyl-CH$_3$), 20.9 (amine-CH$_3$); FTIR (ATR) v/cm^{-1} 3047, 2908, 2852, 1618, 1573 st, 1406 st, 1277 st. 1021 st, 951; HRMS (ESI) m / z calcd for C$_{31}$H$_{32}$Br$_2$N$_3$ORh (M + Na)$^+$ 745.9865, found 745.9839.

(acNac^{Ph})RhI$_2$(dmbpy) (9a): This complex was prepared in a manner similar to that described for (acNac^{Ph})RhBr$_2$(dmbpy) (**8a**) by addition of 2 mL of a diethyl ether solution of I$_2$ (72 mg, 0.028 mmol) to **6** (160 mg, 0.028 mmol) in diethyl ether (5 mL). Compound (acNac^{Ph})RhI$_2$(dmbpy) (**9a**) was afforded as a dark brown solid (156 mg, 67% yield). X-ray quality crystals of **9a** were grown by layering a CH$_2$Cl$_2$ solution of the product with pentane (–35 °C). ^{1}H NMR (500 MHz, CD$_2$Cl$_2$) δ 9.60 (d, J = 5.9 Hz, 1H), 7.91 (s, 1H), 7.82 (s, 1H), 7.54 (d, J = 5.9 Hz, 2H), 7.37–7.34 (m, 2H), 7.32 (m 2H), 7.30–7.27 (m, 1H), 7.03 (s, 1H), 6.77 (d, J = 6.1 Hz, 1H), 6.09 (d, J = 6.1 Hz, 1H), 2.61 (s, 3H), 2.46 (s, 3H), 2.37 (s, 6H), 1.92 (s, 3H), 1.59 (s, 3H); ^{13}C NMR (126 MHz, CD$_2$Cl$_2$) δ 174.5 (C=O), 167.4 (qC–N), 157.7 (dmbpy-C=N), 156.7 (dmbpy-C=N), 153.5 (aryl-C), 152.7 (dmbpy-qC), 151.0 (dmbpy-qC), 150.8 (xylyl-C–N), 149.1 (aryl-C), 143.5 (aryl-qC), 140.0 (xylyl-qC), 133.1 (aryl-C), 128.9 (aryl-C), 127.9 (aryl-C), 126.8 (aryl-C), 126.7 (aryl-C), 125.8 (aryl-C), 125.2 (aryl-C), 123.2 (aryl-C), 123.2 (aryl-C), 111.2 (α-qC), 26.6 (dmbpy-CH$_3$), 26.3 (dmbpy-CH$_3$), 21.6 (keto-CH$_3$), 21.5 (xylyl-CH$_3$), 20.9 (amine-CH$_3$); FTIR (ATR) v/cm^{-1} 3050, 2918, 1622, 1570 st, 1409 st, 1277, 961, 704 st; HRMS (ESI) m / z calcd for C$_{31}$H$_{32}$I$_2$N$_3$ORh (M + K)$^+$ 857.9327, found 857.9340.

Crystallographic Methods. X-ray diffraction data were collected on crystals mounted on glass fibers using a Bruker CCD platform diffractometer equipped with a CCD detector. Measurements were carried out at 163 K using Mo Kα (λ = 0.71073 Å) radiation, which was wavelength selected with a single-crystal graphite monochromator. The SMART program package was used to determine unit-cell parameters and to collect data.[33] The raw frame data were processed using SAINT[34] and SADABS[35] to yield the reflection data files. Subsequent calculations were carried out using the SHELXTL[36] program suite. Structures were solved by direct methods and refined on F_2 by full-matrix least-squares techniques. Analytical scattering factors for neutral atoms were used throughout the analyses.[37] Hydrogen atoms were included using a riding model. ORTEP diagrams were generated using ORTEP-3 for Windows. Diffraction data are shown in Tables 2.5 and 2.6.

Table 2.5. X-ray Diffraction Data-Collection and Refinement Parameters for (acNac^{Ph})Rh(CO)$_2$ (**4a**) and (acNac^{Ph})Rh(CO)NMe$_3$ (**4b**).

	4a	4b
empirical formula	$C_{21}H_{20}NO_3Rh$	$C_{23}H_{29}N_2O_2Rh$
formula weight	437.29	468.39
crystal system	triclinic	monoclinic
space group	$P\bar{1}$	$C2/c$
a/Å	9.8471(13)	33.816(2)
b/Å	10.2810(13)	6.5906(4)
c/Å	11.0051(14)	22.0831(15)
α/deg	107.2704(14)	90
β/deg	96.6107(14)	115.4557(7)
γ/deg	111.2566(14)	90
V/Å^3	960.0(2)	4443.8(5)
Z	2	8
refl. collected	10750	24488
indep. refl.	4245 (0.0194)	5276 (0.0308)
R1 (I > 2σ)^a	0.0253	0.0251
wR2 (all data)^a	0.0673	0.0597

^{a}R$_1$ = $\sum||F_o| - |F_c||/\sum|F_o|$; wR$_2$ = $[\sum w(F_o^2 - F_c^2)^2/\sum w(F_o^2)^2]^{1/2}$; GOF = $[\sum w(|F_o| - |F_c|)^2/(n - m)]^{1/2}$.

Table 2.6. X-ray Diffraction Data-Collection and Refinement Parameters for Cl_2-(acNac^{Ph})Rh(dmbpy) (**7b**), (acNac^{Ph})RhBr$_2$(dmbpy) (**8a**), Br$_2$-(acNac^{Ph})Rh(dmbpy) (**8b**), (acNac^{Ph})RhI$_2$(dmbpy) (**9a**), and I$_2$-(acNac^{Ph})Rh(dmbpy) (**9b**).

	7b	8a	8b	9a	9b
empirical formula	$C_{33}H_{36}Cl_6N_3ORh$	$C_{31}H_{32}Br_2N_3ORh \cdot 4(CDCl_3)$	$C_{35}H_{38}Br_2N_5ORh$	$C_{32}H_{34}Cl_2I_2N_3ORh$	$C_{31}H_{32}I_2N_3O Rh \cdot 2(CH_3CN)$
formula weight	806.26	1206.82	807.43	904.23	901.41
crystal system	triclinic	monoclinic	triclinic	triclinic	triclinic
space group	$P\bar{1}$	$P2_1/c$	$P\bar{1}$	$P\bar{1}$	$P\bar{1}$
a/Å	11.6325(4)	11.2457(6)	9.9943(9)	12.3559(18)	10.4576(8)
b/Å	11.8450(5)	24.0821(12)	13.2363(12)	15.914(2)	12.6266(9)
c/Å	13.9099(5)	17.9876(9)	13.8862(13)	17.937(3)	13.9384(10)
α/deg	75.0037(4)	90	88.8484(12)	74.381(2)	93.4257(9)
β/deg	87.3844(4)	107.7857(7)	77.0126(11)	86.263(2)	97.2717(8)
γ/deg	79.9524(5)	90	76.9211(12)	86.953(2)	103.9766(8)
V/Å^3	1822.94(12)	4638.6(4)	1742.6(3)	3387.2(9)	1763.8(2)
Z	2	4	2	4	2
refl. collected	22872	56998	14972	15279	21273
indep. refl.	9038 (0.0139)	11655 (0.0338)	7945 (0.0204)	15279	8724 (0.0163)
R1 (I > 2σ)^a	0.0370	0.027	0.0325	0.081	0.0204
wR2 (all data)^a	0.0892	0.0608	0.0842	0.123	0.0506

^{a}R$_1$ = $\sum||F_o| - |F_c||/\sum|F_o|$; wR$_2$ = $[\sum w(F_o^2 - F_c^2)^2/\sum w(F_o^2)^2]^{1/2}$; GOF = $[\sum w(|F_o| - |F_c|)^2/(n - m)]^{1/2}$.

2.5 References

[1] (a) Schwab, P. F. H.; Diegoli, S.; Biancardo, M.; Bignozzi, C. A. *Inorg. Chem.* **2003**, *42*, 6613–6615. (b) Damas, A.; Gullo, M. P.; Rager, M. N.; Jutand, A.; Barbieri, A.; Amouri, H. *Chem. Commun.* **2013,** *49*, 3796–3798. (c) Grange, C. S.; Meijer, A. J. H. M.; Ward, M. D. *Dalton Trans.* **2010**, *39*, 200–211.

[2] (a) Linfoot, C. L.; Richardson, P.; McCall, K. L.; Durrant, J. R.; Morandeira, A.; Robertson, N. *Solar Energy* **2011**, *85*, 1195–1203. (b) Geary, E. A. M.; Yellowlees, L. J.; Jack, L. A.; Oswald, I. D. H.; Parsons, S.; Hirata, N.; Durrant, J. R.; Robertson, N. *Inorg. Chem.* **2005**, *44*, 242–250 (c) Islam, A.; Sugihara, H.; Hara, K.; Singh, L. P.; Katoh, R.; Yanagida, M.; Takahashi, Y.; Murata, S.; Arakawa, H.; Fujihashi, G. *Inorg. Chem.* **2001**, *40*, 5371–5380. (d) Diwan, K.; Chauhan, R.; Singh, S. K.; Singh, B.; Drew, M. G. B.; Bahadur, L.; Singh, N. *New J. Chem.* **2014**, *38*, 97–108. (e) Verma, S.; Kar, P.; Das, A.; Ghosh, H. N. *Chem. Eur. J.* **2011**, *17*, 1561–1568.

[3] (a) Kramer, W. W.; Cameron, L. A.; Zarkesh, R. A.; Ziller, J. W.; Heyduk, A. F. *Inorg. Chem.* **2014**, *53*, 8825–8837. (b) Seraya, E.; Luan, Z.; Law, M.; Heyduk, A.F. *Inorg. Chem.* **2015**, *54*, 7571–7578 (c) Pevny, F.; Zabel, M.; Winter, R. F.; Rausch, A. F.; Yersin, H.; Tuczek, F.; Záliš, S. *Chem. Commun.* **2011**, *47*, 6302–6304.

[3] (d) Weinstein, J. A.; Tierney, M. T.; Davies, E. S.; Base, K.; Robeiro, A. A.; Grinstaff, M. W. *Inorg. Chem*. **2006**, *45*, 4544–4555. (e) Best, J.; Sazanovich, I. V.; Adams, H.; Bennett, R. D.; Davies, E. S.; Meijer, A. J. H. M.; Towrie, M.; Tikhomirov, S. A.; Bouganov, O. V.; Ward, M. D.; Weinstein, J. A. *Inorg. Chem*. **2010**, *49*, 10041–10056. (f) V. Anbalagan, V.; Srivastava, T. *Polyhedron*, **2004**, *23*, 3173–3183.

[4] (a) Zuleta, J. A.; Bevilacqua, J. M.; Rehm, J. M.; Eisenberg, R. *Inorg. Chem*. **1992**, *31*, 1332–1337. (b) Cocker, T. M.; Bachman, R. E. *Inorg. Chem*. **2001**, *40*, 1550–1556. (c) Chen, C.-T.; Liao, S.-Y.; Lin, K.-J.; Chen, C.-H.; Lin, T.-Y. J. *Inorg. Chem*. **1999**, *38*, 2734–2741. (d) Vogler, A.; Kunkely, H.; Hlavatsch, J.; Merz, A. *Inorg. Chem*. **1984**, *23*, 506–509. (e) Wootoon, J. L.; Zink, J. I. *J. Phys. Chem*. **1995**, *99*, 7251–7257. (f) Paw, W.; Cummings, S. D.; Mansour, M. A.; Connick, W. B.; Geiger, D. K.; Eisenberg, R. *Coord. Chem. Rev*. **1998**, *171*, 125–150. (g) Cummings, S. D.; Eisenberg, R. *J. Am. Chem. Soc.* **1996**, *118*, 1949–1960. (h) Connick, W. B.; Geiger, D.; Eisenberg, R. *Inorg. Chem*. **1999**, *38*, 3264–3265. (i) M. Hissler, J. E. McGarrah, W. B. Connick, D. K. Geiger, S. D. Cummings and R. Eisenberg, *Coord. Chem. Rev.*, **2000**, 208, 115–137.

[5] (a) Juris, A.; Balzani, V.; Barigelletti, F.; Campagna, S.; Belser, P. L.; Von Zelewsky, A. *Coord. Chem. Rev*. **1988**, *84*, 85–277. (b) McCusker, J. K. *Acc. Chem. Res*. **2003**, *36*, 876–887. (c) Watson, D. F.; Meyer, G. J. *Annu. Rev. Phys. Chem*. **2005**, *56*, 119–156

[6] (a) Maurya, M. *Coord. Chem. Rev*. **2003**, *237*, 163–181. (b) Bennett, M. A.; Byrnes, M. J.; Kováčik, I. J. *Organomet. Chem*. **2004**, *689*, 4463–4474. (c) Suslov, D. S.; Pahomova, M. V.; Abramov, P.A.; Bykov, M. V., Tkach, V. S. *Catal. Commun*. **2015**, *67*, 11–15. (d) Aromí, G.; Gamez, P.; Reedijk, *J. Coord. Chem. Rev* **2008**, *252*, 964–989.

[7] Radwan, Y. K.; Maity, A.; Teets, T. S. *Inorg. Chem*. **2015**, *54*, 7122–7131.

[8] (a) Bourget-Merle, L.; Lappert, M. F.; Severn, J. R. *Chem. Rev*. **2002**, *102*, 3031–3065 (b). Mindiola, D. J. *Acc. Chem. Res*. **2006**, *39*, 813–821. (c) Spielmann, J.; Piesik, D.; Wittkamp, B.; Jansen, G.; Harder, S. *Chem. Commun*. **2009**, 3455–3456. (d) Fan, H.; Adhikari, D.; Saleh, A. A.; Clark, R. L.; Zuno-Cruz, F. J.; Sanchez Cabrera G.; Huffman, J. C.; Pink, M.; Mindiola, D. J.; Baik, M.-H. *J. Am. Chem. Soc*. **2008**, *130*, 17351–17361. (e) Pfirrmann, S.; Limberg, C.; Herwig, C.; Stößer, R.; Ziemer, B. *Angew. Chem. Int. Ed*. **2009**, *48*, 3357–3361.

[9] (a) Yao, Y.; Zhang, Z.; Peng, H.; Zhang, Y.; Shen, Q.; Lin, J. *Inorg. Chem*. **2006**, *45*, 2175–2183. (b) Xue, M.; Zheng, Y.; Hong, Y.; Yao, Y.; Xu, F.; Zhang, Y.; Shen, Q. *Dalton Trans*. **2015**, *44*, 20075–20086. (c) Yao, Y.; Xue, M.; Luo, Y.; Zhang, Z.; Jiao, R.; Zhang, Y.; Shen, Q.; Wong, W.; Yu, K.; Sun, J. *J. Organomet. Chem.* **2003**, *678*, 108–116.

[10] (a) Cui, C.; Roesky, H. W.; Schmidt, H.-G.; Noltemeyer, M.; Hao, H.; Cimpoesu, F. *Angew. Chem., Int. Ed*. **2000**, *39*, 4274–4276. (b) Driess, M.; Yao, S.; Brym, M.; van Wüllen, C.; Lentz, D. *J. Am. Chem. Soc*. **2006**, *128*, 9628–9629. (c) Roesky, H. W. ; Singh, S.; Jancik, V.; Chandrasekhar, V. *Acc. Chem. Res*. **2004**, *37*, 969–981. (d) Henderson, M. J.: Kennard, H. W. C.; Raston L.; Smith, G. *J. Chem. Soc. Chem. Commun*. **1990**, 1203–1204. (e) Tsai, Y-C. Coord. *Chem. Rev*. **2012**, *256*, 722–758.

[11] (a) Chamberlain, B. M.; Cheng, M.; Moore, D. R.; Ovitt, T. M.; Lobkovsky, E. B.; Coates, G. W. *J. Am. Chem. Soc.* **2001**, *123*, 3229–3238. (b) Hayes, P. G.; Piers, W. E.; McDonald, R. *J. Am. Chem. Soc.* **2002**, *124*, 2132–2133. (c) Li, X.-F.; Dai, K.; Ye, W.-P.; Pan, L.; Li, Y.-S. *Organometallics* **2004**, *23*, 1223–1230.

[12] (a) Holland, P. L.; Tolman, W. B. *J. Am. Chem. Soc.* **1999**, *121*, 7270–7271. (b) Jang, E. S.; McMullin, C. L.; Kaß, M.; Meyer, K.; Cundari, T. R.; Warren, T. H. *J. Am. Chem. Soc.* **2014**, *136*, 10930–10940. (c) MacLeod, K. C.; Vinyard, D. J.; Holland, P. L. *J. Am. Chem. Soc.* **2014**, *136*, 10226–10229. (d) Basuli, F.; Bailey, B. C.; Tomaszewski, J.; Huffman, J. C.; Mindiola, D. J. *J. Am. Chem. Soc.* **2003**, *125*, 6052–6053. (e) Thompson, R.; Chen, C.-H.; Pink, M.; Wu, G.; Mindiola, D. J. *J. Am. Chem. Soc.* **2014**, *136*, 8197–8200. (f) Kogut, E.; Wiencko, H. L.; Zhang, L.; Cordeau, D. E.; Warren, T. H. *J. Am. Chem. Soc.* **2005,** *127*, 11248–11249. (g) Cramer, C. J. Tolman, W. B. *Acc. Chem. Res.* **2007**, *40,* 601–608. (h) Monillas, W. H.; Yap, G. P. A.; MacAdams, L. A.; Theopold, K. H. *J. Am. Chem. Soc.* **2007**, *129*, 8090–8091. (i) Ding, K.; Brennessel, W. W.; Holland, P. L. *J. Am. Chem. Soc.* **2009**, *131*, 10804–10805.

[13] Khusniyarov, M. M.; Bill, E.; Weyhermüller, T.; Bothe, E.; Wieghardt, K. *Angew. Chem. Int. Ed.* **2011**, *50*, 1652–1655.

[14] Takaichi, J.; Morimoto, Y.; Ohkubo, K.; Shimokawa, C.; Hojo, T.; Mori, S.; Asahara, H.; Sugimoto, H.; Fujieda, N.; Nishiwaki, N.; Fukuzumi, S.; Itoh, S. *Inorg. Chem.* **2014**, *53*, 6159–6169.

[15] Marshak, M. P.; Chambers, M. B.; Nocera, D. G. *Inorg. Chem.* **2012**, *51*, 11190–11197.

[16] Shaffer, D. W.; Ryken, S. A.; Zarkesh, R. A.; Heyduk, A. F. *Inorg. Chem.* **2012**, *51*, 12122–12131

[17] Moilanen, J.; Borau-Garcia, J.; Roesler, R.; Tuononen, H. M. *Chem. Commun.* **2012**, *48*, 8949–8951.

[18] Eisenstein, O.; Hitchcock, P. B.; Khvostov, A. V.; Lappert, M. F.; Maron, L.; Perrin, L.; Protchenko, A. V. *J. Am. Chem. Soc.* **2003**, *125*, 10790–10791.

[19] Phillips, A. D.; Thommes, K.; Scopelliti, R.; Gandolfi, C.; Albrecht, M.; Severin, K.; Schreiber, D. F.; Dyson, P. J. *Organometallics* **2011**, *30*, 6119–6132.

[20] Herzberg, G.; Narahari Rao, K. *J. Chem. Phys.* **1949**, *17, 1099*.

[21] Geier, S. J.; Chapman, E. E.; McIsaac, D. I.; Vogels, C. M.; Decken, A.; Westcott, S. A. *Inorg. Chem. Comm.* **2006**, *9,* 788–791.

[22] (a) Swanick, K. N.; Ladouceur, S.; Zysman-Colman, E.; Ding, Z. *RSC Advances* **2013**, *3*, 19961–19964. (b) Chirdon, D. N.; Transue, W. J.; Kagalwala, H. N.; Kaur, A.; Maurer, A. B.; Pintauer, T.; Bernhard, S. *Inorg. Chem.* **2014**, *53*, 1487–1499. (c) Zhao, Q.; Liu, S.; Shi, M.; Li, F.; Jing, H.; Yi, T.; Huang, C. *Organometallics* **2007**, *26*, 5922–5930. (d) Corio, P.; Rubin, J. C.; *J. Phys. Chem.* **1995**, *99* 13217–13223. (e) Winkler, K.; Płońska, M. E.; Rećko, K.; Dobrzyński, L. *Electrochimica Acta* **2006**, *51*, 4544–4553.

[23] (a) van Koten, G.; Terheijden, J.; van Beek, J. A. M.; Wehman- Ooyevaar, I. C. M.; Muller, F.; Stam, C. H. *Organometallics* **1990**, *9*, 903–912. (b) Van Zyl, G. J.; Lamprecht, G. J.; Leipoldt, J. G. *Inorg. Chim. Acta* **1987**, *129*, 35–37. (c) Canty, A. J. *Acc. Chem. Res*. **1992**, *25*, 83–90. (d) Bickelhaupt, F. M.; Baerends, E. J.; Ravenek, W. *Inorg. Chem*. **1990**, *29*, 350–354. (e) Braunstein, P.; Chauvin, Y.; Fischer, J.; Olivier, H.; Strohmann, C.; Toronto, D. V. *New J. Chem*. **2000**, *24*, 437–445. (f) Cuervo, D.; Díez, J.; Gamasa, M. P.; Gimeno, J.; Paredes, P. *Eur. J. Inorg. Chem*. **2006**, 599–608. (g) Collman J. P.; Hegedus, L. S.; Norton, J. R.; Finke, R. G. *Principles and Applications of Organotransition Metal Chemistry,* University Science Books; Mill Valley: California, 1987. (h) Crabtree, R. H. *The Organometallic Chemistry of the Transition Metals*, 4th ed.; Wiley: New Jersey, 2005. (i) Rendina, L. M.; Puddephatt, R, J. *Chem. Rev*. **1997**, *6*, 1735–1754 (j) Cook, P. M.; Dahl, L. F.; Hopgood, D.; Jenkins, R. A. *J. Chem. Soc. Dalton Trans.* **1973**, 294–301.

[24] (a) Rogachev, A. Y.; Hoffmann, R. *J. Am. Chem. Soc*. **2013**, *135*, 3262–3275. (b) Alsters, P. L.; Engel, P. F.; Hogerheide, M. P.; Copijn, M.; Spek, A. L.; van Koten, G. *Organometallics* **1993**, *12*, 1831–1844.

[25] (a) Skinner, C. E.; Jones, M. M. *J. Am. Chem. Soc*. **1969**, *91*, 4405–4408. (b) Bickelhaupt, F. M.; Baerends, E. J.; Ravenek, W. *Inorg. Chem*. **1990**, *29*, 350–354. (c) Morgan, K. A.; Jones, M. M. J. *Inorg. Nucl. Chem*. **1972**, *34*, 275–296 (d) Jones, M. M.; Morgan, K. A. J. *Inorg. Nucl. Chem*. **1972**, *34*, 259–274. (e) Van Zyl, G. J.; Lamprecht, G. J.; Leipoldt, J. G. *Inorg. Chim. Acta* **1987**, *129*, 35–37.

[26] (a)Grice, K. A.; Scheuermann, M. L.; .Goldberg, K. I.; *Top. Organomet .Chem*. **2011**, 35, 1–28. (b) Puddephatt, R, J. *Angew. Chem. Int. Ed*. **2002**, *41*, 261–263.

[27] (a) Pruchnik, F. P.; Jutarska, A.; Ciunik, Z.; Pruchnik, M. *Inorg. Chim. Acta* **2004**, *357*, 3019–3026. (b) Rak, M.; Pruchnik, F. P.; Ciunik, L. Z.; Lafolet, F.; Chardon-Noblat, S.; Deronzier, A. *Eur. J. Inorg. Chem.* **2009**, *2009*, 111–118. (c) Ollagnier, C. M. A.; Perera, S. D.; Fitchett, C. M.; Draper, S. M. *Dalton Trans.* **2008**, 283–290. (d) Baker, A. T.; Tikkanen, W. R.; Kaska, W.C.; Ford, P. C. *Inorg. Chem*. **1984**, *23*, 3254–3256.

[28] (a) Otto S.; Roodt, A. *Acta Cryst.* **2002**, *C58*, m565–m566. (b) Panthi, B. D.; Gipson, S. L.; Franken, A. *Organometallics* **2010**, *29*, 5890–5896. (c) Magriz, A.; Gómez-Bujedo, S.; Álvarez, E.; Fernández, R.; Lassaletta, J. M. *Organometallics* **2010**, *29*, 5941–5945. (d) Adams, C. J.; Baber, R. A.; Connelly, N. G.; Harding, P.; Hayward, O. D.; Kandiah, M.; Orpen, A. G. *Dalton Trans.* **2007**, 1325–1333. (e) Yang, L.; Krüger, A.; Neels, A.; Albrecht, M. *Organometallics* **2008**, *27*, 3161–3171.

[29] (a) Tanase, T.; Yoshii, A.; Otaki, R.; Nakamae, K.; Mikita, Y.; Kure, B.; Nakajima, T. *J. Organomet. Chem*. **2015**, *797*, 37–45. (b) Ito, J.; Miyakawa, T.; Nishiyama H. *J. Organomet. Chem*. **2015**, *794*, 318–322. (c) Arras, J.; Speth, H.; Mayer, H. A.; Wesemann, L. *Organometallics* **2015**, *34*, 3629–3636.

[30] (a) Gómez, F. J.; Kamber, N. E.; Deschamps, N. M.; Cole, A. P.; Wender, P. A.; Waymouth, R. M. *Organometallics* **2007**, *26*, 4541–4545. (b) Barcelo, F. L.; Besteiro, J. C.; Lahuerta, P.; Foces-Foces, C.; Cano, F. H.; MartinezRipoll, M. *J. Organomet. Chem*. **1984**, *270*, 343–351.

[30] (c) English, R. B. de V. Steyn. M. M.; Haines, R. J. *Polyhedron* **1987**, *6,* 1503–1507. (d) Barcelo, F. L.; Lahuerta, P.; Udela, M. A. *J. Organomet. Chem*. **1988**, *7*, 584–590.

[31] Cherkasov, V. K.; Druzhkov, N.O.; Kocherova, T. O.; Shavyrin, A. S.; Fukin, G. K. *Tetrahedron* **2012**, 68, 1422–1426.

[32] Connelly, N. G.; Geiger, W. E. *Chem. Rev.* **1996**, 96, 877–910.

[33] SMART Software Users Guide, Version 5.1, Bruker Analytical X-Ray Systems, Inc.; Madison, WI 1999.

[34] SAINT Software Users Guide, Version 6.0, Bruker Analytical X-Ray Systems, Inc.; Madison, WI 1999

[35] G. M. Sheldrick, SADABS, Version 2.10, Bruker Analytical X-Ray Systems, Inc.; Madison, WI 2002.

[36] G. M. Sheldrick, SHELXTL Version 6.12, Bruker Analytical X-Ray Systems, Inc.; Madison, WI 2001

[37] *International Tables for X-Ray Crystallography* 1992, Vol. C., Dordrecht: Kluwer Academic Publishers.

Chapter 3

Octahedral Ruthenium(II) Complexes of the Redox-Active Catecholate

and Bipyridine Ligands

3.1 Introduction

Transition metal complexes with controlled charge-transfer (CT) properties are of continuous research interest in photocatalysis[1] and solar-energy conversion.[2,3] Among various coordination complexes, donor-acceptor complexes of mixed redox-active ligands offer fundamentally intriguing CT patterns defined by tunable absorptive and electronic characteristics, solvatochromism, and relatively long-lived excited-states.[4,5] Classical donor-acceptor systems are exemplified by square-planar complexes of group 10 metals coordinated by a set of two electronically different quinonato ligands: the fully reduced catecholate (or dithiolate) ligand (donor) and the fully oxidized *ortho*-diiminoquinone ligand (acceptor).[4,5] Inherently, these square-planar complexes support ligand-to-ligand charge-transfer (LL'CT) excited states where the pertinent, low-energy transition is derived predominately from the catecholate-based HOMO and the diimine-centered LUMO (catecholate-to-diimine transition). Both orbitals can be tuned independently by chemical manipulations of the respective ligands leading to increased control over the charge-transfer energy. Furthermore, LL'CT is directional in nature and most accessible when the donor-acceptor pair is physically juxtaposed in a coplanar relationship, which in turn facilitates strong electronic coupling of the ligand-based orbitals. As such, the bulk of relevant research has focused on LL'CT systems of group 10 metals where the coplanar ligand arrangement is effectively accommodated by the square-planar, d^8 metal center. However, the same d^8 metal configuration that intrinsically favors LL'CT is also coordinately unsaturated and, thus, can potentially compromise the overall charge-transfer performance through associative ligand-exchange or photochemical quenching pathways.[6]
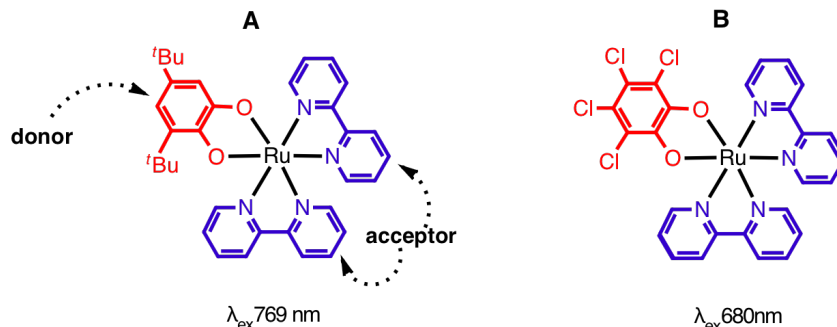
Figure 3.1. Chemical structures of octahedral ruthenium(II) complexes with established LL'CT properties. The individual excitation energies are also shown.

While significantly less explored, non-square planar LL'CT systems, with one redox-active ligand acting as an electron donor and another as an electron acceptor, are also known for octahedral d^6 metal complexes. For example, tunable LL'CT transitions were independently suggested for di- and mononuclear rhodium(III) centers with redox-active ligands.[7] Likewise, visible-energy, ligand-to-ligand charge-transfer is a documented phenomenon with Lever's pioneering studies of non-innocent ruthenium(II)-quinonoid motifs.[8] Lever's ruthenium complexes are shown in Figure 3.1 containing a d^6 metal center coordinated by a single catecholate donor ligand and two identical bipyridine acceptor ligands. As such, the octahedral bis(bipyridine)(catecholate) configuration differs from classical LL'CT complexes in that the donor-acceptor ligand pairs are juxtaposed in a non-coplanar fashion. Hence, the resulting LL'CT transitions were reported to exhibit ill-resolved and weakly intense absorptions ascribed to poor ligand orbital mixing and the large reorganization energy.[8]

In principle, it should be possible to devise a coplanar donor-acceptor configuration for the octahedral d^6 ruthenium ion. This alternative configuration must be designed such that only one catecholate donor ligand and one bipyridine acceptor would be placed in the basal plane of the octahedral metal with the two apical positons accommodated by

59

innocent spectator ligands (e.g. PPh$_3$, Figure 3.2a). In this manner, the classical donor-acceptor configuration reminiscent of group 10 metals could be preserved for directional ligand-to-ligand charge transfer. The resulting system may offer the joint benefits of better controlled CT performance common to the d^8 metals and the substitutionally inert environment common to the d^6 metals.

(a)   R = H (**12a**); Br (**13a**)

(b)   R = H (**12b**); Br (**13b**)
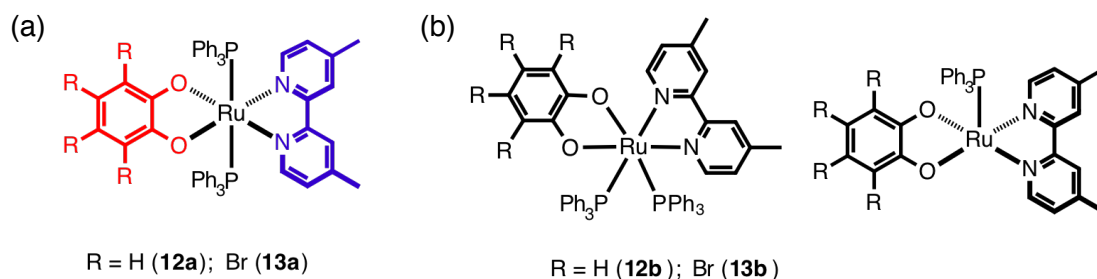
Figure 3.2. (a) Proposed chemical structure of new ruthenium(II) donor-acceptor complexes with coplanar redox-active ligands. (b) Possible structures of ruthenium (II) complexes with alternative arrangements of the same ligands.

In this work, the postulated donor-acceptor framework was targeted for six-coordinate ruthenium centers formulated as (R-cat)Ru(dmbpy)(PPh$_3$)$_2$ (where (PPh$_3$)$_2$ = *trans*-bis(triphenylphosphine); dmbpy = 4,4'-dimethyl-2,2'-bipyridine; R-cat = catecholate (H$_4$-cat) **12a**, tetrabromocatecholate (Br$_4$-cat) **13a**) (Figure 3.2a). New complexes were prepared by sequential coordination of the two types of redox-active ligands to Ru(PPh$_3$)$_3$Cl$_2$, leading to retention of one or both triphenylphosphine ligand(s) as innocent spectators. Preliminary characterization is described for individual complexes of the general formula (R-cat)Ru(dmbpy)(PPh$_3$)$_n$ (where (PPh$_3$)$_n$ = mono or bis(triphenylphosphine) with undefined juxtaposition; R-cat = H$_4$-cat (**12**), Br$_4$-cat (**13**)), which was achieved by a combination of mass spectrometry, spectroscopy, electrochemistry, and X-ray crystallographic methods. Thus far, the findings suggest conflicting assignments of the ruthenium(II) coordination environment: X-ray diffraction

patterns unequivocally disclosed octahedral coordination complexes with non-coplanar donor-acceptor pairs and their spectator ligands shown as *cis*-disposed whereas the solution spectroscopic data produced ambiguity in the structure-type assignment. Further studies are in need to resolve the observed contradictions.

3.2 Results and Discussion

3.2.1 Synthesis and Characterization

The new complexes were prepared by sequential installation of the two redox-active ligands on a ruthenium(II) center, as described in Scheme 3.1. Coordination of the individual catechol proligands to Ru(PPh$_3$)$_3$Cl$_2$ was achieved in the presence of *tert*-butylamine, leading to room-temperature displacement of the two chlorides to produce five-coordinate (R-cat)Ru(PPh$_3$)$_3$ complex (where R-cat is catecholate **11a** or tetrabromocatecholate **11b**). Coordination of the diimine ligand to **11** required heating an equimolar toluene mixture of the 5-coordinate synthon and 4,4'-dimethyl-2,2'-bipyridine at 120 °C. To avoid retention of free triphenylphosphine, which is produced stoichiometrically in the latter step, the solid (R-cat)Ru(dmbpy)(PPh$_3$)$_n$ products were subjected to thorough washings with diethyl ether. The chemical identities of the isolated compounds were verified by electrospray ionization-mass spectrometry (ESI-MS). It should be noted that the chemical structures for putative complexes **12b** and **13b** (where (PPh$_3$)$_2$ = *cis*-bis(triphenylphosphine)) are suggested in Scheme 3.1 on the basis of their X-ray diffraction data. Additional species with different coordination numbers or in a different coordination environment may also exist, as shown in Figure 3.2).

Scheme 3.1 Two-step synthesis of (R-cat)Ru(dmbpy)(PPh$_3$)$_n$ complexes from Ru(PPh$_3$)$_3$Cl$_2$.

11a: 75%   **11b**: 48%
12b: 84%   **13b**: 72%
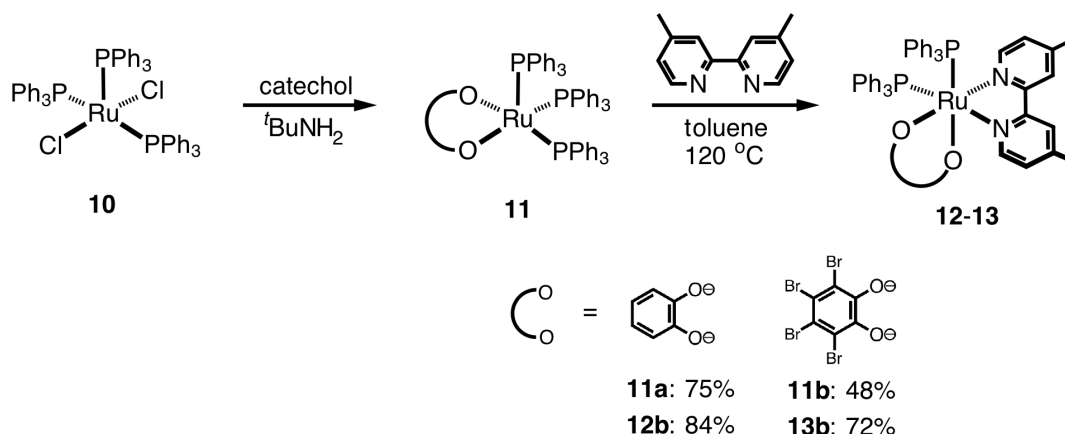
High-quality, single crystals of (R-cat)Ru(dmbpy)(PPh$_3$)$_n$ complexes were obtained by liquid-liquid diffusion-assisted crystallization. The confirmed structures are shown as ORTEP diagrams in Figure 3.3 with the bond angles and distances included in Table 3.1. In both cases, the Ru center revealed pseudo-octahedral geometry comprised of *cis*-disposed auxiliary ligands and the catecholate-bipyridine pair juxtaposed in a non-coplanar arrangement. As shown, the equatorial coordination set is occupied by the dmbpy ligand, one of the dioxolenyl donor atoms, and the monodentate spectator ligand. For (H$_4$-cat)Ru(dmbpy)(PPh$_3$)$_2$ (**12b**), the equatorial site associated with the spectator ligand is filled by one of the two triphenylphosphine groups. The analogous site shows an acetonitrile molecule *in lieu* of PPh$_3$ for the structure derived from (Br$_4$-cat)Ru(dmbpy)(PPh$_3$)$_2$ (**13b**), which had most likely displaced the phosphine ligand during crystal growth to yield (Br$_4$-cat)Ru(dmbpy)(PPh$_3$)(CH$_3$CN) (**13b'**). In both complexes, the remaining apical sites are coordinated by an independent triphenylphosphine ligand and the second oxygen atom of the catecholate fragment. These sites are defined by the O(2)-Ru(1)-P(1) angle of 171.05(6)° in **12b** and 177.32(4)° in **13b'** (Figure 3.3). The *cis-*

62

disposed PPh$_3$ ligands in the former complex are characterized by a large angular distortion pertaining to the P(2)-Ru(1)-P(1) angle of 101.84(3)°, where the axial phosphine is shown tilted away from the equatorial counterpart. In comparison to **12b**, the inclusion of equatorial CH$_3$CN group revealed a marked contraction of the N(3)-Ru(1)-P(1) angle for **13b'** (93.83(5)°).
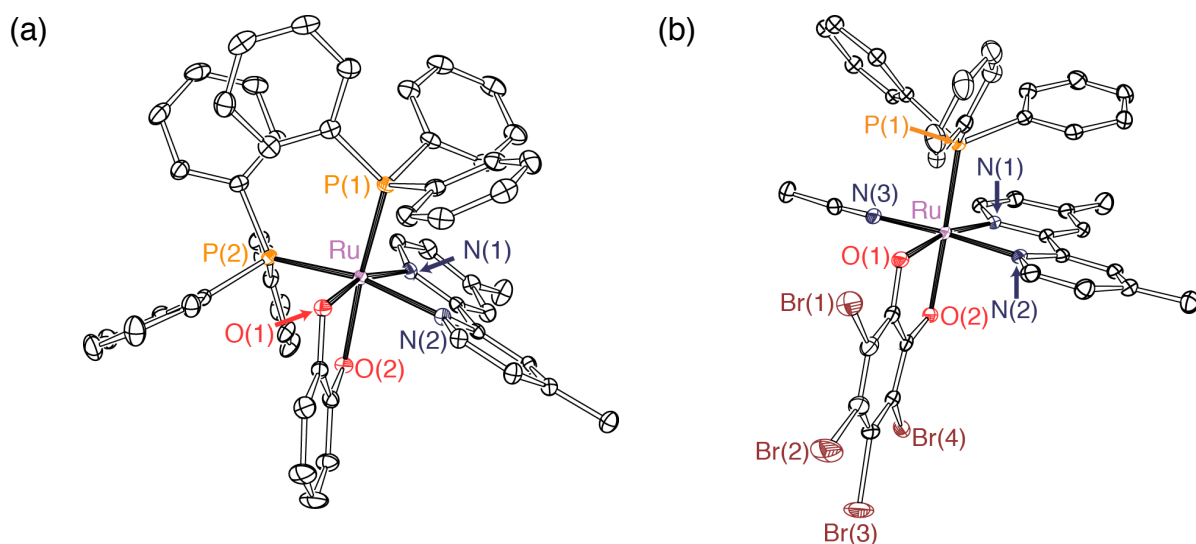
Figure 3.3. ORTEP diagrams of (a) (H$_4$-cat)Ru(dmbpy)(PPh$_3$)$_2$ (**12b**) and (b) (Br$_4$-cat)Ru(dmbpy)(PPh$_3$)(CH$_3$CN) (**13b'**). Ellipsoids are shown at 50% probability. Hydrogen atoms and solvent molecules have been omitted for clarity.

The ligand bond metrics were in support of the ground-state structures having the catecholate donor ligand in the fully reduced form and the dmbpy acceptor ligand in the fully oxidized form. Specifically, the C–C and N–C bond distances of the individual dmbpy ligands match the range observed for other bipyridine complexes of ruthenium(II).[9] The C–O bonds of the parent catechol average 1.339(4) Å for (H$_4$-cat)Ru(dmbpy)(PPh$_3$)$_2$, which is within the range expected for dianionic catecholates on ruthenium ions.[10] Likewise, the average ligand C–C bond distance (1.393(5) Å) at the positions that would be assignable to localized double bonds, defined by the C(14)-C(15) and C(16)-C(17) bonds, is slightly longer than the average C–C bond distance of reported ruthenium-semiquinonate

structures.[11]   The analogous average C–O and C–C bond distances for the brominated

species (**13b'**) are 1.318(2) Å and 1.407(3) Å, respectively.   Once again the pertinent

distances are in accordance with the pattern of bond lengths found for other dianionic

tetrahalocatecholate ligands on ruthenum centers.[12]

Table 3.1. Selected Metrical Parameters for the Solid-State Structures of $(H_4\text{-cat})Ru(dmbpy)(PPh_3)_2$ (**12b**) and $(Br_4\text{-cat})Ru(dmbpy)(PPh_3)(CH_3CN)$ (**13b'**).

Bond	Length (Å)	Bond	Angle (deg)	Bond	Length (Å)	Bond	Angle (deg)
Ru(1)-N(1)	2.076(2)	O(2)-Ru(1)-P(1)	171.05(6)	Ru(1)-N(1)	2.0540(17)	O(2)-Ru(1)-P(1)	177.32(4)
Ru(1)-N(2)	2.103(2)	O(1)-Ru(1)-N(1)	163.12(9)	Ru(1)-N(2)	2.0435(16	O(1)-Ru(1)-N(1)	168.46(6)
N(1)-C(5)	1.358(4)	N(2)-Ru(1)-P(2)	165.43(7)	N(1)-C(5)	1.369(2)	N(2)-Ru(1)-N(3)	174.63(7)
N(2)-C(6)	1.359(4)	P(2)-Ru(1)-P(1)	101.84(3)	N(2)-C(6)	1.360(2)	N(3)-Ru(1)-P(1)	93.83(5)
C(5)-C(6)	1.479(4)	O(1)-Ru(1)-N(2)	87.55(9)	C(5)-C(6)	1.467(3)	O(1)-Ru(1)-N(2)	92.42(6)
Ru(1)-O(1)	2.076(2)	N(1)-Ru(1)-N(2)	77.88(9)	Ru(1)-O(1)	2.0831(14)	N(1)-Ru(1)-N(2)	79.38(7)
Ru(1)-O(2)	2.094(2)			Ru(1)-O(2)	2.1162(14)		
O(1)-C(13)	1.342(4)			O(1)-C(13)	1.320(2)		
O(2)-C(18)	1.337(4)			O(2)-C(18)	1.316(2)		
C(13)-C(18)	1.429(4)			C(13)-C(18)	1.439(3)		
C(14)-C(15)	1.397(5)			C(14)-C(15)	1.408(3)		
C(15)-C(16)	1.386(5)			C(15)-C(16)	1.386(3)		
C(16)-C(17)	1.389(5)			C(16)-C(17)	1.406(3)		
C(17)-C(18)	1.403(4)			C(17)-C(18)	1.400(3)		
Ru(1)-P(1)	2.2981(8)			Ru(1)-P(1)	2.2834(6)		
Ru(1)-P(2)	2.3461(8)			Ru(1)-N(3)	2.0312(18)		

The structural characteristics of $(R\text{-cat})Ru(dmbpy)(PPh_3)_n$ complexes were probed

by NMR spectroscopic techniques. As shown in Figure 3.4a, the ^1H NMR spectrum of $(H_4\text{-}$

cat$)Ru(dmbpy)(PPh_3)_n$ (**12**) collected in $CDCl_3$ produced broad and difficult-to-assign

patterns of aromatic resonances, the bulk of which must be due to triphenylphosphine

protons. The alkyl region of the spectrum, where dimethyl substitution of the dmbpy-

ligand backbone is expected, revealed a poorly resolved combination of broad resonances

around 2.34 and 2.24 ppm. The ^{31}P NMR spectrum of $(H_4\text{-cat})Ru(dmbpy)(PPh_3)_n$ was

dominated by a set of two well-defined resonances at 25.3 ppm and –4.1 ppm, with the latter signal being close to that of free triphenylphosphine (–4.0 ppm). Altogether, the NMR data of **12** appeared to deviate from the spectral pattern of the C_1-symmetric structure (**12b**) we had confirmed initially through our X-ray diffraction data (Figure 3.3a). The absence of two individual resonances in the ^{31}P NMR spectrum of putative (H_4-cat)Ru(dmbpy)(PPh$_3$)$_2$, which would be consistent with non-equivalent nuclei of the *cis*-disposed PPh$_3$ groups, points to the likelihood of alternative conformers being prevalent in solution. The sharp signal at 25.3 ppm is indicative of ruthenium species that either possess a set of two equivalent ^{31}P nuclei or only one ^{31}P nucleus. The former possibility would be in accordance with (H_4-cat)Ru(dmbpy)(PPh$_3$)$_2$ displaying C_{2v} symmetry in solution, where the two PPh$_3$ ligands must be mutually *trans* (**12a**) (Figure 3.2a). Alternatively, dissociation of PPh$_3$ from the six-coordinate complex to yield a five-coordinate metal center of type (H_4-cat)Ru(dmbpy)PPh$_3$ would help explain the single ^{31}P nucleus situtation (Figure 3.2b). This contention is further supported by the minor signal seen at –4.1 ppm (free PPh$_3$).

The structural features of (Br$_4$-cat)Ru(dmbpy)(PPh$_3$)$_n$ (**13**) proved challenging to identify by solution NMR spectroscopy. As shown in Figure 3.4b, the ^{1}H NMR spectrum of the room-temperature sample was silent. Likewise, the ^{31}P NMR spectrum of **13** was rather uninformative displaying no detectable signals apart from the previously seen singlet at –4.1 ppm that is once again ascribable to free triphenylphosphine. The labile nature of the bulky phosphine ligands was independently verified by X-ray crystallographic analysis of **13**, which clearly revealed retention of only one of the two PPh$_3$ groups within the six-coordinate environment of **13** and exchange of another for the CH$_3$CN ligand (Figure 3.3b).

Altogether, the results in Figure 3.4b suggest that **13** must be involved in a rapid ligand exchange process in solution that is unobservable on an NMR time scale. Temperature-dependent NMR studies of the (R-cat)Ru(dmbpy)(PPh$_3$)$_n$ complexes will be necessary to help identify the nature of solution-based dynamics.
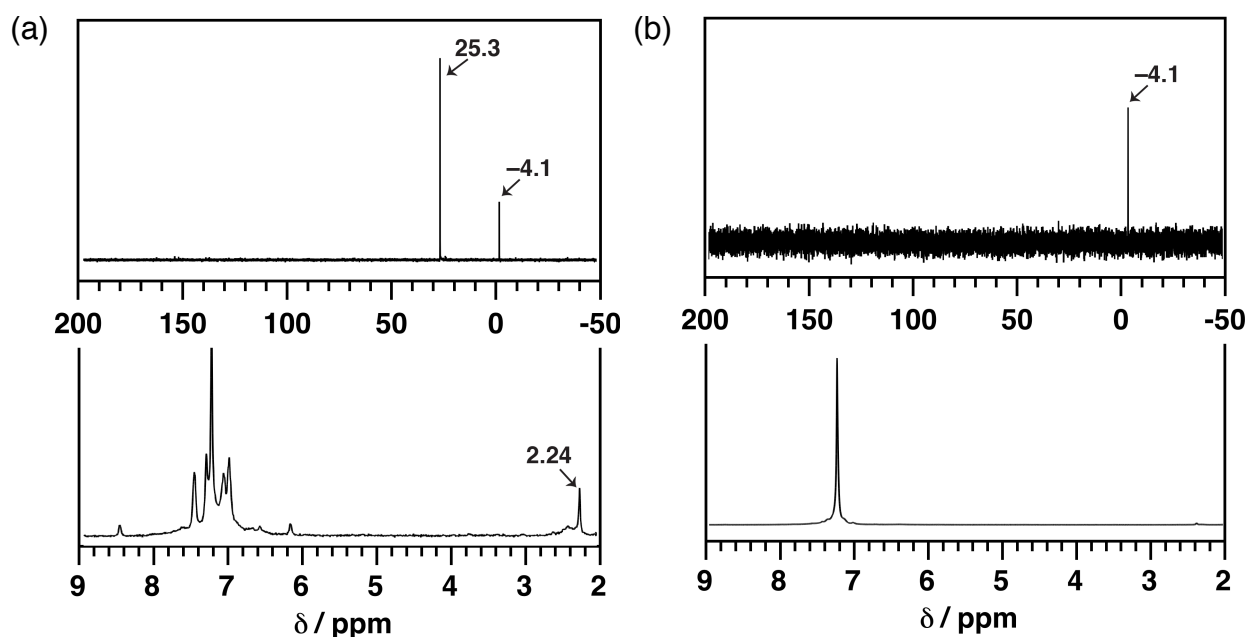
Figure 3.4. ^{1}H and ^{31}P NMR spectra of (a) (H$_4$-cat)Ru(dmbpy)(PPh$_3$)$_n$ (**12**) and (b) (Br$_4$-cat)Ru(dmbpy)(PPh$_3$)$_n$ (**13**) collected in CDCl$_3$ at 298K.

3.2.2 Absorptive Characteristics of (R-cat)Ru(dmbpy)(PPh$_3$)$_n$ Complexes

The new ruthenium complexes were subjected to absorption spectroscopic analysis in order to gain further insight into their solution characteristics. The individual absorption spectra for (H$_4$-cat)Ru(dmbpy)(PPh$_3$)$_n$ (**12**) and (Br$_4$-cat)Ru(dmbpy)(PPh$_3$)$_n$ (**13**) are included Figure 3.5, collected in CH$_2$Cl$_2$ at 298K. The spectral region of **13** was comprised of one visible- and one NIR-energy electronic transitions with well-defined maxima displayed at 610 and 927 nm, respectively. The relative intensities of the two bands proved to vary in the presence of significant quantities of PPh$_3$ (1000 eq), leading to a marked increase in the 610 nm band and decrease in the 927 nm band (Figure 3.5b). The

observed changes indicate an equilibrium between at least two types of ruthenium species, which could be the five- and six-coordinate forms accessed through dissociation of the triphenylphosphine ligand. Accordingly, the lower coordination number (927 nm) and the higher coordination number (610 nm) of Ru^{II} center may both exist at room temperature, at low analyte concentrations in CH_2Cl_2 ($\leq$ 0.03 µM), whereas with excess PPh_3 the six-coordinate environment of type $(Br_4\text{-cat})Ru(dmbpy)(PPh_3)_2$ may be more favored.
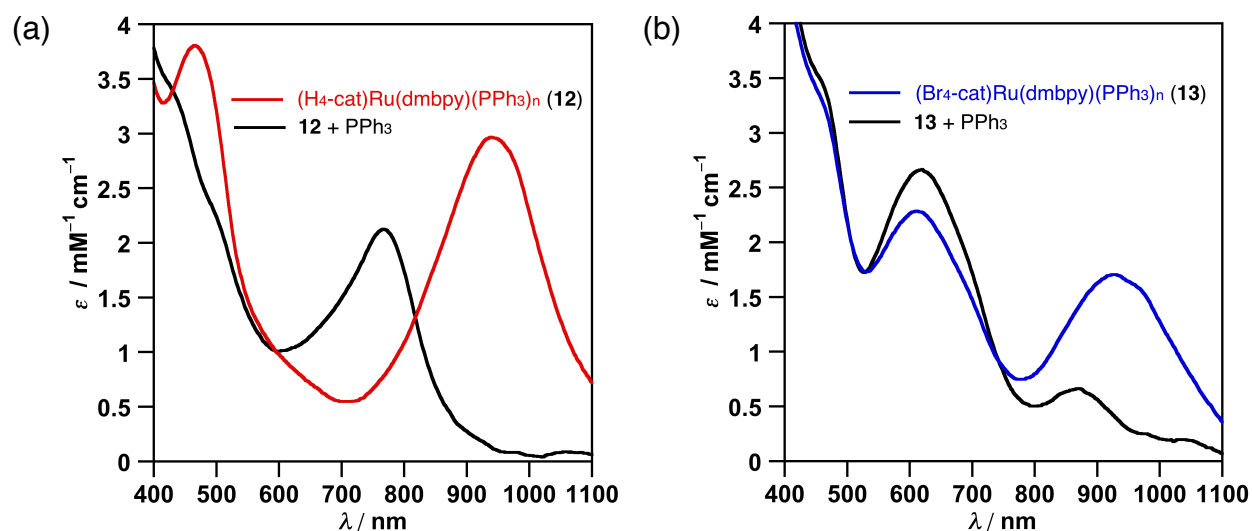
Figure 3.5. UV-vis-NIR absorption spectra of (a) $(H_4\text{-cat})Ru(dmbpy)(PPh_3)_n$ (**12**) and (b) $(Br_4\text{-}$ cat$)Ru(dmbpy)(PPh_3)_n$ (**13**) in CH_2Cl_2 at 298K. Both spectra are shown with and without 1000 equivalents of PPh_3. Molar extinction coefficients were estimated using the six-coordinate structure.

The electronic absorption spectrum of $(H_4\text{-cat})Ru(dmbpy)(PPh_3)_n$ (**12**) revealed one vis-NIR transition at 940 nm and one visible-energy transition at 450 nm (Figure 3.5a). Analogous to the solution electronic absorption experiments performed on complex **13**, addition of excess PPh_3 to the CH_2Cl_2 sample of **12** gave a significantly blue-shifted absorption band at 777 nm. The emergence of the new band was accompanied by depletion of the optical intensity associated with the 940- and 450-nm absorptions. Hence, both of the initially seen electronic transitions are most likely derived from the same

species of **12**, the electronic and structural integrity of which is sensitive to the presence of excessive amounts of PPh_3.
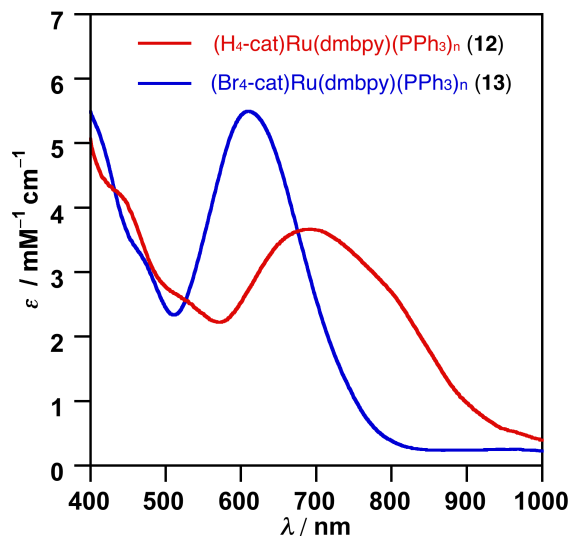
Figure 3.6. UV-vis-NIR absorption spectra of (a) $(H_4\text{-cat})Ru(dmbpy)(PPh_3)_n$ (**12**) and (b) $(Br_4\text{-cat})Ru(dmbpy)(PPh_3)_n$ (**13**) in THF at 298K. Respective molar extinction coefficients were estimated from the six-coordinate structure.

For comparison, the absorptive properties of $(R\text{-cat})Ru(dmbpy)(PPh_3)_n$ complexes were examined in THF solutions at 298K. As shown in Figure 3.6, the spectra of **12** and **13** were each dominated by one main electronic transition in the vis-NIR-energy range. The former complex (**12**) revealed a broad absorption band feature with a lambda maximum at 692 nm (3670 $M^{-1}cm^{-1}$). The vis-NIR spectrum of the brominated variant (**13**) showed a more narrow and blue-shifted transition with a maximum absorption displayed at λ_{max} = 612 nm (5490 $M^{-1}cm^{-1}$). The absence of additional electronic transitions for either $(H_4\text{-cat})Ru(dmbpy)(PPh_3)_n$ (**12**) or $(Br_4\text{-cat})Ru(dmbpy)(PPh_3)_n$ (**13**) suggests that only one type of coordination environment is favored for ruthenium in THF. On closer inspection, it can be seen that the individual band energies for the same complexes in THF compare well to the blue-shifted absorptions in CH_2Cl_2, which were postulated to be derived from the six-coordinate ruthenium species.

3.2.3 Electrochemical Behavior of (R-cat)Ru(dmbpy)(PPh$_3$)$_n$ Complexes
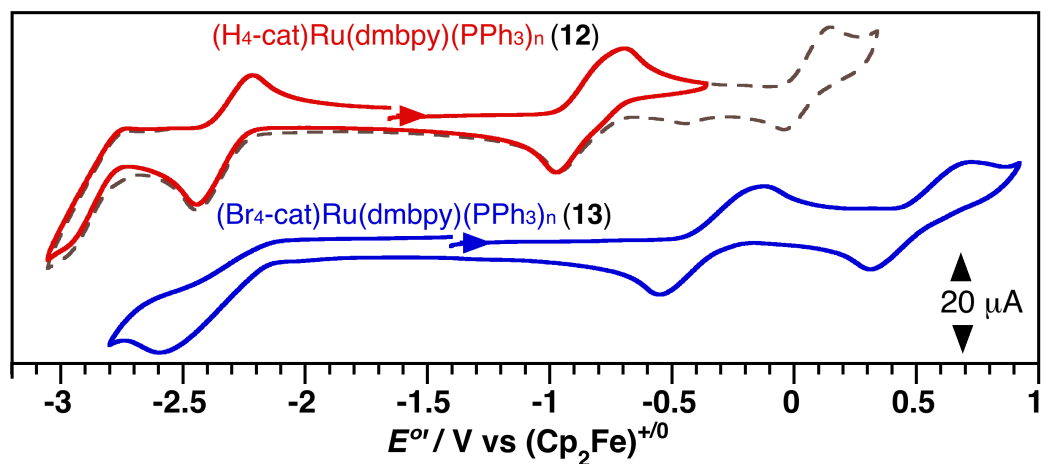
Figure 3.7. Cyclic voltammograms of (H$_4$-cat)Ru(dmbpy)(PPh$_3$)$_n$ (**12**) and (Br$_4$-cat)Ru(dmbpy)(PPh$_3$)$_n$ (**13**) recorded in THF. Measurements were made at a scan rate of 200 mV/s with 1.0 mM analyte and 0.10 M [^{n}Bu$_4$N][PF$_6$]. Potentials referenced to Cp$_2$Fe$^{+/0}$ couple.

The ground-state redox properties of (R-cat)Ru(dmbpy)(PPh$_3$)$_n$ complexes were elucidated in solution. Figure 3.7 compares the cyclic voltammograms (CVs) of the complexes measured in THF with a glassy carbon electrode and a 0.1 M [^{n}Bu$_4$N][PF$_6$] electrolyte. The relevant electrochemical potentials for both complexes are listed in Table 3.2. The reduction window of (H$_4$-cat)Ru(dmbpy)(PPh$_3$)$_n$ (**12**) was comprised of a partially reversible event at –2.33 V and an irreversible event at –2.96 V (versus Cp$_2$Fe$^{+/0}$ couple). In regards to (Br$_4$-cat)Ru(dmbpy)(PPh$_3$)$_n$ (**13**), analogous reductions were found with irreversible characteristics at –2.35 V and –2.92 V (the redox potential of the latter event was detectable through differential pulse voltammetry but was obscured by the reductive edge of the CV window). The cathodic potential sets are virtually identical between the two complexes and, thus, must be due to the transfer of two successive electrons into the dmbpy ligand. A set of two well-behaved oxidations was also observed for both ruthenium species. Complex (H$_4$-cat)Ru(dmbpy)(PPh$_3$)$_n$ (**12**) showed a reversible redox wave at –0.89 V and

another partially reversible, oxidation centered around 0.00 V. The second complex, (Br$_4$-cat)Ru(dmbpy)(PPh$_3$)$_n$ (**13**), revealed comparably reversible yet anodically shifted oxidations at −0.44 V and 0.38 V. The respective shifts in potentials are significantly different, between **12** and **13** (± 450; ± 380 mV), suggestive of strong dependence of each redox event on the catecholate ligand substitution. Though ruthenium-centered oxidations cannot be ruled out at this point, the observed shifts are in accordance with the Hammett σ rule and may involve the [R-cat/R-sq$^\bullet$]$^+$ and [R-sq$^\bullet$/R-q]$^{2+}$ redox couples.[10a,13] In both complexes multiple, ill-behaved anodic events were additionally detectable beyond the 1.0 V potential range (not shown), which could be the product of metal- and/or ligand-based oxidations.

Table 3.2. Electrochemical Potentials for (H$_4$-cat)Ru(dmbpy)(PPh$_3$)$_n$ (**12**) and (Br$_4$-cat)Ru(dmbpy)(PPh$_3$)$_n$ (**13**) in THF.[a]

complex	$E_1^{\circ\prime}$	$E_2^{\circ\prime\,b}$	$E_3^{\circ\prime}$	$E_4^{\circ\prime}$
12	−2.96	−2.33	−0.89	0.00
13	−2.92	−2.35	−0.44	0.38

[a]All potentials were referenced to Cp$_2$Fe$^{+/0}$. [b]This reduction process had a significant enough return current to be measured as $E_{1/2}$ for compounds **12** but is reported as E_{pc} for **13**.

3.2.4 Preliminary Interpretation

Definitive identification of (R-cat)Ru(dmbpy)(PPh$_3$)$_n$ species proved challenging to establish thus far. The solid-state structure of (H$_4$-cat)Ru(dmbpy)(PPh$_3$)$_2$ (**12**) revealed a six-coordinate ruthenium center containing *cis*-disposed PPh$_3$ ligands and non-coplanar arranged catecholate and bipyridine ligands. The verified C$_1$-symmetric configuration for **12** was in contradiction to the ^{31}P NMR data that was more consistent with (H$_4$-cat)Ru(dmbpy)(PPh$_3$)$_2$ possessing C$_{2v}$ symmetry in CDCl$_3$. In addition, the ^{31}P NMR data showed signs of uncoordinated PPh$_3$, signaling that ligand dissociation from **12** to give a

five-coordinate complex is also plausible. The postulated, five-coordinate product was not observable through electrospray ionization-mass spectrometry, though it cannot be ruled out at the moment. Altogether, the data points to more than one type of species being present for $(H_4\text{-cat})Ru(dmbpy)(PPh_3)_n$ (**12**).

X-ray crystallographic analysis of the species derived from $(Br_4\text{-cat})Ru(dmbpy)(PPh_3)_n$ (**13**) revealed a six-coordinate ruthenium center with non-coplanar arranged catecholate and bipyridine ligands. Furthermore, the *cis*-disposed auxiliary ligands of the complex included one CH_3CN molecule and one PPh_3 ligand, which indicated that the bulky phosphine groups are amenable toward ligand exchange. The NMR data in $CDCl_3$ showed dynamic behavior for **13** with signs of uncoordinated PPh_3 as the only detectable species. This observation was in further support of $(Br_4\text{-cat})Ru(dmbpy)(PPh_3)_n$ participating in rapid dissociation-reassociation ligand exchange processes. Though undetectable through NMR spectroscopy, the identity of six-coordinate $(Br_4\text{-cat})Ru(dmbpy)(PPh_3)_2$ complex was confirmed by electrospray ionization-mass spectrometry. Further analysis will be necessary to establish the elusive solution configuration(s) of **13**.

Ambiguity in the structural identification of $(R\text{-cat})Ru(dmbpy)(PPh_3)_n$ complexes made it difficult to assign their charge-transfer properties. The C_{2v}-symmetric configuration of octahedral complexes **12a** and **13a** would result in the low-energy LL'CT transitions (π cat $\rightarrow$ π^* bpy) whereas the C_1-symmetric configuration of octahedral complexes **12b** and **13b** would favor the low-lying MLCT transitions ($Ru^{II} \rightarrow \pi^*$ bpy). This prediction does not propose mutually exclusive excited states but only suggests that the ground-state, electronic configuration of the ruthenium complex should dramatically

influence the charge-transfer character and the extent to which it would manifest. The individual (R-cat)Ru(dmbpy)(PPh$_3$)$_n$ complexes showed only one, well-resolved electronic transition in the vis-NIR range of the electromagnetic spectrum when they were examined in THF. However, the exact nature of charge-transfer cannot be deduced for either **12** or **13** given the current uncertainty associated with their individual structures. The CT elucidation was further complicated by the proclivity of the electronic transitions to show sensitivity toward PPh$_3$, when examined in CH$_2$Cl$_2$.

3.3 Summary

In the present study, a non-classical LL'CT molecular design was pursued with ruthenium(II) centers of the redox-active catecholate donor and bipyridine acceptor ligands. The relevant donor-acceptor CT pair was sought in a coplanar configuration at octahedral ruthenium centers defined as (R-cat)Ru(dmbpy)(PPh$_3$)$_2$ (where (PPh$_3$)$_2$ = *trans*-bis(triphenylphosphine); dmbpy = 4,4'-dimethyl-2,2'-bipyridine; R-cat = catecholate (H$_4$-cat) **12a**, tetrabromocatecholate (Br$_4$-cat) **13a**). Sequential coordination of the two redox-active ligands to Ru(PPh$_3$)$_3$Cl$_2$ yielded new complexes with the general formula (R-cat)Ru(dmbpy)(PPh$_3$)$_n$ (where (PPh$_3$)$_n$ mono or bis(triphenylphosphine); R-cat = H$_4$-cat (**12**) or Br$_4$-cat (**13**)). X-ray quality crystals of the individual products indicated that both contain Ru^{II} in a six-coordinate octahedral environment with non-coplanar donor-acceptor pairs. However, characterization of the putative products by solution spectroscopic techniques provided evidence that alternative ruthenium configurations must also be accessed, as suggested through their absorptive properties and the NMR data. In general, the complexes yielded well-behaved redox chemistry characterized by significant

differences between their oxidation potentials but minor differences between their reduction potentials.

Further studies could help resolve conflicting details concerning the identities of the (R-cat)Ru(dmbpy)(PPh$_3$)$_n$ complexes. In-depth X-ray crystallography experiments will be necessary to potentially reveal additional ruthenium structures provided that they are stable in the solid state. In addition, it will be critical to probe the solution structure and dynamics for each complex by variable-temperature NMR techniques. Thus far, our findings suggest that the ground-state configuration of the ruthenium(II) ion, with chosen ligand combinations, is a structurally complex system to elucidate. To establish validation of its donor-acceptor CT excited states, a deeper understanding of the structural and electronic parameters must first be achieved.

3.4 Experimental

General Considerations. The complexes described are air- and moisture-sensitive, necessitating their synthesis to be carried out under an inert atmosphere of nitrogen using standard Schlenk, vacuum-line, and glovebox techniques. All reactions were carried out in dry and degassed solvents. Hydrocarbon solvents were sparged with argon and then deoxygenated and dried by passage through Q5 and activated alumina columns, respectively. Ethereal and halogenated solvents were sparged with argon and dried by passage through two activated alumina columns. Tetrabromocatechol, 3,5-di-*tert*-butylcatechol, and 4,4-dimethyl-2,2-bipyridine were purchased from Sigma-Aldrich and used as received. Complexes (PPh$_3$)$_3$RuCl$_2$ (**10**) and (H$_4$-cat)Ru(PPh$_3$)$_3$ (**11a**) were reported previously[14] though herein compound **11a** was accessed by a new route.

Physical Methods. NMR spectra were collected on Bruker Avance 400 and 500 MHz spectrometers. Chemical shifts were reported using the standard δ notation in parts per million and referenced with residual ^{1}H and ^{13}C isotopic impurities of the solvent. Infrared spectra were recorded as neat solids using a Jasco FT/IR-4700-ATR-PRO ONE Spectrophotometer. Electronic absorption spectra were recorded in dry, degassed THF and CH_2Cl_2 solvents in one-centimeter cuvettes using a Shimadzu UV-1700 Spectrometer.

Electrochemical Methods. Cyclic voltammetry (CV) voltammetry experiments were performed on a Gamry Series G 300 Potentiostat/Galvanostat/ZRA (Gamry Instruments, Warminster, PA, U.S.A.) using a 3.0 mm glassy carbon working electrode, a platinum wire auxiliary electrode, and a silver wire reference electrode. Measurements were recorded in a nitrogen-filled glovebox at ambient temperature and a scan rate of 200 mV/s. Sample concentrations were based on 1.0 mM THF solutions containing 100 mM $[^nBu_4N][PF_6]$ as the supporting electrolyte. All potentials were referenced to the $[Cp_2Fe^{+/0}]$ couple using ferrocene or decamethylferrocene (-0.47 V vs $Cp_2Fe^{+/0}$) as an internal standard.[15] Decamethylferrocene was purified by sublimation under reduced pressure and tetrabutylammonium hexafluorophosphate was recrystallized from ethanol three times and dried under vacuum.

(H_4-cat)Ru(PPh$_3$)$_3$ (11a): Compound **11a** was prepared by an unpublished procedure: to a suspension of (PPh$_3$)$_3$RuCl$_2$ (446 mg, 0.470 mmol) and catechol (52 mg, 0.47 mmol) in CH_2Cl_2 (10 mL) was added *tert*-butylamine (142 µL, 1.88 mmol). After 12 h of stirring at room temperature, the reaction mixture was filtered to remove *tert*-butylamine hydrochloride. The deep blue filtrate was stripped down to a minimum amount of CH_2Cl_2 (2 mL) and diluted with pentane (15 mL) to facilitate precipitation of the product.

The resulting precipitate was collected on a frit, washed with diethyl ether and pentane, and dried under vacuum to afford (H_4-cat)Ru(PPh$_3$)$_3$ as a dark blue solid (325 mg, 75%). The NMR spectra of **11a** are in agreement with the literature data.[14] ^{31}P NMR (162 MHz, CDCl$_3$) δ 55.6; ^{1}H NMR (400 MHz, CDCl$_3$) δ 7.15 (m, 9H), 7.02 (m, 18H), 6.88 (m,18H), 6.82 (dd, J = 5.8, 3.5 Hz, 2H), 6.52 (dd, J = 5.8, 3.5 Hz, 2H); ^{13}C NMR (126 MHz, CDCl$_3$) δ 163.2 (s, C–O), 136.9-136.4 (m, i-C of PPh$_3$), 135.15-135.07, (m, o-CH of PPh$_3$), 129.1 (s, p-CH of PPh$_3$), 127.5-127.4 (m, m-CH of PPh$_3$), 116.8 (s, cat CH), 116.2 (s, cat CH).

(Br_4-cat)Ru(PPh$_3$)$_3$ (11b): To a suspension of (PPh$_3$)$_3$RuCl$_2$ (452 mg, 0.472 mmol) and tetrabromocatechol (201 mg, 0.472 mmol) in CH$_2$Cl$_2$ (10 mL) was added *tert*-butylamine (142 μL, 1.89 mmol). After 12 h of stirring at room temperature, the reaction mixture was filtered to remove *tert*-butylamine hydrochloride. The deep blue filtrate was stripped down to a minimum amount of CH$_2$Cl$_2$ (2 mL) and diluted with pentane (20 mL) to facilitate precipitation of the product. The resulting precipitate was collected on a frit, washed with diethyl ether and pentane, and dried under vacuum to afford (Br_4-cat)Ru(PPh$_3$)$_3$ (**11b**) as a dark blue solid (280 mg, 48%). ^{31}P NMR (162 MHz, CDCl$_3$) δ 53.1; ^{1}H NMR (500 MHz, CDCl$_3$) δ 7.21 (m, 9H), 7.04 (m, 18H), 6.93 (m, 18H); ^{13}C NMR (126 MHz, CDCl$_3$) δ 159.7 (s, C–O), 135.6-135.1 (m, i-CH and o-CH of PPh$_3$), 129.5 (s, p-CH of PPh$_3$), 127.87-127.80 (m, m-CH of PPh$_3$), 112.9 (s, cat C–Br), 111.5 (s, cat C–Br); FTIR (KBr) ν/cm^{-1} 3049, 2971, 2888, 1481, 1263 st, 1080 st, 926 st, 733 st, 693 st; HRMS (ESI) m / z calcd for C$_{60}$H$_{45}$Br$_4$O$_2$P$_3$Ru (M)$^+$ 1311.8391, found 1311.8405.

Preliminary Characterization for (R-cat)Ru(dmbpy)(PPh$_3$)$_n$ Complexes:

(H$_4$-cat)Ru(dmbpy)(PPh$_3$)$_n$ (12): An air-tight, 50 mL Straus tube was charged with (H$_4$-cat)Ru(PPh$_3$)$_3$ (**11a**) (193 mg, 0.193 mmol), toluene (6 mL), and 4,4'-dimethyl-2,2'-bipyridine (36 mg, 0.19 mmol). The reaction vessel was partially evacuated and sealed followed by heating at 120 °C for 12 h. The solvent was stripped down to a minimum amount of toluene (1.5 mL) and recrystallized, under a glovebox atmosphere by addition of pentane (10 mL). The solid was collected on a frit, washed with pentane and diethyl ether, and dried under vacuum to afford (H$_4$-cat)Ru(dmbpy)(PPh$_3$)$_n$ (**12**) as a dark brown solid (150 mg, 84%). X-ray quality crystals of (H$_4$-cat)Ru(dmbpy)(PPh$_3$)$_2$ **12b** were grown by liquid/liquid diffusion of CH$_3$CN containing **12** into CH$_2$Cl$_2$ (–35 °C). ^{31}P NMR (162 MHz, CDCl$_3$) δ 25.3; FTIR (KBr) v/cm^{-1} 3041, 1617, 1472 st, 1430, 1265, 1248 st, 1086 st, 926 st, 724 st; HRMS (ESI) m / z calcd for C$_{54}$H$_{46}$N$_2$O$_2$P$_2$Ru (M)$^+$ 918.2094, found 918.2073.

(Br$_4$-cat)Ru(dmbpy)(PPh$_3$)$_n$ (13): An air-tight, 50 mL Straus tube was charged with (Br$_4$-cat)Ru(PPh$_3$)$_3$ (**11b**) (164 mg, 0.125 mmol), toluene (5 mL), and 4,4'-dimethyl-2,2'-bipyridine (23 mg, 0.13 mmol). The reaction vessel was partially evacuated and sealed followed by heating at 120 °C for 12 h. The solvent was stripped down to 1.5 mL of toluene and recrystallized by addition of pentane (10 mL), under a glovebox atmosphere. The solid was collected on a frit, washed with pentane and diethyl ether, and dried under vacuum to afford **13** as a dark green product (110 mg, 72%). X-ray quality crystals of (Br$_4$-cat)Ru(dmbpy)(PPh$_3$)(CH$_3$CN) (**13b'**) were grown by liquid/liquid diffusion of CH$_3$CN containing **13** into THF (–35 °C). FTIR (KBr) v/cm^{-1} 3051, 1434 st, 1266, 1092 st, 1059 st, 1045, 736 st, 688 st; HRMS (ESI) m / z calcd for C$_{54}$H$_{42}$Br$_4$N$_2$O$_2$P$_2$Ru (M)$^+$ 1233.8478, found 1233.8452.

Crystallographic Methods. X-ray diffraction data were collected on crystals mounted on glass fibers using a Bruker CCD platform diffractometer equipped with a CCD detector. Measurements were carried out at 163 K using Mo Kα (λ = 0.71073 Å) radiation, which was wavelength selected with a single-crystal graphite monochromator. The SMART program package was used to determine unit-cell parameters and to collect data.[16] The raw frame data were processed using SAINT[17] and SADABS[18] to yield the reflection data files. Subsequent calculations were carried out using the SHELXTL[19] program suite. Structures were solved by direct methods and refined on F2 by full-matrix least-squares techniques. Analytical scattering factors for neutral atoms were used throughout the analyses.[20] Hydrogen atoms were included using a riding model. ORTEP diagrams were generated using ORTEP-3 for Windows. Diffraction data are shown in Table 3.3.

Table 3.3. X-ray Diffraction Data-Collection and Refinement Parameters for (H$_4$-cat)Ru(dmbpy)(PPh$_3$)$_2$ (**12b**) and (Br$_4$-cat)Ru(dmbpy)(PPh$_3$)(CH$_3$CN) (**13b'**).

	12b	**13b'**
empirical formula	C$_{54}$H$_{46}$N$_2$O$_2$PRu•CH$_2$Cl$_2$	C$_{42}$H$_{36}$Br$_4$N$_5$O$_2$PRu•(C$_4$H$_8$O)•2(CH$_3$CN)
formula weight	1002.86	1166.24
crystal system	triclinic	triclinic
space group	$P\bar{1}$	$P\bar{1}$
a/Å	11.0674(5)	12.7106(5)
b/Å	11.2682(5)	13.0704(5)
c/Å	19.1105(8)	15.2694(5)
α/deg	96.0595(6)	81.7368(5)
β/deg	98.4595(6)	96.6107(14)
γ/deg	98.8802(6)	68.1120(4)
V/Å^3	2308.93(18)	2220.48(14)
Z	2	2
refl. collected	28927	27915
indep. refl.	11463 (0.0332)	11052 (0.0189)
R1 (I > 2σ)^a	0.0479	0.0275
wR2 (all data)^a	0.1273	0.0635

^{a}R$_1$ = $\sum||F_o| - |F_c||/\sum|F_o|$; wR$_2$ = $[\sum w(F_o^2 - F_c^2)^2/\sum w(F_o^2)^2]^{1/2}$; GOF = $[\sum w(|F_o| - |F_c|)^2/(n - m)]^{1/2}$.

3.5 References

[1] (a) Zheng, B.; Sabatini, R. P.; Fu, W.-F.; Eum, M.-S.; Brennessel, W. W.; Wang, L.; McCamant, D. W.; Eisenberg, R. *Proc. Natl. Acad. Sci.* **2015**, *112*, E3987–E3996. (b) Zhang, D.; Bin, Y.; Tallorin, L.; Tse, F.; Hernandez, B.; Mathias, E. V.; Stewart, T.; Bau, R.; Selke, M. *Inorg. Chem.* **2013**, *52*, 1676–1678. (c) Zarkadoulas, A.; Koutsouri, E.; Mitsopoulou, C. A. *Coord. Chem. Rev.* **2012**, *256*, 2424–2434. (d) Zhang, J.; Du, P.; Schneider, J.; Jarosz, P.; Eisenberg, R. *J. Am. Chem. Soc.* **2007**, *129*, 7726–7727.

[2] (a) Kärkäs, M. D.; Johnston, E. V.; Verho, O.; Åkermark, B. *Acc. Chem. Res.* **2014**, *47*, 100–111. (b) Adeloye, A. O.; Ajibade, P.A. *Molecules* **2014**, *19*, 12421–12460. (c) Hagfeldt, A.; Boschloo, G.; Sun, L.; Kloo, L.; Pettersson, H. *Chem. Rev.* **2010**, *110*, 6595–6663. (d) Grätzel, M. *J. Photochem. and Photobiol. C: Photochem. Rev.* **2003**, *4*, 145–153. (d) Linfoot, C. L.; Richardson, P.; McCall, K. L.; Durrant, J. R.; Morandeira, A.; Robertson, N. *Solar Energy* **2011**, *85*, 1195–1203. (e) Geary, E. A. M.; Yellowlees, L. J.; Jack, L. A.; Oswald, I. D. H.; Parsons, S.; Hirata, N.; Durrant, J. R.; Robertson, N. *Inorg. Chem.* **2005**, *44*, 242–250 (f) Islam, A.; Sugihara, H.; Hara, K.; Singh, L. P.; Katoh, R.; Yanagida, M.; Takahashi, Y.; Murata, S.; Arakawa, H.; Fujihashi, G. *Inorg. Chem.* **2001**, *40*, 5371–5380. (g) Diwan, K.; Chauhan, R.; Singh, S. K.; Singh, B.; Drew, M. G. B.; Bahadur, L.; Singh, N. *New J. Chem.* **2014**, *38*, 97–108. (h) Verma, S.; Kar, P.; Das, A.; Ghosh, H. N. *Chem. Eur. J.* **2011**, *17*, 1561–1568.

[3] (a) Knoll, J. D.; Albani, B. A.; Turro, C. *Acc. Chem. Res.* **2015**, *48*, 2280–2287. (b) Wenger, O. S. *Acc. Chem. Res.* **2013**, *46*, 1517–1526. (c) Schwab, P. F. H.; Diegoli, S.; Biancardo, M.; Bignozzi, C. A. *Inorg. Chem.* **2003**, *42*, 6613–6615. (d) Damas, A.; Gullo, M. P.; Rager, M. N.; Jutand, A.; Barbieri, A.; Amouri, H. *Chem. Commun.* **2013**, *49*, 3796–3798. (e) Grange, C. S.; Meijer, A. J. H. M.; Ward, M. D. *Dalton Trans.* **2010**, *39*, 200–211.

[4] (a) Cocker, T. M.; Bachman, R. E. *Inorg. Chem.* **2001**, *40*, 1550–1556. (b) Chen, C.-T.; Liao, S.-Y.; Lin, K.-J.; Chen, C.-H.; Lin, T.-Y. J. *Inorg. Chem.* **1999**, *38*, 2734–2741. (c) Vogler, A.; Kunkely, H.; Hlavatsch, J.; Merz, A. *Inorg. Chem.* **1984**, *23*, 506–509. (d) Wootoon, J. L.; Zink, J. I. *J. Phys. Chem.* **1995**, *99*, 7251-7257.

[5] (a) Hissler, M.; McGarrah, J. E.; Connick, W. B.; Geiger, D. K.; Cummings, S. D.; Eisenberg, R. *Coord. Chem. Rev.*, **2000**, 208, 115–137. (b) Zuleta, J. A.; Bevilacqua, J. M.; Rehm, J. M.; Eisenberg, R. *Inorg. Chem.* **1992**, *31*, 1332–1337. (c) Cummings, S. D.; Eisenberg, R. *J. Am. Chem. Soc.* **1996**, *118*, 1949–1960. (d) Paw, W.; Cummings, S. D.; Mansour, M. A.; Connick, W. B.; Geiger, D. K.; Eisenberg, R. *Coord. Chem. Rev.* **1998**, *171*, 125–150. (e) Connick, W. B.; Geiger, D.; Eisenberg, R. *Inorg. Chem.* **1999**, *38*, 3264–3265.

[6] (a) Connick, W. B.; Henling; L. M.; Marsh, R. E.; Gray, H. B. *Inorg. Chem.* **1996**, *35*, 6261–6265. (b) Houlding, V. H.; Miskowski, V. M. *Coord. Chem. Rev.* **1991**, *111*, 145–152. (c) Fleeman, W. L.; Connick, W. B. *Comments Inorg. Chem.* **2010**, *23*, 205–230.

[7] (a) Li, Z.; Leed, N. A.; Dickson-Karn, N. M.; Dunbar, K. R.; Turro, C. *Chem. Sci.* **2014**, *5*, 727–737. (b) Shaffer, D. W.; Ryken, S. A.; Zarkesh, R. A.; Heyduk, A. F. *Inorg. Chem.* **2012**, *51*, 12122–12131.

[8] (a) Haga, M.-A.; Dodsworth, E. S.; Lever, A. B. P. *Inorg. Chem.* **1986**, *25*, 447–353. (b) Masui, H.; Lever, A. B. P.; Auburn, P. R. *Inorg. Chem.* **1991**, *30*, 2402–2410.

[9] (a) De Araujo, M. P.; de Figueiredo, A. T.; Bogado, A. L.; Poelhsitz, Von, G.; Ellena, J.; Castellano, E. E.; Donnici, C. L.; Comasseto, J. V.; Batista, A. A. *Organometallics* **2005**, *24*, 6159–6168. (b) Kepert, C. M.; Deacon, G. B.; Sahely, N.; Spiccia, L.; Fallon, G. D.; Skelton, B. W.; White, A. H. *Inorg. Chem.* **2004**, *43*, 2818–2827; (c) Ortiz-Frade, L.; Manríquez, J.; González, I.; Ruiz-Azura, L.; Moreno-Esparza, R. *Polyhedron* **2010**, *29*, 328–332; (d) Yoshikawa, N.; Yamabe, S.; Sakaki, S.; Kanehisa, N.; Inoue, T.; Takashima, H. *J. Mol. Struct.* **2015**, *1094*, 98–108; (e) Prinaka, D.; Mondal, T. K.; Mobin, S. M.; Sarkar, B.; Lahirin, G. K.; *Inorg. Chim. Acta* **2010**, *363*, 2945–2954.

[10] (a) Bag, N.; Pramanik, A.; Lahiri, G. K.; Chakravorty, A. *Inorg. Chem.* **1992**, *31*, 40–45. (b) Monfette, S.; Duarte Silva, J. A.; Gorelsky, S. I.; Dalgarno, S. J.; Santos, dos, E. N.; Araujo, M. H.; Fogg, D. E. *Can. J. Chem.* **2009**, *87*, 361–367. (c) Boone, R. St.; Pierpont, C. G. *Polyhedron* **1990**, 9, 2267-2272.

[11] (a) Bhattacharya, S.; Pierpont, C. G. *Inorg. Chem.* **1991**, *30*, 1511–1516. (b) Kobayashi, K.; Ohtsu, H.; Wada, T.; Kato, T.; Tanaka, K. *J. Am. Chem. Soc.* **2003**, *125*, 6729–6739. (c) Boone, R. St.; Pierpont, C. G. *Inorg. Chem.* **1987**, 26, 1769-1773.

[12] (a) Ingram, J. D.; Costa, P. J.; Adams, H.; Ward, M. D.; Félix, V.; Thomas, J. A. *Inorg. Chem.* **2012**, *51*, 10483–10494. (b) Bardaji, M.; Brown, N. C.; Connelly, N. G.; Davies, R.; Orpen, A. G.; Rosair, G. M.; Seear, N. R. . *J. Organomet. Chem.* **1994**, *474*, C21–C23.

[13] Wada, T.; Yamanaka, M.; Fujihara, T.; Miyazato, Y.; Tanaka, K. *Inorg. Chem.* **2006**, *45*, 8887–8894.

[14] Monfette, S.; Duarte Silva, J. A.; Gorelsky, S. I.; Dalgarno, S. J.; Santos, dos, E. N.; Araujo, M. H.; Fogg, D. E. *Can. J. Chem.* **2009**, *87*, 361–367.

[15] Connelly, N. G.; Geiger, W. E. Chem. Rev. **1996**, 96, 877–910.

[16] SMART Software Users Guide, Version 5.1, Bruker Analytical X-Ray Systems, Inc.; Madison, WI 1999.

[17] SAINT Software Users Guide, Version 6.0, Bruker Analytical X-Ray Systems, Inc.; Madison, WI 1999

[18] G. M. Sheldrick, SADABS, Version 2.10, Bruker Analytical X-Ray Systems, Inc.; Madison, WI 2002.

[19] G. M. Sheldrick, SHELXTL Version 6.12, Bruker Analytical X-Ray Systems, Inc.; Madison, WI 2001

[20] *International Tables for X-Ray Crystallography* 1992, Vol. C., Dordrecht: Kluwer Academic Publishers.

Part 2: Chapter 4

Introduction to Phosphonic Acid Anchoring Groups

4.1 Surface Chemistry

Integration of single molecules into nanostructured surfaces plays an important role in realizing molecular electronics, photocatalysis, and photovoltaic schemes.[1] Many of such applications require fabrication of technologies built from close-packed monolayers of individual molecules on transparent metal oxide semiconductor (MOS) arrays. For example, MOS nanostructures are commonly found in optoelectronic devices,[2] biological probes,[3] and dye-sensitized solar cells (DSSCs),[4] where they serve as a scaffold layer for loading the designated molecules. It is well recognized that the ability to incorporate functional molecules into MOSs with atomically precise manipulations, one at a time in a controlled fashion, bears a crucial influence on the overall device performance.[1a] Hence, the emergence of metal oxide semiconductors has stimulated the expansion of surface modifiable approaches by leveraging various binding modes at the surface interface based on covalent attachment, hydrogen bonding, electrostatic interactions, or physical entrapment.[5]
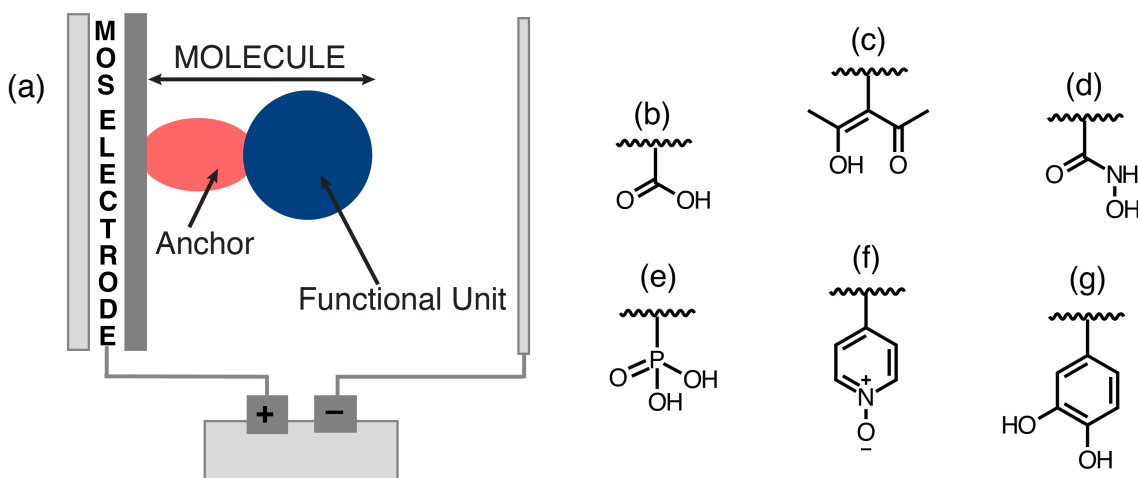
Figure 4.1. Schematic representation of (a) a single-molecule junction showing linkage to a metal-oxide semiconductor (MOS) surface via a generic anchoring group. Possible anchoring groups include (b) carboxylates, (c) acetylacetonates, (d) hydroxamates, (e) phosphonates, (f) pyridine-*N*-oxides, and (g) catecholates.

81

Among the surface functionalization methods involving organically modified metal-oxide materials, it is becoming increasingly important to rely on chemical anchoring groups.[1c,6] A chemical anchoring group is defined as an atom, or group of atoms, appended to a specific site of the molecule to be immobilized that is able to form strong covalent linkages with the surface. Figure 4.1a shows a schematic representation of a single-molecule-MOS junction with anchoring-group connectivity. In the simplest case, the key molecular components are comprised of a functional unit, the part of the individual molecule expected to perform a designated task, and the anchoring group at the molecular terminus. Covalent binding furnishes strong electronic coupling between the molecule and the metal oxide nanostructure while the terminal nature of the linker allows to orient the individual molecules such that the transport of charges through them can proceed in a directional manner. Furthermore, the chemical identity of the terminal linker can be systematically varied in order to study the anchor-group influence on the overall device performance. A multitude of anchoring groups are known to bind photoactive and redox-active molecules to metal oxide materials (Figure 4.1b).[1a,c] Of particular interest are those types of anchors that, in addition to being chemically robust, can facilitate rapid and irreversible injections of charges from the anchored species into the semiconductor material.

4.2. Phosphonic Acid Anchoring Groups

Phosphonate derivatives have garnered increasing attention recently in applications targeting the functionalization of nanostructured metal oxide surfaces with "surface-tethering" molecules (Figure 4.1e).[7] The use of phosphonic acid anchors offers several key advantages for deriving chemically modified MOS junctions: (a) strong phosphorous

oxygen-metal bonds (P–O–M), (b) compatibility with a wide range of metal ions, (c) stability under oxidative, aqueous, and/or variable pH conditions, (d) increased resistance to desorption, and (e) availability of multiple phosphonylation strategies.[7,8] The chemical stability of P–O–M bonds has been demonstrated through the numerous metal phosphonate and phosphate compounds documented in the last several decades.[9] Likewise, the rich coordination chemistry of phosphonic acids is well established with various metal ions, ranging from tetravalent cations like Ti^{IV} and Sn^{IV} to higher-valent cations like Mo^{VI} and W^{VI}.[8] As shown in Figure 4.2, the phosphonic acid group can bind to an oxide surface via monodentate, bidentate, or tridentate modes.[7-9a] In addition, the bonds can be classified as either bridging where each acid oxygen is bound to a different metal atom or chelating where multiple oxygen atoms are bound to the same metal atom. The number of metal atoms bonded to each of the three oxygen atoms can significantly vary according to the nature and oxidation state of the metal, reaction conditions, and the steric bulk of the immobilized organic component.[7] The covalent nature of available binding modes accounts for the strong resistance of phosphonate-functionalized molecules to desorb from the surface. In general, the described binding modes are produced by a surface condensation reaction between the phosphonic acid moiety and metallic oxide sites, giving rise to firmly chemisorbed molecular scaffolds through their P–O bonds.[2,10] As such, the P–O–M bonds of the formed monolayers impart structural integrity to the modified material, rendering it generally recalcitrant toward hydrolysis. Finally, the wide selection of synthetic routes for phosphonic acids has proven valuable in guiding materials chemists in the preparation of phosphonate-functionalized nanostructured arrays.[7]
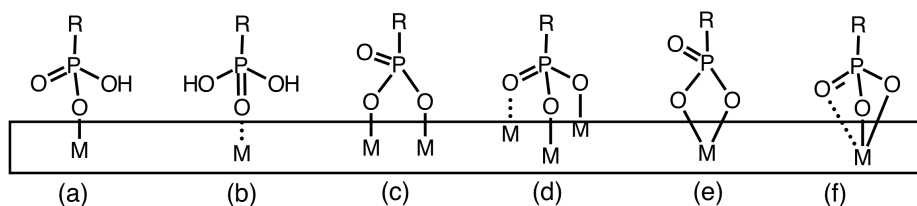
Figure 4.2. Possible binding modes of phosphonic acids to a metal-oxide surface including (a-b) monodentate (c) bridging bidentate and (d) bridging tridentate as well as (e) chelating bidentate and (f) chelating tridendate interactions. The R group represents an organic backbone of immobilized molecules.

With respect to the installation of phosphonic acids on organic substrates, two main approaches can be considered: (a) direct introduction of these groups to the organic backbone or (b) coupling of simple organic molecules, with pre-installed phosphonate anchors, with more complex organic substrates (Figure 4.3). In the former case, the phosphonate group is typically added in the final steps of the synthesis for the molecule to be immobilized. Common chemical methods based on this strategy include the Michaelis-Arbuzov reaction, transition metal-catalyzed cross-coupling reactions, and hydrophosphorylation.[7] The individual examples of these reactions are illustrated in Figure 4.4. The Michaelis-Arbuzov reaction is useful when functionalization of alkyl halides is required, which is achieved by heating the alkyl halide with a triester phosphite (Figure 4.4a).[11] Conversely, the cross-coupling chemistry is better suited for aromatic or vinyl halides. The sp^2-hybridized carbon halide is coupled with a dialkyl phosphite under catalysis with late transitions metals, the role of which is typically fulfilled by palladium, copper, and nickel (Figure 4.4b).[12] Late metal catalysts are also important when the phosphonate-group addition is sought across alkenes or terminal alkynes (Figure 4.4c). The frequently employed hydrophosphorylation catalysts are based on palladium, rhodium, nickel, and copper.[13]
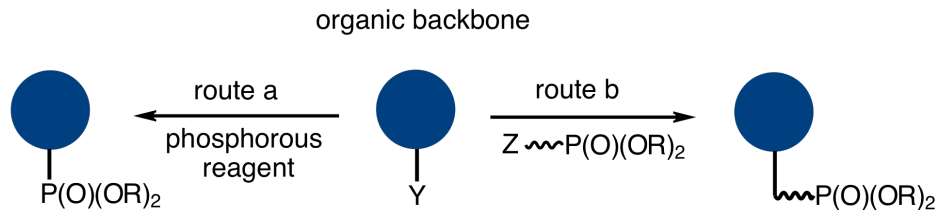
Figure 4.3. Two principal strategies toward functional phosphonylated molecules involving (a) direct incorporation of phosphorous reagents into the organic backbone or (b) coupling of the organic backbone with simple substrates containing pre-installed phosphonate groups.

The indirect coupling of phosphonate derivatives is advantageous when chemically sophisticated substrates are implicated, especially if they are sensitive toward metal-catalyzed reactions. This approach exploits simple organic compounds containing pre-installed phosphonate groups for coupling with the synthetically elaborate molecules (Figure 4.3b). A generic phosphonate derivative is defined in Figure 4.3b as $Z-(CH_2)_n-(PO_3R_2)$ (where Z is a terminal primary amine, alcohol, or aldehyde moiety while $(CH_2)_n$ is a carbon spacer of varying length), which reacts with select organic residues that would be imbedded in the organic backbone.[14] Figure 4.4d exemplifies the synthesis of primary amine derivatives, $NH_2-(CH_2)_n-(PO_3H_2)$, for coupling with carboxylic acid residues.

Regardless of how molecular species are functionalized, through direct use of phosphorous reagents on indirect coupling with phosphonate derivatives, the most frequently employed reagents contain phosphonate esters rather than phosphonic acids, which are much more difficult to handle and purify. At a later point, the phosphonic acids can be accessed from their phosphonate ester counterparts by post-synthetic deprotection strategies. Common deprotections include hydrolysis by refluxing in concentrated hydrochloric acid or the McKenna's method, when milder reaction conditions are needed for sensitive substrates.[7] The latter reaction utilizes bromotrimethylsilane that converts the phosphonate ester groups into hydrolytically labile trimethylsilyl phosphonate esters.[15]
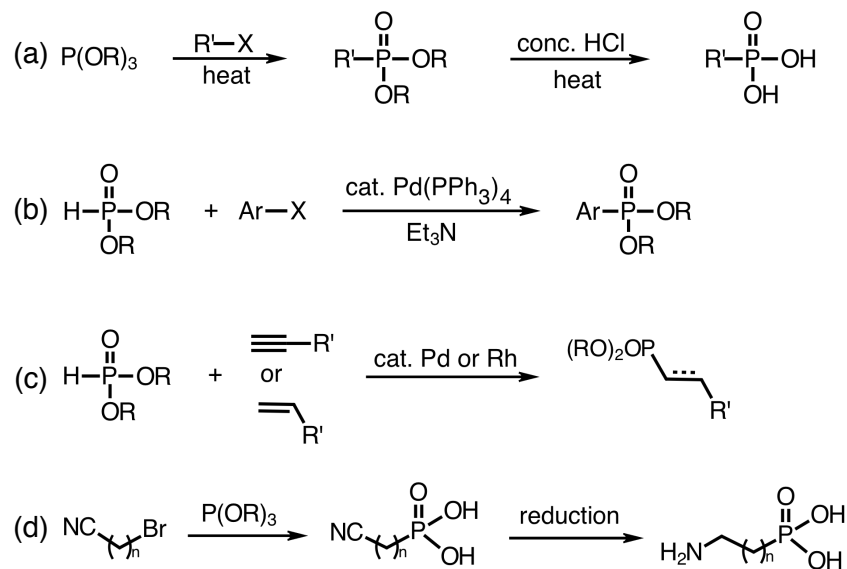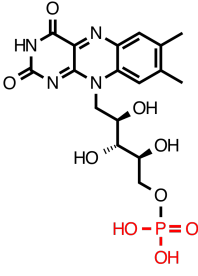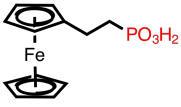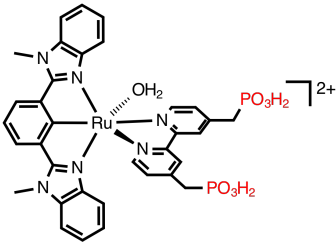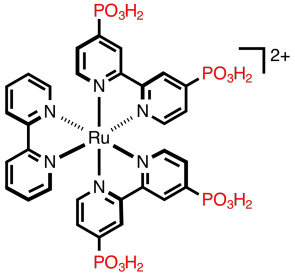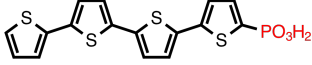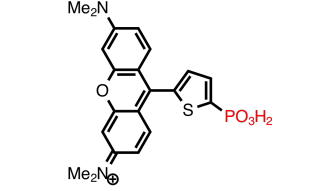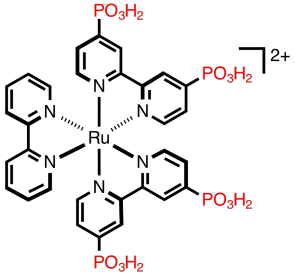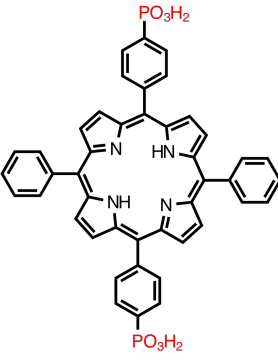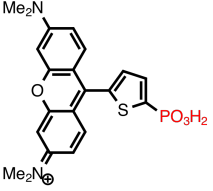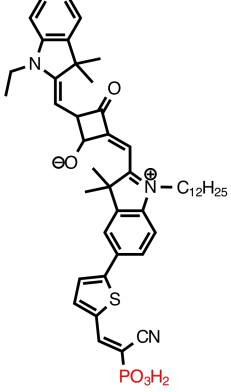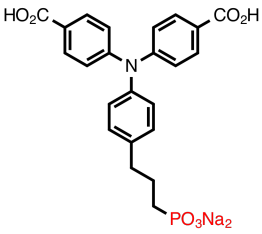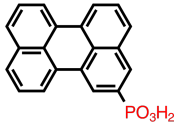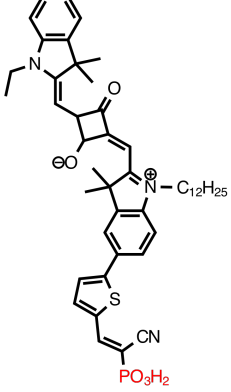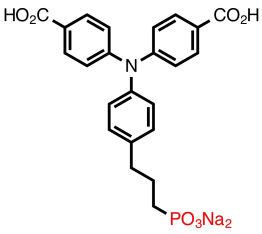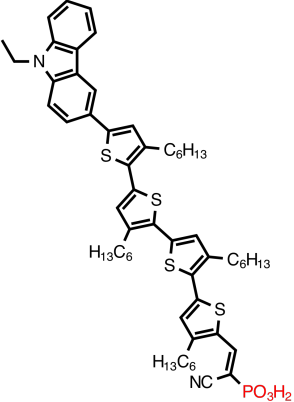
Figure 4.4. General synthetic routes for direct installation of phosphonates via (a) Michaelis-Arbuzov reaction, (b) transition metal-catalyzed cross-coupling reactions, and (c) hydrophosphorylation. R and R' correspond to commonly modified alkyl and/or aryl groups. (d) Representative synthesis of the $Z-(CH_2)_n-(PO_3R_2)$ reagent (where $Z = NH_2$) for subsequent coupling with complex organic structures.

4.3 Applications of Phosphonate Anchors

The utility of phosphonic acid anchoring groups for metal oxide surfaces is exemplified by numerous applications targeting molecular electronics and dye-sensitized solar cells (DSSCs). For example, redox-active organophosphorous compounds are known to undergo chemisorption on tin-doped indium oxide electrodes (ITO), which allows to tune the electrode reactivity for integration in bio-electroanalytical devices and electrocatalytic reactors.[10] Table 4.1 illustrates the chemical structures of relevant redox-active probes (**a-b**) that were reported to form robust layers on the ITO surface. Likewise, polyconjugated thiophenes (**c**) with terminal phosphonic acid groups were shown to form stable monolayers with ITO electrodes for improved charge transport in organic light emitting diodes (OLEDs).[16] Alternatively, a phosphonate-functionalized ruthenium complex

(**d**) was found to effect electrocatalytic water oxidation on the same type of surface.[17] Phosphonic acids have also gained increasing applications in dye-sensitized solar cells where the attachement of molecular dyes on titanium dioxide nanoparticles (TiO_2) collectively produces a working electrode for the cell. Ruthenium-bipyridine dyes (**e**) with different numbers of anchoring groups were studied extensively in the last decades, leading to the observation that a single phosphonate group is sufficient for maintaining contact with the TiO_2 surface (Table 4.1).[18] Similarly, a multitude of examples concerning phosphonylated porphyrin dyes (**f**) have been described that show comparable DSSC performance to that of the porphyrin congeners functionalized with alternative anchoring groups.[19] Finally, the phosphonate anchor is becoming prevalent among organic dyes derived from a wide selection of molecular structures including rhodamines(**g**),[20] perylenes (**h**),[21] squaraines (**i**),[22] triarylamines (**j**),[23] and carbazoles (**k**),[24] as shown in Table 4.1. Altogether, the described examples underscore that the phosphonate-group chemistry will continue to gain relevance in the area of applied materials science and advanced technology.

Table 4.1. Collection of Representative Optoelectronic Compounds and Molecular Dyes with Phosphonate Anchor Groups.

Entry	Structure	Entry	Structure	Entry	Structure
a		b		d	
		b			
e		f		g	
				h	
i		j		k	

4.4. Contributions of This Disseration

Despite its far-reaching influence, the phosphonic acid group shows a scant presence in the field of redox-active ligands, which are applicable in electrocatalysis[25] and photovoltaic schemes.[26] The well-established redox chemistry in our own laboratory has stimulated our interest in developing straightforward phosphonylation routes for several commonly used redox-active ligands, which will be detailed in the next three chapters of

this disseration. Chapter 5 describes the synthesis of two new catecholate ligands with phosphonate diester groups. The influence of the phosphonate diester group on the redox properties for the two catecholates is discussed in the context of square-planar donor-acceptor complexes of Pd^{II}. The binding properties of the phosphonylated complexes are assessed on the surface of titanium dioxide. Chapter 6 reports on the synthesis of the redox-active β-diketiminate ligand containing a phosphonate diester substituent appended at the central carbon of the ligand backbone. The electronic properties of the new ligand are examined in charge-transfer complexes of Rh^{I} and Rh^{III} centers. Chapter 7 details a general route for the preparation of redox-active amido-bis(phenolate) ligands, [ONO], with doubly substituted phosphonate diester groups. Based on this route, two independent ONO-ligand derivatives are accessed with different solubility characteristics. The functionalized redox-active ligands developed in this work should prove useful in heterogeneous applications such as dyes for sensitized solar cells and redox-based catalysts for electrochemical cells.

4.5. References

[1] (a) Leary, E.; La Rosa, A.; González, M. T.; Rubio-Bollinger, G.; Agraïtab, N.; Martín, N. *Chem. Soc. Rev*. **2015**, *44*, 920–942. (b) Chen, X.; Shen, S.; Guo, L.; Mao, S. S. *Chem. Rev*. **2010**, *110*, 6503– 6570. (c) Young, K. J.; Martini, L. A.; Milot, R. L.; Snoeberger III, R. C.; Batista, V. S.; Schmuttenmaer, C. A.; Crabtree, R. H.; Brudvig, G. W. *Coord. Chem. Rev*. **2012**, *256*, 2503–2520 (d) Gordon, R. *MRS Bull*. **2000**, 52–57. (e) Thomas, G. *Nature* **1997**, 389, 907–908.

[2] (a) Hotchkiss, P. J.; Jones, S. C.; Paniagua, S. A.; Sharma, A.; Kippelen, B.; Armstrong, N. R.; Marder, S. R. *Acc. Chem. Res.* **2012**, *45*, 337–346.

[3] (a) Liu, H.; Queffélec, C.; Charlier, C.; Defontaine, A.; Fateh, A.; Tellier, C.; Talham, D. R.; Bujoli, B. *Langmuir* **2014**, *30*, 13949–13955. (b) Clearfield, A.; Demadis, K. D. Metal Phosphonate Chemistry, from Synthesis to Applications.; RSC Publishing: Cambridge, U.K., 2012; p 655 (c) Benbenishty-Shamir, H.; Gilert, R.; Gotman, I.; Gutmanas, E. Y.; Sukenik, C. N. *Langmuir* **2011**, *27*, 12082–12089.

[4] (a) Grätzel, M. *J. Photochem. Photobiol. C: Photochem. Rev.* **2003**, *4*, 145–153. (b) Hagfeldt, A.; Boschloo, G.; Sun, L.; Kloo, L.; Pettersson, H. *Chem. Rev.* **2010**, *110*, 6595–6663. (c) Narayan, M. R. *Renew. Sust. Energ. Rev.* **2016**, *16*, 208–215.

[5] Kalyanasundaram, K. *Coord. Chem. Rev.* **1998**, 177, 347–414.

[6] Zhang, L.; Cole, J. M. *ACS Appl. Mater. Interfaces* **2015**, *7*, 3427–3455.

[7] Queffélec, C.; Petit, M.; Janvier, P.; Knight, D. A.; Bujoli, B. *Chem. Rev.* **2012**, *112*, 3777–3807.

[8] Guerrero, G.; Alauzun, J. G.; Granier, M.; Laurencin, D.; Mutin, P. H. *Dalton Trans.* **2013**, *42*, 12569–12585.

[9] (a) Guerrero, G.; Mutin, P. H.; Vioux, A. *Chem. Mater.* **2001**, *13*, 4367–4373.(b) Alberti, G.; Casciola, M.; Costantino, U.; Vivani, R. *Adv. Mater.* **1996**, *8*, 291–303. (c) Clearfield, A. *Prog. Inorg. Chem.* **1998**, *47*, 371–510.

[10] (a) Forget, A.; Limoges, B.; Balland, V. *Langmuir* **2015**, *31*, 1931–1940. (b) Forget, A.; Tucker, T.; Brett, M. J.; Balland. V. *Chem. Commun.* **2015**, *51*, 6944–6947

[11] Bhattacharya, A. K.; Thyagarajan, G. *Chem. Rev*. **1981**, *81*, 415–430.

[12] (a) Gelman, D.; Jiang, L.; Buchwald, S. L. *Org. Lett.* **2003**, *5*, 2315–2318. (b) Huang, C.; Tang, X.; Fu, H. A.; Jiang, Y. Y.; Zhao, Y. F. *J. Org. Chem.* **2006**, *71*, 5020–5022. (c) Rao, H. H.; Jin, Y.; Fu, H.; Jiang, Y. Y.; Zhao, Y. F. *Chem. Eur. J.* **2006**, *12*, 3636–3646. (d) Ogawa, T.; Usuki, N.; Ono, N. *J. Chem. Soc., Perkin Trans*. **1998**, 2953–2958. (e) Balthazor, T. M.; Grabiak, R. C. *J. Org. Chem.* **1980**, *45*, 5425–5426. (f) Lu, X. Y.; Zhu, J. Y.; Huang, J. L.; Tao, X. C. *J. Mol. Catal.* **1987**, *41*, 235. (g) Markl, G.; Gschwendner, K.; Rotzer, I.; Kreitmeier, P. *Helv. Chim. Acta* **2004**, *87*, 825–844.

[13] (a) Han, L. B.; Tanaka, M. *J. Am. Chem. Soc.* **1996**, *118*, 1571–1572. (b) Zhao, C. Q.; Han, L. B.; Goto, M.; Tanaka, M. *Angew. Chem., Int. Ed.* **2001**, *40*, 1929–1932. (c) Goulioukina, N. S.; Dolgina, T. M.; Beletskaya, I. P.; Henry, J. C.; Lavergne, D.; Ratovelomanana-Vidal, V.; Genet, J. P. *Tetrahedron: Asymmetry* **2001**, 12, 319–327. (d) Han, L. B.; Zhang, C.; Yazawa, H.; Shimada, S. *J. Am. Chem. Soc.* **2004**, *126*, 5080–5081. (e) Gao, Y. X.; Wang, G.; Chen, L.; Xu, P. X.; Zhao, Y. F.; Zhou, Y. B.; Han, L. B. *J. Am. Chem. Soc*. **2009**, *131*, 7956–7957.

[14] (a) Li, F.; Shishkin, E.; Mastro, M. A.; Hite, J. K.; Eddy, C. R.; Edgar, J. H.; Ito, T. *Langmuir* **2010**, 26, 10725–10730. (b) Deniaud, D.; Schollorn, B.; Mansuy, D.; Rouxel, J.; Battioni, P.; Bujoli, B. *Chem. Mater*. **1995**, *7*, 995–1000. (c) Levesque, G.; Arsene, P.; Fanneau-Bellenger, V.; Pham, T. N. *Biomacromolecules* **2000**, *1*, 387–399. (d) Tully, S. E.; Cravatt, B. F. *J. Am. Chem. Soc.* **2010**, *132*, 3264–3265. (e) Douglass, M. R.; Stern, C. L.; Marks, T. J. *J. Am. Chem. Soc*. **2001**, *123*, 10221–10222.

[15] Mustafa, D. A.; Kashemirov, B. A.; McKenna, C. E. *Tetrahedron Lett*. **2011**, *52*, 2285–2287.

[16] Hanson, E. L.; Guo, J.; Koch, N.; Schwartz, J.; Bernasek, S. L. *J. Am. Chem. Soc.* **2005**, *127*, 10058–10062.

[17] Chen, Z.; Concepcion, J. J.; Hull, J. F.; Hoertz, P. G.; Meyer, T. J. *Dalton Trans.* **2010**, *39*, 6950–6952.

[18] (a) Park, H.; Bae, E.; Lee, J.-J.; Park, J.; Choi, W. *J. Phys. Chem. B* **2006**, *110*, 8740–8749. (b) Bae, E.; Choi, W.; Park, J.; Shin, H. S.; Kim, S. B.; Lee, J. S. *J. Phys. Chem. B* **2004**, *108*, 14093–14101. (c) Gillaizeau-Gauthier, I.; Odobel, F.; Alebbi, M.; Argazzi, R.; Costa, E.; Bignozzi, C. A.; Qu, P.; Meyer, G. J. *Inorg. Chem.* **2001**, *40*, 6073–6079. (d) Norris, M. R.; Concepcion, J. J.; Glasson, C. R. K.; Fang, Z.; Lapides, A. M.; Ashford, D. L.; Templeton, J. L.; Meyer, T. J. *Inorg. Chem.* **2013**, *52*, 12492–12501.

[19] (a) Odobel, F.; Blart, E.; Lagreé, M.; Villieras, M.; Boujtita, H.; El Murr, N.; Caramori, S.; Alberto Bignozzi, C. *J. Mater. Chem.* **2003**, *13*, 502–510. (b) Brennan, B. J.; Llansola Portolés, M. J.; Liddell, P. A.; Moore, T. A.; Moore, A. L.; Gust, D. *Phys. Chem. Chem. Phys.* **2013**, *15*, 16605–16614. (c) Nayak, A.; Roy, S.; Sherman, B. D.; Alibabaei, L.; Lapides, A. M.; Brennaman, M. K.; Wee, K.-R.; Meyer, T. J. *ACS Appl. Mater. Interfaces* **2016**, *8*, 3853–3860. (d) Nayak, A.; Knauf, R. R.; Hanson, K.; Alibabaei, L.; Concepcion, J. J.; Ashford, D. L.; Dempsey, J. L.; Meyer, T. J. *Chem. Sci.* **2014**, *5*, 3115–3119. (e) Splan, K. E.; Hupp, J. T. *Langmuir* **2004**, *20*, 10560–10566. (f) Loewe, R. S.; Ambroise, A.; Muthukumaran, K.; Padmaja, K.; Lysenko, A. B.; Mathur, G.; Li, Q.; Bocian, D. F.; Misra, V.; Lindsey, J. S. *J. Org. Chem.* **2004**, *69*, 1453–1460.

[20] Mulhern, K. R.; Orchard, A.; Watson, D. F.; Detty, M. R. *Langmuir* **2012**, *28*, 7071–7082.

[21] (a) Ambrosio, F.; Martsinovich, N.; Troisi, A. *J. Phys. Chem. C* **2012**, *116*, 2622–2629. (b) Ernstorfer, R. Spectroscopic Investigation of Photoinduced Heterogeneous Electron Transfer. Ph.D. Dissertation, Free University of Berlin, *Dahlem*, Berlin, 2004.

[22] Jradi, F. M.; Kang, X.; O'Neil, D.; Pajares, G.; Getmanenko, Y. A.; Szymanski, P.; Parker, T. C.; El-Sayed, M. A.; Marder, S. R. *Chem. Mater.* **2015**, *27*, 2480–2487.

[23] Westermark, K.; Tingry, S.; Persson, P.; Rensmo, H.; Lunell, S.; Hagfeldt, A.; Siegbahn, H. *J. Phys. Chem. B* **2001**, *105*, 7182–7187.

[24] Murakami, T. M.; Yoshida, E.; Koumura, N. *Electrochim. Acta* **2014**, *131*, 174–183.

[25] (a) Lacy, D. C.; McCrory, C. C. L.; Peters, J. C. *Inorg. Chem.* **2014**, *53*, 4980–4988. (b) Isobe, H.; Tanaka, K.; Shen, J.-R.; Yamaguchi, K. *Inorg. Chem.* **2014**, *53*, 3973–3984. (c) Muckerman, J. T.; Polyansky, D. E.; Wada, T.; Tanaka, K.; Fujita, E. *Inorg. Chem.* **2008**, *47*, 1787–1802. (d) Luca, O. R.; Crabtree, R. H. *Chem. Soc. Rev.* **2013**, *42*, 1440–1459. (e) Benson, E. E.; Kubiak, C. P.; Sathrum, A. J.; Smieja, M. M. *Chem. Soc. Rev.* **2009**, *38*, 89–99. (f) Smieja, J. M.; Sampson, M. D.; Grice, K. A.; Benson, E. E.; Roehlich, J. D.; Kubiak, C. P. *Inorg. Chem.* **2010**, *49*, 9283–9289. (g) Kubiak, C. P. *Inorg. Chem.* **2013**, *52*, 5663–5676.

[26] (a) Linfoot, C. L.; Richardson, P.; McCall, K. L.; Durrant, J. R.; Morandeira, A.; Robertson, N. *Solar Energy* **2011,** *85*, 1195–1203. (b) Geary, E. A. M.; Yellowlees, L. J.; Jack, L. A.; Oswald, I. D. H.; Parsons, S.; Hirata, N.; Durrant, J. R.; Robertson, N. *Inorg. Chem*. **2005**, *44*, 242–250 (c) Islam, A.; Sugihara, H.; Hara, K.; Singh, L. P.; Katoh, R.; Yanagida, M.; Takahashi, Y.; Murata, S.; Arakawa, H.; Fujihashi, G. *Inorg. Chem.* **2001**, *40*, 5371–5380. (d) Diwan, K.; Chauhan, R.; Singh, S. K.; Singh, B.; Drew, M. G. B.; Bahadur, L.; Singh, N. *New J. Chem*. **2014**, *38*, 97–108. (e) Verma, S.; Kar, P.; Das, A.; Ghosh, H. N. *Chem. Eur. J.* **2011**, *17*, 1561–1568.

Chapter 5

Synthesis of Catecholate Ligands with Phosphonate Anchoring Groups

5.1 Introduction

Ligands of the *o*-dioxolene family (catecholates) are enjoying a renaissance in coordination chemistry having once again become the subject of recent research interests. Due to the fundamental capacity of catecholate ligands to access three oxidation states when coordinated to a metal ion,[1] coordination complexes incorporating these ligands are often characterized by intriguing electronic or magnetic properties, which in turn leads to diverse potential applications. The utility of redox-active catecholates and their derivatives has expanded rapidly in recent years to include applications in electrocatalytic oxidation of water,[2] multielectron stoichiometric and catalytic C–C coupling reactions,[3] heterolytic activation of H_2,[4] homolytic activation of disulfides and O_2,[5] dioxygenase-type chemistry,[6] and the aerial oxidation of primary alcohols.[7] Also recently, the employment of catecholato ligands was documented in the context of transition-metal catalysis tailored for hydrogenation of unsaturated hydrocarbons[8] and olefin polymerization.[9] Our group[10] and others[11] have studied catecholate-diimine and related complexes of group 10 metals as charge-transfer complexes for use in dye-sensitized solar cells.[12]

Most of the abovementioned studies involving complexes of the catecholate ligands and their derivatives have been performed in homogeneous solutions or with molecular complexes integrated into polymer matrices.[8,13] In several applications, including catalysis, electrocatalysis, and dye sensitization, immobilization of catecholate coordination complexes on a solid support would be advantageous. One of the best-established mechanisms for the immobilization of functional compounds on metal oxide surfaces is to employ a phosphonic acid linker;[14] however, effective methods for installing $-PO_3H_2$ groups onto catecholate-type ligands are limited.[15] To the best of our knowledge, only one such

method has been reported, affording a symmetrical catechol with benzylic phosphonate groups at both the 3 and 6 positions of the catechol ring.[16] Conversely, straightforward and scalable strategies for the installation of phosphonate anchoring groups at the more remote 4/5 positions of the catechol have not been reported.
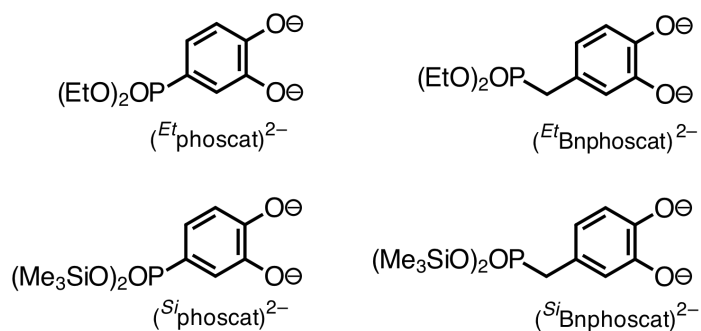
Figure 5.1. New catecholate-ligand derivatives with the ethyl-protected phosphonate groups (top) and the silyl-protected phosphonate groups (bottom).

In this work, we report synthetic strategies for installing a phosphonate anchoring group at the 4-position of the catechol ring. The first derivative, 4-diethoxyphosphorylbenzene-1,2-diol, (^{Et}phoscat)$^{2-}$, contains an ethyl-protected phosphonate group attached directly to the 4-position of the catecholate as shown in Figure 5.1. The second derivative, 4-(diethoxyphosphorylmethyl)benzene-1,2-diol, (^{Et}Bnphoscat)^{2}, contains a single methylene spacer unit between the ethyl-protected phosphonate group and the 4-position of the catecholate ring (Figure 5.1). These two derivatives required significantly different synthetic routes and were expected to confer different electronic character to the catecholate moiety. To characterize the impact that these anchoring groups have on the electronic properties of the catecholate ligands, new square-planar palladium(II) complexes of the phosphonate-functionalized catecholates have been prepared and their spectroscopic and electrochemical features have been measured. Finally, preliminary studies have been conducted to test the binding of these anchored-

catecholate complexes to metal-oxide surfaces, which required *in situ* elaboration of (^{Et}phoscat)$^{2-}$ and (^{Et}Bnphoscat)$^{2-}$ to the silylated derivatives (^{Si}phoscat)$^{2-}$ and (^{Si}Bnphoscat)$^{2-}$, respectively, also shown in Figure 5.1.

5.2 Results and Discussion

5.2.1 Synthesis

Two distinct synthetic routes were required to access the new catecholate proligands (^{Et}phoscat)H$_2$ and (^{Et}Bnphoscat)H$_2$. The (^{Et}phoscat)H$_2$ derivative was prepared from pyrocatechol (**15**) by a three-step synthesis with an overall yield of 37% as shown in Scheme 5.1a. The route to (^{Et}phoscat)H$_2$ involved initial protection of pyrocatechol by treatment with phosphorous trichloride and acetone to afford the corresponding acetanide (**16**). In the next step, the phosphonate diester group was installed using diethylphosphite by a manganese(III)-promoted direct phosphonylation reaction.[17] This reaction proceeds with good regioselectivity, resulting in phosphonylation of the 4-position of the catechol ring (**17a**) with 5:1 selectivity over phosphonylation of the 3-position (**17b**, *ortho* to the oxygen). Attempts to separate the two isomers were not successful; therefore, a mixture of **17a** and **17b** was carried through the next step. The target (^{Et}phoscat)H$_2$ proligand was revealed upon removal of the acetanide protecting group with boron trichloride. Purification of the unmasked catechol by column chromatography on silica gel allowed isolation of the pure 4-phosphonylated regioisomer, 4-diethoxyphosphorylbenzene-1,2-diol, (^{Et}phoscat)H$_2$.

According to the procedure outlined in Scheme 5.1b, the complementary diethyl benzylphosphonate-functionalized catechol, (^{Et}Bnphoscat)H$_2$, was prepared by a six-step synthesis from protocatechuic acid (**18**), in an overall yield of 26% (the lowest yielding step

is 64%). The route to (^{Et}Bnphoscat)H$_2$ commenced with esterification of protocatechuic

acid followed by protection of the catechol functionality with the acetanide using

phosphorous trichloride and acetone. Reduction of the ethyl ester of **20** with lithium

aluminum hydride followed by the addition of phosphorous tribromide gave

benzylbromide derivative **22**. Thermolysis of the benzylbromide derivative in neat

triethylphosphite using Michaelis-Arbuzov conditions gave the ethyl-protected

benzylphosphonate, **23**, which was unmasked on treatment with boron trichloride to afford

(^{Et}Bnphoscat)H$_2$.

Scheme 5.1. Synthesis of (a) (^{Et}phoscat)H$_2$ and (b) (^{Et}Bnphoscat)H$_2$.
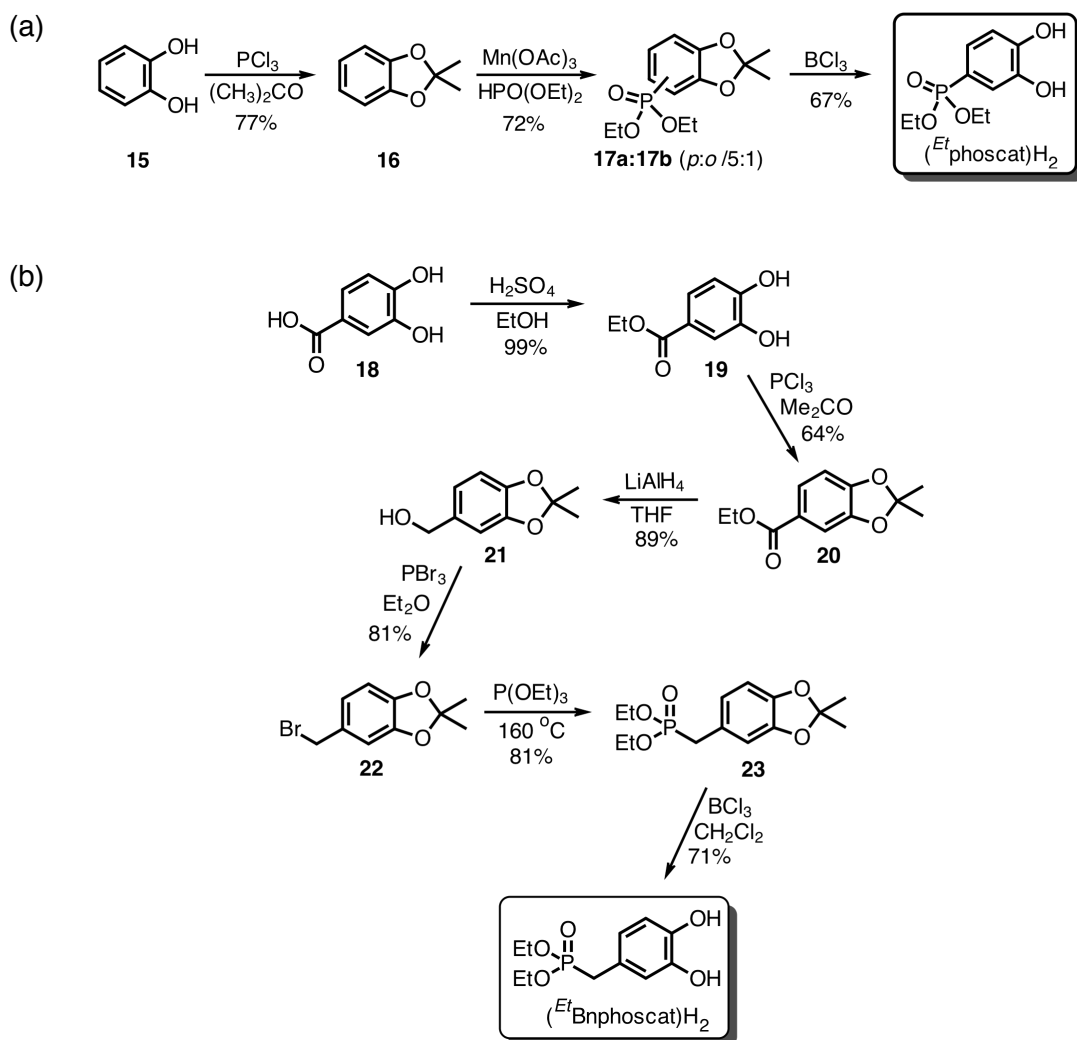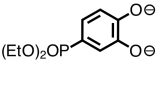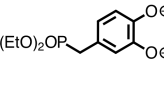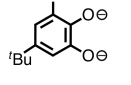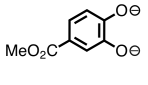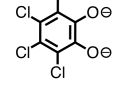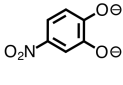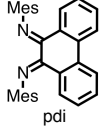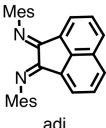
Table 5.1. One-Pot Synthesis of (catecholate)Pd(diimine) Complexes.

$(MeCN)_2PdCl_2 \xrightarrow[\text{CH}_2\text{Cl}_2]{\substack{\textit{i.} \text{ diimine} \\ \textit{ii.} \text{ catechol, 2 } ^t\text{BuNH}_2}} (\text{catecholate})\text{Pd}^{II}(\text{diimine})$

diimine \ catecholate	(^{Et}phoscat)$^{2-}$	(^{Et}Bnphoscat)$^{2-}$	(cat^{t}Bu$_2$)$^{2-}$	(catCO$_2$Me)$^{2-}$	(catCl$_4$)$^{2-}$	(catNO$_2$)$^{2-}$
pdi	(^{Et}phoscat)Pd(pdi) 66%	(^{Et}Bnphoscat)Pd(pdi) 77%	(cat^{t}Bu$_2$)Pd(pdi) 73%	(catCO$_2$Me)Pd(pdi) 81%	(catCl$_4$)Pd(pdi) 79%	—
adi	^{Et}phoscat)Pd(adi) 88%	—	((cat^{t}Bu$_2$)Pd(adi) 67%	(catCO$_2$Me)Pd(adi) 50%	—	(catNO$_2$)Pd(adi) 55%

To benchmark the impact that phosphonate and benzylphosphonate groups have on the electronic properties of the catecholate ligand, new square-planar donor-acceptor complexes of palladium(II) were prepared. The square-planar complexes of the formula (catecholate)Pd(pdi) (catecholate = (^{Et}phoscat)$^{2-}$ or (^{Et}Bnphoscat)$^{2-}$; pdi = *N,N'*-(mesityl)phenanthrene-9,10-diimine) were readily accessed using a one-pot, two-step reaction illustrated in Table 5.1. Addition of pdi to (MeCN)$_2$PdCl$_2$ gave (pdi)PdCl$_2$, which was subsequently treated with either (^{Et}phoscat)H$_2$ or (^{Et}Bnphoscat)H$_2$ in the presence of *tert*-butylamine to afford (^{Et}phoscat)Pd(pdi) or (^{Et}Bnphoscat)Pd(pdi), respectively. To better gauge the electronic properties of coordinated (^{Et}phoscat)$^{2-}$ and (^{Et}Bnphoscat)$^{2-}$ ligands, additional derivatives were prepared from the same pdi ligand but alternative catecholates including 3,5-di-*tert*-butylcatecholate (cat^{t}Bu$_2$)$^{2-}$, methyl 3,4-dihydroxybenzoate (catCO$_2$Me)$^{2-}$, and tetrachlorocatecholate (catCl$_4$)$^{2-}$ (Table 5.1).

A related set of palladium derivatives was accessed through the introduction of a complementary diimine acceptor ligand, *N,N'*-(mesityl)acenaphthenediimine (adi), on palladium. As shown in Table 5.1, the identity of the adi ligand was maintained constant

among the (catecholate)Pd(adi) family of complexes whereas the electronic structure of the catecholate ring was once again subjected to systematic variation. Specifically, (^{Et}phoscat)$^{2-}$, (cat^{t}Bu$_2$)$^{2-}$, (catCO$_2$Me)$^{2-}$, and 4-nitrocatecholate (catNO$_2$)$^{2-}$ were selected as donor ligands, allowing to further confirm the electronic impact of the phosphonate group on the redox ability of the catecholate ligand.

Scheme 5.2. Synthesis of (^{Si}phoscat)Pd(pdi) complex featuring the catecholate ligand with a 4-bis((trimethylsilyl)oxy)phosphonate group.
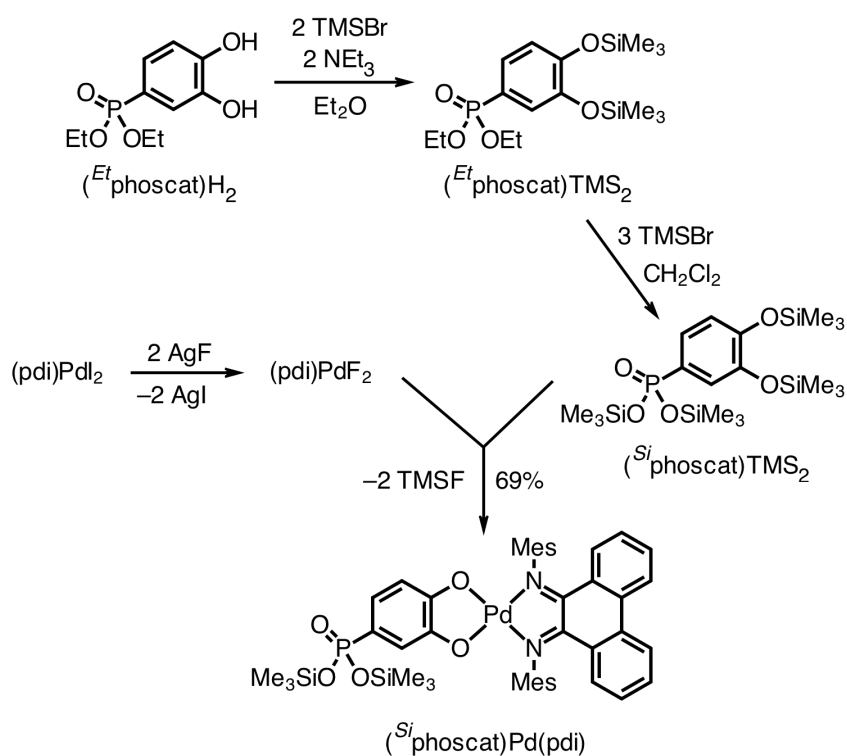
The phosphonate groups of (^{Et}phoscat)$^{2-}$ and (^{Et}Bnphoscat)$^{2-}$ are characterized by chemically robust diethyl ester protecting groups that were expected to impede the binding of the phosphonate anchoring group to metal oxide-based surfaces. As such, silylated derivatives of both ligand platforms were sought. However, all attempts to isolate silylated proligands led to decomposition. Instead a multi-step strategy was devised to generate the silylated proligand and immediately bind it to a palladium center, affording two new

complexes: (^{Si}phoscat)Pd(pdi) and (^{Si}Bnphoscat)Pd(pdi). As shown in Scheme 5.2, the conversion of the 4-(diethyl)phosphonate substituent of (^{Et}phoscat)H$_2$ to a 4-bis((trimethylsilyl)oxy)phosphonate group was achieved by a two-step silylation procedure with bromotrimethylsilane (TMSBr). Initial treatment of (^{Et}phoscat)H$_2$ with TMSBr in the presence of base in diethyl ether resulted in the silylation of both o-dioxolenyl oxygens. The putative (^{Et}phoscat)TMS$_2$ derivative was not isolated and purified but rather it was taken on to (^{Si}phoscat)TMS$_2$ by treatment with excess TMSBr reagent in CH$_2$Cl$_2$, leading to dealkylative silylation of the ethyl-protected phosphonate group under McKenna conditions.[18] Again, putative (^{Si}phoscat)TMS$_2$ was not isolated but rather it was immediately added to (pdi)PdF$_2$, which was generated from a mixture of (pdi)PdI$_2$ and AgF. The palladium fluoride synthon reacted preferentially at the catecholate site to eliminate fluorotrimethylsilane and produce (^{Si}phoscat)Pd(pdi) in 69% yield based on the initial quantity of (pdi)PdI$_2$. An analogous strategy was used for (^{Et}Bnphoscat)H$_2$ to afford (^{Si}Bnphoscat)Pd(pdi) in 67% yield.

The new palladium complexes were characterized as square-planar, (catecholate)Pd(diimine) complexes on the basis of their ^{1}H and ^{13}C NMR spectra, ESI mass spectra, electronic spectroscopies, and electrochemical data. Notably, the phosphonate-containing complexes, (^{Et}phoscat)Pd(pdi), (^{Et}Bnphoscat)Pd(pdi), and (^{Et}phoscat)Pd(adi), are only C_s symmetric owing to the phosphonate anchoring group in the 4-position of the catecholate ring. This asymmetry is transferred to the respective pdi and adi ligand backbones, as evidenced in the ^{1}H and ^{13}C NMR resonances of the individual complexes. In the case of coordinated (^{Et}phoscat)$^{2-}$ ligand, the ^{1}H NMR resonances for the 3 and 5 position of the catecholate ring are shifted downfield relative to the same (^{Et}Bnphoscat)$^{2-}$

resonances, which can be ascribed to the electron withdrawing nature of the phosphonate group when attached directly to the aromatic ring. The TMS-protected complexes (^{Si}phoscat)Pd(pdi) and (^{Si}Bnphoscat)Pd(pdi) show virtually identical ^{1}H and ^{13}C NMR spectral features to the ethyl-protected analogues, excepting the appearance of singlet resonances associated with the SiMe$_3$ groups and disappearance of the resonances associated with the O–CH$_2$CH$_3$ groups. With the exception of symmetric (catCl$_4$)Pd(pdi) structure, the ^{1}H and ^{13}C NMR spectra for all remaining complexes show C_s-symmetric characteristics.

5.2.2 Electronic Properties of (catecholate)Pd(diimine) Complexes
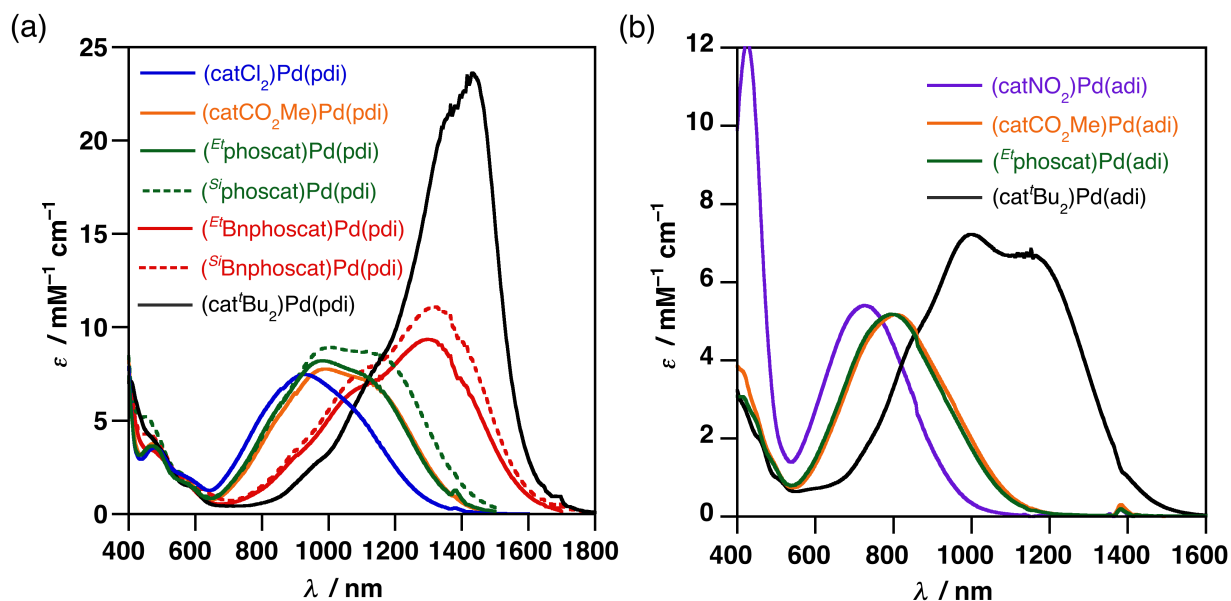
Figure 5.2. Electronic absorption spectra of (a) (catecholate)Pd(pdi) complexes and (b) (catecholate)Pd(adi) complexes, measured in CH$_2$Cl$_2$ at 298K.

The new (catecholate)Pd(diimine) complexes all display characteristic ligand-to-ligand charge-transfer (LL'CT) transitions in the vis-NIR portions of the electromagnetic spectrum. Figure 5.2a shows the electronic absorption spectra for the seven palladium complexes coordinated by identical pdi ligand but electronically different catecholates,

measured in CH_2Cl_2 solutions at 298K. The pertinent band energies and extinction coefficients are listed in Table 5.2. The individual spectra reveal visibly appreciable energy differences with respect to the onset of the LL'CT absorption that track well with the relative donor capacity of the catecholate ligand. Namely, a hypsochromic shift in the lowest-energy charge-transfer band is prominent among the catecholate series in the following order: $(cat^tBu_2)^{2-}$ < $(^RBnphoscat)^{2-}$ < $(^Rphoscat)^{2-}$ = $(catCO_2Me)^{2-}$ < $(catCl_4)^{2-}$; which is generally accompanied by a sizable hypochromic effect. As expected, the identity of the phosphonate protecting groups has no effect on the energy or intensity of the lowest-energy charge-transfer band, with the spectrum of $(^{Et}phoscat)Pd(pdi)$ being identical to that of $(^{Si}phoscat)Pd(pdi)$ and the spectrum of $(^{Et}Bnphoscat)Pd(pdi)$ being identical to that of $(^{Si}Bnphoscat)Pd(pdi)$. Conversely, and consistent with the NMR results, installation of the phosphonate group directly to the catecholate ring has a greater electronic impact than the installation of the phosphonate group through a methylene spacer. As such, the lowest-energy charge-transfer band of the $(^Rphoscat)Pd(pdi)$ complexes (R = diethyl or bis(trimethylsilyl)) is blue shifted by approximately 300 nm relative to the lowest-energy charge-transfer band of the $(^RBnphoscat)Pd(pdi)$ complexes, consistent with the phosphonate group acting as an electron-withdrawing group when attached directly to the catecholate ligand.

Predictable LL'CT characteristics are evident among the remaining complexes of the formula (catecholat)Pd(adi). By analogy to the first set of palladium derivatives, the complexes supported by the adi ligand reveal a hypsochromic shift in the LL'CT band that manifests within the catecholate series in the following order: $(cat^tBu_2)^{2-}$ < $(^Rphoscat)^{2-}$ = $(catCO_2Me)^{2-}$ < $(catNO_2)^{2-}$, as shown in Figure 5.2b. Similarly, the identity of the α-diimine

acceptor has a pronounced influence on the energy of the charge-transfer band whenever the donor-ligand identity is preserved. Specifically, the ligand-to-ligand charge-transfer band red shifts to lower energy, with a concomitant increase in the extinction coefficient, as the diimine is changed from adi to pdi. For example, (^{Et}phoscat)Pd(adi) shows an absorption maximum at 794 nm with an extinction coefficient of 5180 $M^{-1}cm^{-1}$ while in the case of (^{Et}phoscat)Pd(pdi) the absorption maximum is shifted to 894 nm with an extinction coefficient of 8210 $M^{-1}cm^{-1}$ (Table 5.2). In like manner, (catCO$_2$Me)Pd(adi) has an absorption maximum at 800 nm with an extinction coefficient of 5170 $M^{-1}cm^{-1}$ whereas the lower-energy absorption of (catCO$_2$Me)Pd(pdi) is shifted to λ_{max} = 990 nm with an extinction coefficient 7360 $M^{-1}cm^{-1}$. The observed trend in both the absorption energies and the intensities is attributed to more delocalized π* orbitals of the pdi ligand as compared to those of the adi congener.

Table 5.2. Electronic Absorption Spectroscopic Measurements[a] and Electrochemical Data[b] for (catecholate)Pd(diimine) Complexes.

Complex	λ_{max}/nm	ε/$M^{-1}cm^{-1}$	$E°'_1$/[Pd]$^{1-/2-}$	$E°'_2$/[Pd]$^{0/1-}$	$E°'_3$/[Pd]$^{+1/0}$	$E°'_4$/[Pd]$^{+2/+1}$
(cat^{t}Bu$_2$)Pd(pdi)	1414	23620	−1.80	−0.95	−0.15	0.60
(^{Et}Bnphoscat)Pd(pdi)	1292	9360	−1.75	−0.98	−0.09	0.58
(^{Si}Bnphoscat)Pd(pdi)	1322	11090	−−	−−	−−	−−
(^{Et}phoscat)Pd(pdi)	984	8210	−1.74	−0.95	0.10	0.67
(^{Si}phoscat)Pd(pdi)	1014	8940	−−	−−	−−	−−
(catCO$_2$Me)Pd(pdi)	990	7360	−1.68	−0.91	0.13	0.69
(catCl$_4$)Pd(pdi)	928	7400	−1.59	−0.79	0.37	0.89
(cat^{t}Bu$_2$)Pd(adi)	1002	7220	−2.12	−1.21	−0.17	0.71
(^{Et}phoscat)Pd(adi)	794	5180	−2.12	−1.15	0.14	0.85
(catCO$_2$Me)Pd(adi)	800	5170	−2.04	−1.09	0.20	0.92
(catNO$_2$)Pd(adi)	726	5400	−2.02	−1.06	0.38	1.01

[a]All LL'CT transitions were recorded in CH$_2$Cl$_2$ at 298K. [b]Redox potentials were measured in THF at a glassy-carbon electrode using 0.1 M [^{n}Bu$_4$N][PF$_6$] as the supporting electrolyte (referenced to [Cp$_2$Fe]$^{+/0}$).

5.2.3 Electrochemical Properties of (catecholate)Pd(diimine) Complexes
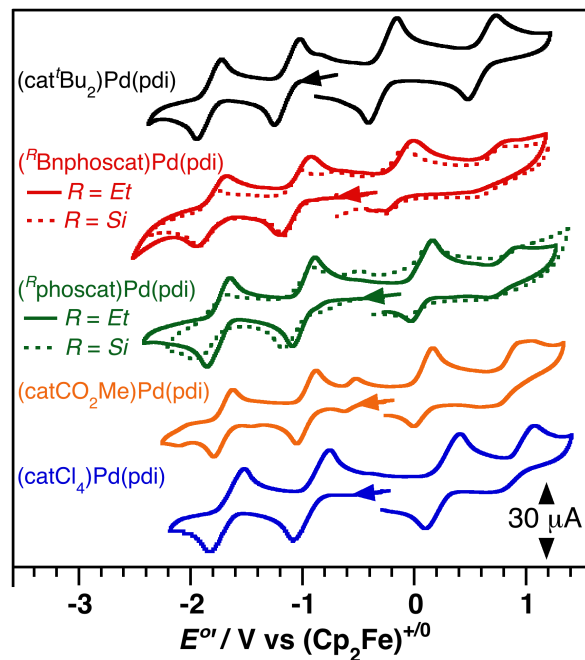
Figure 5.3. Cyclic voltammetry plots for (catecholate)Pd(pdi) complexes. Data was acquired on 1 mM samples dissolved in CH_2Cl_2 containing 0.1 M [$^nBu_4N$][PF_6] using a glassy-carbon electrode and a scan rate of 200 mV sec^{-1}. Potentials were referenced to [Cp_2Fe]$^{+/0}$ using an internal standard.

Electrochemical analyses of the (catecholate)Pd(diimine) complexes further support the hypothesis that substituents on the catecholate ligand modulate the HOMO energy of the complexes while changes to the diimine-ligand backbone modulate the LUMO. Figure 5.3 shows the cyclic voltammetry profiles for the (catecholate)Pd(pdi) family of complexes, recorded on CH_2Cl_2 solutions of the complex (1 mM) containing 100 mM [$^nBu_4N$][PF_6] as the supporting electrolyte. Table 5.3 contains the redox potentials for each complex referenced to [Cp_2Fe]$^{+/0}$ using an internal standard. In all cases, the voltammograms revealed two reversible ($i_{pa}/i_{pc} \cong 1$) one-electron reductions and two partially reversible oxidations ($i_{pa}/i_{pc} < 1$). Consistent with previous reports of square-planar palladium complexes bearing redox-active ligands, these redox processes can be assigned as being localized on the ligands, with the palladium center remaining in the +2 oxidation state.[19] The reductions for

104

all seven complexes occur in narrow ranges of -1.0 ± 0.1 V ($E^{\circ\prime}_1$) and -1.7 ± 0.1 V ($E^{\circ\prime}_2$). Given that these reductions show relatively minor dependence on the identity of the catecholate ligand, they can be assigned as primarily pdi-localized reductions. The oxidative processes for all seven complexes show a marked sensitivity to the identity of the catecholate ligand and vary linearly with the Hammett σ constant of catecholate substituents (Figure 5.4a).[20] An anodic shift of 530 mV is observed in the first oxidative process across the catecholate series with the potentials following the trend: $(cat^tBu_2)^{2-}$ < $(^RBnphoscat)^{2-}$ < $(^Rphoscat)^{2-}$ = $(catCO_2Me)^{2-}$ < $(catCl_4)^{2-}$. A similar trend is observed in the second oxidation across the series though it displays less reversible features. In general, the observed trends confirm that $(cat^tBu_2)Pd(pdi)$ is the easiest complex to oxidize and $(catCl_4)Pd(pdi)$ is the hardest to oxidize. The phosphonate-containing complexes fall in the middle with $(^RBnphoscat)Pd(pdi)$ being approximately 200 mV easier to oxidize than $(^Rphoscat)Pd(pdi)$. Hence, the electrochemical data is consistent with the phosphonate group acting as an electron-withdrawing substituent when bound directly to the catecholate and with the methylene spacer once again acting to insulate the catecholate from the electronic effects of the phosphonate group.

Table 5.3. Electrochemical Data for (catecholate)Pd(pdi) Complexes in CH_2Cl_2.[a]

Complex	$E^{\circ\prime}_1/[Pd]^{1-/2-}$	$E^{\circ\prime}_2/[Pd]^{0/1-}$	$E^{\circ\prime}_3/[Pd]^{+1/0}$	$E^{\circ\prime}_4/[Pd]^{+2/+1}$
$(cat^tBu_2)Pd(pdi)$	−1.79	−1.11	−0.26	0.61
$(^{Et}Bnphoscat)Pd(pdi)$	−1.75	−1.03	−0.14	0.65
$(^{Si}Bnphoscat)Pd(pdi)$	−1.83	−1.06	−0.17	0.67
$(^{Et}phoscat)Pd(pdi)$	−1.72	−0.97	0.07	0.79
$(^{Si}phoscat)Pd(pdi)$	−1.76	−1.00	0.02	0.80
$(catCO_2Me)Pd(pdi)$	−1.70	−0.96	0.06	0.82
$(catCl_4)Pd(pdi)$	−1.65	−0.89	0.27	0.90

[a]Potentials were measured at a glassy-carbon electrode using 0.1 M $[^nBu_4N][PF_6]$ as the supporting electrolyte (referenced to $[Cp_2Fe]^{+/0}$).
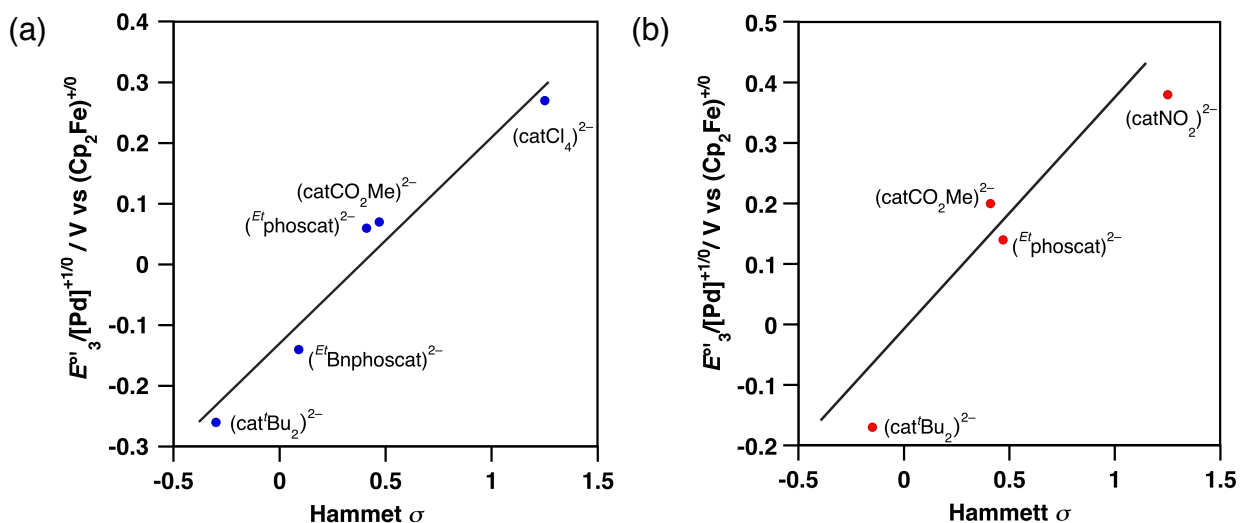
Figure 5.4. Hammett plots of (a) (catecholate)Pd(pdi) and (b) (catecholate)Pd(adi) complexes showing dependence of the first oxidation ($E^{\circ\prime}_3$) in CH_2Cl_2 or THF, respectively, on the catecholate substitution.

The electrochemical data of the (catecholate)Pd(adi) family of complexes parallels the trends established for the (catecholate)Pd(pdi) counterparts. Table 5.2 gives the redox potentials of both series of complexes measured in THF with 1 mM analyte solutions containing 100 mM [$^{n}Bu_4N$][PF_6] as the supporting electrolyte. In regard to the first reversible oxidation, the individual potentials of the adi containing complexes once again vary linearly with the Hammett σ constant of catecholate substituents (Figure 5.4b). In particular, an anodic shift of 550 mV is evident across the catecholate series, with (^{Et}phoscat)Pd(adi) displaying less oxidizable potential than (cat$^{t}Bu_2$)Pd(adi) but more oxidizable potential than (catNO$_2$)Pd(adi). Conversely, minimal shifts in potentials are seen among the two sets of reversible reductions, recorded within narrow ranges of -1.1 ± 0.1 V ($E^{\circ\prime}_1$) and and -2.1 ± 0.1 V ($E^{\circ\prime}_2$). For these redox responses, the lack of sensitivity toward catecholate substitution is consistent with two sequential electrons being displaced out of the adi-centered LUMO. The influence of the diimine ligand on the cathodic responses is further discernable on comparison of the individual families of palladium derivatives. For

106

example, the complexes of the pdi ligand are reduced in THF within more positive potenital ranges, –0.9 ± 0.1 V ($E^{o\prime}_1$) and –1.7 ± 0.1 V ($E^{o\prime}_2$), as compared to the adi complexes. These more facile reductions are in agreement with low-lying LUMO energy associated with the pdi ligand.

5.2.4 Binding of (^{R}phoscat)Pd(pdi) and (^{R}Bnphoscat)Pd(pdi) to Nanocrystalline TiO$_2$

Having defined the molecular structure-electronic property correlations of the phosphonate-containing catecholate ligands, we set out to examine the efficacy of both the ethyl- and silyl-protected phosphonate groups for binding to metal oxide surfaces. Given their low-cost, chemical stability, and well-established protocols for binding phosphonate-functionalized small molecules, nanocrystalline TiO$_2$ films were used to test both (^{R}phoscat)Pd(pdi) and (^{R}Bnphoscat)Pd(pdi) complexes. Under all conditions tested, the ethyl-protected derivatives, (^{Et}phoscat)Pd(pdi) and (^{Et}Bnphoscat)Pd(pdi), failed to bind to the TiO$_2$ films. For these ethyl-protected derivatives, the conditions required to remove the robust ethyl groups generally cleaved the Pd–O linkage first, resulting in complete decomposition of the palladium complex as indicated by the observation of free pdi ligand by both NMR spectroscopy and mass spectrometry. In the case of the silyl-protected derivatives, (^{Si}phoscat)Pd(pdi) and (^{Si}Bnphoscat)Pd(pdi), the trimethyl silyl groups were readily hydrolyzed under the mildly protic environment provided by methanol, resulting in the binding of both complexes to the semiconductor surface. In a typical experiment, nanocrystalline TiO$_2$ films prepared on a standard silica glass slide were soaked in a 0.5 mM methanolic solution of either (^{Si}phoscat)Pd(pdi) or (^{Si}Bnphoscat)Pd(pdi), and the absorption spectrum of the film was monitored as a function of time. As shown in Figure 5.5, within eight hours of soaking in the dye solution, strong charge-transfer absorptions

were observed in the visible-to-near-IR portions of the absorption spectrum, consistent with the binding of either (^{OH}phoscat)Pd(pdi) or (^{OH}Bnphoscat)Pd(pdi) to the TiO$_2$ surface (*OH* corresponds to the hydrolyzed –PO$_3$H$_2$ anchors). The ready binding of the silyl-protected phosphonate-containing complexes as compared to the ethyl-protected derivatives highlights the importance of choosing phosphonate protecting groups with chemistries that are compatible with the potentially reactive metal-ligand bond linkages.
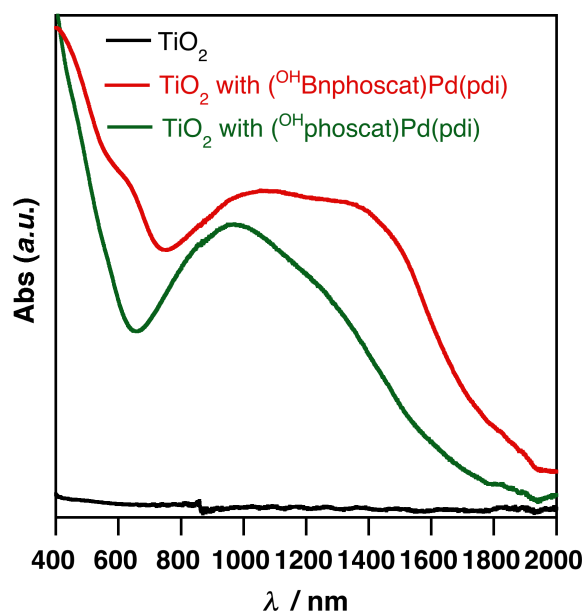
Figure 5.5. Absorption spectra of TiO$_2$ film before and after the 8-hour treatment with 0.5 mM methanolic solutions of (^{Si}phoscat)Pd(pdi) and (^{Si}Bnphoscat)Pd(pdi), showing the lower-energy LL'CT bands of (^{OH}phoscat)Pd(pdi) and (^{OH}Bnphoscat)Pd(pdi), respectively.

5.3 Summary

New catecholate ligands containing protected phosphonate anchoring groups in the 4-position of the catecholate ring were synthesized. The catechol 4-diethoxyphosphorylbenzene-1,2-diol, (^{Et}phoscat)H$_2$, was prepared in three steps from pyrocatechol; whereas, the catechol 4-(diethoxyphosphorylmethyl)benzene-1,2-diol, (^{Et}Bnphoscat)H$_2$, containing a methylene spacer between the catecholate ring and phosphonate anchor, was prepared from protocatechuic acid in six linear steps. A series of

charge-transfer complexes of the formulae (catecholate)Pd(pdi) (pdi = *N,N′*-bis(mesityl)phenanthrene-9,10-diimine) and (catecholate)Pd(adi) (*N,N'*-(mesityl)-acenaphthenediimine (adi)) were also prepared to evaluate the electronic impact of directly attaching the phosphonate group to the catecholate ligand versus attaching it through a methylene linker. Electronic spectroscopy and cyclic voltammetry of the complexes showed that the phosphonate substituent is a significant electron-withdrawing group,[21] when installed directly on the aromatic ring of the catecholate ligand, and, thus, perturbs the donor ability of the (^{*R*}phoscat)$^{2-}$ derivatives. On the other hand, the incorporation of a single methylene linker into the (^{*R*}Bnphoscat)$^{2-}$ derivatives serves to effectively preserve the donating properties of the catecholate ligand.

Both catechol derivatives, (^{*Et*}phoscat)$^{2-}$ and (^{*R*}Bnphoscat)$^{2-}$, were further elaborated to their trimethylsilyl-protected counterparts to facilitate their binding to nanocrystalline metal oxides. The synthesis and application of (^{*Si*}phoscat)Pd(pdi) and (^{*Si*}Bnphoscat)Pd(pdi) demonstrated that the phosphonate groups of both silylated derivatives enable for robust binding to TiO$_2$. Furthermore, and in contrast to the previously reported di-*ortho*-phosphonylated catecholate ligand,[31] the *para*-phosphonylated catechols described here have the anchoring group further removed from the metal-chelating site, which should help to minimize competing interactions between the metal binding site and the metal oxide surface for immobilized dyes. As a result, the phosphonylated catecholate ligands, (^{*R*}phoscat)$^{2-}$ and (^{*R*}Bnphoscat)$^{2-}$, reported herein should prove useful in applications such as catecholate-based dyes for sensitized solar cells or in electrochemical cells employing catecholate-based catalysts.

5.4 Experimental

General Considerations. All manipulations involving the synthesis of ligands were performed under air, unless otherwise noted, employing reagents and solvents purchased from commercial suppliers and used as received. Column chromatography was performed with 230-400 mesh silica gel using flash column techniques. Palladium complexes were synthesized and studied under an inert atmosphere of nitrogen using standard glovebox techniques and dry, degassed solvents. Hydrocarbon solvents were sparged with argon and then deoxygenated and dried by passage through Q5 and activated alumina columns, respectively. Ethereal and halogenated solvents were sparged with argon and dried by passage through two activated alumina columns. Tetrachlorocatechol and 3,5-di-*tert*-butylcatechol were purchased from Sigma-Aldrich and used as received. The diimine ligands, *N,N′*-(mesityl)phenanthrene-9,10-diimine (pdi)[22] and *N,N′*-bis(mesityl)-acenapthylene-1,2-diimine (adi),[23] $(MeCN)_2PdCl_2$[24], and the catecholate-ligand derivatives, 2,2-dimethyl-1,3-benzodioxole[25] (**16**), ethyl 3,4-dihydroxybenzoate (**19**),[26] 3,4-dihydroxybenzoate $((catCO_2Me)^{2-})$[27], and 4-nitrocatecholate $((catNO_2)^{2-})$,[28] were prepared by previously described methods.

Physical Methods. NMR spectra were collected on Bruker Avance 400 and 500 MHz spectrometers. Chemical shifts were reported using the standard δ notation in parts per million and referenced using residual ^1H and ^{13}C isotopic impurities of the solvent. Infrared spectra were recorded as KBr pellets or as neat liquids using a Perkin-Elmer Spectrum One FTIR spectrophotometer. Electronic absorption spectra were recorded as solutions in dry, degassed CH_2Cl_2 in one-centimeter quartz cuvettes using a Perkin-Elmer Lambda 900 UV-vis spectrophotometer.

Electrochemical Methods. Cyclic voltammetry (CV) and differential pulse voltammetry (DPV) experiments were performed on a Gamry Series G 300 Potentiostat/ Galvanostat/ZRA (Gamry Instruments, Warminster, PA, U.S.A.) using a 3.0 mm glassy carbon working electrode, a platinum wire auxiliary electrode, and a silver wire reference electrode. Measurements were recorded in a nitrogen-filled glovebox at ambient temperature and a scan rate of 200 mV/s. Sample concentrations were based on 1.0 mM CH_2Cl_2 or THF solutions containing 100 mM $[^nBu_4N][PF_6]$ as the supporting electrolyte. All potentials were referenced to the $[Cp_2Fe]^{+/0}$ couple using ferrocene or decamethylferrocene (−0.59 V or −0.47 V vs $[Cp_2Fe]^{+/0}$ in CH_2Cl_2 or THF, respectively) as an internal standard.[29] Decamethylferrocene was purified by sublimation under reduced pressure and tetrabutyl-ammonium hexafluorophosphate was recrystallized from ethanol three times and dried under vacuum.

TiO$_2$ Binding Studies. The binding of anchor-functionalized catecholate complexes was studied using 6 μm thick films of nanocrystalline anatase TiO_2 (20 nm average particle size) on glass slides prepared according to a literature procedure.[30] The films were soaked in 0.5 mM solutions of the complex dissolved in methanol. To check for binding the films were removed from the solution, rinsed with clean solvent, and the UV-vis-NIR and FT-IR spectra were recorded. UV-vis-NIR spectra of films were recorded on a Perkin-Elmer Lambda 950 spectrophotometer equipped with a 60 mm integrating sphere. FT-IR spectra were recorded on a Thermo Scientific Nicolet 6700 spectrophotometer equipped with a PIKE Technologies Gladi ATR.

Diethyl (2,2-dimethylbenzo[1,3]dioxol-5-yl)phosphonate (17a) and Diethyl (2,2-dimethylbenzo[1,3]dioxol-4-yl)phosphonate (17b): To a solution of **16** (3.3 g, 22 mmol) and diethyl phosphite (5.7 mL, 44 mmol) in 70 mL of glacial acetic acid was added $Mn(OAc)_3 \cdot H_2O$ (15 g, 56 mmol). The mixture was heated at 100 °C for 2 h while stirring in air. After cooling to room temperature, the reaction mixture was quenched with water (100 mL) and extracted with ethyl acetate (70 mL, then 2 x 40 mL). The combined organic layers were dried over anhydrous Na_2SO_4, and concentrated to dryness. The crude product was purified by column chromatography on silica-gel (ethyl acetate:toluene/55:45) to give an inseparable mixture of regioisomers **17a** and **17b** in a 5-to-1 ratio as an orange oil in a combined yield of 72% (4.5 g). Alternatively, the crude product may also be purified by vacuum distillation (135 °C, 0.60 mmHg). Both isomers were carried on to the next step. ^{31}P NMR (162 MHz, $CDCl_3$, major) δ 20.7; ^{1}H NMR (500 MHz, $CDCl_3$, major) δ 7.23 (dd, J = 14.1, 8.2 Hz, 1H), 7.01 (d, J = 13.2 Hz, 1H), 6.69 (dd, J = 7.9, 4.0 Hz, 1H), 4.09-3.91 (m, 4H), 1.58 (s, 6H), 1.21(t, J = 7.4 Hz, 6H); ^{13}C NMR (125 MHz, $CDCl_3$, major) δ 151.2 (d, J = 3.7 Hz, aryl-C−O), 147.9 (d, J = 22.2 Hz, aryl-C−O), 127.1 (d, J = 11.1 Hz, aryl-C), 121.0 (d, J = 193.7 Hz, aryl-qC), 119.1 ($C(CH_3)_2$), 111.1 (d, J = 12.5 Hz, aryl-C), 108.6 (d, J = 19.0 Hz, aryl-C), 62.1 (d, J = 5.5 Hz, CH_2−O), 26.0 (CH_3), 16.4 (d, J = 6.9 Hz, CH_3); ^{31}P NMR (162 MHz, $CDCl_3$, minor) δ 16.04. Some of the ^{1}H and the ^{13}C resonances of the minor regioisomer **17b** were obscured by those of the major isomer, and thus, characteristic signals are listed as follows: ^{1}H NMR (500 MHz, $CDCl_3$, minor) δ 7.08 (dd, J = 12.8, 7.7 Hz, 1H), 6.77 (appar d, J = 7.5 Hz, 1H), 6.74 (dd, J = 7.7, 3.7= Hz, 1H), 4.09-3.91 (m, 4H, minor and major), 1.61 (s, 6H), 1.24-1.20 (t, J = 7.4 Hz, 6H, minor and major); ^{13}C NMR (125 MHz, $CDCl_3$, minor) δ 149.3 (d, J = 3.2 Hz, aryl-C−O), 147.7 (d, J = 13.0 Hz, aryl-C−O), 124.7 (d, J = 6.9 Hz, aryl-C), 121.2 (d, J =

14.8 Hz, aryl-C), 119.1 (C(CH$_3$)$_2$, minor and major), 112.3 (d, J = 2.8 Hz, aryl-C), 109.5 (d, J = 190.5 Hz, aryl-qC), 62.4 (d, J = 5.5 Hz, CH$_2$-O), 25.9 (CH$_3$), 16.4-16.3 (CH$_3$, minor and major); FTIR (neat) v/cm^{-1} 3060, 2989, 2906, 1654, 1604, 1495 st, 1380, 1251 st, 1039 st, 963 st; HRMS (ESI) m / z calcd for C$_{13}$H$_{19}$O$_5$P (M + Na)$^+$ 309.0868, found 309.0869.

4-diethoxyphosphorylbenzene-1,2-diol (^{Et}phoscat)H$_2$: To a solution of **17a** and **17b** (4.0 g, 14 mmol) in dry CH$_2$Cl$_2$ (200 mL), was added BCl$_3$ (100 mL, 1M in hexanes) at –78 °C under a nitrogen atmosphere. The mixture was stirred at the same temperature for 12 h and then allowed to warm slowly to room temperature. The solvent was removed *in vacuo* to give an oily residue that was purified by silica gel column chromatography (ethyl acetate:hexanes/40:60) to afford the product, (^{Et}phoscat)H$_2$, as a single regioisomer in 67% yield (2.3 g). ^{31}P NMR (162 MHz, CDCl$_3$) δ 21.8; ^{1}H NMR (500 MHz, CDCl$_3$) δ 9.70 (s, 1H), 7.66 (d, J = 15.0 Hz, 1H), 7.13 (dd, J = 12.6, 8.1 Hz, 1H), 6.97-6.95 (m, 1H and s, 1H), 4.13-3.99 (4H, m), 1.30 (t, J = 7.2 Hz, 6H); ^{13}C NMR (125 MHz, CDCl$_3$) δ 149.9 (d, J = 3.6 Hz, aryl-C–O), 141.1 (d, J = 21.3 Hz, aryl-C–O), 124.6 (d, J = 9.7 Hz, aryl-C), 119.3 (d, J = 3.41 Hz, aryl-C), 117.8 (d, J = 195.6 Hz, aryl-qC), 115.6 (d, J = 18.1 Hz, aryl-C), 62.9 (d, J = 5.1 Hz, CH$_2$–O), 16.5 (d, J = 6.5 Hz, CH$_3$); FTIR (neat) v/cm^{-1} 3521 br, 2986, 2252, 2840, 2766, 1707, 1593 st, 1511, 1423, 1283, 1009, 949, 760; HRMS (ESI) m / z calcd for C$_{10}$H$_{15}$O$_5$P (M + Na)$^+$ 269.0555, found 269.0553.

Ethyl 2,2-dimethylbenzo[1,3]dioxole-5-carboxylate (20): To a stirred solution of **19** (23.4 g, 128 mmol) and acetone (56 mL) in 80 mL of benzene, was added slowly phosphorous trichloride (12.0 mL, 137 mmol). The mixture was stirred open to air at room temperature until the evolution of HCl gas ceased, at which point the reaction flask was capped and allowed to stir for an additional 12 h. The reaction was quenched by pouring it

over K_2CO_3 (75 g). The solution was filtered and the precipitate rinsed with benzene. Extraction with 10% NaOH solution and drying over anhydrous Na_2SO_4 afforded product **20** in pure form as a yellow oil (18 g, 64%). While **20** is a known compound, its ^{13}C NMR data has not been reported.[31] ^{1}H NMR (500 MHz, CDCl$_3$) δ 7.61 (dd, J = 8.2, 1.7 Hz, 1H), 7.38 (d, J = 1.7 Hz, 1H), 6.73 (d, J = 8.2 Hz, 1H), 4.32 (q, J = 7.1 Hz, 2H), 1.69 (s, 6H), 1.36 (t, J = 7.1 Hz, 3H); ^{13}C NMR (125 MHz, CDCl$_3$) δ 166.5 (q, C=O), 151.7 (aryl-C−O), 147.8 (aryl-C−O), 125.1 (aryl-C), 124.2 (aryl-qC), 119.4 (C(CH$_3$)$_2$), 109.7 (aryl-C), 108.1 (aryl-C), 61.1 (CH$_2$−O), 26.2 ((CH$_3$)$_2$C), 14.7 (CH$_3$); FTIR (neat) v/cm^{-1} 2991, 2937, 1714 st, 1622, 1607, 1495 st, 1445 st, 1371, 1281 st, 1213 st, 1096, 1020, 980, 839, 821; HRMS (ESI) m / z calcd for $C_{12}H_{14}O_4$ (M + Na)$^+$ 245.0790, found 245.0789.

(2,2-dimethylbenzo[1,3]dioxol-5-yl)methanol (21): Compound **21** was prepared from 2.77 g of **20** (12.0 mmol) and 1.97 g of LiAlH$_4$ (52.0 mmol) in cold THF using a slightly modified literature procedure.[32] Standard aqueous workup afforded 2.0 g of **21** as a yellow oil (89% yield). The ^{1}H and ^{13}C NMR spectra of **21** are in agreement with the literature data.

5-(bromomethyl)-2,2-dimethylbenzo[1,3]dioxole (22): To a cold (0 °C) solution of dioxole **21** (2.0 g, 11 mmol) and pyridine (0.95 mL, 12 mmol) in anhydrous Et$_2$O (21 mL) was added dropwise a solution of PBr$_3$ (0.41 mL, 4.3 mmol) in Et$_2$O (20 mL). The mixture was stirred for 2 h at room temperature and then quenched with ice-water (40 mL). The organic layer was separated, washed with ice-cold, 1 N HCl solution (5 mL) and dried with anhydrous Na$_2$SO$_4$. The removal of solvent by rotary evaporation yielded benzyl bromide **22** as a colorless oil (2.2 g, 81%), which was sufficiently pure to be used directly in the next step. ^{1}H NMR (400 MHz, CDCl$_3$) δ 6.81 (d, J = 7.9 Hz, 1H), 6.78 (s, 1H), 6.65 (d, J = 7.9 Hz,

2H), 4.46 (s, 2H), 1.67 (s, 6H); ^{13}C NMR (125 MHz, CDCl$_3$) δ 148.1 (aryl-C−O), 148.0 (aryl-C−O), 131.1 (aryl-C), 122.5 (aryl-qC), 118.8 (aryl-qC), 109.6 (aryl-C), 108.4 (aryl-C), 35.0 (CH$_2$−Br), 26.2 ((CH$_3$)$_2$C); FTIR (neat) v/cm^{-1} FTIR (KBr) v/cm^{-1} 2989, 2935, 1600, 1494 st, 1448, 1257 st, 1209 st, 979, 835; HRMS (CI, positive) m / z calcd for C$_{10}$H$_{11}$BrO$_2$ (M)$^+$ 241.9942, found 241.9953

Diethyl ((2,2-dimethylbenzo[1,3]dioxol-5-yl)methyl)phosphonate (23): A solution of benzyl bromide **22** (11 g, 45 mmol) in neat triethyl phosphite (7.8 mL, 45 mmol) was refluxed for 12 h. Upon the completion of the reaction, the obtained crude material was purified by silica gel column chromatography (EtOAc:hexanes/42:58) to afford **23** as a yellow oil (11 g, 81%). ^{31}P NMR (162 MHz, CDCl$_3$, major) δ 28.0; ^{1}H NMR (500 MHz, CDCl$_3$) δ 6.66-6.59 (m, 3H), 3.98 (appar q, J = 7.3 Hz, 4H), 3.02 (d, J = 11.0 Hz, 2H), 1.61 (s, 6H), 1.21 (appar t, J = 7.3 Hz, 6H); ^{13}C NMR (125 MHz, CDCl$_3$) δ 147.8 (d, J = 3.2 Hz, aryl-C−O), 146.7 (d, J = 3.2 Hz, aryl-C−O), 124.4 (d, J = 9.7 Hz, aryl-qC), 122.5 (d, J = 7.9 Hz, aryl-C), 118.1 (C(CH$_3$)$_2$), 110.4 (d, J = 6.0 Hz, aryl-C), 108.3 (d, J = 3.2 Hz, aryl-C), 62.3 (d, J = 6.9 Hz, CH$_2$-O), 34.1 (d, J = 139.2 Hz, CH$_2$−P), 26.0 (CH$_3$), 16.6 (d, J = 6.0 Hz, CH$_3$); FTIR (neat) v/cm^{-1} 2988, 2911, 1650, 1609, 1498 st, 1380, 1231 st, 1048 st, 957 st 825 st; HRMS (ESI) m / z calcd for C$_{14}$H$_{21}$O$_5$P (M + Na)$^+$ 323.1024, found 323.1028.

4-(diethoxyphosphorylmethyl)benzene-1,2-diol (^{Et}Bnphoscat)H$_2$: To a solution of **23** (2.5 g, 8.0 mmol) in dry CH$_2$Cl$_2$ (200 mL), was added BCl$_3$ (20 mL, 1M in hexanes) at −78 °C under a nitrogen atmosphere. The mixture was stirred at the same temperature for 12 h and then allowed to warm slowly to room temperature and quenched with MeOH (4 mL). The solvent was removed *in vacuo* to give an oily residue, which was purified by silica gel column chromatography (gradient MeOH:CHCl$_3$/7:93) to afford product (^{Et}Bnphoscat)H$_2$

as a white solid (1.5 g, 71%). ^{31}P NMR (162 MHz, CDCl$_3$) δ 29.5; ^{1}H NMR (500 MHz, CDCl$_3$) δ

8.18 (s, 1H), 7.01 (s, 1H), 6.91 (s, 1H), 6.66 (d, J = 8.6, 1H), 6.55 (d, J = 8.6, 1H), 4.02 (m, 4H),

3.06 (d, J = 20.5 Hz, 2H), 1.26 (t, J = 7.2 Hz, 6H). ^{13}C NMR (125 MHz, CDCl$_3$) δ 145.1 (d, J = 3.2

Hz, aryl-C–O), 140.0 (d, J = 3.6 Hz, aryl-C–O), 122.0 (d, J = 9.3Hz, aryl-qC), 121.8 (d, J = 6.94

Hz, aryl-C), 116.8 (d, J = 6.0 Hz, aryl-C), 115.6 (d, J = 3.2 Hz, aryl-C), 63.2 (d, J = 7.4 Hz,

CH$_2$–O), 33.6 (d, J = 140.6 Hz, CH$_2$–P), 16.7 (d, J = 6.0 Hz, CH$_3$); FTIR (KBr) v/cm^{-1} 3395 br,

3170 br, 2988, 1612, 1536, 1448, 1365, 1274, 1160, 1010, 860. HRMS (ESI) m / z calcd for

C$_{11}$H$_{17}$O$_5$P (M + Na)$^+$ 283.0711, found 283.0704.

(^{Et}**phoscat)Pd(pdi):** A mixture of (CH$_3$CN)$_2$PdCl$_2$ (127 mg, 0.500 mmol) and *N,N′*-

bis(mesityl)phenanthrene-9,10-diimine (222 mg, 0.500 mmol) was stirred in CH$_2$Cl$_2$ (5 mL)

at room temperature for 12 h. To the resulting dark red solution, (^{Et}phoscat)H$_2$ (123 mg,

0.500 mmol) was added followed by *tert*-butylamine (105 μL, 1.00 mmol). After 12 h of

stirring at the same temperature, the reaction mixture was filtered to remove *tert*-

butylamine hydrochloride and the solvent removed under vacuum. The solid residue was

recrystallized from a minimum amount of dichloromethane and pentane (–35 °C) to give

the product as a dark brown solid (260 mg, 66% yield). ^{31}P NMR (162 MHz, CDCl$_3$) δ 25.64;

^{1}H NMR (500 MHz, CDCl$_3$) δ 8.15 (d, J = 8.0 Hz, 2H), 7.62 (appar t, J = 7.7 Hz, 2H), 7.37 (d, J =

8.3 Hz, 1H), 7.32 (d, J = 8.3 Hz, 1H), 7.12 (appar q, J = 7.3 Hz, 2H), 7.05 (s, 4H), 6.82-6.74 (m,

2H), 6.38 (dd, J = 8.1 Hz, J = 5.0 Hz, 1H), 4.00-3.83 (m, 4H), 2.43 (s, 3H), 2.42 (s, 3H), 2.29 (s,

12H), 1.20 (t, J = 7.1 Hz, 6H); ^{13}C NMR (125 MHz, CDCl$_3$) δ 169.5 (d, J = 3.2 Hz, aryl-C–O),

164.7 (d, J = 20.8 Hz, aryl-C–O), 163.1 (C=N), 162.9 (C=N), 144.4 (mesityl-C–N), 144.3

(mesityl-C–N), 138.0 (mesityl-qC), 137.9 (mesityl-qC), 134.11 (pdi qC), 134.10 (pdi qC),

133.7 (pdi aryl-C), 133.6 (pdi ary-C), 130.2 (mesityl-C), 129.69 (pdi aryl-C), 129.67 (pdi

aryl-C), 129.1 (meistyl-qC), 129.0 (mesityl-qC), 128.63 (pdi aryl-C), 128.56 (pdi aryl-C), 126.6 (pdi qC), 126.5 (pdi qC), 125.12 (pdi aryl-C), 125.10 (pdi aryl-C), 122.2 (d, J = 11.1 Hz, cat aryl-C), 119.6 (d, J = 12.5 Hz, cat aryl-C), 116.4 (d, J = 19.4 Hz, cat aryl-C), 113.3 (d, J = 190.0 Hz cat aryl-qC), 61.6 (d, J = 4.6 Hz, C–O), 21.65 (mesityl-CH_3), 21.64 (mesityl-CH_3), 19.1 (mesityl-CH_3), 19.0 (mesityl-CH_3), 16.7 (d, J = 6.9 Hz, CH_3); FTIR (KBr) v/cm^{-1} 3543, 3478, 3417, 3247, 2972, 2906, 2862, 1637, 1615, 1497, 1470, 1352, 1308 st, 1050, 1023; UV–vis–NIR (CH_2Cl_2) λ_{max}/nm (ε/M^{-1} cm^{-1}): 984 (8210); HRMS (ESI) m / z calcd for $C_{42}H_{43}N_2O_5PPd$ (M + Na)$^+$ 815.1858, found 815.1871.

(^{Et}**Bnphoscat)Pd(pdi):** This complex was prepared in a manner similar to that described for (^{Et}phoscat)Pd(pdi) using (^{Et}Bnphoscat)H_2 (135 mg, 0.500 mmol). Recrystallization from THF and pentane (–35 °C) afforded the product as a brown solid (313 mg, 77%). ^{31}P NMR (162 MHz, CDCl$_3$) δ 29.5; ^{1}H NMR (500 MHz, CDCl$_3$) δ 8.16 (d, J = 8.3 Hz, 2H), 7.59 (appar t, J = 7.3 Hz, 2H), 7.33 (d, J = 8.4 Hz, 1H), 7.30 (d, J = 8.4 Hz, 1H), 7.09 (appar td, J = 8.3 Hz, 3.3 Hz, 2H), 7.04 (s, 4H), 6.35 (s, 1H), 6.34 (d, J = 8.0 Hz, 1H), 6.26 (d, J = 8.0 Hz, 1H), 3.94 (m, 4H), 2.96 (d, J = 20.8 Hz, 2H), 2.42 (s, 3H), 2.41 (s, 3H), 2.29 (s, 12H), 1.19 (t, J = 7.2 Hz, 6H); ^{13}C NMR (125 MHz, CDCl$_3$) δ 165.6 (aryl-C–O), 164.9 (aryl-C–O), 161.77 (C=N) , 161.70 (C=N), 144.73 (mesityl-C–N), 144.68 (mesityl-C–N), 137.49 (mesityl-qC), 137.46 (mesityl-qC), 133.61 (pdi qC), 133.59 (pdi qC), 132.7 (pdi aryl-C), 130.00 (pdi aryl-C), 129.97 (pdi-aryl-C), 129.5 (mesityl-qC), 129.34 (pdi aryl-C), 129.31 (pdi-arylC), 128.0 (pdi-arylC), 126.8 (pdi-qC), 124.9 (pdi-arylC), 120.0 (d, J = 9.3 Hz, cat qC), 119.3 (d, J = 6.0 Hz, cat aryl-C), 118.1 (d, J = 6.5 Hz, cat aryl-C), 116.2 (d, J = 2.3 Hz, cat aryl-C), 62.3 (d, J = 6.9 Hz, C–O), 33.7 (d, J = 137.3 Hz, CH_2-P), 21.6 (mesityl-CH_3), 19.08 (mesityl-CH_3), 19.07 (mesityl-CH_3), 16.7 (d, J = 6.5 Hz, CH_3); FTIR (KBr) v/cm^{-1} 3570, 3541, 3470,

3405, 2958, 2900, 1635, 1597, 1436, 1357, 1310, 1025 st, 954; UV-vis-NIR (CH$_2$Cl$_2$) λ_{max}/nm (ε/M^{-1} cm^{-1}): 1298 (9360); HRMS (ESI) m / z calcd for C$_{43}$H$_{45}$N$_2$O$_5$PPd (M + Na)$^+$ 829.2015, found 829.2024.

(cat^{t}Bu$_2$)Pd(pdi): This complex was prepared in a manner similar to that described for (^{Et}phoscat)Pd(pdi) using 3,5-di-*tert*-butylcatechol (111 mg, 0.500 mmol). Recrystallization from dichloromethane and pentane (–35 °C) afforded the product as a dark brown solid (360 mg, 73%). ^{1}H NMR (500 MHz, CDCl$_3$) δ 8.20 (appar t, J = 7.5 Hz, 2H), 7.57-7.50 (m, 2H and m,1H), 7.30 (d, J = 8.3 Hz, 1H), 7.11-7.05 (appar quint, J = 8.0 Hz 2H), 7.04 (s, 2H), 7.00 (s, 2H), 6.42, (br s, 1H), 6.39 (s, 1H), 2.44 (s, 3H), 2.42 (d, 3H), 2.31 (s, 6H), 2.30 (s, 6H), 1.17 (s, 9H), 1.02 (s, 9 H); ^{13}C NMR (125 MHz, CDCl$_3$) δ 167.5 (aryl-C–O), 164.0 (aryl-C–O), 159.3 (C=N), 158.6 (C=N), 145.50 (mesityl-C–N), 145.48 (mesityl-C–N), 142.8 (cat aryl-qC), 138.0 (cat aryl-qC), 136.9, (mesityl-qC) 136.8 (mesityl-qC), 132.7 (pdi qC), 132.5 (pdi qC), 131.0 (pdi aryl-C), 130.9 (pdi aryl-C), 130.3 (mesityl-qC), 129.9 (mesityl-qC), 129.8 (mesityl-C), 129.7 (mesityl-C), 128.8 (pdi aryl-C), 128.7 (pdi aryl-C), 127.24 (pdi qC), 127.20 (pdi qC), 127.1 (pdi aryl-C), 127.0 (pdi aryl-C), 124.5 (pdi aryl-C), 114.7 (cat aryl-C), 113.3 (cat aryl-C), 34.7 (C(CH$_3$)$_3$), 32.0 (cat CH$_3$), 29.5 (cat CH$_3$), 21.7 (mesityl-CH$_3$), 21.5 (mesityl-CH$_3$), 19.2 (mesityl-CH$_3$), 19.0 (mesityl-CH$_3$); FTIR (KBr) v/cm^{-1} 3538, 3478, 3412, 3236, 2945, 2895, 2892, 1637, 1615, 1476, 1492, 1349, 1133, 1083 st, 1045, 1020; UV-vis-NIR (CH$_2$Cl$_2$) λ_{max}/nm (ε/M^{-1} cm^{-1}): 1414 (23620); HRMS (ESI) m / z calcd for C$_{46}$H$_{50}$N$_2$O$_2$Pd (M + Na)$^+$ 791.2822, found 791.2803.

(catCO$_2$Me)Pd(pdi): This was prepared in a manner similar to that described for (^{Et}phoscat)Pd(pdi) using 4-(methoxycarbonyl)catechol (84 mg, 0.50 mmol). Recrystallization from dichloromethane and pentane afforded a dark brown solid (289 mg,

81%). ^{1}H NMR (500 MHz, CDCl$_3$) δ 8.11 (d, J = 8.0 Hz, 2H), 7.61 (appar t, J = 7.7 Hz, 2H), 7.31 (d, J = 8.5 Hz, 1 H), 7.28 (d, J = 9.0 Hz, 1 H), 7.12-7.07 (m, 2H and m, 1H), 7.04-7.02 (s, 4H and m, 1H), 6.33 (d, J = 8.5 Hz, 1H), 3.73 (s, 3 H), 2.42 (s, 3 H), 2.40 (s, 3 H), 2.30 (s, 12 H); ^{13}C NMR (125 MHz, CDCl$_3$) δ 170.3 (aryl-C–O), 168.6 (C=O), 164.0 (aryl-C–O), 163.3 (C=N), 163.1 (C=N), 144.22 (mesityl-C–N), 144.16 (mesityl-C–N), 137.93 (mesityl-qC), 137.88 (mesityl-qC), 134.14 (pdi qC), 134.11 (pdi qC), 133.84 (pdi aryl-C), 133.79 (pdi aryl-C), 130.22(mesityl-C), 130.19 (mesityl-C), 129.6 (pdi aryl-C), 129.01(pdi aryl-C), 129.00 (pdi aryl-C), 128.54 (mesityl-qC), 128.46 (mesityl-qC), 126.37 (pdi qC), 126.31 (pdi qC), 125.22 (pdi aryl-C), 125.20 (pdi aryl-C), 120.5 (cat aryl-C), 117.9 (cat qC), 116.9 (cat aryl-C), 115.5 (cat aryl-C), 51.4 (CH$_3$–O), 21.60 (mesityl-CH$_3$), 21.57 (mesityl-CH$_3$), 18.94(mesityl-CH$_3$), 18.91 (mesityl-CH$_3$); FTIR (KBr) v/cm^{-1} 3554, 3478, 3417, 3230, 2972, 2912, 2939, 1698, 1637, 1615, 1593, 1563, 1497, 1434, 1355, 1281 st, 1196, 1108, 1083; UV-vis-NIR (CH$_2$Cl$_2$) λ_{max}/nm (ε/M^{-1} cm^{-1}): 990 (7360); HRMS (ESI) m / z calcd for C$_{40}$H$_{36}$N$_2$O$_4$Pd (M + Na)$^+$ 737.1623, found 737.1599.

(catCl$_4$)Pd(pdi): This complex was prepared in a manner similar to that described for (^{Et}phoscat)Pd(pdi) using tetrachlorocatechol (124 mg, 0.500 mmol). Recrystallization from dichloromethane and pentane (–35 °C) afforded the product as a dark brown solid (312 mg, 79%). ^{1}H NMR (500 MHz, CDCl$_3$) δ 8.16 (d, J = 8.3 Hz, 2H), 7.66 (appar t, J = 7.7 Hz, 2H), 7.51 (d, J = 8.3 Hz, 2H), 7.16 (apart t J = 7.7 Hz, 2H), 7.08 (s, 4H), 2.41 (s, 6H), 2.31 (s, 12H); ^{13}C NMR (125 MHz, CDCl$_3$) δ 163.9 (C=N), 159.1 (aryl-C–O), 143.9 (mesityl-C–N), 138.5 (mesityl-qC), 134.4 (pdi aryl-C and pdi qC), 130.3 (mesityl-C), 130.0 (pdi aryl-C), 129.0 (mesity- qC), 128.9 (pdi aryl-C), 126.3 (pdi qC), 125.2 (pdi aryl-C), 117.8 (aryl-C–Cl), 116.7 (aryl-C–Cl), 21.6 (mesityl-CH$_3$), 19.1 (mesityl-CH$_3$); FTIR (KBr) v/cm^{-1} 3538, 3406,

3236, 2972, 2906, 1638, 1617, 1595, 1469, 1417 st, 1355, 1307, 1261 st, 1199, 1032, 972; UV-vis-NIR (CH_2Cl_2) λ_{max}/nm (ε/M^{-1} cm^{-1}): 932 (7400); HRMS (ESI) m / z calcd for $C_{38}H_{30}Cl_4N_2O_2Pd$ (M + Na)$^+$ 816.9985, found 816.9960.

(^{Et}phoscat)Pd(adi): A mixture of ($CH_3CN)_2PdCl_2$ (127 mg, 0.500 mmol) and N,N'-bis(mesityl)acenapthylene-1,2-diimine (208 mg, 0.500 mmol) was stirred in CH_2Cl_2 (5 mL) at room temperature for 12 h. To the resulting red solution, (^{Et}phoscat)H_2 (123 mg, 0.500 mmol) was added followed by $tert$-butylamine (105 μL, 1.00 mmol). After 12 h of stirring at the same temperature, the reaction mixture was filtered to rid of triethylammonium chloride and the solvent was removed under vacuum. The solid residue was recrystallized from a minimum amount of dichloromethane and pentane to give a green crystalline product (338 mg, 88% yield). ^{31}P NMR (162 MHz, $CDCl_3$) δ 25.60; ^{1}H NMR (500 MHz, $CDCl_3$) δ 8.10 (d, J = 8.4 Hz, 2H), 7.51 (m, 2H), 7.07 (s, 4H), 6.84-6.77 (m, 2H and m, 2H) 6.44 (dd, J = 7.5, 5.0 Hz, 1H), 4.00-3.83 (m, 4H), 2.42-2.40 (s,12H and s, 6H), 1.20 (t, J = 7.1 Hz, 3H); ^{13}C NMR (125 MHz, $CDCl_3$) δ 172.6 (C=N), 172.5 (C=N), 169.0 (d, J = 3.7 Hz, aryl-C–O), 164.0 (d, J = 20.3 Hz, aryl-C–O), 145.4 (adi qC), 141.1 (mesityl-C–N), 141.0 (mesityl-C–N), 138.5 (mesityl-qC), 138.4 (mesityl-qC), 131.90 (adi aryl-C), 131.88 (adi aryl-C), 131.6 (adi qC), 130.1 (mesityl-C), 130.0 (mesityl-C), 129.95 (mesityl-qC), 129.90 (adi aryl-C), 129.83 (adi aryl-C) 129.81 (mesityl-qC), 121.82 (adi qC), 121.80 (adi qC), 124.50 (adi aryl-C), 124.47 (adi aryl-C), 122.3 (d, J = 12.0 Hz, cat aryl-C), 118.5 (d, J = 12.0 Hz, cat aryl-C), 115.9 (d, J = 20.3 Hz, cat aryl-C), 112.9 (d, J = 191.0 Hz, cat aryl-qC), 61.5 (d, J = 4.6 Hz, CH_2–O), 21.6 (mesityl-CH_3), 18.6 (mesityl-CH_3), 18.5 (mesityl-CH_3), 16.7 (d, J = 6.9 Hz, CH_3); FTIR (KBr) v/cm^{-1} 3560, 3472, 3412, 3230, 2975, 2851, 1637, 1617, 1479, 1274 st, 1226, 1032, 962;

UV-vis-NIR (CH_2Cl_2) λ_{max}/nm (ε/M^{-1} cm^{-1}): 794 (5180); HRMS (ESI) *m* / *z* calcd for $C_{40}H_{41}N_2O_5PPd$ (M + Na)$^+$ 789.1701, found 789.1697.

(cat^{t}Bu$_2$)Pd(adi): This complex was prepared in a manner similar to that described for (^{Et}phoscat)Pd(adi) using 3,5-di-*tert*-butylcatechol (111 mg, 0.500 mmol). Recrystallization from dichloromethane and pentane afforded a dark green solid (247mg, 67%). ^{1}H NMR (500 MHz, CDCl$_3$) δ 8.05 (appar t, *J* = 7.6 Hz, 2H), 7.47 (appar quint, *J* = 7.6 Hz, 2H), 7.06 (s, 4H), 7.03 (d, *J* = 7.0 Hz), 6.73 (d, *J* = 7.0 Hz), 6.44 (s, 1H), 6.37 (s, 1H), 2.45-2.44 (s, 12H and s, 3H), 2.39 (s, 3H), 1.17 (s, 9H), 1.06 (s, 9H); ^{13}C NMR (125 MHz, CDCl$_3$) δ 171.5 (C=N), 170.4 (C=N), 163.7 (aryl-C–O), 159.5 (aryl-C–O), 144.0 (PDI qC), 142.0 (mesityl-C–N), 141.5 (mesityl-C–N), 138.7 (cat aryl-qC), 137.8 (mesityl-qC), 137.7 (mesityl-qC), 135.2 (cat aryl-qC), 131.5 (adi qC), 131.2 (adi aryl-C), 131.1 (adi aryl-C), 130.1 (mesityl-C), 130.0 (mesityl-qC), 129.8 (mesityl-qC), 129.5 (adi aryl-C), 129.42-129.40 (mesityl-C and adi aryl-C), 126.7 (adi qC), 126.4 (adi qC), 123.8 (adi aryl-C), 123.6 (adi aryl-C), 112.0 (cat aryl-C), 111.1 (cat aryl-C), 34.5 ($C(CH_3)_3$), 34.3 ($C(CH_3)_3$), 32.4 (CH_3), 29.5 (CH_3), 21.6 (mesityl-CH_3), 21.5 (mesityl-CH_3), 18.6 (mesityl-CH_3), 18.4 (mesityl-CH_3); FTIR (KBr) *v*/cm^{-1} 3538, 3478, 3406,. 3230, 2944, 2857, 1692, 1638, 1615, 1560, 1536, 1478, 1417, 1288 st, 1190, 1156, 1037, 977; UV-vis-NIR (CH_2Cl_2) λ_{max}/nm (ε/M^{-1} cm^{-1}): 1002 (7220); HRMS (ESI) *m* / *z* calcd for $C_{44}H_{48}N_2O_2Pd$ (M + Na)$^+$ 765.2665, found 765.2673.

(catCO$_2$Me)Pd(adi): This complex was prepared in a manner similar to that described for (^{Et}phoscat)Pd(adi) using 4-(methoxycarbonyl)catechol (84 mg, 0.50 mmol). Recrystallization from dichloromethane and pentane afforded a dark green solid (170 mg, 50%). ^{1}H NMR (500 MHz, CDCl$_3$) δ 8.10 (d, *J* = 8.2 Hz, 2H), 7.50 (td, *J* = 8.2, 2.3 Hz, 2H), 7.13 (d *J* = 8.2, 1H), 7.07-7.05 (s, 4H and d, 1H), 6.82 (d, *J* = 7.1 Hz, 1H), 6.79 (d, *J* = 7.1 Hz, 1H),

6.38 (d, J = 8.2 Hz, 1H), 3.72 (s, 3H), 2.43-2.41 (s, 12H and s, 6H); ^{13}C NMR (125 MHz, CDCl$_3$) δ 172.6 (C=N), 172.4 (C=N), 170.03 (aryl-C–O), 168.6 (C=O), 163.5 (aryl-C–O), 145.4 (adi qC), 141.1 (mesityl-C–N), 141.0 (mesityl-C–N), 138.5 (mesityl-qC), 138.4 (mesityl-qC), 131.89 (adi aryl-C), 131.86 (adi aryl-C), 131.6 (adi qC), 130.2 (mesityl-C), 130.1 (mesityl-C), 129.9 (mesityl qC), 129.8 (mesityl qC), 129.6 (adi aryl-C), 125.82 (adi qC), 125.78 (adi qC), 124.5 (adi aryl-C), 124.4 (adi aryl-C), 120.2 (cat aryl-C), 117.7 (cat aryl-qC), 116.5 (cat aryl-C), 115.0 (cat aryl-C), 51.4 (C–O), 21.6 (mesityl-CH$_3$), 18.6 (mesityl-CH$_3$), 18.5 (mesityl-CH$_3$); FTIR (KBr) ν/cm^{-1} 3543, 3483, 3413, 3225, 2967, 2945, 2906, 1698, 1637, 1613, 1569, 1484, 1434, 1289 st, 1193, 1105, 1080; UV-vis-NIR (CH$_2$Cl$_2$) λ_{max}/nm (ε/M^{-1} cm^{-1}): 800 (5170); HRMS (ESI) m / z calcd for C$_{38}$H$_{34}$N$_2$O$_4$Pd (M +Na)$^+$ 711.1465, found 711.1484.

(catNO$_2$)Pd(adi): This complex was prepared in a manner similar to that described for (^{Et}phoscat)Pd(adi) using 4-nitrocatechol (78 mg, 0.50 mmol). Recrystallization from dichloromethane and ethyl ether afforded a dark green solid (180 mg, 55%). ^{1}H NMR (500 MHz, CDCl$_3$) δ 8.13 (d, J = 8.2 Hz, 2H), 7.54 (m, 2H), 7.42 (d, J = 9.0 Hz, 1H), 7.23 (s, 1H), 7.10 (s, 4H), 6.87 (d, J = 7.1 Hz, 1H), 6.83 (d, J = 7.1 Hz, 1H), 6.29 (d, J = 9.0 Hz, 1H), 2.43 (s, 18H); ^{13}C NMR (125 MHz, CDCl$_3$) δ 173.3 (aryl-C–O), 163.6 (aryl-C–O), 146.0 (adi qC), 145.8 (adi qC), 140.9 (C=N), 140.7 (C=N), 138.9 (mesityl-qC), 138.7 (mesityl-qC), 138.1 (aryl-C–NO$_2$), 132.23 (mesityl-qC), 132.20 (mesityl-qC), 131.7 (adi qC), 130.3 (mesityl-C), 130.0 (mesityl-qC), 129.8 (adi aryl-C), 125.5 (adi qC), 124.8 (adi aryl-C), 124.7 (adi aryl-C), 115.5 (cat aryl-C), 114.0 (cat aryl-C), 110.5 (cat aryl-C), 21.7 (mesityl-CH$_3$), 18.6 (mesityl-CH$_3$), 18.5 (mesityl-CH$_3$); FTIR (KBr) ν/cm^{-1} 3576, 3472, 3417, 3252, 2978, 2857, 1629, 1602, 1550, 1484, 1349, 1259 st, 1067, 1042; UV-vis-NIR (CH$_2$Cl$_2$) λ_{max}/nm (ε/M^{-1} cm^{-1}): 726 (5400); HRMS (ESI) m / z calcd for C$_{36}$H$_{31}$N$_3$O$_4$Pd (M + Na)$^+$ 698.1261, found 698.1261.

(pdi)PdCl₂: A mixture of $(CH_3CN)_2PdCl_2$ (262 mg, 1.01 mmol) and N,N'-bis(mesityl)phenanthrene-9,10-diimine (443 mg, 1.01 mmol) was stirred in CH_2Cl_2 (10 mL) at room temperature for 18 h. The resulting dark red solution was concentrated to dryness under vacuum to afford the product as a brown solid (507 mg, 81% yield). ¹H NMR (400 MHz, CDCl₃) δ 8.07 (d, J = 8.2 Hz, 2H), 7.63 (appar t, J = 7.4 Hz, 2H), 7.18 (d, J = 8.4 Hz, 2H), 7.07 (appar t, J = 7.8 Hz, 2H) 7.02 (s, 4H), 2.37 (s, 6H), 2.32 (s, 12 H); ¹³C NMR (125 MHz, CDCl₃T) δ 167.1 (C=N), 145.0 (mesityl-C–N), 138.3 (mesityl-qC), 135.5 (pdi aryl-C), 135.4 (pdi qC), 130.2 (mesityl-C), 130.1 (pdi aryl-C), 130.0 (mesityl-qC), 128.4 (pdi aryl-C), 126.0 (pdi qC), 125.2 (pdi aryl-C), 21.6 (mesityl-CH₃), 19.0 (mesityl-CH₃); FTIR (KBr) v/cm⁻¹ 2923, 1593, 1476, 1434, 1347, 1292, 1182, 1028, 906, 872, 725, 603; HRMS (ESI) m / z calcd for $C_{32}H_{30}Cl_2N_2Pd$ (M + Na)⁺ 641.0725, found 641.0701

(pdi)PdI₂: A mixture of (pdi)PdCl₂ (927 mg, 1.50 mmol) and sodium iodide (782 mg, 5.25 mmol) was vigorously stirred in CH_2Cl_2 (5 mL) at room temperature for 18 h. The resulting dark brown solution was filtered and the filtrate concentrated to dryness under vacuum to afford the product as a dark brown solid (2.06 mg, 91% yield). ¹H NMR (500 MHz, CDCl₃) δ 8.04 (d, J = 8.0 Hz, 2H), 7.62 (appar t, J = 7.3 Hz, 2H), 7.31 (d, J = 8.5 Hz, 2 H), 7.06 (appar t, J = 7.4 Hz, 2H), 7.03 (s, 4H), 2.38 (s, 6 H), 2.30 (s, 12 H); ¹³C NMR (125 MHz, CDCl₃T) δ 166.6 (C=N), 147.1 (mesityl-C–N), 137.3 (mesityl-qC), 135.2 (pdi aryl-C), 134.9 (pdi qC), 129.9 (mesityl-C), 129.8 (pdi aryl-C), 129.5 (mesityl-qC), 128.2 (pdi aryl-C), 126.9 (pdi qC), 125.7 (pdi aryl-C), 21.5 (mesityl-CH₃), 19.7 (mesityl-CH₃); FTIR (KBr) v/cm⁻¹ 2906, 2851, 2226, 1592, 1441, 1345, 1304, 1249, 1167, 1034, 909, 762, 724 st; HRMS (ESI) m / z calcd for $C_{32}H_{30}I_2N_2Pd$ (M + Na)⁺ 824.9443, found 824.9418.

(**^{Si}phoscat)Pd(pdi):** To a solution of (^{Et}phoscat)H$_2$ (148 mg, 0.600 mmol) and triethylamine (172 μL, 1.23 mmol) in Et$_2$O (10 mL) was added bromotrimethylsilane (162 μL, 1.23 mmol) at −78 °C and the reaction was allowed to warm to room temperature. After stirring for 3 h at room temperature, the reaction mixture was filtered to remove triethylammonium bromide and the solvent was removed under vacuum. The obtained yellow oil (222 mg, 0.570 mmol) was subsequently dissolved in CH$_2$Cl$_2$ (5 mL) and treated with bromotrimethylsilane (225 μL, 1.71 mmol). After stirring for 12 h at room temperature, the reaction mixture was concentrated to dryness under vacuum to remove excess bromotrimethylsilane affording a yellow residue. In a separate vial, (pdi)PdI$_2$ (443 mg, 0.570 mmol) and AgF (216 mg, 1.71 mmol) were combined in 10 mL of CH$_2$Cl$_2$ at ambient temperature for 12 h while protecting the sample from light to prepare (pdi)PdF$_2$. The yellow residue (putatively (^{Si}phoscat)TMS$_2$), was then dissolved in a small aliquot of CH$_2$Cl$_2$ (3 mL) and added to the solution of (pdi)PdF$_2$ and stirred an additional 12 h in the absence of light. The reaction mixture was filtered through a pad of celite and concentrated to dryness under vacuum. The solid residue was recrystallized from a minimum amount of dichloromethane and pentane to give complex (^{Si}phoscat)Pd(pdi) as a brown solid (347 mg, 69% yield). ^{31}P NMR (162 MHz, CDCl$_3$) δ 6.3; ^{1}H NMR (500 MHz, CDCl$_3$T) δ 8.15 (d, J = 8.11 Hz, 2H), 7.62 (appar t, J = 7.6 Hz, 2H), 7.40 (d, J = 8.5 Hz, 1H), 7.33 (d, J = 8.5 Hz, 1H), 7.10 (appar q, J = 7.8 Hz, 2H), 7.05 (s, 4H), 6.82 (d, J = 15.2 Hz), 6.66 (dd, J = 13.6 Hz, 8.0 Hz, 1H), 6.36 (dd, J = 8.0 Hz, 5.0 Hz, 1H), 2.43 (s, 3H), 2.42 (s, 3H), 2.30 (s, 6H), 2.29 (s, 6H), 0.16 (s, 18H); ^{13}C NMR (125 MHz, CDCl$_3$T) δ 168.2 (d, J = 3.2 Hz, aryl-C–O), 164.5 (d, J = 21.5 Hz, aryl-C–O), 162.9 (C=N), 162.7 (C=N), 144.4 (mesityl-C–N), 144.3 (mesityl-C–N), 137.8 (mesityl-qC), 137.7 (mesityl-qC), 134.0 (pdi qC), 133.55 (pdi aryl-C), 133.52 (pdi aryl-C),

130.1 (mesityl-C), 129.6 (pdi aryl-C), 129.16 (mesityl-C), 129.12 (mesityl-C), 128.44 (pdi aryl-C), 128.36 (pdi aryl-C), 126.56 (pdi qC), 126.55 (pdi qC), 125.17 (pdi aryl-C), 125.15 (pdi aryl-C), 121.0 (d, J = 11.5 Hz, cat aryl-C), 119.2 (d, J = 12.8 Hz, cat aryl-C), 117.4 (cat aryl-qC), 116.0 (d, J = 20.0 Hz, cat aryl-C), 21.6 (mesityl-CH_3), 19.1 (mesityl-CH_3), 19.0 (mesityl-CH_3), 1.35 (Si-(CH3)$_3$); FTIR (KBr) v/cm^{-1} 2939, 1652, 1602, 1470, 1418, 1353, 1303, 1254, 1161, 1081, 1010, 840, 766, 716, 717, 598, 535; UV-vis-NIR (CH_2Cl_2) λ_{max}/nm (ε/M^{-1} cm^{-1}): 1014 (8940); HRMS (ESI) m / z calcd for $C_{44}H_{51}N_2O_5PPdSi_2$ (M)$^+$ 880.2125, found 880.2142.

(^{Si}**Bnphoscat)Pd(pdi):** To a solution of (^{Et}Bnphoscat)H$_2$ (156 μL, 0.600 mmol) and triethylamine (172 μL, 1.23 mmol) in THF (10 mL) was added bromotrimethylsilane (162 μL, 1.23 mmol) at −78 °C and the reaction was warmed to room temperature and stirred for 3 h. The reaction mixture was filtered to remove triethylammonium bromide and the solvent was removed under vacuum. The obtained yellow oil (236 mg, 0.580 mmol) was subsequently dissolved in CH_2Cl_2 (5 mL) and treated with bromotrimethylsilane (230 μL, 1.7 mmol). After stirring for 12 h at room temperature, the reaction mixture was stripped to dryness to remove excess bromotrimethylsilane, after which point the yellow compound (putatively (^{Si}Bnphoscat)TMS$_2$), was redissolved in CH_2Cl_2 (3 mL) and added to a suspension of (pdi)PdI$_2$ (455 mg, 0.580 mmol) and AgF (220 mg, 1.7 mmol) in CH_2Cl_2 (10 mL) (which had been pre-stirred for 12 h in the absence of light). After stirring for 12 additional hours in the dark, the reaction mixture was filtered through a pad of celite and concentrated to dryness under vacuum to afford **22** as a brown solid (349 mg, 67%). ^{31}P NMR (162 MHz, CDCl$_3$T) δ 11.2; ^{1}H NMR (500 MHz, CDCl$_3$T) δ 8.16 (d, J = 8.15 Hz, 2 H), 7.59 (td, J = 7.6 Hz, 3.5Hz, 2H), 7.38 (d, J = 8.5 Hz, 1H), 7.30 (d, J = 8.5 Hz, 1H), 7.09 (appar q, J = 7.6 Hz, 2 H),

7.03 (s, 2 H), 7.00 (s, 2 H), 6.32 (d, J = 8.0 Hz, 1H), 6.25 (s, 1H), 6.16 (d, J = 8.0 Hz, 1H), 2.87 (d, J = 21.2 Hz, 2 H), 2.41 (s, 6 H), 2.29 (s, 6H), 2.28 (s, 6H), 0.15 (s, 18 H); ^{13}C NMR (125 MHz, CDCl$_3$T) δ 165.7 (d, J = 2.8 Hz, aryl-C–O), 165.0 (d, J = 3.0 Hz, aryl-C–O), 161.5 (C=N), 161.3 (C=N), 144.9 (mesityl-C–N), 144.7 (mesityl-C–N), 137.34 (mesityl-qC), 137.27 (mesityl-qC), 133.5 (pdi qC), 132.50 (pdi aryl-C), 132.48 (pdi aryl-C), 130.0 (mesityl-C), 129.8 (mesityl-C), 129.61 (pdi aryl-C), 129.3 (mesityl-qC), 129.2 (mesityl-qC), 127.9 (pdi aryl-C), 126.89 (pdi qC), 126.86 (pdi qC), 124.9 (pdi aryl-C), 121.8 (d, J = 10.5 Hz, cat qC), 119.5 (d, J = 7.0 Hz, cat aryl-C), 118.2 (d, J = 6.2 Hz, cat aryl-C), 116.2 (d, J = 2.4 Hz, cat aryl-C), 21.63 (mesityl-CH$_3$), 21.61 (mesityl-CH$_3$), 19.1 (mesityl-CH$_3$), 19.0 (mesityl-CH$_3$), 1.24 (Si-(CH3)$_3$); FTIR (KBr) v/cm^{-1} 2961, 2901, 1594, 1551, 1487, 1440, 1353, 1303, 1185, 1091, 842, 760, 607; UV-vis-NIR (CH$_2$Cl$_2$) λ_{max}/nm (ε/M^{-1} cm^{-1}): 1322 (11090); HRMS (ESI) m / z calcd for C$_{45}$H$_{53}$N$_2$O$_5$PPdSi$_2$ (M + 3H – 2[(CH$_3$)$_3$Si])$^+$ 751.1568, found 751.1578.

Hammett plots of redox potentials of (catecholate)Pd(diimine) complexes: Plots of the first oxidation potential, defined as E$^{o\prime}_3$/[Pd]$^{+1/0}$, against Hammett σ values for the substituents on the catecholate ligand produced straight lines, which were expressed as least-square methods: E$^{o\prime}_3$ = 0.35$\sigma\prime$–0.13 (R = 0.958) for (catecholate)Pd(pdi) complexes and E$^{o\prime}_3$ = 0.27$\sigma\prime$–0.04 (R = 0.960) for (catecholate)Pd(adi) complexes, where $\sigma\prime$ represents the average of *para* and *meta* Hammett σ parameters. The former set of complexes gave the best linear fit for the redox potentials (E$^{o\prime}_3$) measured in CH$_2$Cl$_2$ (Figure 5.4a). The Hammett plot for the (catecholate)Pd(adi) complexes is based on the redox potentials measured in THF (Figure 5.4b).

5.5 References

[1] Pierpont, C. G. *Coord. Chem. Rev.* **2001**, *216-217,* 99-127.

[2] (a) Muckerman, J. T.; Polyansky, D. E.; Wada, T.; Tanaka, K.; Fujita, E. *Inorg. Chem.* **2008**, *47*, 1787–1802. (b) Isobe, H.; Tanaka, K.; Shen, J.-R.; Yamaguchi, K. *Inorg. Chem.* **2014**, *53*, 3973–3984.

[3] (a) Haneline, M. R.; Heyduk, A. F. *J. Am. Chem. Soc.* **2006**, *128*, 8410–8411. (b) Smith, A. L.; Clapp, L. A.; Hardcastle, K. I.; Soper, J. D. *Polyhedron* **2010**, *29*, 164–169.

[4] (a) Ringenberg, M. R.; Kokatam, S. L.; Heiden, Z. M.; Rauchfuss, T. B. *J. Am. Chem. Soc.* **2008**, *130*, 788–789. (b) Deibel, N.; Schweinfurth, D.; Hohloch, S.; Fiedler, J.; Sarkar, B. *Chem. Commun.* **2012**, *48*, 2388–2390.

[5] (a) Lippert, C. A.; Arnstein, S. A.; Sherrill, C. D.; Soper, J. D. *J. Am. Chem. Soc.* **2010**, *132*, 3879–3892. (b) Lippert, C. A.; Riener, K.; Soper, J. D. *Eur. J. Inorg. Chem.* **2012**, 554–561. (c) Broere, D. L. J.; Metz, L. L.; Reek, J. N. H.; Siegler, M. A.; van der Vlugt, J. I. *Angew. Chem. Int. Ed.* **2014**, *53*, 1–6.

[6] (a) Morris, A. M.; Pierpont, C. G.; Finke, R. G. *Inorg. Chem.* **2009**, *48,* 3496–3498. (b) Yin, C. X.; Finke, R. G. *J. Am. Chem. Soc.* **2005**, *127*, 9003–9013.

[7] Chaudhuri, P.; Wieghardt, K.; Weyhermüller, T.; Paine, T. K.; Mukherjee, S.; Mukherjee, C. *Biol. Chem.* **2006**, *386*, 1023-1033.

[8] (a) Camacho-Bunquin, J.; Siladke, N. A.; Zhang, G.; Niklas, J.; Poluektov, O. G.; Nguyen, S. T.; Miller, J. T.; Hock, A. S. *Organometallics* **2015**, *34,* 947–952. (b) Kraft, S. J.; Zhang, G.; Childers, D.; Dogan, F.; Miller, J. T.; Nguyen, S. T.; Hock, A. S. *Organometallics* **2014**, *33,* 2517–2522.

[9] Kolyakina, E. V.; Poddel'sky, I.; Grishin, D. F. *Polymer Science, Ser. B*, **2014**, *56*, 566–576.

[10] Kramer, W. W.; Cameron, L. A.; Zarkesh, R. A.; Ziller, J. W.; Heyduk, A. F. *Inorg. Chem.* **2014**, *53*, 8825-8837.

[11] (a) Pevny, F.; Zabel, M.; Winter, R. F.; Rausch, A. F.; Yersin, H.; Tuczek, F.; Záliš S. *Chem. Commun.* **2011**, *47,* 6302–6304. (b) Heinze, K.; Reinhardt, S. *Chem. Eur. J.* **2008**, *14*, 9482–9486. (c) Shavaleev, N. M.; Davies, E. S.; Adams, H.; Best, J.; Weinstein, J. A. *Inorg. Chem.* **2008**, *47,* 1532–1547. (d) Weinstein, J. A.; Tierney, M. T.; Davies, E. S.; Base, K.; Robeiro, A. A.; Grinstaff, M. W. *Inorg. Chem.* **2006**, *45,* 4544–4555. (e) Best, J.; Sazanovich, I. V.; Adams, H.; Bennett, R. D.; Davies, E. S.; Meijer, A. J. H. M.; Towrie, M.; Tikhomirov, S. A.; Bouganov, O. V.; Ward, M. D.; Weinstein, J. A. *Inorg. Chem.* **2010**, *49*, 10041–10056. (f) Rauth, G. K.; Pal, S.; Das, D.; Sinha, C.; Slawin, A. M. Z.; Woollins, J. D. *Polyhedron* **2001**, *20*, 363–372.

[12] (a) Linfoot, C. L.; Richardson, P.; McCall, K. L.; Durrant, J. R.; Morandeira, A.; Robertson, N. *Solar Energy* **2011**, *85*, 1195–1203. (b) Geary, E. A. M.; Yellowlees, L. J.; Jack, L. A.; Oswald, I. D. H.; Parsons, S.; Hirata, N.; Durrant, J. R.; Robertson, N. *Inorg. Chem.* **2005**, *44*, 242–250. (c) Islam, A.; Sugihara, H.; Hara, K.; Singh, L. P.; Katoh, R.; Yanagida, M.; Takahashi, Y.; Murata, S.; Arakawa, H.; Fujihashi, G. *Inorg. Chem.* **2001**, *40,* 5371–5380.

[12] (d) Diwan, K.; Chauhan, R.; Singh, S. K.; Singh, B.; Drew, M. G. B.; Bahadur, L.; Singh, N. *New J. Chem.* **2014**, *38*, 97–108.

[13] Kraft, S. J.; Hernández Sánchez, R.; Hock, A.S. *ACS Catal.* **2013**, *3*, 826–830.

[14] Queffélec, C.; Petit, M.; Janvier, P.; Knight, D. A.; Bujoli, B. *Chem. Rev.* **2012**, *112*, 3777–3807.

[15] Saito, S.; Kawabata, J. *Helv. Chim. Acta* **2006**, *89*, 1395–1406.

[16] Honda, H.; Matsumoto, T.; Tamura, R.; Kanaizuka, K.; Kobayashi, A.; Kato, M.; Haga, M.-A.; Chang, H.-C. *Chem. Lett.* **2014**, *43*, 1189–1191.

[17] Xu, W.; Zou, J.-P.; Zhang, W. *Tetrahedron Lett.* **2010**, *51*, 2639–2643.

[18] McKenna, C. E.; Higa, M. T.; Cheung, N. H.; McKenna, M. C. *Tetrahedron Lett.* **1977**, 155.

[19] Kokatam, S.; Weyhermüller, T.; Bothe, E.; Chaudhuri, P.; Wieghardt, K. *Inorg. Chem.* **2005**, *44*, 3709-3717.

[20] (a) Kumar, S. B.; Chaudhury, M. *J. Chem. Soc. Dalton Trans.* **1991**, 2169–2174. (b) Wada, T.; Yamanaka, M.; Fujihara, T.; Miyazato, Y.; Tanaka, K. *Inorg. Chem.* **2006**, *45*, 8887–8894. (c) Hansch, C.; Leo, A.; Taft, R. W. *Chem. Rev.* **1997**, *91*, 165-195.

[21] Cheng-Ye, Y.; Wei-Zhen, X.; Meng-Juan, G.; Chi-Ying, Z. *Sci. China Math.* **1964**, *7*, 1510-1515.

[22] Cherkasov, V. K.; Druzhkov, N.O.; Kocherova, T. O.; Shavyrin, A. S.; Fukin, G. K. *Tetrahedron* **2012**, *68*, 1422–1426.

[23] Dastgir, S.; Coleman, K. S.; Cowley, A. R.; Green, M. *Organometallics* **2010**, *29*, 4858.

[24] Rimoldi, M.; Ragaini, F.; Gallo, E.; Ferretti, F.; Macchi, P.; Casati, N. *Dalton Trans.* **2012**, *41*, 3648–3658.

[25] Bikbulatov, R. R.; Timofeeva, T. V.; Zorina, L. V.; Safiev, O. G.; Zorin, V. V.; Rakhmankulov, D. L. *Russ. J. Gen. Chem.* **1996**, *66*, 1805-1806.

[26] Calderon, F. C.; García, J. L.; de la Peña, E. M.; Maya, J. M.; García, J. *Polym. Sci. Part A: Polym. Chem.* **2006**, *44*, 2270–2281.

[27] Rajesh, P. K.; Jarvis, G. G.; Low, P. S. *Tetrahedron Lett.* **2012**, *53*, 1627.

[28] Palumbo, A.; Napolitano, A.; d'Ischia, M. *Bioorg. Med. Chem. Lett.* **2002**, *12*, 13–16.

[29] Connelly, N. G.; Geiger, W. E. *Chem. Rev.* **1996**, *96*, 877–910.

[30] Ito, S.; Murakami, T. N.; Comte, P.; Liska, P.; Grätzel, C.; Nazeeruddin, M. K.; Grätzel, M. *Thin Solid Films* **2008**, *516*, 4613-4619.

[31] Shigemura, R. US Patent/US8148536 B2, April 3, 2012.

[32] Kita, Y.; Arisawa, M.; Gyoten, M.; Nakajima, M.; Hamada, R.; Tohma, H.; Takada, T. *J. Org. Chem.* **1998**, *63,* 6625–6633.

Chapter 6

Synthesis of the *β*-Diketimine Ligand with a Phosphonate Anchoring

Group

6.1 Introduction

The properties and coordination chemistry of monoanionic β-diketiminate ligands (NacNacs) are well established in the literature. The "NacNac" motif is electronically and structurally related to 2,4-pentanedione (acetylacetonato, (acac)⁻) ligand, where the two acac oxygen atoms are exchanged for nitrogen groups. NacNacs have been extensively used to prepare and study a variety of metal coordination complexes in different oxidation states across the periodic table. Furthermore, these ligands afford tunable electronic and steric properties through substitutional changes both within the ligand backbone and at the nitrogen groups. The ease in ligand variation has contributed to the β-diketiminates being investigated as supporting ligands in main-group,[1] transition-metal,[2] and rare-earth[3] coordination chemistry as well as in applications based on small-molecule activation.[4]

One of the most convenient routes for the synthesis of β-diimines is based on the acid-catalyzed condensation of acetylacetone with substituted amines, also known as Schiff-base condensation (Scheme 6.1a).[5] This approach allows for a wide selection of anilines to be installed. Furthermore, the steric demands of the β-diketiminate ligand can be conveniently modulated through the *N*-aryl substituents, by either varying the size of *ortho*-substituents or relocating the substituents from the *ortho*-position to the *meta*- or *para*-position. However, the Schiff base-condensation reaction does not permit much structural variation within the diketonate carbon backbone.

A complementary route toward NacNacs enables for the β-diketonate skeleton to be assembled in a modular fashion via C–C coupling.[5] This strategy employs two separate coupling partners, acetimidoyl chloride and an *N*-acetylimine derivative, both of which can be prepared from acetyl chloride, as shown in Scheme 6.1b. Alternatively, structurally

different coupling partners may be prepared through independent modifications of two

different acyl chloride derivatives. In a typical C–C coupling reaction, the β-diketiminate

ligand is obtained by heating the *in situ* lithitated *N*-acetyliminium salt with imidoyl

chloride. Through this modular synthesis, the β-diiminate steric hindrance can be varied by

changing the chemical substituents at the aromatic nitrogen groups or the β-carbons of the

ligand backbone (at the 1- and 3-position). Further advantages of the C–C coupling reaction

include the ability to derive asymmetric ligand variations and ligands with systematically

tunable electronic properties.

Scheme 6.1. General routes for the synthesis of NacNac ligands via (a) Schiff-base condensation chemistry or (b) C–C coupling. R denotes commonly changed alkyl substituents of the *N*-aryl group.
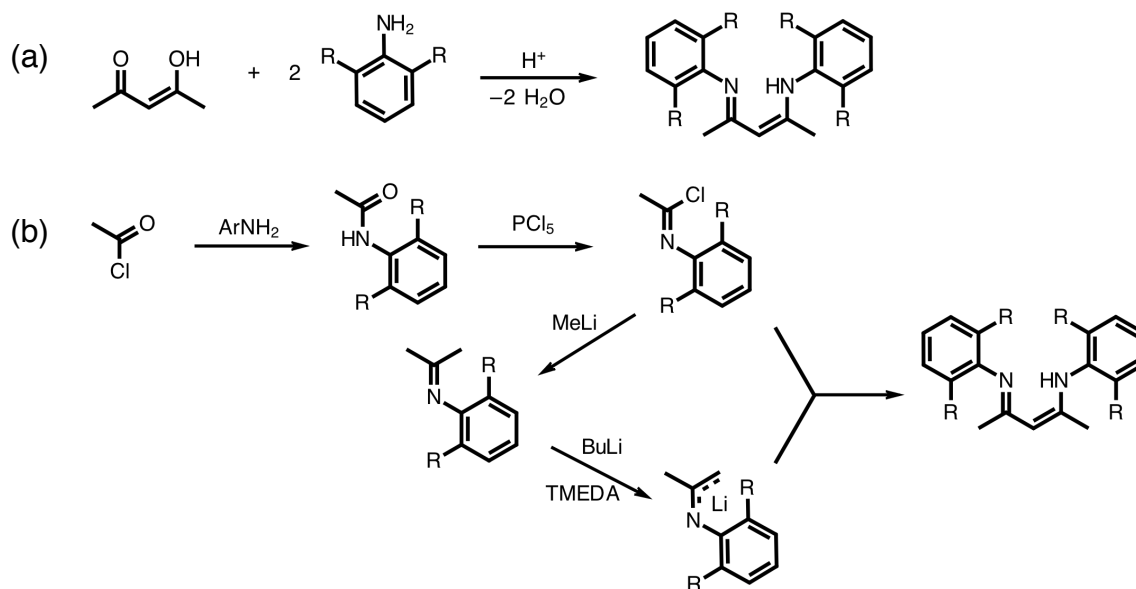
The ease of synthetic accessibility for a wide range of NacNacs has advanced their

popularity not only as auxiliary ligands in coordination chemistry but also as non-innocent

probes in redox events. For example, the proclivity of monoanionic (NacNac)⁻ ligands to

undergo a one-electron oxidation has been showcased for the bis(β-diketiminate)

complexes of cobalt[6] and nickel[7] and for charge-transfer complexes of rhodium,[8]

supported by the *β*-diiminyl donor ((NacNac)⁻) and the *α*-diiminyl acceptor ligands. Complementary redox properties of the (NacNac)⁻ ligand were also discovered recently with coordination complexes of aluminum[9] and ytterbium[10] whose electronic structures were described on the basis of one- and two-electron reduced forms of the ligand, respectively.

Known NacNacs

$(NacNac^{CH3})^-$ $(NacNac^{CF3})^-$

This work
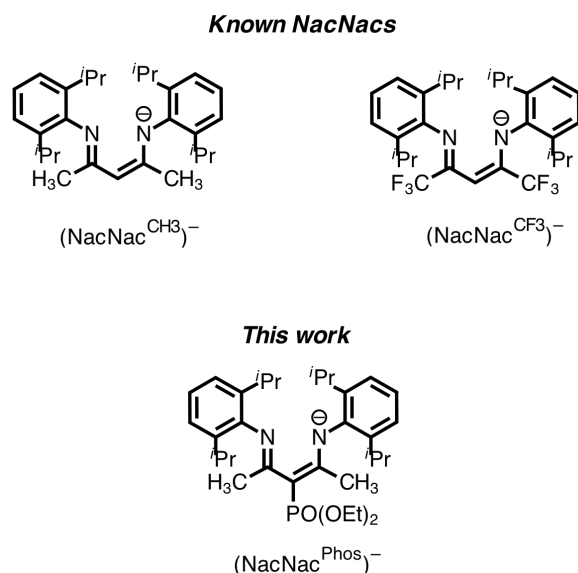
$(NacNac^{Phos})^-$

Figure 6.1 Chemical structures of established *β*-diketiminato ligands, $(NacNac^{CH3})^-$ and $(NacNac^{CF3})^-$ (top), and the phosphonate-functionalized ligand derivative $(NacNac^{Phos})^-$ (bottom).

The evolution of a vast number of *β*-diketiminate complexes with interesting catalytic and redox properties was made possible through fundamental solution studies.[4,6-10] Despite their exciting chemistry in solution, limited reports are known involving the solid-state molecular analogues of soluble NacNac complexes deposited on a high surface area for heterogeneous applications.[11] Heterogeneous catalysis based on single-site reactivity is important in applied sciences due to its general robustness and practically.[12] Such catalysts are assembled on solid-support surfaces by anchoring the catalytically active components through their hydroxyl groups. Typical solid supports

132

include silica and alumina oxides, active carbon, and metal oxide nanoparticles.[13] To the best of our knowledge, the catalytically relevant NacNac metal complexes have not been studied in the context of metallic oxide surface chemistry. The development of suitable anchoring groups for NacNac ligands and their coordination complexes could potentially enable for deeper studies of their catalytic and electronic properties in a controlled fashion.

In this work, a C–C coupling strategy was used to prepare the β-diketiminate ligand, (NacNac^{Phos})⁻ (**29**), containing a diethoxylphosphoryl anchoring group attached directly to the 3-position of the ligand backbone. The ligand was coordinated on a Rh^{I} center of the formula (NacNac^{Phos})Rh(phdi) (**32**) (phdi = phenanthrene-9,10-diimine), which was subsequently oxidized to the Rh^{III} derivative of the formula (NacNac^{Phos})RhCl$_2$(phdi) (**33**). Both rhodium complexes of the new ligand were obtained by a method we had developed previously for related (NacNac^{R})⁻ congeners of Rh^{I} and Rh^{III} centers (where (NacNac^{R})⁻ = *N,N*-bis(2,6-diisopropylphenyl)pentane-2,4-diimine (NacNac^{CH3})⁻; *N,N*-bis(2,6-diisopropyl-phenyl)hexafluoropentane-2,4-diimine, (NacNac^{CF3})⁻).[8]   As shown in Figure 6.1, the phosphonate-free NacNac ligands, (NacNac^{CH3})⁻ and (NacNac^{CF3})⁻, contain a hydrocarbon at the central, *a*-position of the ligand backbone while the two β-carbons are substituted with methyl groups in the former ligand and trifluoromethyl groups in the latter. For these phosphonate-free ligand derivatives, the difference in their β-carbon substituents was found to significantly influence the electronic structure of respective Rh^{III} complexes. Since the phosphonate diester moiety can effectively withdraw electron density from carbon atoms, we set out to examine the impact of the *a*-substituted phosphonate group on the redox behavior of the (NacNac)⁻ ligand. To this end, the electronic properties of the new coordination complexes, (NacNac^{Phos})Rh(phdi) and (NacNac^{Phos})RhCl$_2$(phdi), were

elucidated in solution allowing for systematic comparisons to be drawn between the rhodium complexes with the phosphonate anchors and those without the phosphonate anchors.

6.2 Results and Discussion

6.2.1 Synthesis and Characterization

Scheme 6.2. Synthesis of (NacNac^Phos)H proligand via C–C coupling.
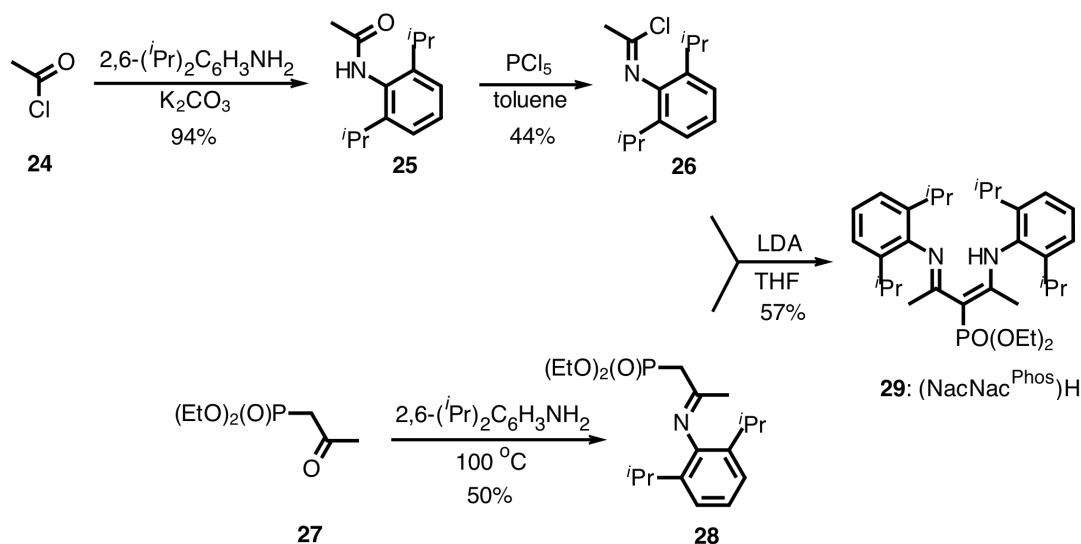
The new β–diketimine proligand, (NacNac^Phos)H (**29**), was prepared by coupling of *N*-arylimine phosphonate **28** and imidoyl chloride **26**. As shown in Scheme 6.2, imidoyl chloride **26** was produced by a condensation reaction between acetyl chloride (**24**) and 2,6-diisopropylanaline followed by dehydration of acetamide **25** with phosphorous pentachloride. The second coupling partner, imine **28**, was accessed by condensation of commercial diethyl (2-oxopropyl)phosphonate (**27**) and 2,6-diisopropylanaline. The (NacNac^Phos)H proligand (**29**) was generated by deprotonation of phosphonylated imine **28** with LDA and treatment with acetimidoyl chloride **26**. The ^{1}H and ^{13}C NMR spectroscopic data of (NacNac^Phos)H in CDCl$_3$ showed symmetric resonances consistent with having the

134

phosphonate substituent in the 3 position of the ligand backbone. The ^{31}P NMR spectrum of the ligand displayed a single resonance at 28.5 ppm, once again confirming one symmetric conformation in solution.

Phosphonylated rhodium complexes of the new ligand, (NacNac^{Phos})Rh(phdi) (**32**) and (NacNac^{Phos})RhCl$_2$(phdi) (**33**), were accessed by an established method[8] and their properties were compared to related rhodium complexes: (NacNac^R)Rh(phdi) and (NacNac^R)RhCl$_2$(phdi) (where R = β-CH$_3$, β-CF$_3$, respectively). As outlined in Scheme 6.3, the rhodium (I) complex was prepared from the ligand exchange reaction of [Rh(μ−Cl)(CO)$_2$]$_2$ synthon with (NacNac^{Phos})K followed by installation of phdi on (NacNac^{Phos})Rh(CO)$_2$ (**31**). The installation of the phdi ligand was accomplished via oxidative substitution of the CO ligands from **31** with trimethyl amine *N*-oxide (TMAO), at elevated temperature. The rhodium (III) derivative, (NacNac^{Phos})RhCl$_2$(phdi), was generated in a separate step via oxidative addition of PhICl$_2$ to (NacNac^{Phos})Rh(phdi).

Scheme 6.3. Synthesis of (NacNac^{Phos})Rh(phdi) (**32**) and (NacNac^{Phos})RhCl$_2$(phdi) (**33**). Ar denotes 2,6-diisopropylphenyl group.
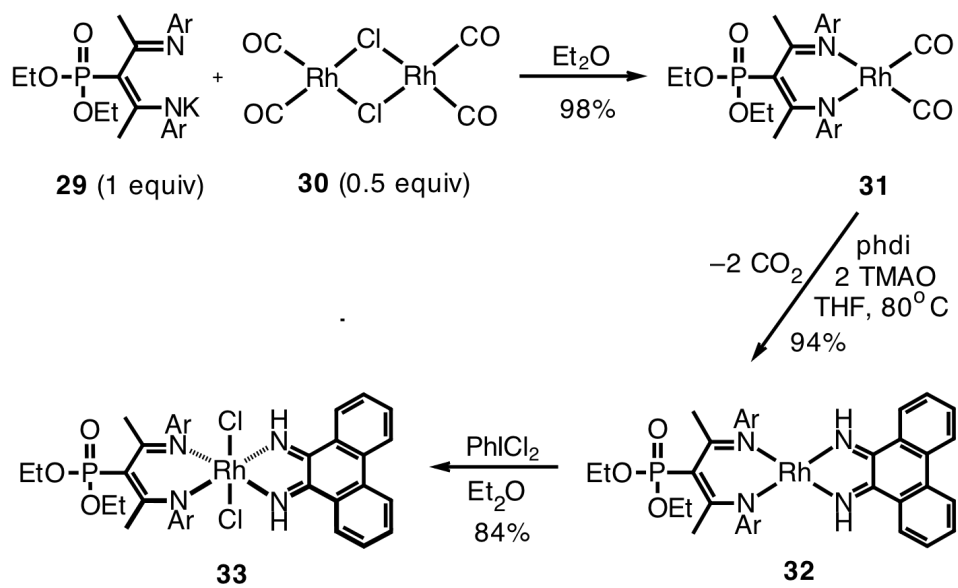
The structural identities of (NacNac^{Phos})RhCl$_2$(phdi) (**33**) and (NacNac^{Phos})Rh(phdi) (**32**) were verified by NMR spectroscopy. The ^{1}H NMR spectra of the complexes in C$_6$D$_6$ were consistent with C_{2v} symmetry in solution, displaying four equivalent isopropyl groups as a single methine resonance at 4.20 ppm for **33** and 3.61 ppm for **32**. In comparison to the Rh^I complex (**32**), the aromatic proton resonances ascribable to the N-2,6-diisopropylphenyl groups for **33** had shifted downfield whereas the resonances due to the phdi-ligand backbone appeared slightly upfield. In addition, the proton resonances associated with the –OCH$_2$CH$_3$ tethers of the phosphonate substituent were found in a more deshielded chemical environment for the complex with the oxidized rhodium center (**33**), as compared to the Rh^I species (**32**), displayed as a multiplet at 4.46 ppm in the former and 4.01 ppm in the latter complex. More subtle electronic differences were reflected in the ^{31}P{^{1}H} NMR spectra of (NacNac^{Phos})RhCl$_2$(phdi) and (NacNac^{Phos})Rh(phdi), showing individual singlet resonances at 30.0 and 29.3 ppm, respectively.

The geometries of octahedral (NacNac^{Phos})RhCl$_2$(phdi) complex and square-planar (NacNac^{Phos})Rh(phdi) complex were verified by single-crystal X-ray diffraction studies. Dark brown crystals of **33** suitable for X-ray diffraction analysis were obtained from a saturated CH$_3$CN solution at –35 °C while dark purple crystals of **32** were grown by layering a saturated diethyl ether solution of the complex over pentane at –35 °C. The respective structures are shown in Figure 6.2 in the form of ORTEP diagrams, with their metrical parameters listed in Table 6.1. The oxidative addition of Cl$_2$ to Rh^I resulted in a notable change in the Rh−N bond distances for coordinated (NacNac^{Phos})$^-$ ligand in **33**. Namely, the Rh−N bond distances between the Rh^{III} center and the nitrogen atoms of (NacNac^{Phos})$^-$ average at 2.035 Å, which is approximately 0.04 Å longer than the averaged Rh−N distance

for **32**. The bond lengthening is in agreement with steric repulsion between the diisopropylphenyl substitutes and the axial chlorides. In the same complex (**33**), the (NacNac^{Phos})-ligand backbone is visibly puckered up**,** with its partially delocalized C=N bonds tilted upward and away from the basal square plane by approximately 11° (Figure 6.2b). The averaged N–C bond distance of the phdi ligand revealed a slight elongation for (NacNac^{Phos})Rh(phdi) (+0.03 Å), as compared to (NacNac^{Phos})RhCl$_2$(phdi). The N–C bond lengthening for the Rh^I complex (**32**) is accompanied by a shorter NC–CN bond, with its distance shorter by approximately 0.04 Å than the NC–CN bond of the Rh^{III} complex (**33**). The longer C–N and shorter C–C bonds may be due to partial reduction of the phdi ligand at the rhodium(I) center.   Similar bond distances have been reported for compounds described as coordinated by the one-electron reduced form of the phdi ligand.[14] Altogether, the bond metrics of **32** compare well with those reported for the (NacNac^R)Rh(phdi) complexes (R = β-CH$_3$ or β-CF$_3$) while the bond metrics of **33** are well matched with those reported for the (NacNac^R)RhCl$_2$(phdi) derivatives.[8]
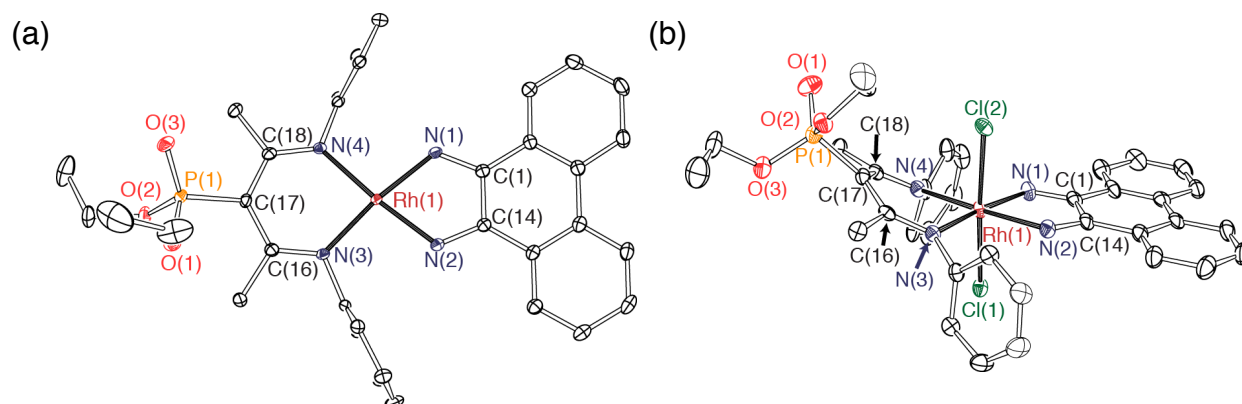
Figure 6.2 ORTEP diagrams of (a) (NacNac^{Phos})Rh(phdi) (**32**) and (b) (NacNac^{Phos})RhCl$_2$(phdi)(**33**). Ellipsoids are shown at 50% probability. Hydrogen atoms, solvent molecules, and the 2,6-diisopropyl substituents have been omitted for clarity.

Table 6.1. Selected Metrical Parameters for Solid-State Structures of (NacNac^{Phos})Rh(phdi) (**32**) and (NacNac^{Phos})RhCl$_2$(phdi) (**33**).

Bond (Å) / Angle (deg)	32	33
Rh(1)-N(3)	2.0097(14)	2.034(3)
Rh(1)-N(4)	1.9988(14)	2.043(3)
N(3)-C(16)	1.331(2)	1.310(5)
N(4)-C(18)	1.325(2)	1.321(5)
C(16)-C(17)	1.430(2)	1.439(5)
C(17)-C(18)	1.434(2)	1.433(5)
N(3)-Rh(1)-N(4)	88.85(6)	88.21(12)
Rh(1)-N(1)	1.9783(15)	2.022(3)
Rh(1)-N(2)	1.9857(15)	2.011(3)
N(1)-C(1)	1.326(2)	1.287(5)
N(2)-C(14)	1.326(2)	1.283(5)
C(1)-C(14)	1.433(2)	1.473(5)
N(1)-Rh(1)-N(2)	76.41(6)	76.14(13)
Cl(1)-Rh(1)-Cl(2)		176.37(3)

6.2.2 Electronic Properties of the Redox-Active (NacNac^{Phos})$^-$ Ligand

The new charge-transfer complexes, (NacNac^{Phos})Rh(phdi) (**32**) and (NacNac^{Phos})RhCl$_2$(phdi) (**33**), displayed diagnostic transitions in the vis-NIR portions of the electromagnetic spectrum. As shown in Figure 6.3a, the visible region of the spectrum for **32** was dominated by a strong absorption band at λ_{max} = 574 nm with an extinction coefficient of 22,200 M^{-1}cm^{-1}. The described charge-transfer band bears close resemblance to the individual, low-energy absorption profiles of (NacNac^{CH3})Rh(phdi) and (NacNac^{CF3})Rh(phdi), with respective energies shifted by no more than 20 nm and the intensities changed by no more than 500 M^{-1}cm^{-1} (Table 6.2). The lack of dependence on the NacNac-ligand substitution indicates that the low energy absorption of (NacNac^{Phos})Rh(phdi) is likely metal-to-ligand charge-transfer (MLCT) in character with molecular orbitals derived from rhodium and the phdi ligand.
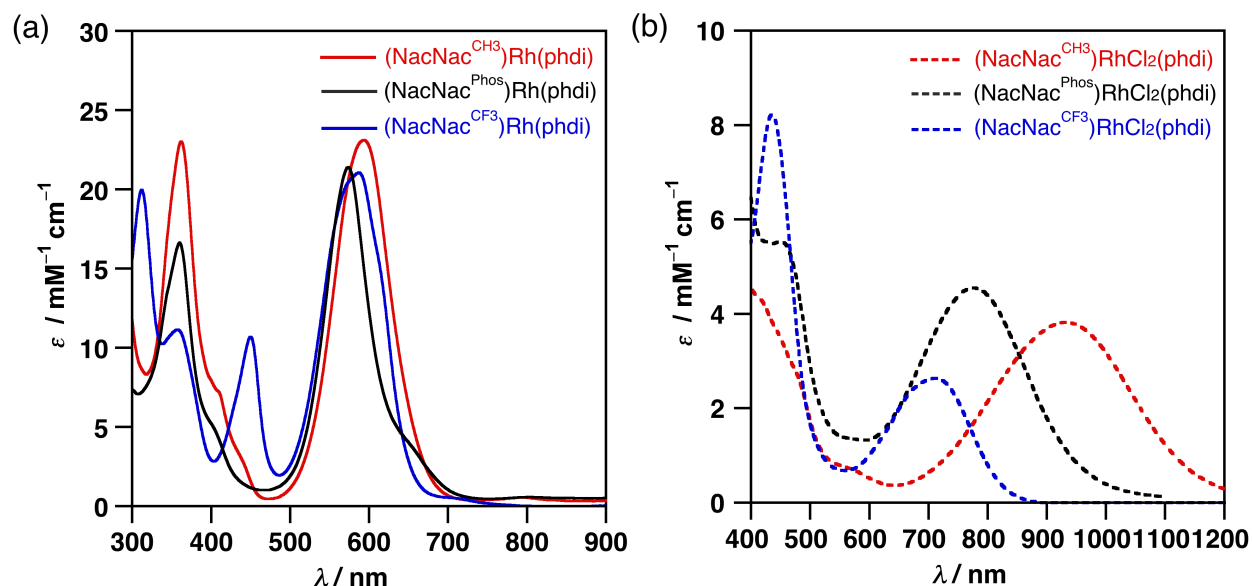
Figure 6.3. Electronic absorption spectra of (a) (NacNac^R)Rh(phdi) complexes and (b) (NacNac^R)RhCl$_2$(phdi) complexes (R = β-CH$_3$, β-CF$_3$, or a-PO(OEt)$_2$) measured in CH$_2$Cl$_2$ at 298K.

Marked differences were observed with respect to the low-energy charge-transfer bands among the oxidized complexes, (NacNac^R)RhCl$_2$(phdi) (Figure 6.3b). For all three rhodium species, the vis-NIR range of the spectrum was dominated by a broad ligand-to-ligand charge-transfer (LL'CT) transition of relatively weak intensity ($\varepsilon \cong 4{,}500$ M^{-1}cm^{-1}). The pertinent electronic transition for **33** was centered at $\lambda_{max} = 775$ nm, revealing a 160-nm blue shift in energy relative to (NacNac^{CH3})RhCl$_2$(phdi) and a 60-nm red shift relative to (NacNac^{CF3})RhCl$_2$(phdi). Sensitivity toward the NacNac ligand substitution signifies that the LL'CT transition must involve significant contributions from the β-diketiminate-centered orbital (HOMO). Furthermore, a clear relationship can be inferred between the donating capacity of the (NacNac^R)$^-$ ligand and the LL'CT energy: on the basis of the lambda max values, and assuming minimal perturbations to the phdi-centered LUMO among the three complexes, the HOMO of (NacNac^{Phos})$^-$ must be slightly elevated in energy relative to that of (NacNac^{CF3})$^-$ but sufficiently dropped in energy relative to that of (NacNac^{CH3})$^-$. The former

observation is consistent with the (NacNac^{Phos})$^-$ monoanion being a stronger donor than (NacNac^{CF3})$^-$ while the latter is consistent with it being a weaker donor than the (NacNac^{CH3})$^-$ counterpart.

Table 6.2 Electronic Absorption Spectroscopic and Electrochemical Data for (NacNac^R)Rh(phdi) and (NacNac^R)RhCl$_2$(phdi) Complexes.[a,b]

Complex	λ_{max}/nm	ε/M^{-1}cm^{-1}	$E^{\circ\prime}_1$	$E^{\circ\prime}_2$	$E^{\circ\prime}_{3(pc)}$	$E^{\circ\prime}_4$	$E^{\circ\prime}_{5(pa)}$	$E^{\circ\prime}_5$
(NacNac^{CH3})Rh(phdi)	593	22,700	−3.08	−2.03	—	0.06	0.79	—
(NacNac^{Phos})Rh(phdi)	574	22,200	−2.75	−1.83	—	0.16	0.73	—
(NacNac^{CF3})Rh(phdi)	587	21,100	−2.69†	−1.79	—	0.37	0.75	—
(NacNac^{CH3})RhCl$_2$(phdi)	935	3,820	−3.10	−2.04	−1.31	0.10††	—	0.34
(NacNac^{Phos})RhCl$_2$(phdi)	775	4,550	−2.77	−1.87	−1.17	0.16††	—	0.45
(NacNac^{CF3})RhCl$_2$(phdi)	713	2,640	−2.79†	−1.73	−1.11	0.34††	—	1.12

[a]R represents β-CH$_3$, β-CF$_3$, a-PO(OEt)$_2$ substituents of the (NacNac)$^-$ ligand. [b]Potentials were measured at a glassy-carbon electrode using 0.1 M [^{n}Bu$_4$N][PF$_6$] as the supporting electrolyte (referenced to [Cp$_2$Fe]$^{+/0}$). †This reduction is reported as E_{pc} for (NacNac^{CF3})Rh(phdi) and (NacNac^{CF3})RhCl$_2$(phdi). ††This daughter oxidation is reported as E_{pa} for all Rh^{III} complexes.

The redox properties of the new rhodium complexes were elucidated by cyclic voltammetric analysis recorded on THF solutions of **32** and **33** (1 mM) containing 100 mM [^{n}Bu$_4$N][PF$_6$] as the supporting electrolyte. Table 6.2 lists the redox potentials for the rhodium compounds with and without the phosphonate diester anchors, referenced to [Cp$_2$Fe]$^{+/0}$. For the Rh^I complex coordinated by the (NacNac^{Phos})$^-$ ligand (**32**), the cathodic CV region was comprised of one reversible reduction at −1.83 V and another partially reversible reduction at −2.75 V (Figure 6.4). These reductions have shifted to more positive potentials in comparison to those of (NacNac^{CH3})Rh(phdi) but appear slightly more negative than those of (NacNac^{CF3})Rh(phdi). The described events were assigned to diimine-centered reductions where the seeming dependence on the NacNac-ligand substitution may have resulted from the varied ability of rhodium to π-backbond with the phdi ligand. For example, the stronger donating capacity of the (NacNac^{CH3})$^-$ ligand furnished a more electron-rich rhodium species, (NacNac^{CH3})Rh(phdi), making it harder to reduce the C=N

bonds of the phdi ligand. Conversely, the $(NacNac^{Phos})^-$ and $(NacNac^{CF3})^-$ ligands are weaker

donor ligands on Rh^I, which led to more facile reductions of the same ligand. The anodic

voltammogram of $(NacNac^{Phos})Rh(phdi)$ (**32**) exhibited a partially reversible oxidation at

0.16 V and an irreversible oxidation near the edge of the solvent window at 0.73 V. The

oxidation at 0.16 V is consistent with a (NacNac)-centered oxidation, the potential of which

is influenced by the $PO(OEt)_2$ substituent. For example, the first-oxidation potential shifted

more negatively for $(NacNac^{CH3})Rh(phdi)$ (–10 mV), where the phosphonate substituent

was absent in the 3-position of the ligand backbone, but shifted more positively for

$(NacNac^{CF3})Rh(phdi)$ (+19 mV) where the fluorinated ligand without the phosphonate

substituent was used instead. Conversely, the second oxidation event of **32** at 0.73 V was

virtually unaffected by the NacNac-ligand identity and is, thus, assigned to a metal-based

redox couple.

The CV plot of $(NacNac^{Phos})RhCl_2(phdi)$ (**33**) revealed electrochemically reactive

behavior, consistent with other $(NacNac^R)RhCl_2(phdi)$ complexes, leading to

electrochemical generation of **32** (Figure 6.4b). When scanning cathodically, the complex

underwent a rapid two-electron reduction at –1.17 V, which was followed by a reversible

reduction at –1.87 V and another slightly reversible reduction at –2.77 V. The anodic region

contained a partially reversible oxidation at 0.45 V followed by a daughter peak at 0.16 V in

response to the first irreversible reduction event (–1.17 V). The two-electron reduction of

$(NacNac^{Phos})RhCl_2(phdi)$ at –1.17 V is attributed to the formation of unstable 20-electron

species, which is presumed to yield $(NacNac^{Phos})Rh^I(phdi)$ (**32**) upon dissociation of

chlorides. The remarkably similar redox features between the two remaining one-electron

reductions of **33** and those of **32**, and the matching daughter oxidation at 0.16 V, further

support the contention that **33** undergoes electrochemical decomposition to give **32** via putative $[(NacNac^{Phos})Rh^{I}Cl_2(phdi)]^{2-}$ intermediate. As shown in Figure 6.4b, the proclivity toward reductive decomposition was common to all three $(NacNac^{R})RhCl_2(phdi)$ compounds, independently of the NacNac-ligand substitution. Conversely, the redox potential of the second oxidation for **33** (0.45 V) fell in the middle of the analogous potentials seen with $(NacNac^{CH3})RhCl_2(phdi)$ at 0.34 V and $(NacNac^{CF3})RhCl_2(phdi)$ at 1.12 V. The strong dependence of the second oxidation on the electronic character of the NacNac ligand mirrors the optical trend seen for the individual LL'CT band energies (*vide supra*). Therefore, the second oxidation most likely occurred on the $(NacNac^{Phos})^-$ fragment of **33**.
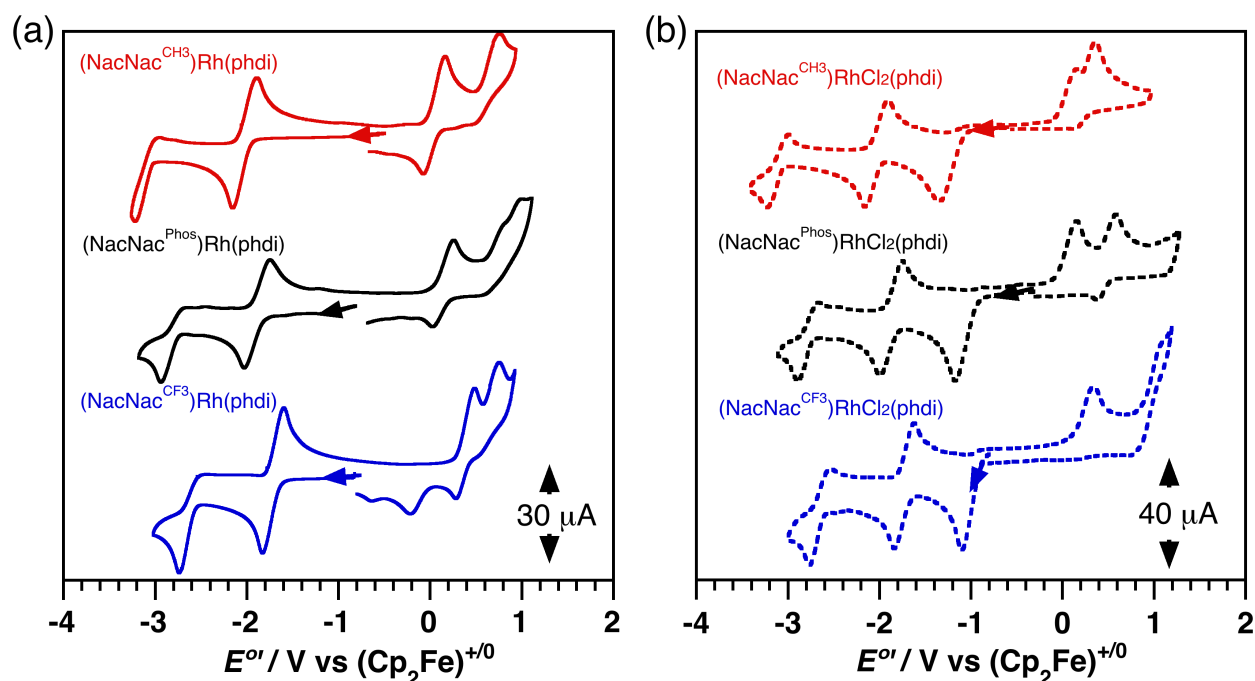
Figure 6.4. Cyclic voltammetry plots for (a) $(NacNac^{R})Rh(phdi)$ and (b) $(NacNac^{R})RhCl_2(phdi)$ complexes. measured in CH_2Cl_2 at 298K. Data acquired at 298 K on 1 mM samples dissolved in THF containing 0.1 M $[^{n}Bu_4N][PF_6]$ using a glassy-carbon electrode and a scan rate of 200 mV sec^{-1}. Potentials were referenced to $[Cp_2Fe]^{+/0}$ using an internal standard.

6.3 Summary

A modular synthetic approach was developed for the β-diiminyl ligand, (NacNac[Phos])[−], containing a phosphonate diester substituent at the central carbon of the ligand backbone. The phosphonylated ligand was derived by preparing two separate components, an imine with the pre-installed phosphonate group and the imidoyl chloride, and then combining the two via C–C coupling. To evaluate the impact that the phosphonate substituent has on the electronic character of the NacNac ligand, the new ligand was elaborated into the charge-transfer complexes of rhodium, including (NacNac[Phos])Rh(phdi) (**32**) and (NacNac[Phos])RhCl$_2$(phdi) (**33**) (phdi = phenanthrene-9,10-diimine). Both rhodium complexes were synthesized by a previously developed method with the former (**32**) derived from [Rh(μ–Cl)(CO)$_2$]$_2$ and the latter by the two-electron oxidation of **32**.

The absorptive and electrochemical features of the charge-transfer complexes with phosphonate anchors were compared to the analogous complexes without the phosphonate anchors. Predictably, the charge-transfer character for (NacNac[Phos])Rh(phdi) demonstrated a lack of dependence on the electronic identity of the NacNac ligand, with main orbital contributions derived from the rhodium(I) metal and the phdi acceptor ligand. In contrast, the low-energy electronic transition of the oxidized complex, (NacNac[Phos])RhCl$_2$(phdi), was ligand-to-ligand charge-transfer in nature with its band energy directly influenced by the donor-ligand substitution according to the trend: (NacNac[CF3])[−]>(NacNac[Phos])[−]>(NacNac[CH3])[−]. A similar trend was established by electrochemical methods for the first oxidation of (NacNac[Phos])Rh(phdi) and the second oxidation of (NacNac[Phos])RhCl$_2$(phdi), in both cases showing NacNac-centered redox behavior. The comparative assessment of the electronic properties for the new complexes confirmed that instalation of the phosphonate anchor

directly in the 3-position of the carbon backbone appreciably perturbs the donor ability of the β–diketimine ligand.

Given the vast presence of the phosphonate group in field of metallic oxide surface interfaces, the (NacNac^{Phos})⁻ ligand exemplifies a rare case of the redox-active donor ligand with its oxidizable properties potentially exploitable not only in homogeneous solutions but also on solid supports. In due course, the diethyl ester groups of the ligand phosphonate substituent may be cleaved off to enable for robust binding of the NacNac coordination complexes on the surface of metal oxides. The resulting complexes may prove important in several applications that target heterogenous catalysis, electrocatalysis, or solar-energy conversion schemes.

6.4 Experimental

General Considerations. All manipulations involving the synthesis of ligands were performed under air, unless otherwise noted, employing reagents and solvents purchased from commercial suppliers and used as received. Column chromatography was performed with 230-400 mesh silica gel using flash column techniques. Rhodium complexes were synthesized and studied under an inert atmosphere of nitrogen using standard glovebox techniques and dry and degassed solvents. Hydrocarbon solvents were sparged with argon and then deoxygenated and dried by passage through Q5 and activated alumina columns, respectively. Ethereal and halogenated solvents were sparged with argon and dried by passage through two activated alumina columns. To test for effective oxygen and water removal, nonchlorinated solvents were treated with a few drops of a purple solution of sodium benzophenone ketyl in tetrahydrofuran. The [Rh(μ-Cl)(CO)$_2$]$_2$ starting material (**30**) was obtained from Heraeus while diethyl (2-oxopropyl)phosphonate and (**27**) was

purchased from Sigma Aldrich and used without further purification. The ligand precursors *N*-(2,6-diisopropylphenyl)acetamide (**25**),[15] *N*-(2,6-diisopropylphenyl)-acetimidoyl chloride (**26**),[16] and phenanthrene-9,10-diimine (phdi)[17] were prepared by reported methods.

Physical Methods. NMR spectra were collected on Bruker Avance 400 and 500 MHz spectrometers. Chemical shifts were reported using the standard δ notation in parts per million and referenced using residual ^{1}H and ^{13}C isotopic impurities of the solvent. Infrared spectra were recorded as neat solids using a Jasco FT/IR-4700-ATR-PRO ONE spectrophotometer. Electronic absorption spectra were recorded in a dry, degassed CH_2Cl_2 solvent in one-centimeter cuvettes using a Shimadzu UV-1700 Spectrometer.

Electrochemical Methods. Cyclic voltammetry (CV) and differential pulse voltammetry (DPV) experiments were performed on a Gamry Series G 300 Potentiostat/Galvanostat/ZRA (Gamry Instruments, Warminster, PA, U.S.A.) using a 3.0 mm glassy carbon working electrode, a platinum wire auxiliary electrode, and a silver wire reference electrode. Measurements were recorded in a nitrogen-filled glovebox at ambient temperature and a scan rate of 200 mV/s. Sample concentrations were based on 1.0 mM THF solutions containing 100 mM $[^n Bu_4 N][PF_6]$ as the supporting electrolyte. All potentials were referenced to the $[Cp_2 Fe]^{+/0}$ couple using ferrocene or decamethylferrocene (0.47 V vs $[Cp_2 Fe]^{+/0}$) as an internal standard.[18] Decamethylferrocene was purified by sublimation under reduced pressure and tetrabutyl-ammonium hexafluorophosphate was recrystallized from ethanol three times and dried under vacuum.

Synthesis of diethyl-(2-((2,6-diisopropylphenyl)imino)propyl)phosphonate (28): A mixture of neat diethyl (2-oxopropyl)phosphonate **27** (750 µL, 3.9 mmol), 2,6-

diisopropylaniline (1.5 mL, 7.8 mmol), and *p*-toluenesulfonic acid monohydrate (30 mg) was heated at 100 °C for 12 h in the presence of anhydrous $CaSO_4$ (1.60 g, 11.8 mmol). The crude mixture was diluted with CH_2Cl_2 (50 mL), filtered, and the solvent was removed *in vacuo* to give a burgundy, oily substance. Analytically pure product had crystallized out of the crude reaction mixture while left sitting undisturbed for 3 days at rt. The obtained crystals were finely ground, filtered, and washed with cold hexanes to afford **28** as a white crystalline powder (689 mg, 50%). ^{31}P NMR (162 MHz, CD_3OD) δ 28.1, 25.3 (imine/ enamine); ^{1}H NMR (500 MHz, CD_3OD) δ 7.87 (d, *J* = 4.3 Hz, 1H), 7.34 (appar t, *J* = 7.6 Hz, 1H), 7.24 (s, 1H), 3.96-3.90 (m, 4H), 3.33 (d, *J* = 13.0 Hz, 1H), 3.12 (sept, *J* = 6.9 Hz, 2 H), 2.33 (s, 6H), 1.29-1.25 (m, 12H), 1.21 (d, *J* = 6.9 Hz, 6H); ^{13}C NMR (125 MHz, CD_3OD) δ 163.0 (d, *J* = 21.1 Hz, C–N), 148.2 (aryl-qC), 134.8 (aryl-qC–N), 129.4 (aryl-C), 124.8 (aryl-C), 73.1 (d, *J* = 217.9 Hz α-CH–P), 61.8 (d, *J* = 5.2 CH_2–O), 29.5 (CH_3), 24.9 (^{i}Pr-CH_3), 23.8 (^{i}Pr-CH_3), 19.03 (^{i}Pr-CH), 19.00 (^{i}Pr-CH), 16.6 (d, *J* = 6.9 Hz, CH_3); FTIR (neat) v/cm^{-1} 3220, 3019, 1604, 1588, 1526, 1462, 1384, 1363, 1330, 1205 st, 1054 st, 1023 st, 933 st, 784 st; HRMS (ESI) *m / z* calcd for $C_{19}H_{32}O_3P$ (M + Na)$^{+}$ 376.2018, found 376.2019.

(NacNac^{Phos})H (29): To a solution of **28** (674 mg, 1.90 mmol) in THF (15 mL) at –10 °C was added lithium diisopropylamide (2.0 M, 1.45 mL) under a nitrogen atmosphere. The reaction mixture was stirred for 0.5 h at that temperature, after which point a degassed solution of imidoyl chloride **26** (454 mg, 1.90 mmol) in THF (15 mL) was introduced via cannula. The resulting reaction mixture was refluxed for 12 h. After cooling to rt, the reaction mixture was washed with $NaHSO_3$ (100 mL) and extracted with ethyl acetate (100 mL X 3). The combined organic layers were washed with brine (200 mL), dried over anhydrous Na_2SO_4, and concentrated *in vacuo*. The crude residue was purified by column

chromatography on silica-gel (ethyl acetate:hexanes/25:75) to give (**29**) as a white crystalline solid (600 mg, 57%). ^{31}P NMR (162 MHz, CDCl$_3$) δ 28.5; ^{1}H NMR (500 MHz, CDCl$_3$) δ 7.17-7.12 (m, 6H), 4.16-4.08 (m, 4H), 2.97 (sept, J = 6.8 Hz, 4H), 2.19 (s, 6H), 1.36 (t, J = 7.1 Hz, 6H), 1.19 (d, J = 6.8 Hz, 12 H), 1.12 (J = 6.8 Hz, 12 H); ^{13}C NMR (125 MHz, CDCl$_3$) δ 170.2 (C=N), 170.0 (C=N), 141.9 (aryl-qC), 139.28 (aryl-qC–N), 139.26 (aryl-qC–N), 125.8 (aryl-C), 123.5 (aryl-C), 89.2 (d, J = 209.9 Hz, α-qC–P), 60.8 (d, J = 5.3 Hz, CH$_2$–O), 28.4 (CH$_3$), 24.3 (^{i}Pr-CH$_3$), 23.5 (^{i}Pr-CH$_3$), 21.2 (^{i}Pr-CH), 16.3 (d, J = 6.9 Hz, –CH$_3$); FTIR (neat) v/cm^{-1} 3207, 3013, 2963, 2868, 1587, 1519, 1464, 1328, 1208 st, 1027 st, 945 st, 787 st; HRMS (ESI) m / z calcd for C$_{33}$H$_{51}$O$_3$P (M + Na)$^+$ 577.3535, found 577.3542.

(NacNac^{Phos})Rh(CO)$_2$ (31): A pre-chilled solution of (NacNac^{Phos})H (**29**) (400 mg, 0.721 mmol) in diethyl ether (10 mL, −78 °C) was added to a vial of potassium hydride (30.4 mg, 0.757 mmol). After stirring at room temperature for 12 h, to the resulting suspension was added [Rh(μ-Cl)(CO)$_2$]$_2$ (**30**) (140 mg, 0.36 mmol) followed by stirring at the same temperature for another 12 h. The dark solution was stripped to dryness, re-dissolved in CH$_2$Cl$_2$, and filtered to remove KCl. The solvent from the filtrate was removed in *vacuo* to afford **31** as a light brown solid (506 mg, 98%). ^{31}P NMR (162 MHz, CDCl$_3$) δ 29.5; ^{1}H NMR (400 MHz, CDCl$_3$) δ 7.18 (m, 6H), 4.10-4.05 (m, 4H), 3.28 (sept, J = 6.7 Hz, 4H), 2.10 (s, 6H), 1.37 (d, J = 6.7 Hz, 12H), 1.33 (t, J = 6.7 Hz, 12H), 1.22 (d, J = 6.7 Hz, 12H); ^{13}C NMR δ 183.4 (d, J = 66.6 Hz, C≡O), 167.4 (d, J = 19.7 Hz, C=N), 154.3 (qC–N), 139.7 (aryl-qC), 126.6 (aryl-C), 124.1 (aryl-C), 77.36 (α-qCH–P), 61.5 (d, J = 6.2 Hz, CH$_2$–O), 28.1 (CH$_3$), 24.4 (^{i}Pr-CH), 24.3 (^{i}Pr-CH$_3$), 24.1 (^{i}Pr-CH$_3$), 16.5 (d, J = 6.8 Hz, –CH$_3$); FTIR (neat) v/cm^{-1} 2961, 2829, 2862, 1524, 1437, 1375 st, 1318 st, 1235 st, 1047 st, 1023 st, 940 st, 779 st, 591 st; HRMS (ESI) m / z calcd for C$_{35}$H$_{50}$N$_2$O$_5$PRh (M + Na)$^+$ 735.2410, found 735.2427.

(NacNac^Phos)Rh(phdi) (32): In a nitrogen-filled glovebox, a solution of **31** (293 mg, 0.411 mmol), TMAO (62 mg, 0.822 mmol), and phenanthrene-9,10-diimine (85 mg, 0.411 mmol) in THF (7 mL) was loaded into a straus tube. The reaction mixture was heated at 100 °C for 12 h. The purple reaction mixture was cooled to rt and stripped to dryness to give analytically pure **32** as a purple crystalline solid (335 mg, 94%). ^{31}P NMR (162 MHz, CDCl$_3$) δ 29.3; ^{1}H NMR (500 MHz, CDCl$_3$) δ 8.01 (appar t, J = 7.4 Hz, 2H), 7.90 (d, J = 7.9 Hz, 2H), 7.76-7.73 (m, 2H), 7.22 (appar t, J = 7.5 Hz, 2H), 7.69 (s, 6H), 4.03-3.95 (m, 4H), 3.28 (sept, J = 6.6 Hz, 4H), 2.73 (s, 6H), 1.33 (d, J = 6.6 Hz, 12H), 1.30 (t, J = 7.0 Hz, 6H), 0.94 (d, J = 6.6 Hz, 12H). ^{13}C NMR δ 162.04 (d, J = 19.5 Hz, C=N), 154.5 (phdi-C=N), 151.4 (aryl-qC–N), 144.7 (aryl-qC), 130.9 (phdi-qC), 129.6 (phdi-qC), 129.5 (phdi-CH), 127.6 (phdi-CH), 126.1 (aryl-CH), 125.1 (phdi-CH), 123.5 (aryl-CH), 118.8 (phdi-CH), 77.4 (α-qCH–P), 61.3 (d, J = 6.3 Hz, CH$_2$–O), 29.0 (^{i}Pr-CH), 25.6 (CH$_3$), 23.4 (^{i}Pr-CH$_3$), 16.4 (d, J = 7.1 Hz, CH$_3$); FTIR (neat) v/cm^{-1} 3310, 2960, 2928, 1515, 1501, 1412, 1315, 1361, 1244, 1097, 1014 st, 1046 st, 934 st, 779 st, 589 st; HRMS (ESI) m / z calcd for C$_{47}$H$_{60}$N$_4$O$_3$PRh (M + H)$^+$ 863.3536, found 863.3529.

(NacNac^Phos)RhCl$_2$(phdi) (33): A solution of PhICl$_2$ (66.5 mg, 0.242 mmol) in Et$_2$O (2 mL) was added to a stirred dark purple solution of **32** (209 mg, 0.242 mmol) in Et$_2$O (3 mL). The reaction turned brown and was left stirring at rt for 12 h. The volume of the solution was reduced down to 2 mL and the resulting brown precipitate was filtered. After repeated washings with cold pentane and drying under vacuum, compound **33** was afforded as a greenish-brown solid (190 mg, 84%). ^{31}P NMR (162 MHz, CDCl$_3$) δ 30.0; ^{1}H NMR (500 MHz, C$_6$D$_6$) δ 10.30 (s, 2H), 7.38 (appar d, J = 7.6 Hz, 4H), 7.30 (appar t, J = 7.5 Hz, 2H), 7.13 (s, 2H), 6.76 (appar t, J = 7.5 Hz, 2H), 6.72 (appar t, J = 7.4 Hz, 2H), 4.41-4.53 (m,

4H), 4.20 (sept, J = 6.5 Hz, 4H), 3.10 (s, 6H), 1.63 (d, J = 6.5 Hz, 12H), 1.30 (d, J = 6.5 Hz, 12H), 1.26 (t, J = 7.0 Hz, 6H); ^{13}C NMR δ 168.9 (d, J = 20.4 Hz, C=N), 168.1 (phdi-C=N), 146.5 (phdi-qC), 145.2 (aryl-qC), 134.4 (phdi-CH), 132.5 (phdi-qC), 129.5 (phdi-CH), 127.3 (phdi-CH), 125.3 (aryl-CH), 124.9 (phdi-qC), 124.7 (aryl-CH), 124.4 (phdi-CH), 77.4 (α-qCH–P), 61.4 (d, J = 5.8 Hz, CH_2–O), 28.9 (^{i}Pr-CH),), 26.5 (CH_3), 26.4 (^{i}Pr-CH_3), 24.9 (^{i}Pr-CH_3), 16.6 (d, J = 7.3 Hz, CH_3); FTIR (neat) v/cm^{-1} 3289, 2972, 2930, 1600, 1544, 1462, 1314, 1227, 1050, 1026 st, 949 st, 930, 752 st, 591 st; HRMS (ESI) m / z calcd for $C_{47}H_{60}N_4O_3Cl_2PRh$ (M + H)$^+$ 933.2913, found 933.2911

Crystallographic Methods. X-ray diffraction data were collected on crystals mounted on glass fibers using a Bruker CCD platform diffractometer equipped with a CCD detector. Measurements were carried out at 163 K using Mo Kα (λ = 0.71073 Å) radiation, which was wavelength selected with a single-crystal graphite monochromator. The SMART program package was used to determine unit-cell parameters and to collect data.[19] The raw frame data were processed using SAINT[20] and SADABS[21] to yield the reflection data files. Subsequent calculations were carried out using the SHELXTL[22] program suite. Structures were solved by direct methods and refined on F_2 by full-matrix least-squares techniques. Analytical scattering factors for neutral atoms were used throughout the analyses.[23] Hydrogen atoms were included using a riding model. ORTEP diagrams were generated using ORTEP-3 for Windows. Diffraction data are shown in Table 6.3

149

Table 6.3. X-ray Diffraction Data Collection and Refinement Parameters for Complexes (NacNac$^{\text{Phos}}$)Rh(phdi) (**32**) and (NacNac$^{\text{Phos}}$)RhCl$_2$(phdi) (**33**).

	32	33
empirical formula	C$_{47}$H$_{60}$N$_4$O$_3$PRh	C$_{53}$H$_{69}$Cl$_2$N$_7$O$_3$PRh
formula weight	862.87	1056.93
crystal system	triclinic	triclinic
space group	$P\bar{1}$	$P2_1/c$
a/Å	8.8549(5)	19.4380(17)
b/Å	11.0734(6)	14.2103(13)
c/Å	23.0945(12)	19.8174(17)
α/deg	76.6983(6)	90
β/deg	79.0316(6)	106.2803(12)
γ/deg	8.8549(5)	90
V/Å^3	2163.1(2)	5254.5(8)
Z	2	4
refl. collected	26348	28927
indep. refl.	10500 (0.0199)	11463 (0.0332)
R1 (I > 2σ)^a	0.0290	0.0479
wR2 (all data)^a	0.0734	0.1273

^{a}R$_1$ = $\sum||F_o| - |F_c||/\sum|F_o|$; wR$_2$ = $[\sum w(F_o^2 - F_c^2)^2/\sum w(F_o^2)^2]^{1/2}$; GOF = $[\sum w(|F_o| - |F_c|)^2/(n - m)]^{1/2}$.

6.5 References

[1] (a) Cui, C.; Roesky, H. W.; Schmidt, H.-G.; Noltemeyer, M.; Hao, H.; Cimpoesu, F. *Angew. Chem., Int. Ed.* **2000**, *39*, 4274–4276. (b) Driess, M.; Yao, S.; Brym, M.; van Wüllen, C.; Lentz, D. *J. Am. Chem. Soc.* **2006**, *128*, 9628–9629. (c) Roesky, H. W.; Singh, S.; Jancik, V.; Chandrasekhar, V. *Acc. Chem. Res.* **2004**, *37*, 969–981. (d) Henderson, M. J.; Kennard, C. H. L.; Raston, C. L.; Smith, G. *J. Chem. Soc. Chem. Commun.* **1990**, 1203–1204. (e) Tsai, Y-C. *Coord. Chem. Rev.* **2012**, *256*, 722–758.

[2] (a) Bourget- Merle, L.; Lappert, M. F.; Severn, J. R. *Chem. Rev.* **2002**, *102*, 3031–3065. (b) Mindiola, D. J. *Acc. Chem. Res.* 2006, 39, 813–821. (c) Spielmann, S.; Piesik, D.; Wittkamp, B.; Jansen, G.; Harder, S. *Chem. Commun.* **2009**, 3455-3456. (d) Fan, H.; Adhikari, D.; Saleh, A. A.; Clark, R. L.; Zuno-Cruz, F. J.; Sanchez Cabrera, G.; Huffman, J. C.; Pink, M.; Mindiola, D. J.; Baik, M.-H. *J. Am. Chem. Soc.* **2008**, *130*, 17351–17361. (e) Pfirrmann, S.; Limberg, C.; Herwig, C.; Stößer, R.; Ziemer, B. *Angew. Chem. Int. Ed.* **2009**, *48*, 3357–3361.

[3] (a) Yao, Y.; Zhang, Z.; Peng, H.; Zhang, Y.; Shen, Q.; Lin, J. *Inorg. Chem.* **2006**, *45*, 2175–2183. (b) Xue, M.; Zheng, Y.; Hong, Y.; Yao, Y.; Xu, F.; Zhang, Y.; Shen, Q. *Dalton Trans.* **2015**, *44*, 20075–20086. (c) Yao, Y.; Xue, M.; Luo, Y.; Zhang, Z.; Jiao, R.; Zhang, Y.; Shen, Q.; Wong, W.; Yu, K.; Sun, J. *J. Organomet. Chem.* **2003**, *678*, 108–116.

[4] (a) Holland, P. L.; Tolman, W. B. *J. Am. Chem. Soc.* **1999**, *121*, 7270–7271. (b) Jang, E. S.; McMullin, C. L.; Kaß, M.; Meyer, K.; Cundari, T. R.; Warren, T. H. *J. Am. Chem. Soc.* **2014,** *136*, 10930–10940. (c) MacLeod, K. C.; Vinyard, D. J.; Holland, P. L. *J. Am. Chem. Soc.* **2014**, *136*, 10226–10229. (d) Basuli, F.; Bailey, B. C.; Tomaszewski, J.; Huffman, J. C.; Mindiola, D. J. *J. Am. Chem. Soc.* **2003**, *125*, 6052–6053. (e) Thompson, R.; Chen, C.-H.; Pink, M.; Wu, G.; Mindiola, D. J. *J. Am. Chem. Soc.* **2014**, *136*, 8197–8200. (f) Kogut, E.; Wiencko, H. L.; Zhang, L.; Cordeau, D. E.; Warren, T. H. *J. Am. Chem. Soc.* **2005**, *127*, 11248–11249. (g) Cramer, C. J.; Tolman, W. B. *Acc. Chem. Res.* **2007**, *40,* 601–608. (h) Kogut, E.; Wiencko, H. L.; Zhang, L.; Cordeau, D. E.; Warren, T. H. *J. Am. Chem. Soc.* **2005**, *127*, 11248–11249 (i) Monillas, W. H.; Yap, G. P. A.; MacAdams, L. A.; Theopold, K. H. *J. Am. Chem. Soc.* **2007**, *129*, 8090–8091. (j) Ding, K.; Brennessel, W. W.; Holland, P. L. *J. Am. Chem. Soc.* **2009**, *131*, 10804. (k) Camp, C.; Grant, L. N.; Bergman, R. G.; Arnold, J. *Chem. Commun.* **2016**, *52*, 5538–5541.

[5] Budzelaar, P. H. M.; Bart van Oort, A.; Orpen, A. G. *Eur. J. Inorg. Chem.* **1998**, 1485–1494

[6] Marshak, M. P.; Chambers, M. B.; Nocera, D. G. *Inorg. Chem.* **2012**, *51*, 11190–11197.

[7] (a) Khusniyarov, M. M.; Bill, E.; Weyhermüller, T.; Bothe, E.; Wieghardt, K. *Angew. Chem. Int. Ed.* **2011**, *50*, 1652–1655. (b) Takaichi, J.; Morimoto, Y.; Ohkubo, K.; Shimokawa, C.; Hojo, T.; Mori, S.; Asahara, H.; Sugimoto, H.; Fujieda, N.; Nishiwaki, N.; Fukuzumi, S.; Itoh, S. *Inorg. Chem.* **2014**, *53*, 6159–6169.

[8] Shaffer, D. W.; Ryken, S. A.; Zarkesh, R. A.; Heyduk, A. F. *Inorg. Chem.* **2012**, *51*, 12122–12131.

[9] Moilanen, J.; Borau-Garcia, J.; Roesler, R.; Tuononen, H. M. *Chem. Commun.* **2012**, *48*, 8949–8951.

[10] Eisenstein, O.; Hitchcock, P. B.; Khvostov, A. V.; Lappert, M. F.; Maron, L.; Perrin, L.; Protchenko, A. V. *J. Am. Chem. Soc.* **2003**, *125*, 10790-10791.

[11] (a) Borah, P.; Zhao, Y. *J. Catal.* **2014**, *318*, 43–52. (b) Li, B.; Zhang, C.; Yang, Y.; Zhu, H.; Roesky, H. W. *Inorg. Chem.* **2015**, *54*, 6641–6646.

[12] Pelletier, J. D. A.; Basset, J.-M. *Acc. Chem. Res.* **2016**, *49*, 664–677.

[13] Ertl, G.; Knözinger, H.; Weitkamp, J., Eds.; Preparation of Solid Catalysts. *In Handbook of Heterogeneous Catalysis*; Wiley-VCH Verlag GmbH: New York, 2008.

[14] (a) Chern, S.-S.; Lee, G.-H.; Peng, S.-M. *J. Chem. Soc., Chem. Commun.* **1994**, 1645–1646. (b) Chern, S.-S.; Liaw, M-C.; Peng, S.-M. *J. Chem. Soc., Chem. Commun.* **1993**, 359–361. (c) Peng, S. M.; Chen, C.-T.; Liaw, D.-S.; Chen, C.-I.; Wang, Y. *Inorg. Chim. Acta* **1985**, *101*, L31–L33.

[15] Boere, R. T.; Klassen,V.; Wolmershaüser, G. *DaltonTrans.* **1998**, 4147–4154.

[16] Liu, P., Wesolek, M.; Danopoulos, A. A.; Braunstein, P. *Organometallics* **2013**, *32*, 6286–6297.

[17] Linder, T.; Sutherland, T. C.; Baumgartner, T. *Chem. Eur. J.* **2010**, *16*, 7101–7105.

[18] Connelly, N. G.; Geiger, W. E. *Chem. Rev.* **1996**, *96*, 877–910.

[19] SMART Software Users Guide, Version 5.1, Bruker Analytical X-Ray Systems, Inc.; Madison, WI 1999.

[20] SAINT Software Users Guide, Version 6.0, Bruker Analytical X-Ray Systems, Inc.; Madison, WI 1999

[21] G. M. Sheldrick, SADABS, Version 2.10, Bruker Analytical X-Ray Systems, Inc.; Madison, WI 2002.

[22] G. M. Sheldrick, SHELXTL Version 6.12, Bruker Analytical X-Ray Systems, Inc.; Madison, WI 2001

[23] *International Tables for X-Ray Crystallography* 1992, Vol. C., Dordrecht: Kluwer Academic Publishers.

Chapter 7

Synthesis of the Redox-Active [ONO] Ligands with Phosphonic

Anchoring Groups

7.1 Introduction

The tridentate amido-bis(phenolate) motif, *N*,*N*-bis(3,5-di-*tert*-butyl-2-phenoxide)amide [ONO], is an established pincer-type ligand that exhibits rich redox chemistry.[1] The well-documented redox activity of the [ONO]-ligand platform is derived from its ability to exits in three distinct oxidation states when coordinated to a metal ion. As shown in Figure 7.1, the amido-bis(phenolate) ligand may be found in the fully reduced catecholate form, the one-electron oxidized semiquinonate form, or the two-electron oxidized quinonate form of the ligand. Owing to its pincer-type topology, coordination of the [ONO] ligand to transition metal ions results in meridional complexes, where the ligand electron valence states can be delocalized over both of the *N*-tethered aromatic rings. As a result, the electron-reservoir role of the [ONO] ligand has proven valuable in recent years, capable of reversibly shuttling electrons between the coordinated ligand and the metal ion. The ability to access and store multiple electron equivalents within the ligand framework is a feature that is crucial for bio-inspired transformations, catalysis, and small-molecule activation chemistry.
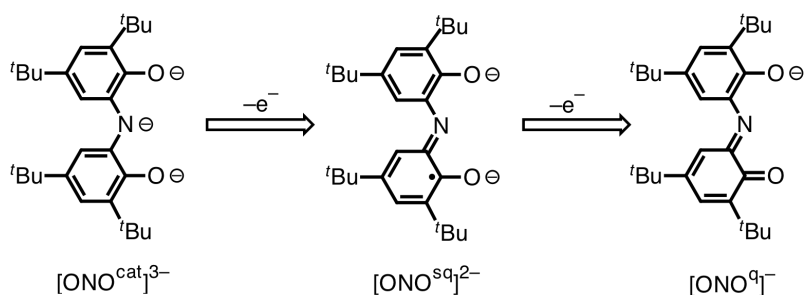
Figure 7.1 Three possible oxidation states of the redox-active [ONO]-ligand platform accessible on coordination to a metal ion.

The mutli-electron reactivity of the amido-bis(phenolate) ligand platform has been harnessed with a wide range of coordination complexes. Our group in particular developed

the [ONO]-ligand chemistry with early, d^0 transition metal ions (group IV/V) revealing their ability to participate in catalytic or substoichiometric transformations. For example, the complexes of tantalum(V) supported by the [ONO] ligand, in the fully reduced $[ONO^{cat}]^{3-}$ form, were shown to effect the insertion of azides into the Ta–C bonds,[2] catalyze the oxidative formation of diaryldiazenes,[3] or induce carbene-transfer reactions with diazoalkanes.[4] Hence, the [ONO] ligand at a formally d^0 metal center proved to mediate two-electron redox processes needed for bond activation or bond forming reactions (however, the ligand non-innocence was not implicated in the carbene-transfer chemistry). In addition, the [ONO] complex of zirconium(IV) possessing the mono-protonated form of the ligand, $[ONHO]^{2-}$, was found by us to effect the four-electron reduction of O_2 by leveraging the dual function of the ligand as an electron and proton reservoir.[5] Alternatively, Wieghardt and coworkers reported the activation of O_2 by the [ONO] copper(II) catalyst with synergistic electron and hydrogen-atom transfer capabilities, which was exploitable in the aerobic oxidation of primary alcohols.[6] More recently, we demonstrated the proclivity of the doubly oxidized $[ONO^q]^-$ ligand platform to effect reductive elimination of disulfides from an iron(III) complex.[7]

Considering the diverse range of mononuclear [ONO] coordination complexes and their rich ligand-based reactivity, it is reasonable to suggest that many more catalytic applications of the tridentate amido-bis(phenolate) motif will be forthcoming. To the best of our knowledge, the multi-electron reactivity patterns of existing [ONO] complexes have not been investigated under conditions other than homogeneous catalysis where the catalysts employed are always present in a liquid suspension. If alternative applications are to be targeted for the [ONO]-based complexes, including electrocatalysis and fuel-forming

reactions, it may be advantageous to design catalyst probes that would be equipped with built-in electrode-surface binding capabilities directly at the redox-active moiety. Given the proven usefulness of metal oxide electrodes in heterogeneous catalysis,[8] we became interested in revising the [ONO]-ligand backbone that would lead to complexes that could be tethered to metal oxide surfaces. This would potentially allow us to harness the unique multi-electron properties of the pincer-type [ONO] ligand outside of solution-based reactivity schemes.

Scheme 7.1. Synthesis of [ONO] proligands via (a) condensation of 3,5-di-*tert*-butylcatechol with aqueous ammonia and (b) the copper(I)-catalyzed *N*-arylation of *o*-aminophenol with *o*-iodophenol.
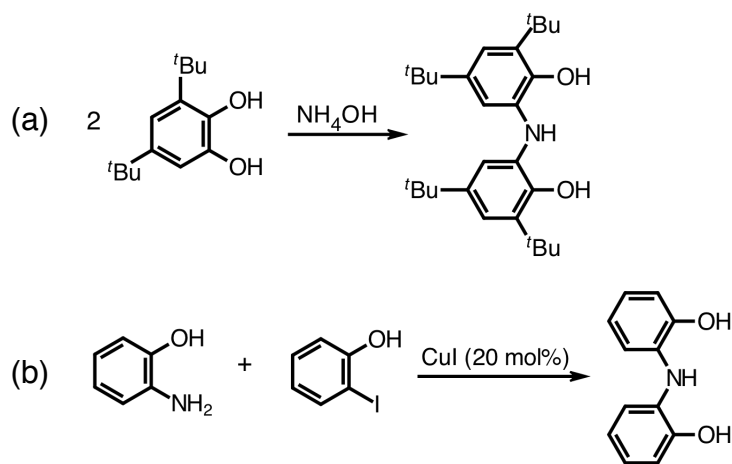
While the parent ligand, *N,N*-bis(3,5-di-*tert*-butyl-2-phenoxide)amide, is readily prepared by stitching together two catechols through condensation with ammonia,[6] this strategy is generally limited to the catechols with bulky di-*tert*-bulyl groups (Scheme 7.1a). The reason why 3,5-di-*tert*-butylcatechol is used in this process is to prevent nucleophilic attack of ammonia on the carbon atoms of the oxidized quinone, formed as a reactive intermediate during homocondensation. However, the same *tert*-bulyl groups sterically preclude the installation of additional substituents (i.e. anchoring groups) on the bis(phenolate) backbone of the [ONO] proligand. More recently, the copper(I)-catalyzed

synthesis of various diphenylamine derivatives was reported by Li and coworkers.[9] The synthesis was achieved by *N*-arylation of 2-aminophenol with aryl iodide derivatives, which yielded symmetric 2-(diphenylamino)phenol when using 2-iodophenol as coupling partner (Scheme 7.1b). In general, the showcased methodology was functional-group tolerant with hydroxyl, cabonyl, alkyl, and halogen groups remaining intact during the course of the reaction. In this manner, the C–N coupling reaction revealed the possibility of building the [ONO]-ligand skeleton in a modular fashion, from two individual components with either symmetrical or unsymmetrical substitutional patterns being potentially targeted for the amido-bis(phenolate) motif.

In this work, we report the strategy for incorporating anchoring groups into the [ONO]-ligand backbone for covalent attachment on metal oxide surfaces. To this end, two symmetric ligand variations containing a phosphonate anchoring group on both of the aromatic rings of the [ONO]-ligand framework were prepared by the C–N coupling reaction (Scheme 7.3). The first derivative, azanediylbis(5-(diethoxyphosphoryl)2-phenol) ([P$_2$-ONO]H$_3$), contains an ethyl-protected phosphonate group attached directly at the 5-position of the *o*-aminophenolate rings. The second derivative, azanediylbis(5-(diethoxyphosphoryl)3-*tert*-butyl-2-phenol) ([P$_2$-ONO^{tBu}]H$_3$), contains a *tert*-butyl substituent at the 3-position of each *o*-aminophenolate ring in addition to the ethyl-protected phosphonate groups attached directly to ring 5-positions. The installation of bulky *tert*-butyl groups on [P$_2$-ONO^{tBu}]H$_3$ was expected to confer different solubility properties relative to the [P$_2$-ONO]H$_3$ congener but preserve the electronic characteristics of the two ligand derivatives. The prospective [ONO] complexes of the new ligand derivatives will be poised for fundamental redox studies under heterogeneous conditions.

7.2 Results and Discussion

Scheme 7.2. Synthetic strategy for the preparation of *o*-aminophenol (**37/43**) and *o*-iodophenol derivatives (**38/44**).

34: R = H
40: R = ^{t}Bu, 91%

35: R = H, 32%
41: R = ^{t}Bu, 69%

36: R = H, 88%
42: R = ^{t}Bu, 94%

37: R = H, 89%
43: R = ^{t}Bu, 88%

38: R = H, 88%
44: R = ^{t}Bu, 99%
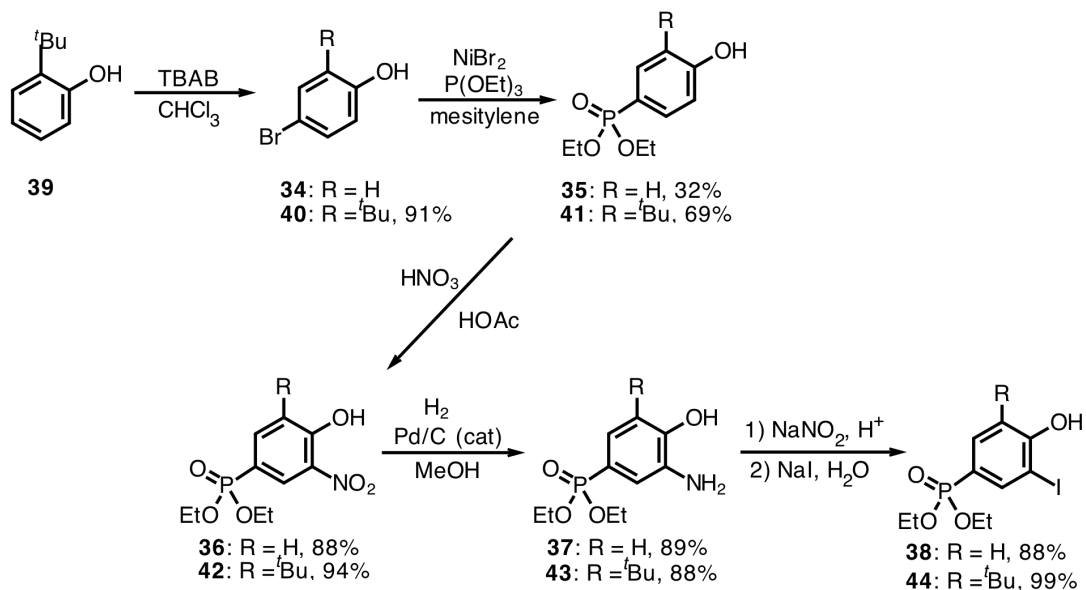
Synthesis of the [P$_2$-ONO]H$_3$ and [P$_2$-ONO$^{t\mathrm{Bu}}$]H$_3$ proligands required first preparing the individual, phosphonate-functionalized synthons for the C–N coupling reaction. Scheme 7.2. shows the relevant sequence that was used to access both types of coupling partners. The ethyl-protected phosphonate group was installed early in the synthesis by the nickel(II)-mediated Arbuzov reaction of either 4-bromophenol (**34**) or 4-bromo-2-(*tert*-butyl)phenol (**40**) with triethylphosphite (compound **40** was prepared in a preceding step by bromination of commercial 2-(*tert*-butyl)phenol **39** with tetrabutylammonium tribromide (TBAB)).[10] Treatment of the phosphonate-functionalized phenol (**35/41**) with concentrated nitric acid added a nitro group to the aromatic ring in the *ortho* position relative to the hydroxyl group of either **36** or **42**. The 2-aminophenol compound was derived next via hydrogenation of the singly nitrated phenol (**36/42**) under palladium catalysis. The second coupling partner, 2-iodophenol (**38/44**), was accessed by a one-pot,

diazotization-iodination reaction of aminophenol derivatives. Treatment of the individual

o-aminophenols (**37/42**) with sodium nitrite in acidic media produced a diazonium salt,

which was not isolated but immediately converted to aromatic iodide **38** or **44** by means of

nucleophilic aromatic substitution with sodium iodide (Scheme 7.2). In general, the

described approach yielded consistently pure phenolic intermediates, thus eliminating the

need for purification outside of routine workup for each successive reaction step.

Furthermore, the phosphonate diester group remained preserved throughout the synthesis,

highlighting the functional group tolerance toward various reaction conditions.

Scheme 7.3. Copper(I)-catalyzed C–N assembly of $[P_2\text{-ONO}]H_3$ and $[P_2\text{-ONO}^{tBu}]H_3$ ligand precursors.
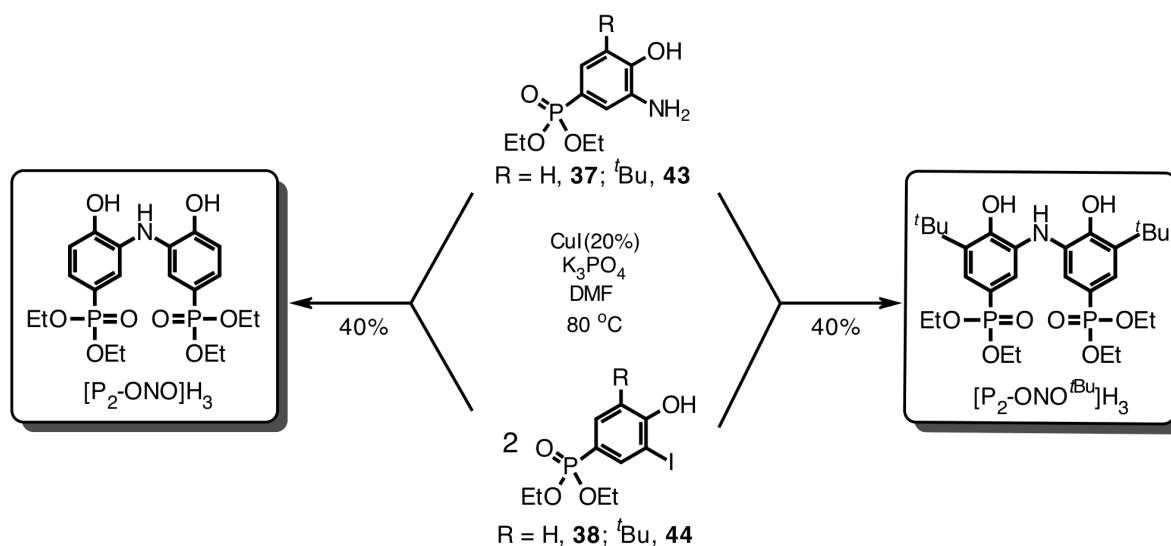
The copper(I)-catalyzed C–N assembly of the [ONO] ligands was performed in air-

free conditions using a 2:1 ratio of 2-aminophenol to 2-iodophenol derivatives. As

established by Li and coworkers,[9] the extra equivalent of the aminophenol substrate was

deemed necessary to restrain formation of triphenylamine compounds, which otherwise

compete with the diphenylamine counterparts. As shown in Scheme 7.3, the coupling

reaction required heating a DMF solution containing the appropriate ratio of 2-

aminophenol (**37/43**) and 2-iodophenol (**38/44**) derivatives in the presence of catalytic

CuI and 2 equivalents tripotassium phosphate. During standard workup, the first ligand derivative, [P$_2$-ONO]H$_3$, was found to readily crystallize from a saturated ethyl acetate solution, thus obviating the need for further purification. In contrast, the bulky *tert*-butyl substituents of [P$_2$-ONO^{tBu}]H$_3$ facilitated the ligand dissolution in polar organic solvents, which had complicated its recrystallization. Therefore, the second [ONO]-ligand derivative was isolated in pure form by means of standard column chromatography techniques. As noted in Scheme 7.3, both proligands were obtained in relatively modest yields of 40%, which suggests that optimization of the coupling conditions will be necessary to eliminate scale-up problems.

The new pincer-type [ONO] proligands were characterized by solution NMR spectroscopy. The ^{1}H NMR spectra of [P$_2$-ONO]H$_3$ and [P$_2$-ONO^{tBu}]H$_3$ in CDCl$_3$ confirmed the symmetrical features of respective bis(phenolato) rings. The key spectral differences between the proton signals of [P$_2$-ONO^{tBu}]H$_3$ and those of [P$_2$-ONO]H$_3$ are associated with the 3-position of the aromatic rings containing *tert*-butyl substituents in the former case and aromatic protons in the latter. Therefore, the [P$_2$-ONO^{tBu}]H$_3$ proligand displayed one fewer proton signal in the aromatic ppm range and one extra singlet resonance at 1.41 ppm (integration of 18H). In regards to the [P$_2$-ONO]H$_3$ counterpart, the extra proton resonance ascribed to the 3-position of the aromatic rings was found at 7.23 ppm (integration of 2H). For both ligands, the proton resonances associated with the O–CH$_2$CH$_3$ tethers of the phosphonate group were observed within the usual spectral range with minimal chemical-shift differences between the two ligand derivatives. Likewise, the ^{31}P NMR spectra of [P$_2$-ONO]H$_3$ and [P$_2$-ONO^{tBu}]H$_3$ gave virtually identical signals centered at 22.5 and 22.0 ppm, respectively, further confirming the virtually indistinguishable electronic characteristics of

the phosphonate moieties. Finally, the ^{13}C NMR characterization of the individual ligands revealed very similar spectra with main spectral differences assignable to the presence of the *tert*-butyl groups for [P$_2$-ONO$^{t\text{Bu}}$]H$_3$ and lack thereof for [P$_2$-ONO]H$_3$.

7.3 Summary and Outlook

Two new redox-active proligands of the amido-bis(phenolate) motif were prepared incorporating a diethoxyphosphoryl substituent within each aromatic ring of the ligand backbone. While both proligands, [P$_2$-ONO]H$_3$ and [P$_2$-ONO$^{t\text{Bu}}$]H$_3$, contain their ethyl-protected phosphonate groups attached directly to the 5-position of the *o*-aminophenolate rings, the second ligand derivative additionally contains *tert*-butyl substituents at the 3-position of the aromatic rings. Both ligand derivatives were synthesized by an adapted copper(I)-catalyzed *N*-arylation of *o*-aminophenols with *o*-iodophenols. The respective phenolic coupling partners were obtained through a sequence of aromatic substitution reactions and functional group interconversions, with the phosphonate anchoring group installed early in the synthesis under Michaelis-Arbuzov conditions. Though only moderately scalable, both syntheses were achieved in a straightforward fashion with minimum purification requirements.

In this work, [P$_2$-ONO]H$_3$ and [P$_2$-ONO$^{t\text{Bu}}$]H$_3$ were contrived for probing their multi-electron reactivity patterns on solid electrode interfaces. Relative to the prototypic [ONO] ligand, *N,N*-bis(3,5-di-*tert*-butyl-2-phenoxide)amide, the introduction of two diethoxyphosphoryl groups directly on the *N*-tethered aromatic rings of the ligands, rather than through a carbon spacer, will be expected to significantly perturb the electron valence states available to [P$_2$-ONO]$^{3-}$ and [P$_2$-ONO$^{t\text{Bu}}$]$^{3-}$. The strong impact of phosphonate anchors on the redox properties of oxidable catecholate ligands was previously confirmed by us in a

161

related study.[11] Therefore, it will be necessary to establish the electronic properties of [P$_2$-ONO]$^{3-}$ and [P$_2$-ONO^{tBu}]$^{3-}$, which can be accomplished by systematically studying transition metal coordination complexes of the new ligands that would be designed based on known [ONO] systems. Based on the observed solubility properties of [P$_2$-ONO^{tBu}]H$_3$ and [P$_2$-ONO]H$_3$, the former ligand derivative with its bulky *tert*-butyl substituents may enable for studies of metal complexes in organic solvents while the latter in aqueous media.

In due course, the surface-tethering capability of the [P$_2$-ONO]H$_3$ and [P$_2$-ONO^{tBu}]H$_3$ proligands may be unmasked by cleaving off the ester tethers of the phosphonate groups. Compatible deprotection strategies will be implemented either by converting the ligand phosphonate ester groups to phosphonic acids or through post-synthetic deprotection of the same groups in the individual [ONO] complexes. The resulting [ONO] complexes with the phosphonic acids should be amenable toward attachment on metal oxide nanoparticles. Such [ONO]-based probes may thus become attractive candidates for heterogeneous catalysis applications on the surface of electrodes where the interfacial chemistry of the catalyst to be immobilized has already been tackled. Considering the exciting multi-electron reactivity patterns of the amido-bis(phenolate) motif, the ligand derivatives described here have the potential to transcend the way in which this type of redox chemistry is currently being leveraged.

7.4 Experimental

General Considerations. All manipulations involving the synthesis of ligands were performed under air, unless otherwise noted, employing reagents and solvents purchased from commercial suppliers and used as received. Column chromatography was performed with 230-400 mesh silica gel using flash column techniques. The ligand precursors diethyl

(4-hydroxyphenyl)phosphonate (**35**)[12] and 4-bromo-2-(*tert*-butyl)phenol (**40**)[7] were prepared by the methods reported.

Physical Methods. NMR spectra were collected on the Bruker Avance 400 and 500 MHz spectrometers. Chemical shifts were reported using the standard δ notation in parts per million and referenced using residual ^{1}H and ^{13}C isotopic impurities of the solvent. Infrared spectra were recorded as neat solids or oils using a Jasco FT/IR-4700-ATR-PRO ONE spectrophotometer.

Synthesis of diethyl (4-hydroxy-3-nitrophenyl)phosphonate (36): To a solution of **35** (3.11 g, 13.5 mmol) in acetic acid (4.5 mL) was added nitric acid (1.00 mL) in 2.7 mL of acetic acid at 40 °C. The reaction was heated at the same temperature for 2 h, after which point the solvent was removed by rotary evaporation. The crude oil was re-dissolved in EtOAc (200 mL) and extracted with water (200 mL). The organic phase was dried over anhydrous Na_2SO_4 and concentrated *in vacuo* to give **36** as a yellow flaky solid (3.26 g, 88%). ^{31}P NMR (162 MHz, $CDCl_3$) δ 16.6; ^{1}H NMR (500 MHz, $CDCl_3$) δ 10.85 (s, 1H), 8.60 (d, *J* = 14.0 Hz, 1H), 7.97 (appar t, *J* = 9.4 Hz, 1H), 7.25 (m, 1H), 4.21-4.10 (m, 4H), 1.35 (t, *J* = 6.9 Hz, 6H); ^{13}C NMR (125 MHz, $CDCl_3$) δ 157.7 (d, *J* = 2.6 Hz, qC–O), 139.8 (d, *J* = 10.3 Hz, aryl-C), 133.5 (d, *J* = 19.5 Hz, qC–NO_2), 129.8 (d, *J* = 13.1 Hz, aryl-C), 121.9 (d, *J* = 198.5 Hz, qC–P), 120.8 (d, *J* = 14.9 Hz, aryl-C), 62.7 (d, *J* = 5.4 Hz, CH_2–O), 16.5 (d, *J* = 6.2 Hz, CH_3); FTIR (neat) v/cm^{-1} 2990, 2903, 2643, 2588, 1581, 1531, 1420, 1352, 1214 st, 1160 st, 1005 st, 837; HRMS (ESI) *m* / *z* calcd for $C_{10}H_{14}NO_6P$ (M + Na)$^+$ 298.0457, found 298.0450.

Synthesis of diethyl (3-amino-4-hydroxyphenyl)phosphonate (37): A solution of **36** (3.00 g, 10.9 mmol) and palladium on carbon (10% by weight, 300 mg) in MeOH (30 mL) was equipped with a balloon of H_2, evacuated, and refilled with H_2 (X 3). The reaction

163

mixture was stirred at room temperature, under a balloon of H_2 for a period of 18 h. The

catalyst was filtered off under N_2 and the solvent was removed under reduced pressure to

give **37** as a dark brown paste (2.37 g, 89%). ^{31}P NMR (162 MHz, CDCl$_3$) δ 22.5; ^{1}H NMR

(500 MHz, CDCl$_3$) δ 7.12 (dd, J = 13.6, 1.5 Hz, 1H), 7.10 (d, J = 13.6 Hz, 1H), 6.94 (dd, J = 7.7,

4.5 Hz, 1H), 4.28-3.98 (m, 4H), 1.30 (t, J = 7.1 Hz, 6H); ^{13}C NMR (125 MHz, CDCl$_3$) δ 149.6 (d,

J = 3.2 Hz, qC–O), 135.4 (d, J = 18.7 Hz, qC–N), 123.9 (d, J = 10.8 Hz, aryl-C), 118.3 (d, J = 12.5

Hz, aryl-C), 117.4 (d, J = 194.6 Hz, qC–P), 115.0 (d, J = 18.2 Hz, aryl-C), 62.3 (d, J = 5.2 Hz,

CH$_2$–O), 16.4 (d, J = 6.7 Hz, CH$_3$); FTIR (neat) v/cm^{-1} 3360-3089 br, 2983, 2760, 2655, 1586,

1515, 1391, 1289 st, 1195 st, 1014 st, 957 st, 792 st, 757 st; HRMS (ESI) m / z calcd for

C$_{10}$H$_{16}$NO$_4$P (M + Na)$^+$ 268.0715, found 268.0724.

Synthesis of diethyl (4-hydroxy-3-iodophenyl)phosphonate (38): To a stirred

solution of **37** (982 mg, 4.00 mmol) in acetone (8 mL) was added conc. HCl (0.85 mL, 10

mmol) at –10 °C. Then a solution of NaNO$_2$ (276 mg, 4.00 mmol) in H$_2$O (1.0 mL) was added

dropwise to the reaction mixture and stirred for 0.5 h at 0 °C. To the diazonium solution

was then added a solution of NaI (1.2 g, 8.0 mmol) in H$_2$O (1.4 mL) and the reaction mixture

was stirred at 0 °C-rt for 12 h. The reaction mixture was diluted with EtOAc (100 mL) and

extracted with H$_2$O (100 mL), a solution of NaHSO$_3$ (6 g) in H$_2$O (100 mL), and H$_2$O (100

mL). Drying of the organic phase with anhydrous Na$_2$SO$_4$ followed by filtration and

evaporation of the solvent under reduced pressure afforded compound **38** as a dark red

paste (1.26 g, 88%). ^{31}P NMR (162 MHz, CDCl$_3$) δ 18.7; ^{1}H NMR (500 MHz, CDCl$_3$) δ 8.09 (dd,

J = 13.2, 1.7 Hz, 1H), 7.63 (ddd, J = 12.6, 8.3, 1.7 Hz, 1H), 7.07 (dd, J = 8.3, 4.1 Hz, 1H),

4.18-4.02 (m, 4), 1.33 (t, J = 7.0 Hz, 6H); ^{13}C NMR (125 MHz, CDCl$_3$) δ 160.6 (d, J = 2.5 Hz, qC–

O), 142.7 (d, J = 11.8 Hz, aryl-C), 133.8 (d, J = 11.2 Hz, aryl-C), 120.2 (d, J = 196.3 Hz, qC–P),

115.3 (d, J = 16.7 Hz, aryl-C), 85.3 (d, J = 19.8 Hz, qC–I), 62.7 (d, J = 5.3 Hz, CH_2–O), 16.4 (d, J = 6.4 Hz, CH_3); FTIR (neat) v/cm^{-1} 3054, 2983, 2901, 2719, 2613, 1587, 1388, 1296, 1182 st, 1126 st, 1013 st, 955 st, 797 st, 768 st; HRMS (ESI) m / z calcd for $C_{10}H_{14}IO_4P$ (M + Na)$^+$ 378.9572, found 378.9579.

Synthesis of azanediylbis(5-(diethoxyphosphoryl)2-phenol) ([P$_2$-ONO]H$_3$): A flame-dried straus tube containing a magnetic stirring bar was charged with 2-aminophenol **37** (1.64 g, 6.68 mmol), 2-iodophenol **38** (1.19 g, 3.34 mmol), CuI (127 mg, 0.668 mmol), and K_3PO_4 (1.45 g, 6.68 mmol). The tube was evacuated and refilled with N_2 (X 3), which was followed by the addition of degassed DMF (5 mL). The tube was sealed and the mixture was heated at 80 °C for 16 h. The resulting mixture was cooled to rt, diluted with H_2O (250 mL) and acidified with conc. HCl to adjust the pH to 6. The aqueous fraction was extracted with ethyl acetate (3 X 200 mL), dried with Na_2SO_4, and the solvent volume was reduced down to 10 mL. The pure compound was obtained by recrystallization from the saturated EtOAc solution while sitting undisturbed at –35 °C for 1 day. After filtration and repeated washings with cold ethyl acetate, proligand **[P$_2$-ONO]H$_3$** was obtained as a salmon-pink solid (600 mg, 40%). ^{31}P NMR (162 MHz, CDCl$_3$) δ 22.5; ^{1}H NMR (500 MHz, CDCl$_3$) δ 7.52 (dd, J = 14.1, 1.5 Hz, 2H), 7.23 (ddd, J = 13.3, 8.1, 1.5 Hz, 2H), 6.97 (dd, J = 8.1, 4.5 Hz, 2H), 4.10-4.01 (m, 8H), 1.31 (t, J = 7.1 Hz, 12 H); ^{13}C NMR (125 MHz, CDCl$_3$) δ 152.7 (d, J = 3.5 Hz, qC–O), 132.9 (d, J = 19.0 Hz, qC–N), 126.5 (d, J = 20.7 Hz, aryl-C), 119.4 (d, J = 12.8 Hz, aryl-C), 118.9 (d, J = 195.5 Hz, qC–P), 115.9 (d, J = 18.2 Hz, aryl-C), 63.5 (d, J = 5.5 Hz, CH_2–O), 16.7 (d, J = 6.3 Hz, CH_3); FTIR (neat) v/cm^{-1} 2988, 2232 br, 1588, 1509, 1408, 1280, 1202 st, 1106, 1009 st, 957 st, 794 st, 766 st; HRMS (ESI) m / z calcd for $C_{20}H_{29}NO_8P_2$ (M + Na)$^+$ 496.1266, found 496.1264.

Synthesis of diethyl (3-(*tert*-butyl)-4-hydroxyphenyl)phosphonate (41): A mixture of **40** (6.14 g, 27.0 mmol), nickel(II) bromide (6.44 g, 29.5 mmol) in mesitylene (30 mL) was heated at 160–180 °C under an atmosphere of nitrogen for 10 min. Degassed triethylphosphite (6.89 mL, 40.2 mmol) was added via cannula. The mixture was heated at the same temperature under an atmosphere of nitrogen for the next 12 h. After cooling to room temperature, the mixture was filtered through Celite, diluted with diethyl ether (250 mL), and extracted with a 10% solution of sodium hydroxide (2 X 250 mL). The aqueous phase was washed twice with diethyl ether (200 mL), acidified by concentrated hydrochloric acid and extracted with diethyl ether (3 X 200 mL). The organic phase was dried with anhydrous Na_2SO_4 and filtered. Removal of solvent under reduced pressure yielded **41** as a white solid (5.32 g, 69%). ^{31}P NMR (162 MHz, $CDCl_3$) δ 23.1; ^1H NMR (500 MHz, $CDCl_3$) δ 7.72 (dd, J = 14.0, 1H), 7.58 (dd, J = 12.8, 8.1 Hz, 1H), 7.04 (dd, J = 8.1, 4.3 Hz, 1H), 4.24-4.13 (m, 4H), 1.48 (s, 9H), 1.42 (t, J = 7.0 Hz, 6H); ^{13}C NMR (125 MHz, $CDCl_3$) δ 160.5 (d, J = 3.5 Hz, qC–O), 137.1 (d, J = 14.7 Hz, qC-^{t}Bu), 131.9, (d, J = 11.6 Hz, aryl-C), 130.9 (d, J = 12.6 Hz, aryl-C), 117.4 (d, J = 196.2 Hz, qC–P), 117.0 (d, J = 17.1 Hz, aryl-C), 62.5 (d, J = 5.3 Hz, CH_2–O), 35.1 (s, $C(CH_3)_3$), 29.6 (s, $(CH_3)_3$), 16.7 (d, J = 6.6 Hz, CH_3); FTIR (neat) v/cm$^-$^{1} 3101, 2948, 2903, 2873, 1592, 1495, 1399, 1278, 1132 st, 1196 st, 1020 st, 959 st, 795 st, 549; HRMS (ESI) m / z calcd for $C_{14}H_{23}NO_4P$ (M + Na)$^+$ 309.1232, found 309.1222.

Synthesis of diethyl (3-(*tert*-butyl)-4-hydroxy-5-nitrophenyl)phosphonate (42): To a solution of **41** (8.76 g, 31.0 mmol) in acetic acid (14 mL) was added nitric acid (2.30 mL) in 6.0 mL of acetic acid at 40 °C. The reaction was heated at the same temperature for 2 h, after which point the solvent was removed by rotary evaporation. The crude oil was re-dissolved in EtOAc (300 mL) and extracted with water (300 mL) followed

by brine (300 mL). The organic phase was dried over anhydrous Na_2SO_4, filtered, and concentrated *in vacuo* to give **42** as a yellow oil (9.67 g, 94%). ^{31}P NMR (162 MHz, CDCl$_3$) δ 17.8; ^1H NMR (500 MHz, CDCl$_3$) δ 11.82 (s, 1H), 8.47 (dd, *J* = 14.8, 1.8 Hz, 1H), 7.95 (dd, *J* = 12.9, 1.8 Hz, 1H), 4.20-4.09 (m, 4H), 1.45 (s, 9H), 1.35 (t, *J* = 7.1 Hz, 6H); ^{13}C NMR (125 MHz, CDCl$_3$) δ 157.9 (d, *J* = 3.0 Hz, qC–O), 142.0 (d, *J* = 13.5 Hz, qC–NO$_2$), 137.0 (d, *J* = 11.6 Hz, aryl-C), 134.3 (d, *J* = 20.1 Hz, qC-^{t}Bu), 128.0 (d, *J* = 12.7 Hz, aryl-C), 120.6 (d, *J* = 198.6 Hz, qC–P), 62.7 (d, *J* = 5.4 Hz, CH$_2$–O), 16.5 (d, *J* = 6.2 Hz, CH$_3$); FTIR (neat) v/cm^{-1} 2962, 2902, 2873, 1607, 1543, 1388, 1354, 1254 st, 1024 st, 964 st, 794; HRMS (ESI) *m / z* calcd for C$_{14}$H$_{14}$NO$_4$P (M + Na)$^+$ 354.1082, found 354.1088.

Synthesis of diethyl (3-amino-5-(*tert*-butyl)-4-hydroxyphenyl)phosphonate (43): A solution of **42** (5.60 g, 19.6 mmol) and palladium on carbon (9% by weight 500 mg) in MeOH (100 mL) was equipped with a balloon of H$_2$, evacuated, and refilled with H$_2$ (X 3). The reaction mixture was stirred under a balloon of H$_2$ for a period of 18 h. The catalyst was filtered off under N$_2$ and the solvent was removed under reduced pressure to give **43** as a brown paste (4.57 g, 89%). ^{31}P NMR (162 MHz, CDCl$_3$) δ 22.4; ^1H NMR (500 MHz, CDCl$_3$) δ 7.99 (d, *J* = 13.1, 1H), 7.65 (d, *J* = 13.4 Hz, 1H), 4.17-4.03 (m, 4H), 1.39 (s, 9H), 1.33 (t, *J* = 7.0 Hz, 6H); ^{13}C NMR (125 MHz, CDCl$_3$) δ 151.1 (qC–O), 137.0 (d, *J* = 17.1 Hz, qC–N), 133.3 (qC-^{t}Bu), 124.4 (aryl-C), 122.4 (aryl-C), 118.5 (d, *J* = 194.6 Hz, qC–P), 62.4 (d, *J* = 5.3 Hz, CH$_2$–O), 35.0 (C(CH$_3$)$_3$), 29.8 ((CH$_3$)$_3$), 16.7 (d, *J* = 6.6 Hz, CH$_3$); FTIR (neat) v/cm^{-1} 3434, 3364, 3260, 3099 br, 2950, 2908, 1648, 1578, 1416 st, 1143 st, 1176 st, 977 st, 795 st; HRMS (ESI) *m / z* calcd for C$_{14}$H$_{24}$NO$_4$P (M + Na)$^+$ 324.1341, found 324.1330.

Synthesis of diethyl (3-(*tert*-butyl)-4-hydroxy-5-iodophenyl)phosphonate (44): A stirred solution of **43** (1.50 g, 4.97 mmol) in concentrated H$_2$SO$_4$ (8 mL) was cooled

to 0°C. Then, a solution of $NaNO_2$ (990 mg, 14 mmol) in H_2O (2.4 mL) was added dropwise

to the reaction mixture and stirred for 0.5 h at 0 °C. To the diazonium solution was then

added a solution of NaI (5.61 g, 33.8 mmol) in H_2O (20 mL) and the mixture was subjected

to sonication at 60 °C for 0.5 h, followed by heating at the same temperature for 1 h. The

reaction mixture was diluted with EtOAc (250 mL) and extracted with H_2O (200 mL), a

solution of $NaHSO_3$ (12 g) in H_2O (200 mL), and H_2O (200 mL). Drying of the organic phase

over anhydrous Na_2SO_4 followed by filtration and evaporation of the solvent under reduced

pressure afforded compound **44** as a dark burgundy oil (2.04 g 99%). ^{31}P NMR (162 MHz,

$CDCl_3$) δ 18.9; ^1H NMR (500 MHz, $CDCl_3$) δ 7.98 (dd, J = 13.5, 1.6 Hz, 1H), 7.62 (dd, J = 13.5,

1.6 Hz, 1H), 4.16-4.02 (m, 4), 1.38 (s, 9H), 1.33 (t, J = 7.1 Hz, 6H); ^{13}C NMR (125 MHz, $CDCl_3$)

δ 156.7 (d, J = 3.3 Hz, qC–O), 140.3 (d, J = 11.8 Hz, aryl-C), 137.8 (d, J = 14.8 Hz, qC-^tBu),

131.5 (d, J = 11.6 Hz, aryl-C), 121.7 (d, J = 194.7 Hz, qC–P), 90.1 (d, J = 21.3 Hz, qC–I), 63.1

(d, J = 5.6 Hz, CH_2–O), 36.0 ($C(CH_3)_3$), 29.5 ($(CH_3)_3$) 16.8 (d, J = 6.6 Hz, CH_3); FTIR (neat) $v/$

cm^{-1} 3440, 2967, 2919, 2767, 1717, 1430, 1260 st, 1141, 1001 st, 795 st, 556; HRMS (ESI)

m / z calcd for $C_{14}H_{22}IO_4P$ (M + Na)$^+$ 435.0198, found 435.0188.

Synthesis of azanediylbis(5-(diethoxyphosphoryl)3-*tert*-butyl-2-phenol) ([P₂-ONO^{tBu}]H₃): A flame-dried straus tube containing a magnetic stirring bar was charged with

2-aminophenol **43** (2.34 g, 7.80 mmol), 2-iodophenol **44** (1.65 mg, 4.00 mmol)**,** CuI (150

mg, 0.78 mmol), and K_3PO_4 (1.70 mg, 8.00 mmol). The tube was evacuated and refilled with

N_2 (X 3), which was followed by the addition of degassed DMF (10 mL). The tube was

sealed and the mixture was heated at 80 °C for 16 h. The resulting mixture was cooled to rt,

diluted with H_2O (200 mL), and acidified with conc. HCl to adjust the pH to 6. The aqueous

fraction was extracted with ethyl acetate (3 X 250 mL), dried with anhydrous Na_2SO_4, and

concentrated down under reduced pressure. The crude compound was purified by column

chromatography on silica gel (diethyl ether: methanol/98:2) using a gradient elution to give

[P₂-ONO^{tBu}]H₃ as an orange solid (936 mg, 40%). ^{31}P NMR (162 MHz, CDCl$_3$) δ 22.0; ^{1}H NMR

(500 MHz, CDCl$_3$) δ 7.41 (d, J = 14.4, 2H), 7.00 (d, J = 13.9, 2H), 4.09-3.97 (m, 8H), 1.41 (s,

18H), 1.31 (t, J = 7.0 Hz, 12 H); ^{13}C NMR (125 MHz, CDCl$_3$) δ 152.3 (d, J = 3.7 Hz, qC–O),

138.1 (d, J = 15.9 Hz, qC–N), 132.9 (d, J = 20.1 Hz, qC-^{t}Bu), 125.9 (d, J = 11.6 Hz, aryl-C),

122.4 (d, J = 11.6 Hz, aryl-C), 119.1 (d, J = 194.6 Hz, qC–P), 62.6 (d, J = 5.5 Hz, CH$_2$–O), 35.3

(C(CH$_3$)$_3$), 29.8 ((CH$_3$)$_3$), 16.6 (d, J = 6.5 Hz, CH$_3$); FTIR (neat) ν/cm^{-1} 3359-2961 br, 2903,

1585, 1424, 1162 st, 1204 st, 960 st, 777, 516; HRMS (ESI) m / z calcd for C$_{28}$H$_{45}$NO$_8$P$_2$ (M +

Na)$^+$ 608.2518, found 608.2512.

7.5 References

[1] O'Reilly, M. E.; Veige, A. S. *Chem. Soc. Rev.* **2014**, *43*, 6325–6369.

[2] Zarkesh, R. A.; Heyduk, A. F. *Organometallics*, **2011**, *30*, 4890–4898.

[3] Zarkesh, R. A.; Ziller, J. W.; Heyduk, A. F. *Angew. Chem., Int. Ed.*, **2008**, *47*, 4715–4718.

[4] Zarkesh, R. A.; Heyduk, A. F. *Organometallics* **2009**, *28*, 6629–6631.

[5] Lu, F.; Zarkesh, R. A.; Heyduk, A. F. *Eur. J. Inorg. Chem.* **2011**, *2012*, 467–470.

[6] Chaudhuri, P.; Hess, M.; Weyhermüller, T.; Wieghardt, K. *Angew. Chem. Int. Ed.* **1999**, *38*, 1095–1098.

[7] Wong, J. L.; Sánchez, R. H.; Logan, J. G.; Zarkesh, R. A.; Ziller, J. W.; Heyduk, A. F. *Chem. Sci.* **2013**, *4*, 1906–1910.

[8] (a) Forget, A.; Limoges, B.; Balland, V. *Langmuir* **2015**, *31*, 1931–1940. (b) Kaliginedi, V.; Ozawa, H.; Kuzume, A.; Maharajan, S.; Pobelov, I. V.; Kwon, H. N.; Mohos, M; Broekmann, P.; Fromm, K. M.; Haga, M; Wandlowski, T.; *Nanoscale* **2015**, *7*, 17685–17692. (c) Sathrum, A. J.; Kubiak, C. P. *J. Phys. Chem. Lett.* **2011**, *2*, 2372–2379. (d) Farran, R.; Jouvenot, D.; Loiseau, F.; Chauvin, J.; Deronzier, A. *Dalton Trans.* **2014**, *43*, 12156–12159. (e) Terada, K.; Kobayashi, K.; Haga, M.-A. *Dalton Trans.* **2008**, 4846–4854. (f) Kanan, M. W.; Nocera, D. G. *Science* **2008**, *321*, 1072–1075. (g) Armistead, P. M.; Thorp, H. H. *Anal. Chem.* **2001**, *73*, 558–564. (h) Kato, M.; Cardona, T.; Rutherford, A. W.; Reisner, E. *J. Am. Chem. Soc.* **2012**, *134*, 8332–8335.

[9] Li, Y.; Wang, H.; Jiang, L.; Sun, F.; Fu, X.; Duan, C. *Eur. J. Org. Chem.* **2010**, 6967–6973.

[10] Williams, A. B.; Weiser, P. T.; Hanson, R. N.; Gunther, J. R.; Katzenellenbogen, J. A. *Org. Lett.* **2009**, *11*, 5370–5373.

[11] Seraya, E.; Luan, Z.; Law, M.; Heyduk, A.F. *Inorg. Chem.* **2015**, *54*, 7571–7578.

[12] Lejeune, N.; Dez, I.; Jaffrès, P-A.; Lohier, J-F.; Madec, P-J.; Oliveira Santos, J. S.; *Eur. J. Inorg. Chem.* **2008**, 138–143.

Synthesis of Phosphonylated *β*-Ketoamine Ligand

Installation of a phosphonate diester group was achieved for the *β*-ketoaminato ligand defined as (acNac^{Phos})H (**49**). The synthetic strategy for (acNac^{Phos})H was comprised of first introducing the phosphonate substituent on 4-iodobenene derivative under Michaelis Arbuzov conditions and then coupling the functionalized arene with 2,4-pentanedione (acac) under copper catalysis.[1] As outlined in Scheme A.1, reduction of 4-iodobenzoic acid with borane reagent yielded (4-iodophenyl)methanol (**45**) that was subsequently treated with phosphorous tribromide to afford 1-(bromomethyl)-4-iodobenzene (**46**). The Michaelis Arbuzov reaction involved refluxing substrate **46** in neat triethyl phosphite, which gave diethyl 4-iodobenzylphosphonate (**47**). The copper(I)-catalyzed Ullman condensation of iodobenzene **47** was employed with 2,4-pentanedione to give (acac^{Phos})H (**48**). Finally, compound **48** was converted to (acNac^{Phos})H (**49**) by an acid-catalyzed Schiff-base condensation of **48** with excess 3,5-dimethylaniline.

Scheme A.1. Synthesis of (acNac^{Phos})H proligand (**49**).
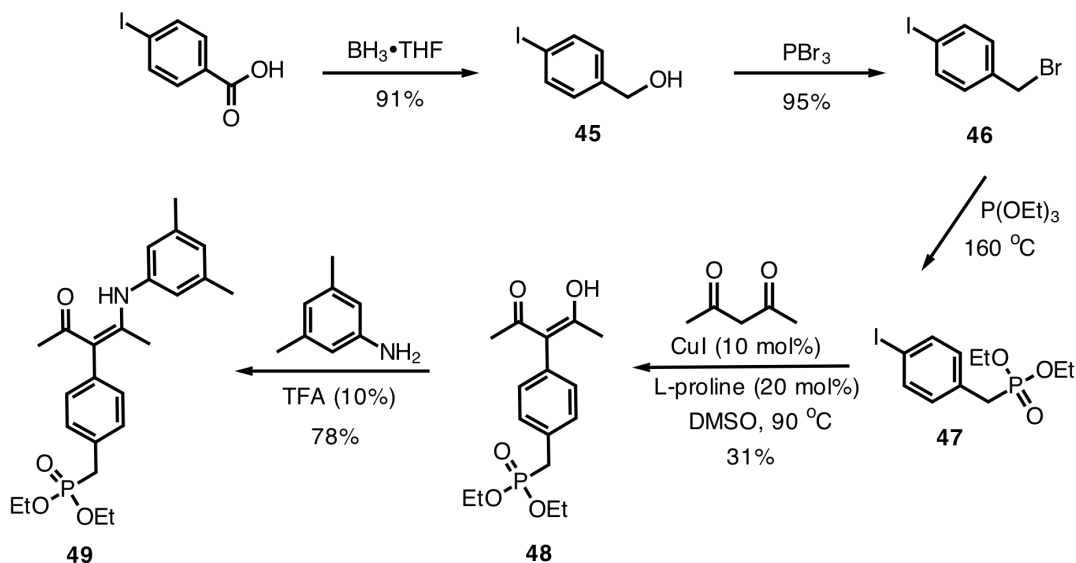
Experimental

(4-iodophenyl)methanol (45): To 4-iodobenzoic acid (2.3 g, 9.4 mmol) diluted in 20 mL THF was slowly added BH_3 (20 mL, 1.0 M in THF) and the reaction mixture was stirred overnight at room temperature. The reaction was quenched with HCl (100 mL, 2 M) followed by extraction with CH_2Cl_2 (70 mL X 3). The combined organic layers were washed with saturated $NaHCO_3$ (150 mL) and brine (150 mL), dried over anhydrous Na_2SO_4, and concentrated to dryness to yield **45** as a white solid (1.70 g, 91%). The ^{1}H NMR spectrum of **45** was in agreement with the literature data.[2] ^{1}H NMR (500 MHz, $CDCl_3$) δ 7.68 (d, 2H, *J* = 8.0 Hz), 7.11 (d, 2H, *J* = 8.0 Hz), 4.65 (s, 2H), 2.04 (br, 1H).

1-(bromomethyl)-4-iodobenzene (46): To a solution of **45** (2.45 g, 10.5 mmol) and pyridine (0.894 mL, 11.0 mmol) in anhydrous Et_2O (50 mL) was added dropwise a solution of PBr_3 (1.033 mL, 11 mmol). The reaction mixture was stirred overnight at room temperature and was then quenched with ice-cold water (50 mL). The organic layer was separated, washed with HCl (1 M, 50 mL), and dried over anhydrous Na_2SO_4. Evaporation *in vacuo* afforded benzyl bromide **46** as a white solid (2.96 g, 95%), with its ^{1}H NMR spectrum matching the literature data.[2] ^{1}H NMR (500 MHz, $CDCl_3$) δ 7.68 (d, *J* = 8.1, 2 H), 7.14 (d, *J* = 8.1, 2 H), 4.42 (s, 2 H).

Diethyl 4-iodobenzylphosphonate (47): A solution of **46** (3.79 g, 12.2 mmol) in neat triethyl phosphite (1.75 mL, 10.2 mmol) was refluxed for 12 h. Upon completion of the reaction, the obtained material was purified by silica gel column chromatography (ethyl acetate:hexanes/40:60) to afford **47** as a yellow oil (2.47 g, 58%). The ^{1}H NMR spectrum

of **47** matched the literature data.[3] ^{1}H NMR (CDCl$_3$, 500 MHz) δ 7.64 (d, J = 8.0 Hz, 2H), 7.05 (d, J = 7.0 Hz, 2H), 4.05-4.01 (m, 4H), 3.09 (d, J = 21.5 Hz, 2H), 1.25 (t, J = 7.0 Hz, 6H).

Diethyl 4-(2,4-dioxopentan-3-yl)benzylphosphonate ((acac^{Phos})H, 48): A mixture of **47** (2.1 g, 5.9 mmol), acetylacetone (1.52 mL, 14.8 mmol), K$_2$CO$_3$ (3.3 g, 23 mmol), CuI (113 mg, 0.593 mmol), and L-proline (137 mg, 1.19 mmol) in 40 mL of DMSO was heated at 90 °C under nitrogen atmosphere for 12 h. The reaction was cooled, poured into HCl (100 mL, 1M), and extracted with ethyl acetate (100 mL X 3). The combined organic layers were washed with brine (200 mL), dried over anhydrous Na$_2$SO$_4$, and concentrated *in vacuo*. The obtained residue was purified by column chromatography on silica-gel (ethyl acetate:hexanes/60:40) to give **48** as a yellow oil (590 mg, 31%). ^{31}P NMR (162 MHz, CDCl$_3$) δ 151.9; ^{1}H NMR (500 MHz, CDCl$_3$) δ 7.34 (d, J = 7.8 Hz, 2H), 7.12 (d, J = 7.8 Hz, 2H), 4.06-3.99 (m, 4H), 3.20 (d, J = 21.7 Hz, 2H), 1.87 (s, 6H), 1.23 (appar t, J = 7.0 Hz, 6H); ^{13}C NMR (126 MHz, CDCl$_3$) δ 191.2 (C=O), 135.8 (d, J = 3.8 Hz, aryl-qC), 131.6 (d, J = 3.0 Hz, aryl-C), 131.3 (d, J = 9.1 Hz, aryl-qC), 130.7 (d, J = 6.6 Hz, aryl-C), 115.0 (α-C), 62.6 (d, J = 6. 8 Hz, CH$_2$-O), 34.3 (d, J = 138.4 Hz, CH$_2$–P), 24.4 (xylyl-CH$_3$), 16.7 (acyl-C), 16.6 (CH$_3$); FTIR (neat) v/cm^{-1} 1240 st (P=O).

Diethyl 4-(2-(3,5-dimethylphenylamino)-4-oxopentenyl) benzyl phosphonate ((acNac^{Phos})H, 49): A solution of **48** (448 mg, 1.37 mmol) and 3,5-dimethylaniline (0.514 mL, 4.12 mmol) was refluxed in ethanol (30 mL) for 12 h, in the presence of several drops of trifluoroacetic acid. The reaction mixture was cooled to room temperature and the solvent was removed under reduced pressure. The crude material was purified by column chromatography on silica-gel (ethyl acetate:hexanes/40:60) to give **49** as a yellow solid

(360 mg, 61%). ^{31}P NMR (162 MHz, CDCl$_3$) δ 151.9; ^{1}H NMR (500 MHz, CDCl$_3$) δ 7.31 (d, J = 7.9 Hz, 2H), 7.17 (d, J = 7.9 Hz, 2H), 6.84 (s, 1H), 6.76 (s, 2H), 4.04-3.96 (m, 4H), 3.20 (d, J = 21.6 Hz, 2H), 2.30 (s, 6H), 1.86 (s, 3H), 1.71 (s, 3H), 1.22 (appar t, J = 7.1 Hz, 6H); ^{13}C NMR (126 MHz, CDCl$_3$) δ 195.7 (C=O), 160.0 (C–N), 139.6 (d, J = 3.8 Hz, aryl-qC), 139.05 (xylyl-qC), 138.99 (xylyl-C–N), 132.5 (d, J = 3.1 Hz, aryl-C), 130.5 (d, J = 6 .6 Hz, aryl-C), 130.3 (d, J = 9.1 Hz, aryl-qC), 127.7 (xylyl-C), 123.4 (xylyl-C), 120.7 (α-qC), 62.5 (d, J = 6.8 Hz, CH$_2$-O), 34.3 (d, J = 138.2 Hz, CH$_2$–P), 29.5 (acyl-C), 21.5 (xylyl-CH$_3$), 18.7 (CH$_3$), 16.7 (d, J = 6.0 Hz, CH$_3$); FTIR (neat) v/cm^{-1} st (N–H), 1589 br (C=O, C=C), 1256 st (P=O).

References

[1] Cherkasov, V. K.; Druzhkov, N.O.; Kocherova, T. O.; Shavyrin, A. S.; Fukin, G. K. *Tetrahedron* **2012**, *68*, 1422–1426.

[2] Cheung, S.; Chow, H.; Ngai, T.; Wei, X. *Chem. Eur. J.* **2002**, *15*, 2278–2288,

[3] Rout, L.; Regati, S.; Zhao, C. *Adv. Synth. Catal.* **2011**, *353*, 3340–3346.

Appendix B

## Synthesis of *N,N*-bis(*tert*-butyl)-*ortho*-dimethylbenzene-1,2-diamide Ligand

Redox-active ligands of the *ortho*-phenylenediamine family were previously studied by us in the context of Group 4 imido complexes.[1] In particular, terminal imido complexes of zirconium(IV) were sought as catalysts for C–H bond activation to form functionalized amines. The desired reactivity on a high-oxidation d^0 zirconium complex required access to multi-electron valence changes, which could be enabled through ligand-based redox chemistry of two identically coordinated *N,N*-bis(neo-pentyl)-*ortho*-phenylenediamide ligands. However, the flexible *N*-neo-pentyl protecting groups of the ligands lacked in steric regulation necessary to produce the terminal imido species for C–H bond activation. Alternatively, undesired μ-imido-bridged Zr^{IV} dimers were isolated. To circumvent the undesired ligand arrangements, the steric parameters of the *ortho*-phenylenediamide ligand were recently revised. The new ligand derivative, *N,N*-bis(*tert*-butyl)-*ortho*-dimethylbenzene-1,2-diamine, $(^{tBu}pda)H_2$ (**51**), contains bulky *tert*-butyl protecting groups on both of its nitrogen donor atoms and two methyl substituents added in the 4- and 5-positions of the aromatic ring (Scheme B.1). These structural changes will be expected to confer enhanced ligand rigidity on the Zr metal center, which may in turn facilitate the isolation of mononuclear terminal imido species.

Scheme B.1. Pd-catalyzed synthesis of $(^{tBu}pda)H_2$ (**51**).
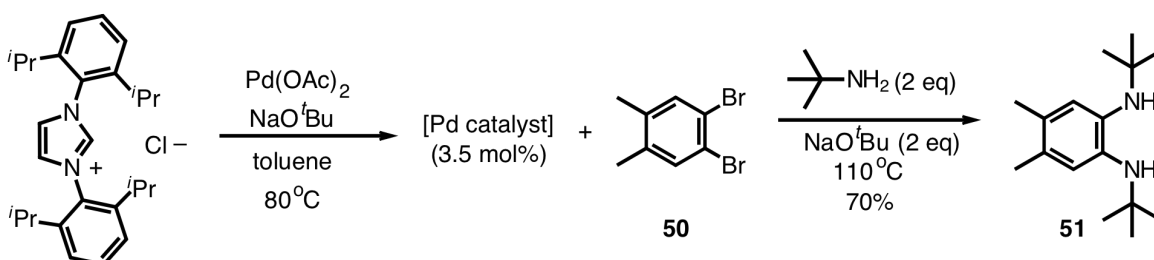
The new redox-active proligand $(^{tBu}pda)H_2$ (**51**) was prepared in a one-step reaction involving the Pd-catalyzed amination of arenes.[2] As shown in Scheme B.1, 4,5-dibromo-*o*-xylene (**50**) was cross-coupled with *tert*-butylamine under basic conditions. The active palladium catalyst was accessed *in situ* by reacting $Pd(OAc)_2$ and 1,3-bis(2,6-diisopropylphenyl)imidazolium chloride in the presence of NaO^tBu. The cross coupling reaction was then performed by heating the toluene mixture of Pd catalyst, aryl dibromide **50**, and *tert*-butylamine (1:2 stochiometry) in the presence of base at 110 °C. It was found that the crude reaction mixture was comprised of mostly $(^{tBu}pda)H_2$ though small quantities of the mono-coupled product were also present, which were separated by column chromatographic techniques. The ^1H NMR spectrum of $(^{tBu}pda)H_2$ in $CDCl_3$ showed symmetric ligand conformation in solution.

Scheme B.2. Metallation of $(^{tBu}pda)^{2-}$ to zirconium(IV).
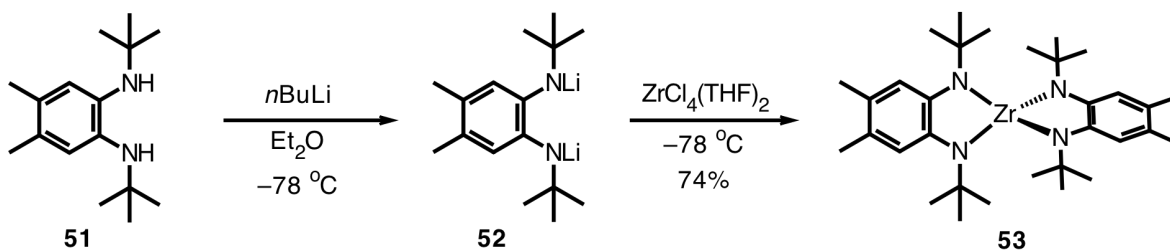
Metallation of dianionic $(^{tBu}pda)^{2-}$ ligand to zirconium(IV) was briefly explored using the method established by us with other *ortho*-phenylenediamine and *ortho*-aminophenol ligand derivatives.[3] The neutral proligand, $(^{tBu}pda)H_2$, was deprotonated with 2 equivalents of *n*BuLi to yield $(^{tBu}pda)Li_2$ (**52**), as shown in Scheme B.2. Treatment of *in-situ* generated lithium dianion (**52**) with 0.5 equivalents of $ZrCl_4(THF)_2$, in diethyl ether at –78 °C, produced four-coordinate zirconium(IV) complex **53**, $Zr(^{tBu}pda)_2$. Analysis of $Zr(^{tBu}pda)_2$ by ^1H NMR spectroscopy in C_6D_6 revealed chemically equivalent $(^{tBu}pda)^{2-}$ fragments with a

notable upfield shift of their aromatic proton resonance (δ 6.79 (s, 2H)), as compared to that of ($^{t\mathrm{Bu}}$pda)Li$_2$ (δ 7.24 (s, 2H)). The structural connectivity of putative complex **53** was derived from low-resolution diffraction data of the crystal grown from a saturated THF product solution (–35 °C). The preliminary structure shown in Figure B.1. confirmed tetrahedral geometry around zirconium.
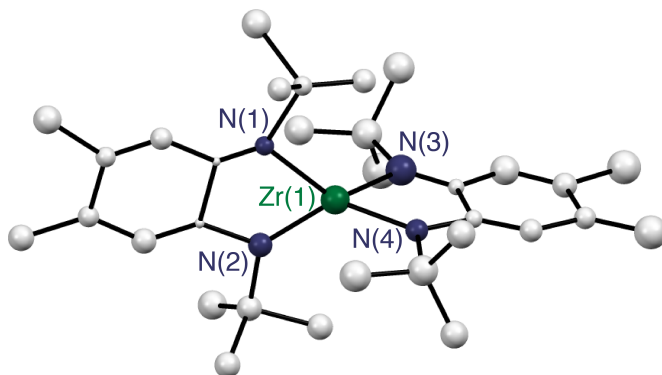

Figure B.1. Preliminary solid-state structure of Zr($^{t\mathrm{Bu}}$pda)$_2$ complex (**53**).

Experimental

General Considerations: All chemical manipulations were carried out under an inert atmosphere of nitrogen using standard Schlenk, vacuum-line, and glovebox techniques. The *ortho*-phenylenediamine proligand, ($^{t\mathrm{Bu}}$pda)H$_2$, was prepared by a procedure adapted from Bielawski and coworkers.[2] Synthesis of ZrCl$_4$(THF)$_2$ was accomplished by literature procedure.[4]

***N,N*-bis(*tert*-butyl)-*ortho*-dimethylbenzene-1,2-diamide (($^{t\mathrm{Bu}}$pda)H$_2$ 51):** A mixture of 1,3-bis(2,6-diisopropylphenyl)imidazolium chloride (85 mg, 0.20 mmol), NaO^{t}Bu (30 mg, 0.31 mmol), Pd(OAc)$_2$ (25 mg, 0.11 mmol), and toluene (5 mL) was stirred at 80 °C under nitrogen for 10 minutes. The catalyst solution was cannula transferred to a toluene mixture (100 mL) containing 4,5-dibromo-*o*-xylene (**50**) (1.50 g, 5.68 mmol), *tert*-butylamine (1.25 mL, 11.9 mmol), and NaO^{t}Bu (1.20 g, 12.5 mmol) and the resulting

mixture was stirred at 110 °C overnight, under nitrogen. After cooling to room temperature, the reaction mixture was filtered to remove residual NaBr salts. The solvent was then removed under reduced pressure and the crude product was purified by column chromatography (ethyl acetate:hexanes/4:96) to afford **51** as an off-white solid (1.0 g, 70% yield). ^{1}H NMR (500 MHz, CDCl$_3$) δ 6.71 (s, 2H), 2.16 (s, 6H), 1.26 (s, 18H); ^{13}C NMR (126 MHz, CDCl$_3$) δ 136.5 (qC–N), 128.4 (qC), 123.1 (aryl-C), 52.4 (C(^{t}Bu)$_3$), 30.3 (CH$_3$), 19.8 (^{t}Bu); FTIR (neat) 3297, 2970, 1510, 1359, 1216 st, 1200 st, 822; HRMS (ESI) m / z calcd for C$_{16}$H$_{28}$N$_2$ (M + H)$^+$ 249.2331, found 249.2325.

Zr($^{t\text{Bu}}$pda)$_2$ (53): To a suspension of ($^{t\text{Bu}}$pda)H$_2$ (**51**) (102 mg, 0.460 mmol) in diethyl ether (3 mL) was added nBuLi (358 μL, 2.58 M hexane solution) at –78 °C. The reaction mixture was allowed to warm to room temperature and was stirred overnight. The next day, the reaction mixture was cooled to –78 °C and ZrCl$_4$(THF)$_2$ (88 mg, 0.23 mmol) was added to putative ($^{t\text{Bu}}$pda)Li$_2$ intermediate (**52**). After stirring for 12 h at rt, the solvent was removed under vacuum to afford Zr($^{t\text{Bu}}$pda)$_2$ **53** as a golden brown solid (150 mg, 74%). ^{1}H NMR (500 MHz, C$_6$D$_6$) δ 6.78 (s, 2H), 2.15 (s, 6H), 1.20 (s, 18H).

References

[1] Ketter, N. A. Expanding the Chemistry of d^0 Transition Metals Through Redox-Active Ligands: Synthesis and Reactivity Studies of Group 4 Metals with Redox-Active Phenylenediamine and Phenanthrenediamine Ligands. Ph.D. Disseration, University of California Irvine, Irvine, CA. 2008.

[2] Khramov, D. M.; Boydston, A. J.; Bielawski, C. W. *Org. Lett.* **2006**, *8*, 1831–1834.

[3] (a) Ketterer, N. A.; Fan, H.; Blackmore, K. J.; Yang, X.; Ziller, J. W.; Baik, M. H.; Heyduk, A. F. *J. Am. Chem. Soc.* **2008**, *130*, 4364–4374; Blackmore, K. J.; Ziller, J. W.; Heyduk, A. F. *Inorg. Chem.* **2005**, *44*, 5559–5561.

[4] Fackler, J. P. *Inorganic Syntheses*; John Wiley and Sons: New York, 1982; Vol. 21.